



# VCU

Virginia Commonwealth University  
VCU Scholars Compass

---

Theses and Dissertations

Graduate School


---

2020

## Formulation and Validation of Nanoparticle Controlled Delivery for Chemotherapeutic Drug Products

Shani L. Levit

Follow this and additional works at: <https://scholarscompass.vcu.edu/etd>

 Part of the [Nanomedicine Commons](#), [Nanoscience and Nanotechnology Commons](#), [Other Biomedical Engineering and Bioengineering Commons](#), [Other Chemical Engineering Commons](#), [Polymer Science Commons](#), and the [Transport Phenomena Commons](#)

© Shani L. Levit

---

Downloaded from

<https://scholarscompass.vcu.edu/etd/6232>

This Dissertation is brought to you for free and open access by the Graduate School at VCU Scholars Compass. It has been accepted for inclusion in Theses and Dissertations by an authorized administrator of VCU Scholars Compass. For more information, please contact [libcompass@vcu.edu](mailto:libcompass@vcu.edu).



# VCU

College of Engineering

Chemical and Life Science Engineering

# Formulation and Validation of Nanoparticle Controlled Delivery for Chemotherapeutic Drug Products

By

Shani L. Levit

A dissertation submitted in partial fulfillment of the requirements for the degree of Doctor of Philosophy in Chemical and Life Science Engineering at Virginia Commonwealth University.

Approved: April 24<sup>th</sup>, 2020

Advisor

Christina Tang, Ph.D.

Assistant Professor, Department of Chemical and Life Science Engineering

Advisory Committee

Christopher A. Lemmon, Ph.D., Department of Biomedical Engineering

Jessika Rojas, Ph.D., Department of Mechanical and Nuclear Engineering

Thomas D. Roper, Ph.D., Department of Chemical and Life Science Engineering and  
Pharmaceutical Engineering

Hu Yang, Ph.D., Department of Chemical and Life Science Engineering

Virginia Commonwealth University

Richmond, Virginia

© Shani L. Levit 2020  
All Rights Reserved

## Acknowledgements

My journey towards my Ph.D. at Virginia Commonwealth University has been filled with the most amazing memories and moments of pure happiness mixed with times of adversity. I am so thankful for the person I have become after facing these obstacles. I have gained so much strength, scientific experience, knowledge, and confidence in myself and my scientific work. I could not have done all of this without the love and support of the people around me.

Firstly, I would like to express immense gratitude to my advisor, Dr. Christina Tang for her guidance, support, and friendship. I would like to thank Dr. Tang for taking me under her wing and giving me the opportunity to pursue a Ph.D. in Chemical Engineering. Dr. Tang has been the best mentor I could ask for and supported me in more ways than I could count. She was a mentor in the lab, teaching me techniques vital for my success in the lab which lead me to become a mentor to younger students. I am thankful for her time and attention to detail though the many hours of revisions and edits which may have been frustrating at times but ultimately helped me flourish as a writer. She was my biggest advocate and proponent for disseminating my research to the scientific community. She encouraged me to present at numerous conferences as well as helped me go over every presentation which made me feel confident about my work. I am thankful for our late evening chats in the lab which I will forever miss. I am thankful for her kindness, generously, and guidance which have helped me get to today.

I would like to thank all the members of my Ph.D. committee, Dr. Christopher Lemmon, Dr. Jessika Rojas, Dr. Thomas Roper, and Dr. Hu Yang, for sparing their valuable time and providing me

with suggestions and feedback with my Ph.D. work. This feedback helped with the successful completion of my dissertation. I would especially like to thank Dr. Roper and Dr. Yang for offering me their laboratory space in order to complete vital elements of my research.

I would also like to thank all of VCU and the Chemical and Life Science Engineering (CLSE) Department for their support. I would like to thank the CLSE department for taking me in and allowing me to meet wonderful professors, mentors, and students along the way. Thank you to those who provided me with guidance on my research, professional development, and fun activities along the way like glass blowing! These experiences have made my time at VCU memorable and exciting.

I owe my deepest gratitude to my parents, Evgeny and Margarita Levit for their support throughout my life. It wouldn't be without your encouragement throughout all my science fairs, school projects, and even art classes that I would be here today receiving my doctorate. I remember my first experience with chemical engineering when I was around 10 years old, my parents bought me a science kit filled with over 100 chemicals, pipettes, and 96-well plates. At the time I thought it was too nerdy, but who knew these tools would be the foundation of my career today. I cannot thank my parents enough for their moral and financial support through these numerous years. Thank you for always pushing me to succeed and do my best in whatever I tried. I love you both so much!

I would like to also thank my grandmother, Maya, for her love and support. She helped raise me to be the person I am today. Thank you for always being there to talk to me, take me to school, teach me a plethora of useful skills, like sewing! You have waited a long time to see me graduate with my doctorate and I am so happy that I can make you proud! Thank you also to my auntie and uncle, Alla and Sasha, for always bringing me laughter and joy. I love you all so much and I hope to see you soon in Israel.

I want to thank my grandma, Lida, and my late grandfather, Lev, for their love and support. My grandfather was a scientist himself and he helped me come up with the most brilliant ideas for my science fair projects in school. I hope I can make him proud.

My brother, David, has been one of my greatest role models. He always did the best at school, sports, and art which made me want to follow in his footsteps. He ate chocolate, so I wanted to eat chocolate. He did swimming, so I wanted to do swimming. He did science fairs, so I wanted to do them too. While I stopped following in his footsteps, I am still inspired by his drive and motivation. Thanks for always being there, David!

One of the best things that my Ph.D. studies at VCU have brought me is my boyfriend, Dr. Ross Petrella. I am so thankful that I was able to meet you. You have been my biggest support, a shoulder to cry on, and the first person I want to share all my good news. I am so happy we were able to quarantine together, which gave me the support I needed to get through the last stage of my Ph.D. I could not have completed this journey without you, Ross. Thank you for being my personal chef, taking me wherever I want to go, and listening to all my complaints. I can't believe I found someone as amazing as you who loves me so much, which makes me love you even more. You are the love of my life and I cannot wait to spend the rest of our lives together.

Lastly, I would also like to thank my friends for filling me with laughter, helping me taking my mind off the stress, and being there for me when I needed it most. I want to thank one of my oldest and dearest friends, Mary Claire Gibson! It was that faithful day on the monkey bars in 6<sup>th</sup> grade that brought us together and solidified a lifelong friendship. Thanks for the support not just during my PhD, but throughout my life thus far! I want to thank my college friends at University of Virginia, Kyra, Ruba, Caitlin, Hale, Lark, Angela, and so many others. I could not have gotten through our Biomedical Engineering classes without you. Thank you to all these wonderful female engineers that showed me I can succeed and thrive as an engineer. To all the friends I met at VCU including Abigail

Casey, Remy Cooper, Rebecca Walker, Simone Gregor, thank you for helping me through the tough times and making my experience at VCU memorable. I also want to thank all my lab members and mentees, especially my lab mate Andrew Harrison, for always making going to lab a fun place! Thank you also to all the friends I met in Richmond who helped take my mind off all the stress!

To all these people and so many others, thank you for everything that has led me here and for your support for years to come!

# Table of Contents

Formulation and Validation of Nanoparticle Controlled Delivery for Chemotherapeutic Drug Products.....	1
Acknowledgements.....	ii
Table of Contents.....	vi
List of Figures.....	viii
List of Tables.....	xiii
Abstract.....	1
1. Chapter 1: Review of Sequential Drug Delivery of Drug Combinations for Chemotherapeutic Treatment of Ovarian Cancer.....	3
1.1. Introduction.....	3
1.2. Clinical Motivation.....	6
1.3. Drug Interaction and Synergy Methods.....	11
1.4. Sequence-Dependent Synergy of Free Chemotherapeutic Drugs.....	17
1.5. Nanoparticle Drug Combinations.....	30
1.6. Modeling Synergy of Drug Combinations.....	41
1.7. Conclusion.....	44
2. Chapter 2: Project Overview.....	47
2.1. Overview.....	47
2.2. Significance and Background.....	48
2.3. Model Drug Selection.....	50
2.4. Prior Art.....	52
2.5. Flash NanoPrecipitation.....	53
2.6. Approach.....	55
2.7. Specific Aims.....	56
2.8. Overview of Dissertation.....	58
3. Chapter 3: Rapid, Single-Step Protein Encapsulation via Flash NanoPrecipitation.....	61
3.1. Introduction.....	61
3.2. Materials and Methods.....	63
3.3. Results and Discussion.....	66
3.4. Conclusions.....	80



4. Chapter 4: Rapid Self-Assembly of Polymer Nanoparticles for Synergistic Codelivery of Paclitaxel and Lapatinib via Flash NanoPrecipitation .....	82
4.1. Introduction .....	83
4.2. Materials and Methods .....	85
4.3. Results and Discussion .....	91
4.4. Conclusion .....	109
5. Chapter 5: Sequence-Dependent Cytotoxicity of Nanoparticle Delivery of Paclitaxel and Lapatinib in Ovarian Cancer Cells .....	110
5.1. Introduction .....	111
5.2. Materials and Methods .....	113
5.3. Results and Discussion .....	120
5.4. Conclusion .....	133
6. Chapter 6: Controlled Drug Release of a Paclitaxel Prodrug from pH-Labile Nanoparticles to Improve Drug Efficacy.....	134
6.1. Introduction .....	135
6.2. Materials and Methods .....	137
6.3. Results and Discussion .....	145
6.4. Conclusion .....	168
7. Chapter 7: Rapid, Room Temperature Nanoparticle Drying and Low Energy Reconstitution via Electrospinning.....	170
7.1. Abstract.....	170
7.2. Introduction .....	171
7.3. Materials and Methods .....	173
7.4. Results .....	177
7.5. Conclusion .....	187
8. Chapter 8: Conclusion.....	189
8.1. Overview of Project Goals .....	189
8.2. Conclusions from Study .....	189
8.3. Future Work and Potential Impact.....	191
9. Vita.....	195
10. References .....	198
Appendix I: Paclitaxel Prodrug Analysis .....	223

## List of Figures

- Figure 1:** Diagram of advantages of drug combination for treating ovarian cancer. (A) Synergy can be observed when the drug combinations act through multiple pathways. (B) Combinations can overcome multi-drug resistance (MDR) mechanisms to increase anticancer activity. (C) Delivery of drug combinations can also reduce toxicity by reducing the necessary doses of each drug. Reprinted from [11], Copyright (2012), with permission from Elsevier..... 5
- Figure 2:** Mechanisms of cancer cell resistance to anticancer therapy ranging from changing expression of proteins to effecting drug accumulation, drug metabolism, and altering gene expression or repair to apoptotic pathways. (A) Reprinted from [33], Copyright © 2013, Springer Nature and (B) reprinted from [34], Copyright © 2014 Kapse-Mistry, Govender, Srivastava and Yegeri..... 8
- Figure 3.** (A) Isobologram with concentrations of drug A and B on the X and Y axis. The line between the IC-50 of drug A and B is the additivity effect of the drug combination. Below the line of additivity is synergy and above is antagonism. (B) and (C) are other visual representations of drug interaction. (B) is a plot of the combination index (CI) versus fraction affected ( $f_A$ ) and (C) dose reduction (DRI) index plotted against the fraction affected ( $f_A$ ). Figure reprinted from [60], Copyright © 2012 Breitinger. Licensee IntechOpen..... 14
- Figure 4.** Isobolograms of sequentially delivered drugs to two human leukemia cells, HM2 cells (closed circles) and HM51 cells (open circles) with (A) cisplatin 24 hours prior to paclitaxel and (B) paclitaxel 24 hours prior to cisplatin. (C) Tumor weight after sequential delivery of paclitaxel and bleomycin with the lowest tumor weight observed with (+) bleomycin administer prior to paclitaxel. (A) and (B) Reprinted from [84], Copyright (1995), with permission from Elsevier. (C) Reprinted from [14], Copyright © 2001, © 2001 Lippincott Williams and permission from Wolters Kluwer. .... 19
- Figure 5.** Representative image of cascade pathway activated by sequential co-delivery of cisplatin and EGCG. Reprinted from [18], Copyright © 2020 by The International Institute of Anticancer Research..... 23
- Figure 6.** Combination index of cells (A) A2780 and (C) OAW42 cells treated with 8-CI-cAMP followed by paclitaxel and (B) A2780 and (D) OAW42 cells treated with the reverse sequence. Drug synergy is dependent on the drug ratio and sequence. Reprinted from [135] with permission from AACR..... 29
- Figure 7.** Diagram of nanoparticle endocytosis and delivery of drug combinations. Delivery of drug combinations targets multiple proteins and results in activation of multiple cascade pathways to induce cell death. Reprinted (adapted) with permission from [157]. Copyright (2011) American Chemical Society..... 35
- Figure 8.** (A) Polymer nanoparticle loaded with three drugs for controlled release. RAP and 17-AAG are loaded in the core while paclitaxel is conjugated to the polymer shell. (B) Synergy is observed when all three drugs are co-delivered across the range of fraction affected. Reprinted (adapted) with permission from [194]. Copyright (2011) American Chemical Society. .... 41
- Figure 9.** Diagrams of (A) PPI network modeling, (B) dynamic pathway modeling, and (C) examples of network motifs that facilitate in determining synergy of drug combinations. Reprinted from [206]. Copyright © 2015, Springer Nature. .... 42
- Figure 10.** Simplified pathway cascade for modeling interaction of cisplatin and PI828. Reprinted (or adapted) from [211], with permission from AACR. .... 44

<b>Figure 11.</b> ABC transporters are responsible for removing drugs from the cell resulting in drug resistance. Lapatinib inhibits the activity of the transporters which sensitizes the cells and increases intracellular chemotherapeutic accumulation. ....	51
<b>Figure 12.</b> Flash NanoPrecipitation (FNP) is a rapid and scalable process with high drug loading. The rapid change in solvent quality during mixing of the solvent stream with the miscible anti-solvent stream in the Confined Impinging Jet (CIJ) Mixer leads to 1) precipitation of core material and 2) self-assembly of block co-polymer. The growth stabilized by block co-polymer adsorption. Nanoparticle size is governed by rate of nucleation and growth relative to self-assembly. ....	54
<b>Figure 13.</b> Two potential pathways of drug delivery from pH-labile nanoparticles. (1) When the nanoparticles are endocytosed the pH decreases resulting in destabilization and drug release or (2) diffusion-limited drug release from the nanoparticle outside the cell. ....	55
<b>Figure 14.</b> Overview of nanoparticle synthesis with Flash NanoPrecipitation to encapsulate paclitaxel and lapatinib with a tannic acid (TA) and iron coordination complex using an amphiphilic block copolymer stabilizer. ....	57
<b>Figure 15.</b> Overview of experimental studies covered in this dissertation. In Chapter 3 we discuss encapsulation of protein followed by the nanoparticle formulation process for encapsulating weakly hydrophobic drugs and synergistic activity of co-loaded nanoparticles in Chapter 4. In Chapter 5 we examine sequential drug delivery in vitro and in Chapter 6 we investigate formulating nanoparticles for controlled release. Lastly, in Chapter 7 we discuss electrospinning nanoparticles to extend their shelf-life.....	59
<b>Figure 16.</b> Precipitation of BSA and TA - Varying BSA:TA ratio. ....	67
<b>Figure 17.</b> Nanoparticles formulated with PS-b-PEG (28 mg/mL) and TA (5mg/mL) dissolved in acetone and rapidly mixed with BSA (9mg/mL) dispersed in water via FNP. ....	67
<b>Figure 18.</b> Dynamic light scattering (DLS) intensity weighted size distribution results of (A) Bovine serum albumin-tannic acid (BSA-TA) complex without the presence of a stabilizer, (B) BSA-TA complex with an amphiphilic block co-polymer, and (C) the BSA-TA complex stabilized with 750kDa polyethylenimine (PEI), immediately upon mixing and after 24 hrs. The BSA-TA complex stabilized with PEI did not change in size after 24 hrs.....	68
<b>Figure 19.</b> Effect of PEI molecular weight on nanoparticle formulation. ....	70
<b>Figure 20.</b> Precipitation of BSA and TA at various pH conditions. ....	72
<b>Figure 21.</b> DLS of the 10kDa PEI nanoparticles formulated under different pH conditions by varying the pH of the BSA stream. ....	72
<b>Figure 22.</b> Schematic of proposed self-assembly mechanisms using 750kDa and 10kDa polyethylenimine (PEI) via Flash NanoPrecipitation (FNP) with PEI stabilizer. In the confined impinging jet (CIJ) mixer the bovine serum albumin (BSA) and tannic acid (TA) interact via hydrogen bonding to form an insoluble complex. Then the complex is immediately diluted in a reservoir containing PEI. The BSA-TA complex interacts with the PEI via electrostatic interaction. High molecular weight 750kDa PEI aggregates template nanoparticle assembly and absorb the BSA-TA precipitate. In contrast, 10kDa PEI adsorbs on the precipitating BSA-TA complex forming a core-shell structure. ....	74

<b>Figure 23.</b> DLS of 10kDa PEI nanoparticles after dialysis.....	77
<b>Figure 24.</b> Effect of nanoparticle dispersion pH on size for (A) 10kDa polyethylenimine nanoparticles (PEI NPs) and (B) 750kDa PEI NPs. The size of the particles was measured 24 hours after adjusting the pH. The 10kDa PEI NPs destabilized under acidic conditions and released bovine serum albumin (BSA). The 750kDa PEI NPs did not change size at acidic pH. ....	77
<b>Figure 25.</b> Overview of nanoparticle synthesis with Flash NanoPrecipitation to encapsulate. paclitaxel and lapatinib with a tannic acid (TA) and iron coordination complex using an amphiphilic block copolymer stabilizer. The organic solvent stream contains the stabilizer, PS-b-PEG, TA, and one or more drugs of interest. The organic stream is rapidly mixed with the aqueous stream containing iron using a CIJ mixer. Upon rapid mixing, the TA and iron from an insoluble complex which facilitates the precipitation and encapsulation of paclitaxel and lapatinib. The resulting nanostructures are kinetically trapped.....	92
<b>Figure 26.</b> Dynamic light scattering of TA-Fe NPs (containing no drugs). ....	92
<b>Figure 27.</b> TEM images of (A) PTX NPs, (B) LAP NPs, and (C) PTX-LAP NPs. ....	94
<b>Figure 28.</b> Representative dynamic light scattering results of uniform (red) paclitaxel nanoparticle (PTX NPs), (blue) lapatinib nanoparticle (LAP NPs), and (purple) co-loaded paclitaxel-lapatinib nanoparticle (PTX-LAP NPs) samples produced at ~100 nm (each DLS curve is the average of n = 4 measurements). Representative transmission electron microscopy (TEM) image of PTX-LAP NPs (scale bar = 200 nm), as inset. ....	95
<b>Figure 29.</b> Dynamic light scattering of LAP NPs. Nanoparticles were formulated at 1mg/mL and 2mg/mL drug concentration in the organic stream. The LAP NP dispersion produced at 2 mg/mL had multiple size peaks at ~150 nm and ~30 nm, while the LAP NPs produced at 1 mg/mL were uniform at ~100 nm.....	97
<b>Figure 30.</b> The cumulative drug release of paclitaxel (PTX) and lapatinib (LAP) from polymer nanoparticles (NPs) from (A) PTX from PTX NPs, (B) LAP from LAP NPs, and (C) PTX and LAP from co-loaded nanoparticles. The graph shows the average $\pm$ standard deviation of 3 replicates of FNP and independent drug release assays.....	100
<b>Figure 31.</b> Dose response curve for cell treated with free PTX (blue) and PTX NPs (red). ....	103
<b>Figure 32.</b> Dose response curve for cell treated with free LAP (blue) and LAP NPs (red). ....	103
<b>Figure 33.</b> Cell cycle analysis of OVCA-432 cells from flow cytometry to compare free drug (in 2% DMSO) and nanoparticle formulations for A) paclitaxel (PTX) and B) lapatinib (LAP). The graph shows the average $\pm$ standard deviation from 3 replicate wells.....	105
<b>Figure 34.</b> Cell cycle distribution of untreated cells and cell treated with TA-Fe NPs. ....	105
<b>Figure 35.</b> The cell viability dose-response curve of OVCA-432 cells when treated with (blue) paclitaxel nanoparticles (PTX NPs) and (red) paclitaxel-lapatinib nanoparticles (PTX-LAP NPs). The PTX-LAP NPs treatment shifts the dose-response curve to lower drug concentrations compared to the PTX NPs treatment. The graph shows the mean $\pm$ standard deviation from one experiment performed with 6 replicate wells. ....	107
<b>Figure 36.</b> Cell viability of OVCA-432 cells after 48 hour treatment with (gray) media, (purple) tannic acid-iron nanoparticles (TA-Fe NPs), (pink) paclitaxel nanoparticles (PTX NPs), (light blue) lapatinib	

nanoparticles (LAP NPs), (green) paclitaxel-lapatinib nanoparticles (PTX-LAP NPs). The cells were treated with a PTX concentration of 0.009  $\mu\text{g/mL}$  and LAP at 0.004  $\mu\text{g/mL}$  based on IC-50 of the PTX-LAP NPs. The cell viability was significantly lower when the cells were treated with PTX-LAP NPs when compared to PTX NPs ( $p < 0.05$ ) and LAP NPs ( $p < 0.05$ ). The graph shows the mean  $\pm$  standard deviation from one experiment performed with 6 replicate wells. .... 108

**Figure 37.** The cell viability was examined for OVCA-432 and OVCAR-3 cells following 24 hour treatment with a single free drug dose. Cells were either treated simultaneously with free paclitaxel and free lapatinib (light blue, PTX + LAP), with free paclitaxel alone (pink, Free PTX), with free lapatinib alone (light orange, Free LAP), or untreated (light grey, Control)..... 124

**Figure 38.** The cell viability was examined for OVCA-432 and OVCAR-3 cells following 24 hour treatment with a single nanoparticle drug dose. Cells were either treated simultaneously with PTX NPs and LAP NPs (dark blue, PTX NPs + LAP NPs), with PTX NPs alone (magenta, PTX NPs), with LAP NPs alone (orange, LAP NPs), or untreated (dark grey, Control). .... 125

**Figure 39.** The cell viability of OVCA-432 cells and OVCAR-3 cells following 48 hour sequential treatment with free paclitaxel and free lapatinib. The cells were either untreated (light grey, Control), or treated with sequential drug delivery over 48 hours: simultaneous treatment of free paclitaxel and free lapatinib (light blue, Free PTX + Free LAP), (pink) paclitaxel followed by lapatinib (pink, Free PTX > Free LAP), and lapatinib followed by paclitaxel (light orange, Free LAP > Free PTX). .... 127

**Figure 40.** The cell viability of OVCA-432 cells and OVCAR-3 cells following 48 hour sequential treatment with PTX NPs and LAP NPs. The cells were either untreated (dark grey, Control), or treated with sequential drug delivery over 48 hours: simultaneous treatment of PTX NPs and LAP NPs (dark blue, PTX NPs + LAP NPs), paclitaxel followed by lapatinib (magenta, PTX NPs > LAP NPs), and lapatinib followed by paclitaxel (orange, LAP NPs > PTX NPs)..... 128

**Figure 41.** The cell cycle distribution for OVCA-432 and OVCAR-3 cells treated with three sequence schedules using free drugs. The cells were either untreated (light grey, Control), simultaneously treated with free paclitaxel and free lapatinib (light blue, PTX + LAP Free), free paclitaxel followed by free lapatinib 24 hrs later (pink, PTX > LAP Free), or free lapatinib followed by free paclitaxel 24 hrs later (light orange, LAP > PTX Free)..... 131

**Figure 42.** The cell cycle distribution for OVCA-432 and OVCAR-3 cells treated with three sequence schedules using nanoparticle formulations. The cells were either untreated (dark grey, Control), simultaneously treated with PTX NPs and LAP NPs (blue, PTX NPs + LAP NPs), PTX NPs followed by LAP NPs 24 hrs later (magenta, PTX NPs > LAP NPs), or LAP NPs followed by PTX NPs 24 hrs later (orange, LAP NPs > PTX NPs). .... 132

**Figure 43.** Two-step synthesis of the paclitaxel-prodrug with  $\alpha$ -tocopherol as the lipid anchor. In the first step the tocopherol lipid anchor is synthesized and in the second step paclitaxel is conjugated to the lipid anchor to form the prodrug..... 139

**Figure 44.** Representative transmission electron microscopy (TEM) images of (A) Pro NPs and (B) Pro-LAP NPs taken at 40kX (scale bar = 200 nm). .... 148

**Figure 45.** (A) The drug release profile of (pink circles) PTX NPs, (orange squares) Pro NPs, (blue rhombus) LAP NPs at pH 7.4 sink conditions. Highlighted in the green square is the (B) close up of the release profile between time 0 to 0.5 days. The average and standard deviation are shown for 3 replicate samples. .... 154

**Figure 46.** (A) The drug release profile of (pink circles) PTX NPs, (orange squares) Pro NPs, (blue rhombus) LAP NPs at pH 4 sink conditions. Highlighted in the green square is the (B) close up of the release profile between time 0 to 0.5 days. The average and standard deviation are shown for 3 replicate samples. .... 155

**Figure 47.** (A) The drug release profile of (pink circles) paclitaxel and (blue rhombus) lapatinib from PTX-LAP NPs and (orange squares) prodrug and (light blue triangle) lapatinib from Pro-LAP NPs at pH 7.4 sink conditions. Highlighted in the green square is the (B) close up of the release profile between time 0 to 0.5 days. The average and standard deviation are shown for 3 replicate samples..... 159

**Figure 48.** (A) The drug release profile of (pink circles) paclitaxel and (blue rhombus) lapatinib from PTX-LAP NPs and (orange squares) prodrug and (light blue triangle) lapatinib from Pro-LAP NPs at pH 4 sink conditions. Highlighted in the green square is the (B) close up of the release profile between time 0 to 0.5 days. The average and standard deviation are shown for 3 replicate samples..... 161

**Figure 49.** Cell cycle analysis of OVCA-432 cells from flow cytometry of (grey) untreated cells, and cells treated with either (pink) free paclitaxel or (green) free prodrug. .... 166

**Figure 50.** Cell cycle analysis of OVCA-432 cells treated with single drug nanoparticles. The cell distribution was compared between (grey) untreated cells, (pink) PTX NPs, and (green) Pro NPs..... 167

**Figure 51.** Cell cycle analysis of OVCA-432 cells treated with co-loaded nanoparticles. The cell distribution was compared between (grey) untreated cells, (pink) PTX-LAP NPs, and (green) Pro-LAP NPs. .... 168

**Figure 52.** SEM images of electrospun PVA fibers loaded with NPs. A) PVA only fibers with an average nanofiber (NF) diameter of  $329 \text{ nm} \pm 34 \text{ nm}$ , B) PVA fibers with 95 nm VE NPs at 0.8 wt.% with an average NF diameter of  $364 \text{ nm} \pm 36 \text{ nm}$ , C) PVA NF with 3.2 wt.% loading of 174 nm VE NPs with an average diameter of  $292 \text{ nm} \pm 47 \text{ nm}$ , and D) PVA fiber with 0.8 wt.% loading of 112 nm PS NPs and NF diameter of  $354 \text{ nm} \pm 31 \text{ nm}$ . All samples electrospun to form continuous, uniform fibers. .... 178

**Figure 53.** Rapid NP reconstitution using low-energy mixing. A) Initial NP-loaded fibers B) Immediate dissolution of PVA fibers upon addition of DI water, and C) Visible confirmation of NP reconstitution after 5 mins of hand-mixing..... 179

**Figure 54.** Particle size distribution measured by dynamic light scattering of 118 nm VE NPs reconstituted within 1 day of drying and after 7 months of storage at ambient conditions. The peak at  $\sim 30 \text{ nm}$  is attributed to the dissolved polymer in the solution and the solution and the peak at  $\sim 160 \text{ nm}$  is attributed to the reconstituted NPs. The NP size is comparable upon reconstitution after 1 day and 7 months of storage at ambient conditions..... 181

**Figure 55.** Particle size distribution measured by dynamic light scattering of the initial NPs, PVA control, and reconstituted (RC) NPs for A) VE NP and B) PS NPs. The second peak for RC NPs shifts to the right indicative of an increase in particle size relative to initial NPs..... 182

## List of Tables

<b>Table 1.</b> BSA recovery in Bradford assay sample preparation .....	66
<b>Table 2.</b> Zeta potential of BSA-TA complex with polymer stabilizers. ....	66
<b>Table 3.</b> Effect of polyelectrolyte stabilizer molecular weight on nanoparticle properties and stability.....	69
<b>Table 4.</b> Size and zeta potential of PEI dispersed in water .....	71
<b>Table 5.</b> Effect of PEI molecular weight on nanoparticle formulation.....	71
<b>Table 6.</b> Effect of pH of the BSA stream and PEI reservoir on 750kDa PEI nanoparticles .....	72
<b>Table 7.</b> Effect of pH of the BSA stream and PEI reservoir on 10kDa PEI nanoparticle formulation .....	73
<b>Table 8.</b> Varying ratio of stabilizer to core for 750kDa PEI nanoparticles.....	75
<b>Table 9.</b> Varying total solids concentration and ratio of BSA to TA by mass for nanoparticles made with 10kDa PEI .....	75
<b>Table 10.</b> Varying Total Solids of 750kDa PEI nanoparticles.....	76
<b>Table 11.</b> Effect of ionic strength on particle stability of 750kDa PEI nanoparticles .....	78
<b>Table 12.</b> Effect of ionic strength on 10kDa PEI nanoparticle properties. ....	78
<b>Table 13.</b> Effect of TA on nanoparticle formulation .....	79
<b>Table 14.</b> Effect of tannic acid (TA) on protein encapsulation.....	80
<b>Table 15.</b> Summary of paclitaxel nanoparticle formulations.....	93
<b>Table 16.</b> Summary of lapatinib nanoparticle formulations. ....	96
<b>Table 17.</b> Effect of varying drug concentration when preparing for formulating PTX-LAP NPs.....	98
<b>Table 18.</b> Comparing nanoparticles size and polydispersity before and after filtration. ....	98
<b>Table 19.</b> Nanoparticle stability.....	98
<b>Table 20.</b> Encapsulation Efficiency and Drug Loading of Nanoparticles. ....	99
<b>Table 21.</b> Cell viability of cell treated with Fe-TA NPs. ....	102
<b>Table 22.</b> IC-50 of paclitaxel, paclitaxel nanoparticles, lapatinib, and lapatinib nanoparticles in OVCA-432 cells.....	104

<b>Table 23.</b> IC-50 and combination index of paclitaxel-lapatinib nanoparticles (PTX-LAP NPs) (co-loaded) compared to simultaneous delivery of paclitaxel nanoparticles (PTX NPs) and lapatinib nanoparticles (LAP NPs) (two single drug-loaded NPs) in OVCA-432 cells.....	109
<b>Table 24.</b> Sequential drug dosing of OVCA-432 cells for evaluating cell viability.....	118
<b>Table 25.</b> Sequential drug dosing of OVCAR-3 cells for evaluating cell viability.....	118
<b>Table 26.</b> Sequential drug dosing of OVCA-432 cells for cell cycle analysis.....	119
<b>Table 27.</b> Sequential drug dosing of OVCAR-3 cells for cell cycle analysis.....	119
<b>Table 28.</b> Nanoparticle Characterization.....	121
<b>Table 29.</b> The IC-50 values for free drug and nanoparticle treated cells.....	122
<b>Table 30.</b> Formulation parameters for single-drug and co-loaded nanoparticles with paclitaxel, prodrug, and lapatinib.....	140
<b>Table 31.</b> Varying the concentration of the PTX-prodrug.....	146
<b>Table 32.</b> Varying ratio of the block co-polymer to core ratio.....	147
<b>Table 33.</b> Varying the prodrug concentrations of Pro-LAP NPs.....	149
<b>Table 34.</b> Varying the BCP: core ratio of Pro-LAP NPs.....	150
<b>Table 35.</b> Size and polydispersity index of nanoparticles.....	151
<b>Table 36.</b> Summary of the encapsulation efficiency and drug loading.....	152
<b>Table 37.</b> Rate constant and $R^2$ of nanoparticle drug release at pH 7.4 conditions fit to the Korsmeyer-Peppas diffusion model.....	157
<b>Table 38.</b> Rate constant and $R^2$ of nanoparticle drug release at pH 4 conditions fit to the Hixson-Crowell diffusion model.....	158
<b>Table 39.</b> The IC-50 of OVCA-432 cells treated with paclitaxel, paclitaxel prodrug, lapatinib in free drug and nanoparticles formulations.....	163
<b>Table 40.</b> IC-50 and combination index of co-loaded nanoparticles in OVCA-432 cells.....	165
<b>Table 41.</b> Characteristics of NPs electrospun fibers.....	177
<b>Table 42.</b> Comparing reconstitution techniques.....	179
<b>Table 43.</b> Dissolving fibers in PBS.....	180
<b>Table 44.</b> Comparing size stability of NPs after storage for 7 months.....	181
<b>Table 45.</b> NP core composition and size influences NP size stability after reconstitution.....	183



<b>Table 46.</b> NP:NF ratio influences NP size stability after reconstitution .....	185
<b>Table 47.</b> NP loading concentration .....	186
<b>Table 48.</b> Comparing drying and reconstitution of dialyzed particles to non-dialyzed particles.....	187

## Abstract

Treating ovarian cancer is challenging due to a variety of genetic mutations and affected cell types attributing to cancer development, diagnosis in advanced stages, and acquired drug resistance mechanisms (MDR) due to chemotherapy treatment. Taxol, a free drug formulation of paclitaxel (PTX), is one of the most widely used chemotherapeutic drugs. Clinically, paclitaxel is used in combination with other drugs such as lapatinib (LAP) to increase treatment efficacy and overcome MDR. In both pre-clinical and clinical studies, sequentially delivering drug combinations have been found to improve drug efficacy. However, there is a challenge with translating pre-clinical results to clinical practice due to a difference in time-scales of treatment schedules, i.e, hours in preclinical studies vs. days to weeks in clinical studies. Furthermore, the drug efficacy of free drug formulations is limited due to poor solubility, poor bioavailability, and severe toxicity. Nanoparticle drug delivery can overcome these limitations with controlled drug release.

Flash NanoPrecipitation (FNP) is developed as a rapid, scalable, self-assembly process that leverages intermolecular interactions to encapsulate hydrophilic macromolecules and weakly hydrophobic drugs ( $\log P < 6$ ) via *in situ* complexation with antioxidants (i.e. tannic acid) formulating a pH-labile platform. A single-step method using FNP was demonstrated by complexing proteins with tannic acid and then stabilized with a polyelectrolyte. These nanoparticles have high encapsulation efficiency of hydrophilic macromolecules (~80%), are stable at physiological conditions, and disassemble upon changes in pH to release their biologic payload.

Next, *in situ* coordination complexation of tannic acid and iron (TA-Fe<sup>3+</sup>) via FNP was used to encapsulate paclitaxel and lapatinib in pH-labile, polymer-stabilized nanoparticles. The drug release at pH 7.4 was driven by Fickian diffusion while at pH 4 drug release was driven by dissolution of the core. Encapsulation of paclitaxel and lapatinib into nanoparticles increased drug potency by 1500-fold

for paclitaxel and 6-fold for LAP *in vitro* with ovarian cancer cell line (OCA-432). When PTX and LAP were co-loaded into the same nanoparticle, they displayed a synergistic interaction indicated by a combination index of 0.23. Sequential drug delivery was also examined with delivery of single-drug nanoparticles using two ovarian cancer cell models with three different treatment schedules. The response was cell-dependent; overall the greatest cytotoxicity was observed with simultaneous drug treatment or paclitaxel delivery followed by delivery of lapatinib 24 hours later. Based on these results, further enhancement of drug efficacy was explored by formulating a paclitaxel prodrug (PTX conjugated to Vitamin E). The drug release of the prodrug from the nanoparticle was faster than paclitaxel due to different driving forces (i.e. compression of core) which facilitated sequential release of the paclitaxel prodrug prior to lapatinib. *In vitro*, there was an 8-fold and a 5-fold increase in drug efficacy of the prodrug relative to paclitaxel in free drug formulations and in nanoparticles, respectively. The potency was further enhanced by co-encapsulation with lapatinib. Overall, these findings provide the foundational methods to increase efficacy of paclitaxel and control drug release from nanoparticle for sequential drug delivery.

While nanoparticle formulations offer advantages over free drugs for sequential drug delivery of drug combinations, the stability of nanoparticle dispersions, which requires cold-chain storage, is an obstacle for translation to clinical practice. While drying the dispersion can improve long-term storage, the main limitations of current drying methods are particle aggregation, high-energy reconstitution, and the use of large amounts of cryoprotectants. A novel, rapid, and room-temperature method for drying nanoparticles via electrospinning was developed. Redispersion by hand-mixing to the original nanoparticle size was achieved when the fiber diameter and nanoparticle diameter were comparable. Overall, the techniques laid out in this dissertation facilitate translation of controlled sequential drug delivery to clinical practice using nanomedicines for treating ovarian cancer.

# 1. Chapter 1: Review of Sequential Drug Delivery of Drug Combinations for Chemotherapeutic Treatment of Ovarian Cancer

---

## 1.1. Introduction

Ovarian cancer is one of the most common forms of cancer among women with over 200,000 new cases of ovarian cancer each year worldwide [1]. Genetically inherited gene mutations are one of the most significant risk factors for ovarian cancer. Other risk factors include age, gynecological conditions, pelvic inflammatory disease, and polycystic ovarian syndrome [1]. Both the prevention and early detection of ovarian cancer are difficult because most cell markers cannot be reliably diagnosed during early stages [1–4]. Therefore, ovarian cancer is primarily diagnosed in advanced stages (stage III) when the 5-year survival rate is only 30% [1].

There are five primary types of ovarian cancer, each with different progression, genetic mutations, and prognoses associated with the disease. These five types of ovarian cancer originate from three cell types: epithelial cells, stromal cells, germ cells. Among these, epithelial ovarian cancer is one of the most common [4]. However, the pathogenesis is still not well understood and there are varieties of mutation profiles that contribute to the development of ovarian cancer. Type I serous and mucinous tumors are associated with the mutation of BRAF and KRAS oncogenes, endometrioid tumors are associated with PTEN gene [1,5]. Type II high-grade serous and carcinosarcoma tumors

have p53, BRCA1, and BRCA 2 gene mutations [4,6]. A more detailed review of ovarian cancer epidemiology is available by Reid et al. [1].

For all types of ovarian cancer, the standard of care includes surgery to remove the majority of the tumor followed by chemotherapy [4]. Surgery entails a hysterectomy, removal of both ovaries, and removal of tumor tissue to reduce volume [6]. However, surgery alone is ineffective at completely treating ovarian cancer, due to the formation of microscopic tumor tissues and macroscopic peritoneal implants that form during advanced stages [7]. For patients with advanced stage ovarian cancer, platinum-based chemotherapy, such as cisplatin, following surgery was the standard of care for over 40 years.

Paclitaxel, extracted from the bark of the Yew tree, was discovered to have anticancer activity and in the 1990's was FDA approved for ovarian cancer treatment [4,8]. Currently, the standard of care is two-drug combination treatment of carboplatin and paclitaxel infusion over 3 hours weekly, for 6 cycles. While this treatment has been found to prolong survival and improve quality of life for patients, it is associated with severe systemic toxicity and many patients experience recurrence. Only a small population have long-term remission [7,9,10]. Treating patients with recurring ovarian cancer and acquired drug resistance mechanisms remains a significant challenge [7].

Sequential treatment with of drug combinations is a common practice for managing recurring ovarian cancer. One of the common sequences is first-line carboplatin and paclitaxel therapy followed by a re-treatment of both drugs at first relapse which has high response rates (~85%). Due to various factors such as the type of ovarian cancer, genetic mutations, and development of resistance mechanisms, selecting appropriate drug combinations as well as treatment schedule is challenging (**Figure 1**). Both clinical and pre-clinical studies have investigated sequence schedules of drug combinations to overcome these limitations [12–14].

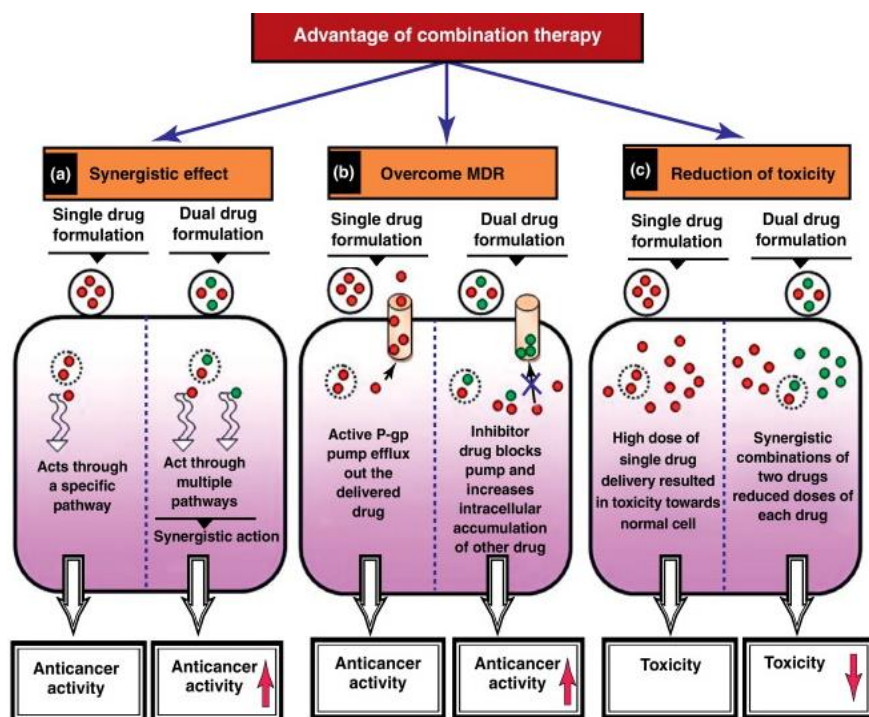


**Figure 1:** Diagram of advantages of drug combination for treating ovarian cancer. (A) Synergy can be observed when the drug combinations act through multiple pathways. (B) Combinations can overcome multi-drug resistance (MDR) mechanisms to increase anticancer activity. (C) Delivery of drug combinations can also reduce toxicity by reducing the necessary doses of each drug. Reprinted from [11], Copyright (2012), with permission from Elsevier

The definition of sequential therapy is an important consideration when developing new drug combinations and translational research. However, there is not a direct comparison between clinical and pre-clinical results due to a difference in time schedules. Clinically, sequences of drug combinations are treated on the order of days to weeks [15–17]. However, *in vitro* and *in vivo* sequential drug treatments are on the order of hours which are on the same timescale as many drug-activated pathways [13,18,19]. This results in a disparity between practices in pre-clinical studies and the clinic. While delivering therapeutic dosages on the same time scale as cellular activity can enhance therapeutic efficacy, two major challenges for transitioning this practice into the clinic are patient compliance and increased cytotoxicity. Nanoparticle drug delivery can overcome these limitations with controlled drug release.

This review will discuss the clinical motivations for sequential chemotherapy for treating ovarian cancer. The focus on this review is combinations of small molecules including platinum chemotherapeutic agents, taxane agents, doxorubicin, targeted protein inhibitory drugs, as well as other therapeutic agents. *In vitro* and *in vivo* drug efficacy are discussed in terms of drug synergy for free-drug delivery of drug combinations. Nanoparticle drug combinations of polymer micelles, dendrimers, and lipid nanoparticles are also reviewed for treatment of ovarian cancer. Lastly, computational modeling and predictive approaches are discussed to facilitate the selection of drug combinations and schedules.

## 1.2. Clinical Motivation

### 1.2.1. Drug Resistance Mechanisms

With chemotherapy treatments, many patients often relapse due to development of drug resistance mechanisms. Drug resistance can be attributed to five factors: 1) Drug inactivation or detoxification, 2) dose intensity, 3) drug efflux, 4) DNA repair, 5) cell death inhibition [20,21]. Ovarian cancer cells are known to form resistance mechanisms to a variety of drugs including cisplatin, carboplatin, and paclitaxel (**Figure 2**) [20].

Cells have mechanisms for detoxification or inactivation of anticancer drugs, particularly platinum therapies, thereby reducing their potency [22,23]. Drugs interact with proteins that either modify, degrade, form drug complexes, or downregulate proteins necessary for metabolic activation of the drug [24,25]. Metallothionein and glutathione are known to play a role in detoxification either by altering drug transportation, enzymatic-catalysis of inactivation of platinum, or inhibiting DNA damage induced by platinum therapies [20]. Some of the proteins involved with the activation and inactivation of the drugs are cytarabine (AraC), cytochrome P450 (CYP), glutathione-S-transferase (GST), and uridine diphospho-glucuronosyltransferase (UGT) [21,24,25].

The drug resistance is also attributed to an increase in drug efflux. Cancer cells can decrease drug accumulation by enhancing drug efflux. The class of ATP-binding cassette (ABC) transporters are membrane proteins that have a role in removing and regulating the transport of substances across the cell membrane. However, in some cancer cells, there is an upregulated expression of the ABC transporters, which facilitate the removal of anticancer drugs thereby lowering intracellular drug accumulation. From the ABC transporter family, three proteins are known to be associated with drug resistance: multidrug resistance protein 1 (MDR1), multidrug resistance-associated protein 1 (MRP1), and breast cancer resistance protein (BCRP). These proteins effect the drug efflux of taxane and kinase inhibitor drugs among others [26,27]. Interestingly, a decrease in platinum drug accumulation is not associated with P-glycoprotein expression while it is a factor for Taxol resistance [20].

Platinum drugs can be particularly susceptible to drug resistance. Platinum therapies induce cytotoxicity by forming lesions in DNA which disrupt DNA synthesis and gene expression. Studies have shown that in cells resistant to platinum therapy, DNA repair is enhanced and the rate of DNA repair may also depend on the affected genomic regions [28,29]. DNA repair mechanism also involves nucleotide excision repair and homologous recombination [30,31].

Drug resistance can also occur by cell inhibition of apoptosis and autophagy pathways. For example, apoptosis can be inhibited by overexpression of antiapoptotic proteins such as B-cell lymphoma 2 (BCL-2) and Akt proteins [21]. Review of drug resistance mechanism can be found elsewhere: [20,21,32].



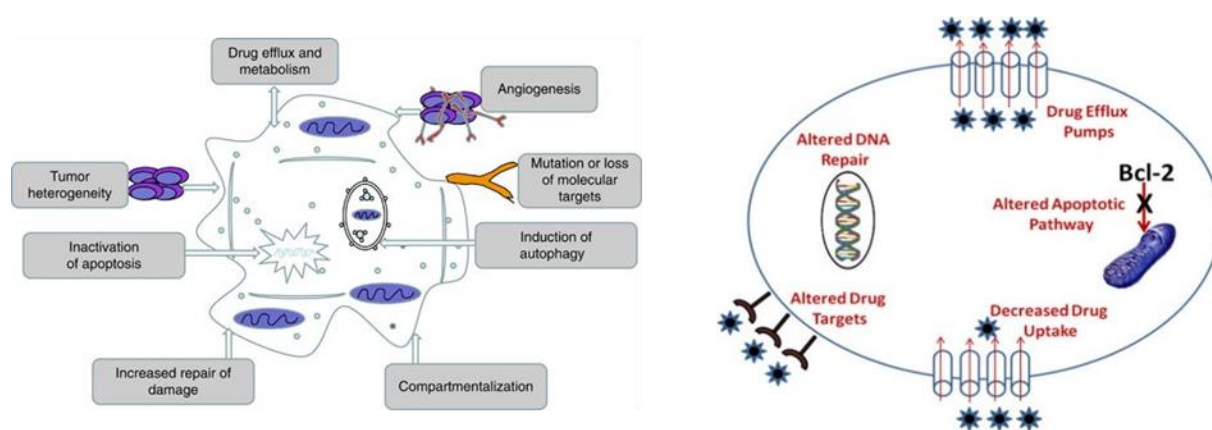


**Figure 2:** Mechanisms of cancer cell resistance to anticancer therapy ranging from changing expression of proteins to effecting drug accumulation, drug metabolism, and altering gene expression or repair to apoptotic pathways. (A) Reprinted from [33], Copyright © 2013, Springer Nature and (B) reprinted from [34], Copyright © 2014 Kapse-Mistry, Govender, Srivastava and Yergeri.

### 1.2.2. Standard of Care & Sequential Treatment

The challenge still remains to treat patients with recurring ovarian cancer while preventing drug resistance mechanisms. Some of the current approaches for treating ovarian cancer with multidrug resistance as well as preventing resistance include 1) combination therapy with noncross-resistant agents; 2) sequential therapy of drug combinations; 3) dose-intense chemotherapy 4) intraperitoneal therapy which exposes cancer cells to higher drug concentration at tumor site; 5) use of signal transduction inhibitors such as tyrosine kinase inhibitors; 6) new drug formulations such as nanoparticles [35]. Although, dose-intense chemotherapy has shown limited efficacy with the maximum dose limitations in clinical setting.

In cases where the time to relapse is within 6 months after first-line treatment, the ovarian cancer is considered platinum resistant [3,7]. The current standard of care is dependent on platinum sensitivity with therapy responses based on a platinum-free interval during second-line therapy leading to improved patient outcomes [36]. Therefore, incorporation of a platinum-free interval has been an important consideration for both platinum-sensitive and -resistant groups. Other studies have investigated methods to overcoming these challenges with combination chemotherapy regimens such

as drug combinations of carboplatin with gemcitabine which was found to improve progression time and progression-free survival compared to platinum treatment alone [37]. The treatment-free or platinum-free intervals have been found to be important for improving patient responses to therapies because the interval can aid in reducing the tumor resistance to therapies. However, after even the first-line treatment, many patients develop drug resistant mechanisms which limit the efficacy of chemotherapies [9].

The second, third, and fourth relapses cycle through etoposide, liposomal doxorubicin, and topotecan, respectively. But there are severe limitations of this sequence due to cumulative toxicity of these drugs and decrease in quality of life for the patient [38].

An alternative sequence approach, the first-line therapy remains carboplatin with paclitaxel, followed by topotecan as the second-line therapy. The reason for the shift is that although the efficacy of topotecan is comparable to single-drug platinum-therapy, it does not induce cumulative toxicity and patient response is higher with minimal pretreatment. This allows for treatment with other chemotherapeutic agents upon the next relapse [39,40].

In an effort to improve patient outcomes, strategies such as maintenance therapy and intraperitoneal drug administration, as well as drug combination treatments, have been investigated [7]. Maintenance therapy has been investigated as a means to prevent relapse [7,41]. One study dosing 12 monthly cycles of paclitaxel found that it produces neurotoxicity and the results were inconclusive [41]. Similarly, maintenance studies with topotecan and epirubicin did not show an improvement in patient survival [42,43]. Intraperitoneal (IP) chemotherapy delivers the anticancer drugs directly into the peritoneal cavity and has been investigated in small-volume ovarian cancers. The advantages of this delivery method is that higher drug concentrations can be delivered to the tumor tissue [44]. While this treatment improves survival, it is not commonly used due to severe toxicity [45].

Currently, the standard of care is two-drug combination treatment of platinum agent with paclitaxel. McGuire et. al. [46] found that drug combinations of paclitaxel and cisplatin significantly improved survival rates. Furthermore, increasing dosage concentrations of paclitaxel and cisplatin was found to improve survival; however, it also increased neurological and gastrointestinal toxicity [47]. This led the change in standard of care to combination of taxol chemotherapeutics with carboplatin, a less toxic platinum agent delivered through infusion over 3 hours in six three-weekly cycles [46,48].

While combinations of paclitaxel and carboplatin reduce some of the cytotoxic effect observed with paclitaxel and cisplatin, patients still experience systemic toxicity. Side effects include myelosuppression, neuropathy, and alopecia [7]. Other studies have found that delivering a weekly schedule of dose-dense paclitaxel improved the survival while minimizing progression [49,50]. A study by Kutsumata et al. investigated delivery of dose-dense paclitaxel and carboplatin (1 hr infusion) on a weekly regimen compared to the standard treatment of paclitaxel and carboplatin (3 hr infusion) every 3 weeks in a phase III trial. The study found that weekly dose-dense therapy of paclitaxel with carboplatin significantly improved patient survival [49]. Another limitation of chemotherapy is the cumulative toxicity with multiple treatments [51]. There is still a need to improve chemotherapy and minimize side effects of the treatment.

Other combinations of chemotherapeutic agents and dosing schedules have also been explored clinically in an effort to overcome drug resistance mechanisms, prevent relapse, and limit systemic toxicity. A Phase I trial examined sequence schedules of gemcitabine in combination with paclitaxel in patients with recurring epithelial ovarian cancer. The study found a schedule of paclitaxel treatment on day 1 and gemcitabine on day 1 as well as day 8 increased patient response rate by 41% and enabled high drug dosing with tolerable toxicity [12]. Another clinical trial examined drug combinations of cyclophosphamide, hexamethylmelamine, adriamycin, and cis-dichlorodiammineplatinum(II) in patients with ovarian carcinomas. The drugs were administered on a 4 -week cycle simultaneously on

day 1 and hexamethylmelamine was given orally on days 1-14. However, this treatment was found to induce severe side effects [52].

More recently, the standard of care has shifted to nanoparticle drug formulations [53]. PEGylated liposomal doxorubicine (Doxil), has been shown to enhance drug efficacy in recurring or resistant ovarian cancers. Initially, Doxil was treated at 50 mg/m<sup>2</sup> every 4 weeks but there was schedule and dose-dependent toxicity associated with this treatment [54,55]. This led to several studies examining reduced dosage to 40 mg/m<sup>2</sup> every 4 weeks which was found to minimize toxicity and enhance treatment efficacy [56]. In order to further improve patient response to treatment, Doxil has been used in combination with other chemotherapies such as carboplatin, paclitaxel, and gemcitabine in a variety of treatment schedules. Overall, the studies found that reducing the dosages of both agents would minimize toxicity and increase therapeutic efficacy [57–59].

Overall clinical practices are shifting to sequential chemotherapy of drug combinations. Selection of appropriate drug combinations is an important consideration to prevent cross-resistant therapies and minimize cumulative toxicities [9]. Certain sequences can enhance drug efficacy, producing a synergistic drug interaction while others can be antagonistic; therefore, exploring efficacy of drug sequence schedules will drive improvements in chemotherapeutic treatments. There also needs to be a consideration for the time scale of sequential treatments conducted in clinical practice, typically on the order of one week, and methods for closing the gap between pre-clinical studies which are conducted on shorter treatment cycles.

### **1.3. Drug Interaction and Synergy Methods**

With the growing approach of drug combination therapies, it is important to understand the interactions of the drugs. Screening studies help to determine the concentrations of the drugs necessary to produce an effective treatment. Therefore, understanding the dose-response interaction of each drug

is vital. Multiple drugs can either exhibit no cross-interaction with each other, producing an additive effect. However, drug combinations can also interact with one another depending on the drug target, downstream pathways activated by the drugs, and other biochemical interactions in the cells. These interactions are classified as either synergistic or antagonistic effects. Synergistic drug interaction is classified as a greater overall effect of two or more drugs than the sum of their individual effects. In the reverse case, when the combination of multiple drugs produces a smaller effect than the sum of the individual components, the drug interaction is antagonistic. This is a particularly important concept for developing new drug combinations and schedules because the combination of the drugs could produce an enhanced cytotoxic effect (synergistic) or inhibit cytotoxicity and induce greater systemic toxicity [60]. There are several methods for quantifying the synergy and drug interaction which are discussed here.

### 1.3.1. Fractional Inhibition Concentration

The fractional inhibition concentration (FIC) is a measure of synergy [61]. It is often used in defining synergistic effects of antibacterial drugs [62–64]. The FIC index is defined by (Eq. 1):

$$\sum FIC = \frac{MIC_{A,B}}{MIC_A} + \frac{MIC_{B,A}}{MIC_B} \quad (\text{Eq. 1})$$

where the minimum inhibitory concentration, *MIC*, of drug *A* in combination is divided by the *MIC* of the drug alone resulting in the FIC of drug *A* (*FIC<sub>A</sub>*) and added to the *FIC<sub>B</sub>* of the second drug in a two drug system. In practice, the FIC is measured with a checkerboard dilution assay of the two selected drugs to measure the inhibitory activity of antibacterial and antibiotic drugs. Then the inhibitory activity is measured with a variety of methods including visual, spectrophotometric, and colorimetric assay from which the *MIC* is determined as the minimum drug concentration of a single drug necessary to inhibit bacterial growth [62].

Generally, synergy is defined for FIC values below 0.5 and values between 0.25 to 0.75 are regarded as weak synergistic. Additive interaction is considered between 0.5 – 4 and values over 4 are defined as antagonistic [62].

### 1.3.2. Interaction Index and Isobologram

The interaction index can also be used to describe the combined effects of two or more drugs with Eq. 2 [65]:

$$I = \frac{D_1}{ID_{X,1}} + \frac{D_2}{ID_{X,2}} \quad (\text{Eq. 2})$$

Where  $D_1$  and  $D_2$  are the concentrations of drug 1 and 2 delivered in combination and  $ID_{X,1}$  and  $ID_{X,2}$  are the drug concentrations that produce the same level of effect,  $X$ , when treated alone. Often it is described at 50% inhibition ( $X = 50\%$ ). The Hill equation (Eq. 3) describes the drug induced effect,  $E$ , measured experimentally and uses the 50% inhibition concentration.

$$E = E_{max} \times \frac{C^h}{IC_{50}^h + C^h} \quad (\text{Eq. 3})$$

Where  $E_{max}$  is the maximum drug effect (near 100%),  $C$  is the drug concentration, and  $h$  is the Hill coefficient that describes the shape of the concentration-effect relationship [60].

When the interaction index is equal to 1, there is no drug interaction. An interaction index below 1 indicates the two drugs are synergistic but when the value is greater than 1 the drugs are antagonistic. This concept is widely represented with an isobologram (**Figure 3A**), which represents the interaction of two drugs [66]. When there is no interaction between the drugs, the activity level is independent of the drug concentration. The isobologram is typically used at 50% inhibition (IC-50) effects and the line connecting the activity of the individual drugs defines zero drug interaction. When the 50% inhibition of the two drugs is below this line, the drugs are displaying synergism and if the concentrations are above the line of additivity, then the drug interaction is antagonistic [60]. The

isobologram is often used as a method for defining drug combination synergy, as it is a simple analysis technique.

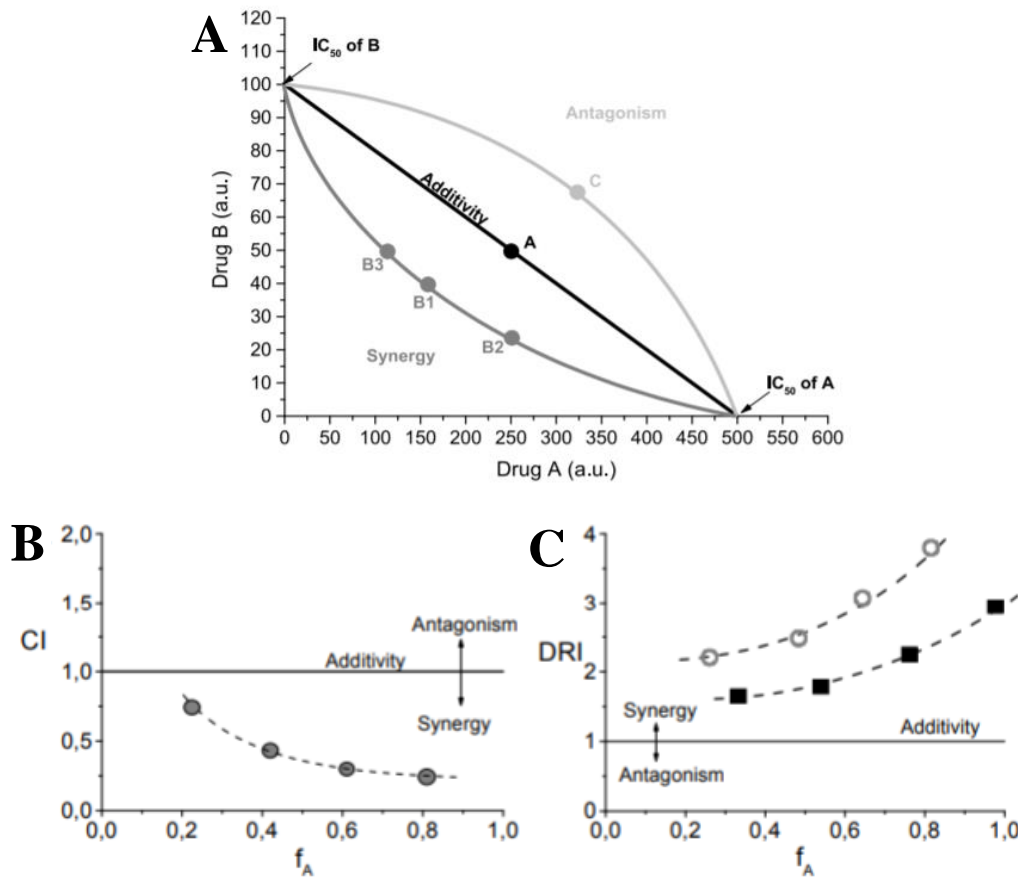


**Figure 3.** (A) Isobologram with concentrations of drug A and B on the X and Y axis. The line between the IC-50 of drug A and B is the additivity effect of the drug combination. Below the line of additivity is synergy and above is antagonism. (B) and (C) are other visual representations of drug interaction. (B) is a plot of the combination index (CI) versus fraction affected ( $f_A$ ) and (C) dose reduction (DRI) index plotted against the fraction affected ( $f_A$ ). Figure reprinted from [60], Copyright © 2012 Breitingner. Licensee IntechOpen.

### 1.3.3. Median Effect Analysis

The median effect analysis (Eq. 4) was derived by Chou et al. [67,68]:

$$\left(\frac{d}{M}\right)^n = \frac{E_d}{1 - E_d} \quad (\text{Eq. 4})$$

Where  $d$  is the drug dose,  $E_d$  is the effect of the drug, and  $M$  is the dose that causes 50% effect or 50% cytotoxicity in the case of chemotherapy which is also defined as the half-maximal inhibitory concentration, IC-50. The  $n$  is the constant from the slope of the dose-response curve. This equation

can be used to understand the interaction between the drug dosage and response. The median effect analysis equation was used as the basis for developing the combination index and dose response index.

#### 1.3.4. Combination Index and Dose Response Index

The median effect analysis and interaction index equations were extended to define the combination index (CI) to describe interaction of multiple drugs and the type of interaction between the drugs [69]. The combination index for multiple drug is defined by Eq. 5:

$$CI = \sum_{j=1}^n \frac{(D)_j}{(ID_X)_j} \quad (\text{Eq. 5})$$

Where  $n$  is the number of drugs in the combination. When the CI is equal to 1 the effect is additive. When the CI is less than 1 the effect is synergistic and when it is above 1 the effect is antagonistic (**Figure 3B**). Furthermore, in the cases of synergistic interaction the dose reduction index (DRI) has been introduced to determine the reduced dose of the drugs necessary to achieve the same effect (Eq. 6) [60].

$$CI = \frac{1}{(DRI)_1} + \frac{1}{(DRI)_2} \quad (\text{Eq. 6})$$

The DRI is defined by Eq. 7.

$$DRI_j = \frac{(ID_X)_j}{(D)_j} \quad (\text{Eq. 7})$$

The DRI is typically plotted against the fraction affected ( $f_a$ ) and described by a Chou-Martin plot (**Figure 3C**) [60]. It should be noted that the concentrations or effect level that are investigated can produce different results for drug interaction and some areas of the dose-response curve of the combination therapy could be further away from the point of single drug treatment, which could result in misinterpretation [70,71]. Furthermore, drug combinations can be biphasic, meaning that the dose-response curve is non-linear and there can be a concentration range in which the drugs are synergistic or antagonistic [60,70].



Additionally, the effect of drug combinations can be unequal for the drugs used. When one or both the drugs have no effect individually but the combination does not affect the outcome it is termed inertism. In the case when the two drugs do not produce an effect individually but in combination they are synergetic, it is termed as coalism [60,72]. In the case of three or more drugs and varying schedules of delivery, determining synergistic interaction can be more complex [60]. In practice, combination index and dose response index are the two most common approaches for defining the synergistic activity of anticancer drugs.

### 1.3.5. Other Models of Drug Interaction

There are several other methods that help describe drug interaction. The Bliss independence model is based on the additivity of probability theory and defined by Eq. 8 when two drugs have no interaction.

$$Y_{ab,P} = Y_a + Y_b - Y_a Y_b \quad (\text{Eq. 8})$$

Where  $Y_a$  and  $Y_b$  are the percent inhibition of drugs  $a$  and  $b$  and  $Y_{ab,P}$  is the percent inhibition of the drug combination [73]. However this model can only be applied to systems with linear drug concentration-inhibition relationships [60].

The Loewe additivity model also describes drug interaction defined by Eq. 9. This model assumes that a drug cannot interact with itself. The Loewe additivity model is used in cases where the drug concentration-inhibition relationship is nonlinear and includes the isobologram [60].

$$\sum_{j=1}^n \frac{x_j}{X_j} \quad (\text{Eq. 9})$$

Where  $x_j$  is defined as the dose of compound  $j$  in combinations that produces an effect,  $y$ . The dose of individual treatment with compound  $j$  that produces the same effect,  $y$ , is represented as  $X_j$ . When the value is less than 1 indicates synergism and greater than 1 indicates antagonism [74].

Drugs can produce a synergistic effect by having one biological target or affect multiple pathways. However, the interaction of drugs can produce an agnostic effect by interfering with their metabolism which could affect the clearance, drug absorption, and tissue distribution of the drugs. Generally, these chemotherapy drugs affect a multitude of pathways and biochemical processes, therefore synergy can be difficult to quantify [60]. The Loewe additivity method is used more over compared to the Bliss Independence model, because the Loewe model takes into account similar mechanisms of action of the two compounds while the Bliss Independence assumes independent mechanisms of action [75]. Overall, characterizing synergy of drug combinations can be a useful tool for screening drugs and predicting the clinical response. There are many different models for determining drug synergy with different assumptions of the drug interaction and most often the isobologram, combination index, and Loewe additivity model are used because they are based on measuring the dose for a certain inhibitory effect.

#### **1.4. Sequence-Dependent Synergy of Free Chemotherapeutic Drugs**

Historically, ovarian cancer has been treated with free drug formulations. Following the development of Taxol, there was a shift to combination therapy of paclitaxel with cisplatin or carboplatin [76–79]. Combination therapy provided several advantages including reducing the toxicity of the drug dose, inhibiting cancer activity with multiple molecular targets, and limiting the development of or overcoming drug resistance mechanisms [79,80]. Combination therapy has also been extended to sequential delivery of free drugs as a method for coordinating the activation of anticancer pathways to optimize drug efficacy. Free drug combinations and sequential drug delivery of small molecules paired with platinum or taxane drugs are discussed in this section as these two agents are most common in chemotherapeutic treatment of ovarian cancer but are also associated with high prevalence of resistance mechanisms.

#### *1.4.1. Platinum Agents with Taxane*

Platinum and taxane combination regimens are often examined because both agents induce cell cycle-dependent effects. Cell cycle arrest at specific phases with sequential delivery could play an important role in the cell cycle arrest leading to cancer cell death [13]. The interaction of these drugs has been examined with various treatment schedules on ovarian cancer models to determine whether the combination provides a synergistic effect.

Sequential delivery of cisplatin with taxane agents has been evaluated on both platinum-resistant and -sensitive cells with cell-dependent outcomes [81,82]. A study by Judson et al. investigated combination of cisplatin with paclitaxel in platinum-resistant and -sensitive cell lines (A2780, A2780CP, 2008, C-13, SKOV-3, OVC 420, OVCA 429, OC-194, OC-494). Paclitaxel alone was found to induce apoptosis in both cisplatin-resistant and -sensitive cell lines; however, the addition of cisplatin inhibited paclitaxel-induced apoptosis in cisplatin-resistant cells. Similar effects were also observed when the drugs were sequentially administered with paclitaxel followed by cisplatin. As cisplatin did not inhibit stabilization of the microtubules nor the expression of Bcl-2, the results suggest that cisplatin targets are downstream of the primarily targets of paclitaxel in cisplatin-resistant cells [83].

Another study on the sequential delivery of paclitaxel and cisplatin was done by Vanhoefer et al. on ovarian adenocarcinoma cells (EOVI and EVO2) from patients pretreated with platinum therapies. Vanhoefer et al. found that treating the cells with paclitaxel 24 hrs prior to cisplatin produced a synergistic effect determined via isobologram analysis. However, when the two drugs were administered simultaneously or in the reverse sequence, the treatment was antagonistic. Furthermore, the study found that pre-exposure to cisplatin resulted in long-lasting antagonistic effects (up to 72 hours post treatment) which could be attributed to a decrease in intracellular accumulation of paclitaxel

due to downregulation of glutathione (inhibiting cytotoxicity) and delaying cell phase transition from S-phase induced by cisplatin to G<sub>2</sub>/M phase induced by paclitaxel. The overall findings of the study found a schedule-dependent synergy of cisplatin plus paclitaxel (**Figure 4A and 4B**) [84].

Second generation platinum therapies have also been considered in combination with taxane drugs to determine the synergistic effect and an optimal sequencing schedule [85–87]. Several studies examined combination of either cisplatin or carboplatin with taxane drugs. Smith et al. evaluated the toxicity of taxane (docetaxel and paclitaxel) with either cisplatin or carboplatin on several human ovarian cancer cell lines (CAOV-3, OVCAR-3, SKOV-3, ES-2, OV-90, TOV-112D, and TOV-21G). Cisplatin was found to be more toxic compared to carboplatin in terms of cell growth inhibition with either doxorubicin or paclitaxel as is reported in other clinical studies [76–78].

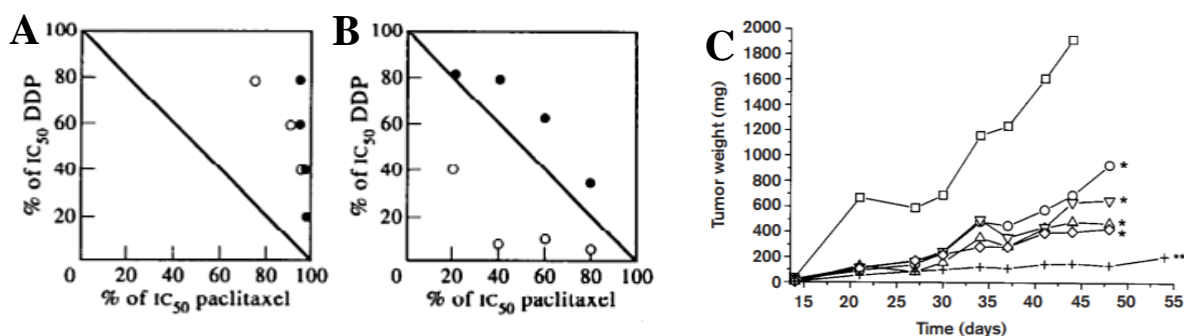


**Figure 4.** Isobolograms of sequentially delivered drugs to two human leukemia cells, HM2 cells (closed circles) and HM51 cells (open circles) with (A) cisplatin 24 hours prior to paclitaxel and (B) paclitaxel 24 hours prior to cisplatin. (C) Tumor weight after sequential delivery of paclitaxel and bleomycin with the lowest tumor weight observed with (+) bleomycin administer prior to paclitaxel. (A) and (B) Reprinted from [84], Copyright (1995), with permission from Elsevier. (C) Reprinted from [14], Copyright © 2001, © 2001 Lippincott Williams and permission from Wolters Kluwer.

The relatively high systemic toxicity of cisplatin led to a shift to carboplatin as well as other platinum therapeutics. Carboplatin plus paclitaxel treatment has been examined on ovarian cancer cell models. A study found that sequential treatment of carboplatin followed by paclitaxel produced a synergistic effect, while reverse sequence and simultaneous treatment produced an additive effect using isobologram analysis. Similar results were also observed in human lung cancer cells (NSCLC,

A549) [14]. Furthermore, another study investigated binary combinations of paclitaxel or colchicine, which like paclitaxel also inhibits tubulin polymerization, with cisplatin, oxaliplatin, YH12 (trans-PtCl<sub>2</sub>(ammino) {imidazo-(1,2- $\alpha$ )pyridine}) and TH1 [(trans-PtCl(NH<sub>3</sub>)<sub>2</sub>)<sub>2</sub> {trans-Pt(3-hydroxypyridine)<sub>2</sub>(H<sub>2</sub>N(CH<sub>2</sub>)<sub>6</sub>NH<sub>2</sub>)<sub>2</sub>}Cl<sub>4</sub>) in different sequences of treatment. Two cells were tested, A2780 and platinum-resistant, A2780CisR and the synergy was evaluated with the combination index. A sequence-dependent synergistic effect was observed. The greatest synergy was observed when paclitaxel or colchicine were administered first followed by the platinum agent 4 hours later. This combination produced a weaker synergistic effect in platinum-resistant cells compared to the A2780 cells. The strongest synergy was observed in both cell lines when they were treated with cisplatin with either paclitaxel or colchicine. However, when the combinations were delivered simultaneously or with pre-treatment of platinum therapy (4 hrs or 24 hrs prior) produced an antagonistic effect in both cisplatin-resistant and -sensitive cell types [18].

Other platinum therapeutic agents such as ZD0473 also been considered. A study investigated the effects on a new generation platinum agent, ZD0473, in combination with paclitaxel *in vitro*. Four different human ovarian carcinoma cells (A2780, A2780CisR, CH1, A2780E6) were examined with and without platinum resistance. In all four cell lines, simultaneous treatment with ZD0473 and paclitaxel produced a synergistic effect as defined by the median effect analysis. Furthermore, ZD0473 administered 24 hrs before paclitaxel produced a synergistic growth inhibitory effect compared to the reverse sequence in 3 of 4 cell lines, with the exception being A2780E6 cells that have inactivated p53 [88]. Interestingly, these results are in contrast to studies with cisplatin and paclitaxel combinations, which showed that paclitaxel delivery prior to cisplatin, produces a synergetic interaction [81,82,84,88].

Overall, there was a sequence dependent synergetic effect of platinum and taxane combination therapies. In the cases when cisplatin was administered, a synergistic effect was observed when the

taxane was administered prior to cisplatin. This was particularly evident in cells with platinum-resistance due to cisplatin treatment. However, with other platinum therapeutic agents, the reverse sequence, platinum followed by taxane, or simultaneous treatment, produced synergism, independent of platinum resistance.

#### 1.4.2. *Platinum Agents with Protein Targeted Inhibitory Drugs*

Inhibitory agents have also been explored for overcoming drug-resistance mechanisms, proliferation or antiapoptotic genes that are expressed by the ovarian cancer cells. These agents include tyrosine kinase inhibitors, Wnt/ $\beta$ -catenin, PARP, Akt, PI3K inhibitors, and histone deacetylase inhibitors [89–95].

Platinum therapies have also been explored in sequential combination with these inhibitory agents with synergistic drug interaction [96,97]. A proteasome inhibitor, bortezomib, was studied in combination with carboplatin, oxaliplatin, or *trans*-bis(3-hydroxypyridine)dichloroplatinum(II) (CH1) on ovarian cancer cells that are platinum-sensitive (A2780 and SKOV-3) and -resistant (A2780CisR and A2780\_ZD0473R). The results found that bortezomib enhances intracellular accumulation of the platinum therapies thereby increasing drug efficacy due to inhibition of platinum-induced down-regulation of copper transporter 1 (CTR1). In the sequence of platinum agent followed by bortezomib was antagonistic in platinum-resistant cells, while for platinum-sensitive cells the sequences did not have a significant impact on drug synergy [96]. The difference in the cell response to the sequential treatment can be attributed to a difference in drug resistance mechanism, i.e. difference in protein recognition and processing of the cells as well as p53 expression. Furthermore, these results provide evidence that chemotherapeutic agents can be paired with drugs that target overexpressed genes for cell specific therapy.

### 1.4.3. Platinum Agents with Other Small Molecule Drugs

Platinum combination therapies have been also explored with a variety of other therapeutic agents as methods to overcome drug resistance and improve drug efficacy. Gemcitabine, vinorelbine, topotecan, and doxorubicin are common chemotherapeutic agents that have been considered in combination with platinum agents [37,88,98–100]. A study examined the effect of administrating ZD0473 with gemcitabine, vinorelbine, topotecan, or doxorubicin using four different human ovarian carcinoma cell lines (A2780, A2780CisR, CH1, A2780E6). The study found a synergistic effect with ZD0473 was combined with topotecan in 3 of 4 cells lines where an antagonistic effect was observed in wild-type p53 A2780 cells. The results for ZD0473 in combination with vinorelbine only produced a synergistic effect in 1 of 4 cells lines. In all 4 cell lines, ZD0473 with doxorubicin resulted in no drug interaction or an antagonistic effect [88]. The difference in the cell response to the drug combinations can be attributed to a difference in drug resistance mechanism, difference in protein recognition and processing of the cells, and p53 expression.

Small molecules including supplements have also shown promising results in combination with chemotherapeutic agents [18]. Yunos et al. examined binary combination of cisplatin (Cis) with either curcumin (Cur), and epigallocatechin-3-gallate (EGCG), supplements (phytochemicals) from plants due to their antioxidant properties, on a A2780 cell line and cisplatin-resistant, A2780CisR cell line. The study examined simultaneous delivery and sequential delivery as well as timing of sequential delivery (at 4 hours or 24 hours). Treating the cells with cisplatin 4 hours before curcumin and EGCG produced the highest synergistic effect; therefore, lower concentrations delivered in a short time period produced the highest cytotoxicity. Curcumin targets pro-apoptotic proteins: p53, BAX, NF-kB, p38, and MAPK. Delivery of cisplatin increases ROS therefore the addition of curcumin or EGCG after cisplatin act to protect the DNA by scavenging free radicals, which results in more platinum-DNA binding compared to the less favorable platinum-thiol binding (**Figure 5**) [18].

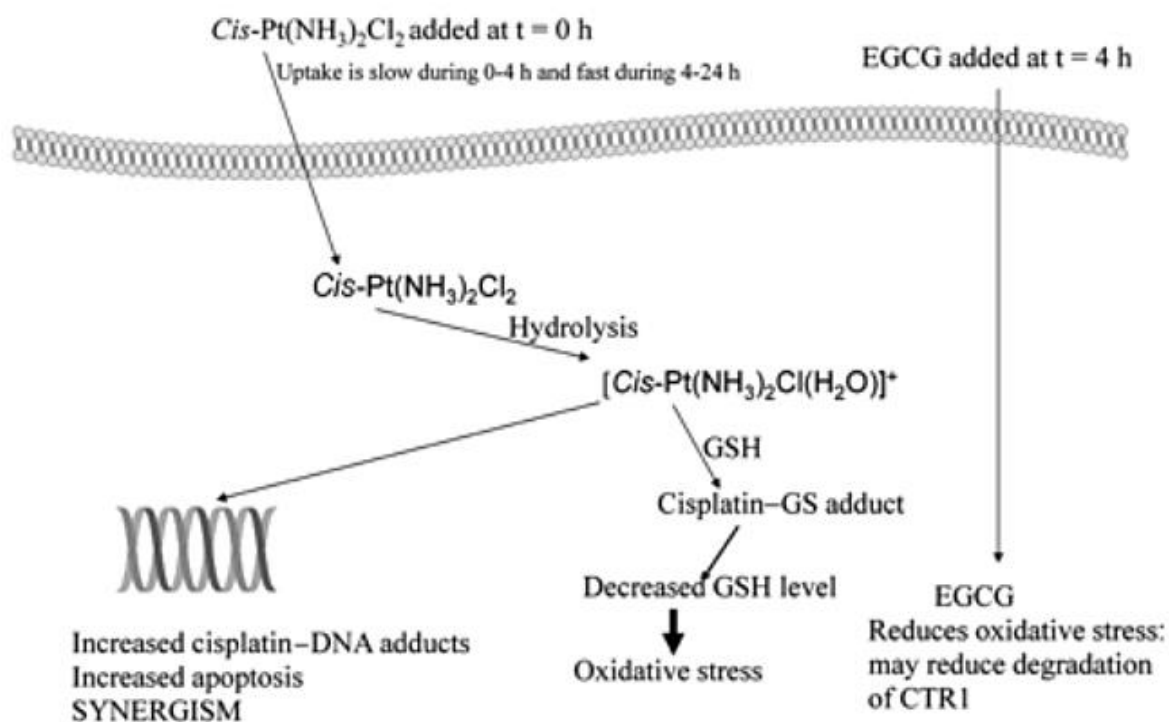


**Figure 5.** Representative image of cascade pathway activated by sequential co-delivery of cisplatin and EGCG. Reprinted from [18], Copyright © 2020 by The International Institute of Anticancer Research.

Platinum therapy has also been examined in combination with arsenic trioxide (ATO), a drug that inhibits growth and induces apoptosis, on suspended and adherent ovarian cancer cells (COC1, A2780, IGROV-1, SKOV-3, and R182). Using Chou-Talalay analysis and the dose-reduction index (DRI), found that the combination of cisplatin plus ATO produced a weakly synergistic interaction in suspended ovarian cancer cells (COC1) and a stronger synergistic interaction in adherent cells that were both platinum-sensitive and -resistant and a DRI from 1.2- to 13.5-fold [101].

Overall, sequential therapy of platinum therapies with various small molecule drugs such as chemotherapeutic agents and antioxidants have shown sequence dependent synergistic activity. Selecting the appropriate sequence is also dependent on the drug combination. Considerations include the relation of the drug targets to the downstream pathway of platinum therapies or if it is being applied



as a counter measure to the negative effects of platinum therapy such as upregulation of pro-cancer proliferating pathways or formation of free radicals.

#### *1.4.4. Taxane Agents with Protein Targeted Inhibitory Drugs*

Other than platinum therapies, taxane agents such as paclitaxel are one of the most widely used anticancer drugs for treating ovarian cancer [102–104]. Paclitaxel targets microtubules in the cell and inhibits polymerization necessary for mitosis leading to cell death [105–107]. The limitations of paclitaxel efficacy are either through acquired or inherent mechanisms of drug resistance and high systemic toxicity. Therefore, paclitaxel is often paired with other agents to improve therapeutic efficacy and patient outcomes [108–114]. One class of drugs is those that target specific proteins to inhibit pro-tumorigenic cell function such as epidermal growth factor receptor (EGFR) inhibitors and histone deacetylase inhibitors among others [111–117]. In this section, we will discuss drug combinations of paclitaxel with protein inhibitor drugs.

Epidermal growth factor receptors are membrane-bound proteins that play a role in signal transduction of critical pathways including proliferation and pro-survival. In cancer, EGFR is often overexpressed or there is an increase in the activation of downstream pathways of EGFR that promote tumor growth. EGFR activity can be targeted with EGFR inhibitors including small molecule drugs such as tyrosine kinase inhibitors and monoclonal antibodies (mAb) [118–122]. An example of these is HB-EGF inhibitor which is a membrane surface EGFR ligand and is involved in MAPK signaling and activation of ERK and Akt. HB-EGF expression is also associated with paclitaxel drug resistance due to activation of anti-apoptotic signaling.

Combination of paclitaxel and CRM197 (HB-EGF inhibitor) was examined for synergistic interaction in treating SKOV-3 cells and SKOV-3 mouse models overexpressing HB-EGF with sequential treatment of CRM197 and paclitaxel. This study found that the combination of these drugs

has an inhibitory effect on cell proliferation and enhanced apoptosis by inhibiting ERK and Akt activation while activating p38 and JNK. The results showed a synergistic effect in both *in vitro* and *in vivo* models [115].

Similarly, other EGFR inhibitors (gefitinib, ZD674, cetuximab) were examined with either docetaxel or paclitaxel with sequential delivery method in esophageal cancer (KYSE30). A synergistic interaction was observed when the chemotherapeutic agent was administered followed by the EGFR inhibitor and an antagonistic interaction was observed in the reverse sequence. The difference in the outcome was attributed to the arrest of cells in the G<sub>2</sub>/M phase [19].

Another study investigated a Akt inhibitor (MK-2206), downstream of EGFR in combination with paclitaxel ovarian cancer cells [117]. The serine/threonine kinase Akt plays a prominent role in promoting cell survival and inhibiting apoptosis; therefore, inhibition of this protein is an important factor in promoting cytotoxicity of cancer therapies [123,124]. The combination treatment of MK-2206 and paclitaxel produced a synergistic interaction in ovarian cancer cells (SKOV-3 and NCI-N87 cells) due to suppression of both Akt and EGFR-2 signaling pathways *in vitro* and *in vivo*. Chemotherapeutic agents were also tested with MK-2206 on ovarian cancer cells (A2780) and a synergistic effect was observed with doxorubicin (topoisomerase inhibitor), camptothecin (topoisomerase inhibitor), gemcitabine (anti-metabolite), 5-FU (anti-metabolite), and carboplatin (DNA cross-linker) [117].

Histone deacetylase and histone acetyl transferases are commonly used as anticancer targets because of their role in gene transcription. By using inhibitors, we can arrest tumor growth and induce apoptosis [125–127]. A study by Modesitt and Parsons examined sequential treatment of vorinostat, a histone deacetylase inhibitor, with paclitaxel on three different cell types (SKOV-3, OVCAR-3, 2774) and a mouse model. The treatments evaluated were paclitaxel alone, vorinostat alone, vorinostat followed by paclitaxel, and paclitaxel followed by vorinostat, as well as simultaneous delivery. The

cell viability of SKOV-3 and OVCAR-3 cells was not significantly lowered by sequential treatment and overall, the combination treatment was not superior to individual drug treatment. The 2774 cells did show higher cytotoxicity when treated with paclitaxel followed by a low dose of vorinostat. The *in vivo* results did not show a difference between sequences of administration. HDAC inhibitors have a role in inducing differentiation, growth arrest, and promoting apoptosis by increasing expression of pro-apoptotic proteins while decreasing anti-apoptotic proteins (survivin). HDAC inhibitors also have a role in altering the expression of p21 which is involved with regulation of cell cycle thereby increasing cell cycle arrest. 2774 cells have a low expression of survivin and low p21 activity which could indicate they are more susceptible to combination treatment with vorinostat compare to the other cell types. The study concludes that the benefits of sequential and combination treatments are cell-dependent and tumor specific; therefore, the treatment needs to be tailored to specific ovarian cancer mutation to optimize therapeutic effects [116].

Cyclooxygenase (COX) inhibitors have also been examined for treating ovarian cancer in drug combinations. COX enzymes play a role in cell migration and tumorigenesis [128–130]. In a study by Li et al., two COX inhibitors, celecoxib and SC-560, two COX inhibitors, were examined alone and in combination with paclitaxel on SKOV-3 carcinoma cells xenografts. Alone, celecoxib and SC-560 significantly decreased tumor volume compared to the control group and the tumor volume was further decreased with the addition of paclitaxel. Interestingly, the results from treatment with celecoxib and SC-560 individually were very similar to two drug combinations with the COX inhibitor and Taxol. The greatest decrease in tumor volume, cyclin D1 expression, and cell proliferation were observed in three-drug combination of both COX inhibitors and paclitaxel. These results suggest that the COX inhibitor drugs decrease expression of cyclin D1 which can inhibit the cell cycle progression from G<sub>1</sub> to S phase, which could limit the efficacy of paclitaxel [131].

The results from studies combining paclitaxel with protein inhibitor drugs suggest that these combinations can improve drug efficacy. The synergistic drug interactions can also be enhanced with sequential delivery of the drugs, but selection of an appropriate drug pair is cell dependent. Sequence of delivery can be synergistic and considerations should include whether the proteins that are inhibited are independent or downstream of the pathway activated by paclitaxel, facilitate paclitaxel accumulation, or the enhance cell cycle arrest.

#### 1.4.5. Taxane Agents with Other Small Molecular Drugs

Other small molecule drugs have also been considered in combination treatments with paclitaxel. For example, drugs that have been used for years in treated cancer such as bleomycin are also being considered in sequential drug dosing. A study found that simultaneous treatment of paclitaxel and bleomycin, which halts cells in G<sub>2</sub> phase, produced a similar synergetic effect compared with sequential dosing of bleomycin followed by paclitaxel in HEY cell line. The results from the study suggest non-overlapping toxicities of the two therapies [14].

Along with traditional anticancer drugs, experimental drugs or existing drug not previously used for cancer treatment are also being considered for sequential drug delivery to improve efficacy of paclitaxel [132–134]. Zibotentan (ZD4054), an endothelin-1 and endothelin A receptor (ET<sub>A</sub>R) antagonist (overexpression of ET<sub>A</sub>R is associated with ovarian carcinomas) has been found to significantly inhibit cancer cell growth. ZD4054 has also been examined in combination with current standard of care therapies (platinum or taxane). Binary combinations with either cisplatinum or paclitaxel were found to significantly inhibit cell proliferation of HEY cells *in vitro*. The results were further improved with the co-treatment of all three drugs which inhibited proliferation *in vitro* and inhibited tumor growth and neovascularization *in vivo* (HEY xenograft). These results support the idea that drug combinations with different target mechanisms can produce synergism [132].

Sequential combinations of Taxol and flavopiridol were also examined on ovarian carcinoma by Song et al.. Flavopiridol is a first cyclin-dependent kinase inhibitor involved in cell cycle regulation. While Taxol and flavopiridol treatment alone on SKOV-3 cells was cytotoxic, sequential combinations resulted in further decrease in cell viability. Sequential delivery of Taxol (treated for 24hrs) followed by flavopiridol (for 24 hrs) produced the greatest synergistic effect with the greatest cell death and highest apoptotic rate *in vitro*. However, *in vivo* (SKOV-3 xenograft) the sequential combination was not synergistic [133].

Another category of drugs that have been examined are those that regulate cellular metabolism. These drugs have also been considered for sequential drug therapy to improve therapeutic efficacy with paclitaxel. Different sequences were evaluated for delivering PTX and 8-Chloro-adenosine 3',5'-Monophosphate (8-Cl-cAMP), an antimetabolite. The study examined two cell lines with different sensitivity to the drugs. Using the Chou-Talalay method, they examined the combination index (CI) at 20%, 50%, and 80% cell kill values while maintaining the same ratio between the two drugs. At 20% kill, paclitaxel followed by 8-Cl-cAMP had the highest CI values, at 50% kill, 8-Cl-cAMP followed by paclitaxel had highest CI for A2780 cells and opposite sequence for OAW42 cells, and at 80% cell kill 8-Cl-cAMP followed by paclitaxel had highest CI. Overall, paclitaxel treatment before 8-Cl-cAMP was the most effective method with highest synergy while 8-Cl-cAMP before paclitaxel had the lowest effectiveness for both cell lines compared to simultaneous treatment. These results suggest pre-exposure of paclitaxel produced greatest synergy (**Figure 6**). 8-Cl-cAMP, like paclitaxel, accumulates the cells in the G<sub>2</sub>-M phase of the cell cycle. Resistance to paclitaxel-induced apoptosis is dependent on activation of the Raf-1 kinase activity. 8-Cl-cAMP exposure inactivates Op18 which has a role in increasing tubulin polymerization thereby increasing the proportion of stabilized tubulin which can be exposed to paclitaxel [135].

Lonidamine (inhibits aerobic glycolysis) has also been used to treat ovarian cancer in combination with Taxol. Orlandi et al., treated A2780 cells with sequential combinations of lonidamine and Taxol and found that the efficacy of the treatment was sequence dependent. Synergy was observed when the cells were treated with Taxol prior to lonidamine while an antagonistic interaction was observed in the reverse sequence or simultaneous treatment. Lonidamine was determined to not modify the effects induced by Taxol (cell cycle arrest, tubulin polymerization, and apoptosis) and instead impacted the induction of the Bax protein as well as other targets [136].

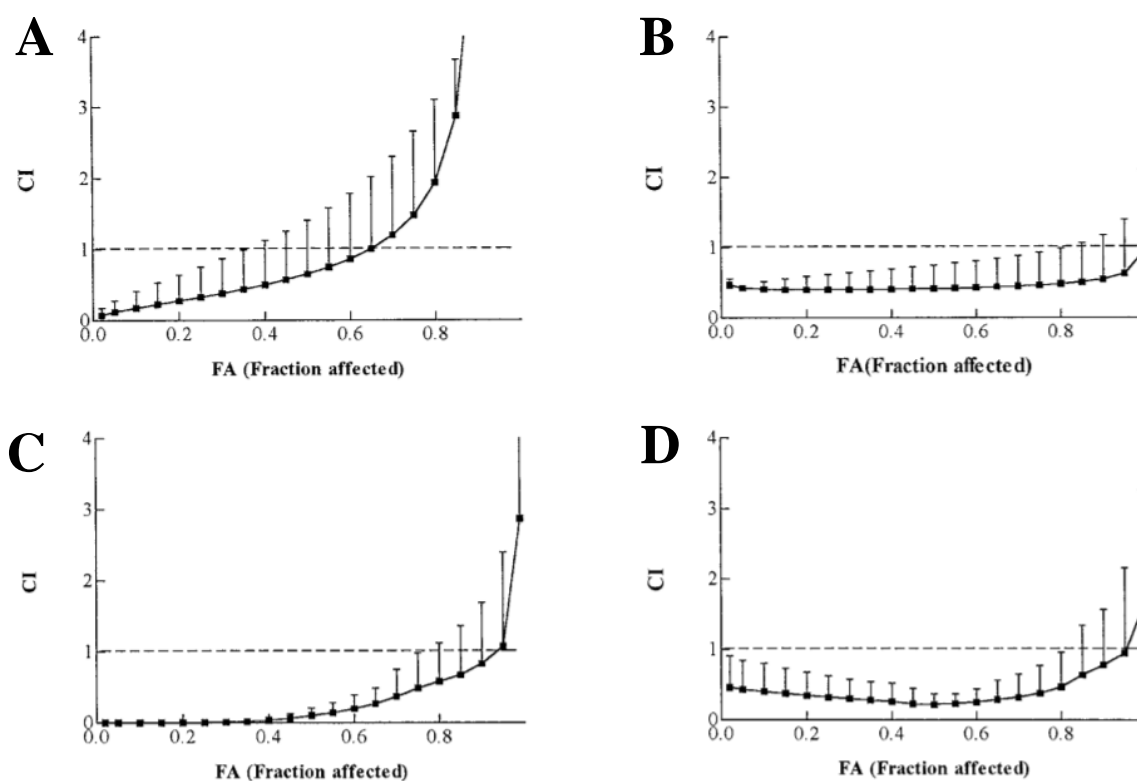


**Figure 6.** Combination index of cells (A) A2780 and (C) OAW42 cells treated with 8-CI-cAMP followed by paclitaxel and (B) A2780 and (D) OAW42 cells treated with the reverse sequence. Drug synergy is dependent on the drug ratio and sequence. Reprinted from [135] with permission from AACR.

Synergistic drug interactions have been observed between sequential delivery of paclitaxel and various small molecule drugs. Often synergy is dependent upon drug combination but it is also worth noting that in many cases, delivery of paclitaxel prior to the secondary drug agent enhances treatment

efficacy. These observations could be attributed to the regulatory pathways inhibited or activated by the drug combination leading to first cell cycle arrest and then inducing cell death.

## 1.5. Nanoparticle Drug Combinations

Studies and clinical practices with free drugs have shown the advantages of drug combinations for treating ovarian cancer, as previously discussed. However, there are many limitations of free drug formulations. The safety and efficacy of anticancer drugs are limited by their high systemic toxicity and poorly water-soluble. This leads to the challenge of balance delivering a safe dose while maintaining high enough bioavailability to target tissue for an efficacious dose. Furthermore, it is difficult to compare sequential treatment between pre-clinical and clinical studies due to a disparity between sequence cycles that is on the order of hours versus days. There is also limited control over the timing of drug delivery at the target sight with both techniques due to low targeting specificity. Filling the gap between drug delivery schedules conducted at the clinical setting compared to those done on the bench top also needs to be addressed in order to facilitate translational research.

Nanoparticles can address many of these challenges. Encapsulation of the drugs paired with controlled and sustained drug release can facilitate in minimizing toxicity and improving controls over the drug pharmacokinetics [137–139]. Furthermore, the nanoparticles can be designed for both passive and active targeting while mitigating immunogenicity with techniques such as PEGylation and increase control over sequential drug delivery at the target sight [140]. In this review, we will cover applications of polymer-based nanoparticles for simultaneous and sequential delivery of drug combinations. Detailed reviews of liposomal-based nanoparticles can be found here: [141,142]. There are many advantages of polymer-based nanoparticle vehicles over liposomes including greater payload of hydrophobic molecules which encompass the majority of anticancer drugs, size control, relatively

greater structural integrity and stability, greater control over particle design in terms of polymer selection, functional groups, and drug release kinetics.

### *1.5.1. Polymer Nanoparticles and Micelles*

Encapsulating chemotherapeutic agents into polymer micelles is one approach for improving drug efficacy and overcoming limitations such as drug solubility. Polymer micelles are often formulated with amphiphilic macromolecules that have a hydrophilic and hydrophobic block. The structure of the block co-polymers allows for assembly of a single layer micelle with a hydrophobic core and hydrophilic shell. The structure of the micelles is spherical although other morphologies such as rods and tubules have also been investigated [143–146]. Thorough reviews of micellar nanoparticles for chemotherapeutic treatment of cancer can be found elsewhere [147–149].

The formulation of polymeric micelles leverages the self-assembly nature of the amphiphilic polymer structures. Some of the self-assembly formulation methods include ultrasonication, thin-film dispersion, and Flash NanoPrecipitation (FNP) [147–150]. Based on the polymer selection, the surface chemistry, degradation rate, and size of the nanoparticles can be tuned. Drugs can be loaded into micelles by either precipitating the drugs into the hydrophobic core or conjugating the drugs to the polymers. The advantages of polymer micelles as a carrier for chemotherapeutic agents are high drug loading, sustained drug release, and the micelles can be tailored for responsive drug release [147–150]. In this review, we will focus on nanoparticles encapsulating platinum and taxane agents in combination with small molecules drugs for the treatment of ovarian cancer.

#### *1.5.1.1. Combination Drug Delivery with Platinum Drug Agents*

Core-shell polymer nanoparticles have also been investigated to deliver platinum-based agents for ovarian cancer treatment. For example, core-shell coordinated polymer nanoparticles formulated



with a 1,2-dioleoyl-*sn*-glycero-3-phosphate (DOPA) core and DSPE-PEG shell co-encapsulated carboplatin and gemcitabine monophosphate. These nanoparticles were used to treat platinum-resistant cells (A2780/CDPP) *in vitro*. A synergetic interaction was observed in platinum-resistant cells. The advantages of delivering carboplatin and gemcitabine in nanoparticle formulation were extending blood circulation times, increasing drug uptake by 5-fold, and reducing tumor weight 12-fold compared to free drug combination of platinum-resistant xenografts [151]. Polymer micelle carriers have also been used in delivery of oxoplatin with curcumin. A triblock copolymer was utilized to formulate the nanoparticles with oxoplatin conjugated to the amine-bearing polymer and curcumin encapsulated into the core via self-assembly. The co-administration of curcumin and oxoplatin on A2780 cells resulted in slight synergistic interaction with free drugs (CI ~0.8). The two drugs were also administered in co-loaded micelles to A2780 cells and a strong synergistic interaction (CI ~0.3) was observed; however, two single-drug micelles produced a weaker synergistic interaction [152]. Gemcitabine has also been examined in nanoparticle combinations with doxorubicin. A study by Liu et al. determined that the doxorubicin/gemcitabine micelles improved the synergistic interaction and endocytosis of the drugs [153].

#### **1.5.1.2. Combination Drug Delivery with Taxane-based Agents**

With the therapeutic efficacy observed with free drug delivery of taxane-based drug combinations, a similar approach has also been applied to polymer nanoparticle drug delivery. In a study by Devalapally et al., poly(ethylene oxide) modified poly(epsilon-caprolactone) (PEO-PCL) nanoparticles were co-encapsulated with tamoxifen (estrogen receptor modulator) and paclitaxel to enhance drug efficacy in MDR ovarian cancer. The synergy of the drug combination was examined *in vitro* on wild-type (SKOV-3) and MDR positive cells (SKOV-3<sub>TR</sub>) as well as xenografts of the two cell lines. Co-administering paclitaxel (20mg/kg) and tamoxifen (70mg/kg) in PEO-PCL nanoparticles

reduced the IC-50 of paclitaxel by 10-fold in SKOV-3 cells, and 2-fold in SKOV-3<sub>TR</sub> and effectively suppressed tumor growth in drug-sensitive and -resistant models with low systemic toxicity. These results suggest that administering tamoxifen enhances the cytotoxicity of paclitaxel to aid in overcoming drug resistance [154].

Protein specific inhibitors have also been co-encapsulated with paclitaxel in polymer nanoparticles [155,156]. Katragadda et al., examined combinations of paclitaxel with tanespimycin (17-AAG, antineoplastic antibiotic that inhibits cytosolic functions) in polymer micelles *in vivo*. The authors determined that the co-loaded (paclitaxel-17-AAG) in 1,2-Distearoyl-*sn*-glycero-3-phosphoethanolamine-*N*-[methoxy(polyethylene glycol)-2000] (PEG-DSPE) micelles increased tumor drug concentration by 3.5- and 1.7-fold and significantly arrested tumor growth compared to equivalent free drug combinations in ovarian tumor (SKOV-3) xenografts [156].

Three-drug combinations have also been examined with paclitaxel co-encapsulated with cyclopamine (hedgehog inhibitor) and gossypol (Bcl-2 inhibitor) in poly(ethylene glycol)-block-poly( $\epsilon$ -caprolactone) (PEG-b-PCL) micelles. Cyclopamine and gossypol loaded alone in the micelles exhibited minimal cytotoxic effects. *In vitro*, the 3-drug micelles did not exhibit significantly more potency compared to paclitaxel micelles in 2D cell model (SKOV-3 and ES-2). However, in 3D ES-2 model the treatment results in disaggregation of the spheroid, possibly due to multiple mechanisms including inhibition of Hedgehog signaling by cyclopamine aiding in reversing taxane resistance. *In vivo*, the 3-drug micelles significantly reduced tumor volume and extended survival time compared to paclitaxel micelles alone [155].

Drugs that affect the metabolic activity of cancer cells are also an important class of drugs that have been considered with paclitaxel in both free drug and nanoparticle formulations. Lonidamine was co-administer with paclitaxel in EGFR-targeted PCL nanoparticles to facilitate in overcoming MDR. Co-delivery of paclitaxel and lonidamine in nanoparticles resulted in a greater reduction in cell

viability of MDR ovarian cells (SKOV-3<sub>TR</sub>, OVCAR-5) compared to the equivalent drug concentrations delivered in single-drug nanoparticles and free drug formulations. The results from the study suggest that lonidamine promotes mitochondrial binding of pro-apoptotic Bcl-2 proteins in combination with microtubule stabilization induced by paclitaxel which facilitates in overcoming MDR. The benefit of co-delivering these drugs in a EGFR-targeted nanoparticle platform allows for active targeting of EGFR that is overexpressed by MDR cells and sustained drug release on the order of several days enabling greater drug efficacy compared to free formulations (**Figure 7**) [157].

Alternative therapeutic agents have also been examined in nanoparticle formulations. Paclitaxel has often been paired with curcumin as a method for treating ovarian cancers [158–162]. While this approach is promising, nanoparticles formulations have encapsulated these drugs to improve drug efficacy. Boztas et al., encapsulated curcumin and paclitaxel in poly( $\beta$ -cyclodextrin triazine) (PCDT) nanoparticles via complexation to the polymer. Interestingly, delivering curcumin nanoparticles significantly improved cytotoxicity compared to the free drug form but delivering paclitaxel nanoparticles did not affect the cytotoxicity. When both the curcumin and paclitaxel nanoparticles were co-delivered, a synergistic effect was observed *in vitro* on A2780 and SKOV-3 cells compared to co-delivery of the free formulation that did not display a synergistic interaction. Additionally, the co-delivery of two particles resulted in significantly higher cell death. The benefits of this particle platform are the improved drug solubility and bioavailability [158]. Tacrolimus (FK506) has previously been prescribed as an immunosuppressive drug for organ transplant and has also now been also examined for treating ovarian cancer. Tacrolimus was co-encapsulated with paclitaxel in polymer micelles (poly(ethylene glycol)- poly( $\epsilon$ - caprolactone) (MPEG-PCL)) to overcome MDR. The advantages of this nanoparticle platform is that it is a one-step solid dispersion method that does not require organic solvents and high drug loading. When the nanoparticles were examined *in vitro*, the co-loaded nanoparticle exhibited greater cytotoxicity effect in MDR cells

(A2780/T) compared to paclitaxel-sensitive cells (A2780). Furthermore, co-delivering paclitaxel and FK506 in the micelles increased the intracellular paclitaxel concentration, G<sub>2</sub>/M arrest, and greater apoptosis of drug-resistant cells compared to drug-sensitive cells or micelles encapsulating only paclitaxel [163].

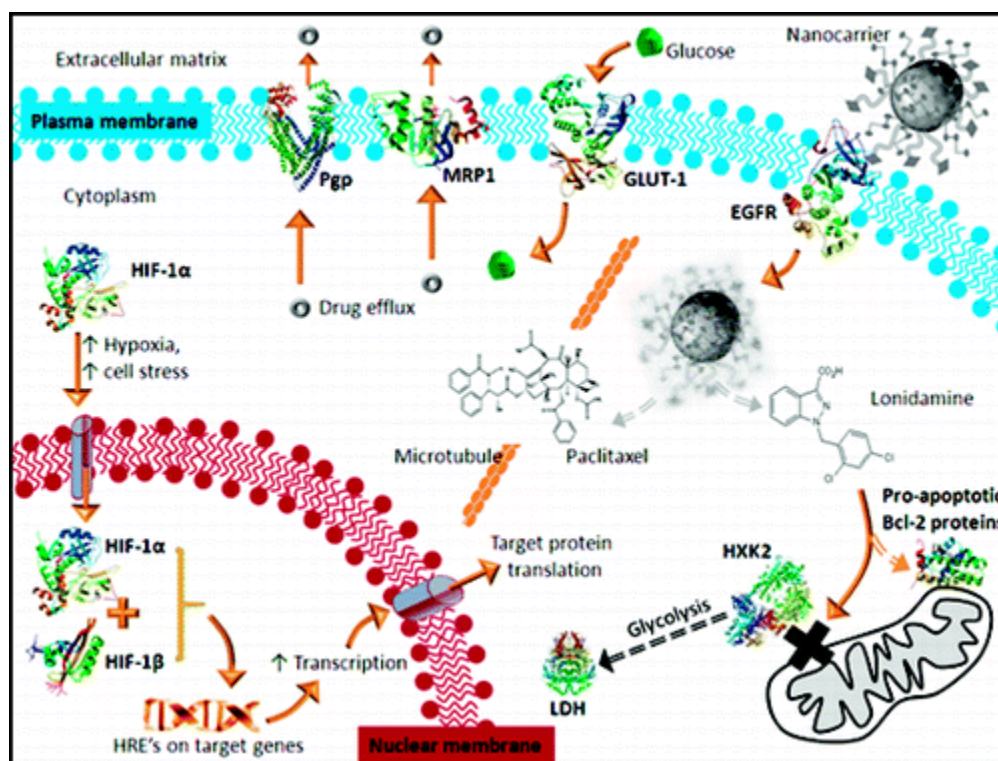


**Figure 7.** Diagram of nanoparticle endocytosis and delivery of drug combinations. Delivery of drug combinations targets multiple proteins and results in activation of multiple cascade pathways to induce cell death. Reprinted (adapted) with permission from [157]. Copyright (2011) American Chemical Society.

### 1.5.2. Dendrimers

Dendrimers are another type of polymer nanoparticles with hyper-branched structures. Dendrimers are comprised of multiple branches of long polymer strands with each branch referred to as a generation. The structure allows for tailoring of the branches and chemical composition to tune the size, hydrophobicity, surface charge, drug encapsulation, and targeting. Drugs can either be loaded in dendrimers by covalently conjugating to the polymer branches or entrapped in the dendrimer core cavities by electrostatic or hydrophobic interaction. Applications and formulations of dendrimers can be found elsewhere [164–166].

Dendrimers have also been investigated as vehicles for co-delivery of anticancer drugs. Platinum drugs such as cisplatin have been examined in co-loaded dendrimers to improve drug efficacy. Cisplatin was co-loaded with paclitaxel in three layer linear dendritic telodendrimer micelles. The telodendrimer was formulated by complexing cisplatin to the carboxylic acid groups between adjacent branches and conjugating paclitaxel to the interior layer. Paclitaxel exhibited fast release while cisplatin exhibited relatively slower release. *In vitro* study on SKOV-3, ES-2, and Hela cells and found that at a ratio of 2:1 cisplatin to paclitaxel was synergistic for all cells types. With a xenograft model, the co-loaded nanoparticles had the highest accumulation in the tumor tissue, decreased tumor volume, and increased survival time, which suggests increased drug efficacy and reduced renal toxicity of co-loaded nanoparticles. Encapsulation into nanoparticles could increase PTX bioavailability to tumor tissue while delivering slow dosage of cisplatin to improve overall efficacy [167].

In another example, Guo et al., cisplatin and doxorubicin were co-delivered using fourth-generation polyamidoamine dendrimers (HA@PAMAM-PT-Dox). The dendrimers were modified with hyaluronic acid (HA) and the drugs were covalently conjugating to the fourth generation of the dendrimer. The cytotoxic activity of the dendrimer was examined *in vitro* with a breast cancer cell model (MCF-7 and MDA-MB-231) and found that the HA@PAMAM-PT-Dox nanoparticles induced greater reduction in cell viability at lower concentrations and synergistic activity compared to both the dendrimers containing only cisplatin and the free drugs. The co-loaded dendrimers were also examined *in vivo* using MDA-MB-231 xenografts and determined that the HA@PAMAM-PT-Dox inhibited tumor growth as well as reduce the toxicity [168].

Dendrimers have also been examined for combination drug delivery of paclitaxel co-encapsulated with other anticancer drugs and have displayed synergistic activity. Zou et al., combined paclitaxel and borneol (P-gp inhibition effects) in PEG-PAMAM dendrimers via a one-step

precipitation method. The authors found that the P-gp inhibitory activity of borneol increased the intracellular paclitaxel concentration. Furthermore, the dendrimer drug combination exhibited higher cytotoxicity and apoptosis *in vitro* (A2780/PTX cells) as well as a significant decrease in tumor volume *in vivo* (A780/PTX bearing mice) compared with the free drug formulations [169].

Other drug combinations have also been considered in dendrimers for enhancing drug efficacy. Co-encapsulation of doxorubicin and bortezomib in telodendrimers have shown synergy *in vitro* (SKOV-3 and H929 cells) and improved anticancer activity *in vivo* (SKOV-3 xenograft). The nanoparticles were formulated by spatial separation of the two drugs, doxorubicin conjugated to the interior and bortezomib conjugated in the intermediate generations of the dendrimer. The nanoparticles displayed synergistic interaction at a wide range of drug ratios [170].

Another dendritic approach is using peptide dendrimers with added properties of enzyme-responsive drug delivery. For example, a tetra-peptide sequence (Gly-Phe-Leu-Gly) was utilized for responsive release of doxorubicin from PEGylated dendrimers to improve drug accumulation and antitumor activity [171]. Such approaches can be coordinated with multiple drugs for sequential drug release. Similarly, pH-responsive dendrimers have also been used for delivering drug combinations. A study synthesized a 5 generation EDA-PPI dendrimer with glycine-tBOC and folic acid-fMOC loaded with methotrexate and tretinoin with slight improvement in drug efficacy with co-encapsulation [172,173]. Synergistic or enhanced anti-cancer activity has also been found with a variety of dendrimer drug combinations in lung, breast, and brain tumors [174,175].

### 1.5.3. Lipid Nanoparticles

Lipid nanoparticles combine the advantages of liposomes and polymer micelles in that they are a single lipid layer with a hydrophobic core and hydrophilic outer shell. Lipid nanoparticles can be formulated with solid or liquid lipids, nanostructured lipid carriers and lipid drug conjugates. As

with micelles, the lipids can be modified for controlled release. There are various methods in which lipid nanoparticle can be prepared including high pressure homogenization, solvent emulsification- evaporation, or emulsions. Detailed reviews discussing formulation of lipid nanoparticles can be found elsewhere [176,177]

Lipid nanoparticles have also been examined for enhancing the drug efficacy and synergy of drug combinations. For example, a combination of paclitaxel and curcumin (downregulate ABC transporters) have been encapsulated in oil-in-water nanoemulsions with flaxseed oil prepared by high-energy ultrasonication. The paclitaxel and curcumin nanoemulsions were found to enhance the cytotoxic effect and increase apoptosis, however the drug combination was only slightly synergistic (CI = 0.93) in both drug-sensitive cells (SKOV-3) and additive effect in drug-resistant cells (SKOV-3<sub>TR</sub>) and similar effects were observed with free drug form [178].

Along with traditional lipid nanoparticles, lipid-polymer hybrid nanoparticles have also been examined for delivering drug combinations to overcome cancer resistance mechanisms. Zhang et al., examined encapsulating paclitaxel and tetrandrine (P-glycoprotein inhibitor) in iRGD peptide by conjugating paclitaxel to the polymer core and precipitating tetrandrine in the core creating a core-shell structure. The core-shell structure allowed for sequential release of the two drugs with release of tetrandrine prior to paclitaxel. The co-loaded nanoparticles increased the intracellular paclitaxel accumulation mediated by tetrandrine resulting in an increase apoptosis in A2780/PTX cells [179].

A similar lipid nanoparticle formulation has been applied to co-delivery of doxorubicin and triptolide (herbal extract with antitumor activity). Lipid-polymer hybrid nanoparticles were formulated with monomethoxy-poly(ethylene glycol)-*S-S*-hexadecyl (mPEG-*S-S*-C<sub>16</sub>), soybean lecithin, and poly(D,L-lactide-co-glycolide) (PLGA) and the drugs were loaded via self-assembly. This nanoparticle formulation allowed for reduction-sensitive simultaneous drug release. *In vitro* the co-loaded nanoparticles were synergistic over a wide range of concentrations with a 1:0.2 ratio of

doxorubicin and triptolide exhibiting the strongest synergy. Furthermore, *in vivo* co-loaded nanoparticles significantly decreased tumor volume even compared to two single-drug loaded nanoparticles indicating spatiotemporal effect [180].

Another unique formulation was created by Lee et al., in which they co-delivered doxorubicin and cisplatin in single polymer-caged nanobins. The nanobins were formulated by lipid-templated polymer platform with the doxorubicin encapsulated in the core and cisplatin conjugated to the polymer shell. The benefits of this nanoparticle platform are that the drug loading and surface chemistry is tunable, and they allow for sustained drug release on the order of several days. The nanoparticle drug combination displayed synergism in ovarian cancer cells (OVAR-3) as well as breast cancer cells compared to both free drug and single-drug nanobins resulting in enhancement of cytotoxicity of each drug [181]. Other formulations of drug combinations encapsulated in lipid-polymer nanoparticles have displayed synergistic activity such as doxorubicin with paclitaxel [182] and doxorubicin with indocyanine green [183] in other forms of cancer.

#### 1.5.4. Sequential Drug Delivery with Nanoparticles

Sequential combination therapy with free drug formulations has been shown to improve drug efficacy and overcome resistance mechanisms. A similar approach can be applied to nanoparticle drug formulations to further enhance drug efficacy [184–190]. However, few studies have examined sequential drug delivery with nanoparticle formulation of anticancer drugs in ovarian cancer. Previous studies have shown that the optimal drug delivery sequence is cell-specific; therefore a greater attention needs to be placed on the effects of sequential delivery with nanoparticles on ovarian cancer treatment.

With nanoparticle formulations, several sequential delivery methods can be applied such as combination of nanoparticles with free drugs, two single-drug loaded nanoparticles, or co-



encapsulation. The two former approaches can be easily modulated by controlling when the two drugs are delivered. The release of two drugs can be coordinated using various approaches such as coordinating diffusion rates with either drug hydrophobicity (prodrug approach) or selection of the core-shell [191,192]. Additionally, co-encapsulation provides the benefits of spatial and temporal control of multiple drugs [193].

For example, combinations of three drugs have also been co-encapsulated into PLA-b-PEG nanoparticles to facilitate with multiple target approach via controlled drug release. Three anticancer drugs: paclitaxel, 17-allylamino-17-demethoxygeldanamycin (17-AAG), and rapamycin, were encapsulated in the particle core. *In vitro*, the drug release rate was found to be dependent on the hydrophobicity of the drugs (17-AAG > PTX > RAP) and the 3-drug loaded nanoparticles were found to have strong synergistic interaction in breast cancer cells (**Figure 8**) [194,195].

There have been many applications of these techniques with single-drug nanoparticles; however, few studies have extended the approaches to co-encapsulated nanoparticles [196–198]. Stimuli-responsive drug release of drug combinations from nanoparticle is one such approach and reviews of stimuli-responsive nanoparticle platforms can be found in [192,199–204]. By utilizing stimuli-responsive platforms and controlled drug release, we can address the gap between pre-clinical and clinical studies in terms of drug delivery time-frame.

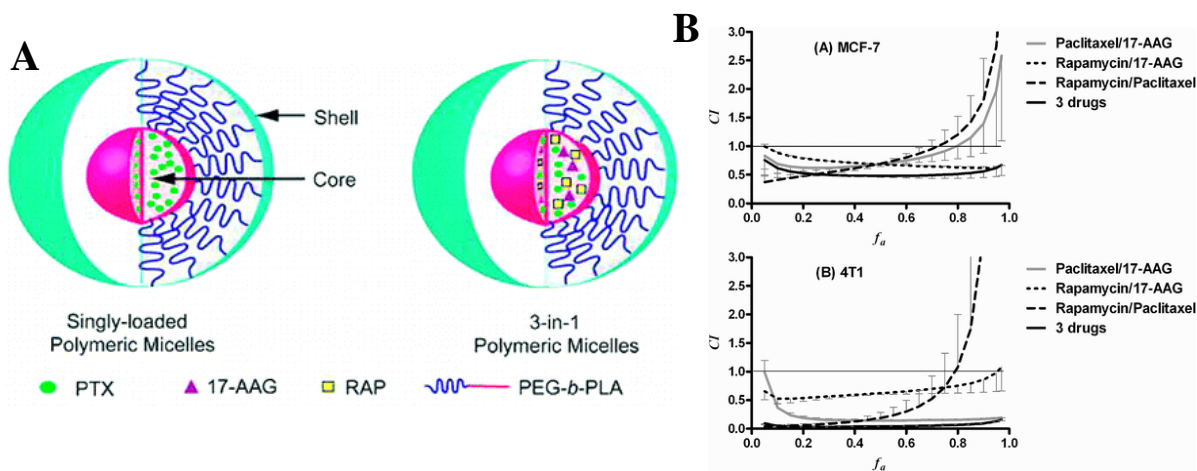


**Figure 8.** (A) Polymer nanoparticle loaded with three drugs for controlled release. RAP and 17-AAG are loaded in the core while paclitaxel is conjugated to the polymer shell. (B) Synergy is observed when all three drugs are co-delivered across the range of fraction affected. Reprinted (adapted) with permission from [194]. Copyright (2011) American Chemical Society.

## 1.6. Modeling Synergy of Drug Combinations

Conventional approach of dose-response quantification can be resource-intensive and does not provide a comprehensive understanding of complex biological systems and mechanisms of synergy. Furthermore, screening various drug combinations and treatment schedules for various types of cancers is very time-intensive. An alternative approach for further understanding the interaction of drug combinations is through systems biology modeling. This approach is based on protein interaction networks and drug activated cascades. Some studies have explored whether expression of key oncogenes can provide a guideline for determining synergistic drug combinations for treating ovarian cancer. For example, BRCA expression is found in over 50% of epithelial ovarian cancers therefore providing a screen for first-line therapies [205].

One method for predicting synergy of combinations is protein-protein interaction (PPI) network which is based on the functional associations of key proteins (activations/ inhibition) and drug targets to predict synergy. In these cases, synergy can be evaluated based on topology score and agent

score. The topology score is based on topology relationship between targets and drugs while agent score is based on the phenotype similarities of drugs [206]. The PPI network methods provide information about feedback structure and cascade pathways of drug targets (**Figure 9A**). A similar approach is dynamic pathway simulation which models the dynamic behavior of drugs and mechanisms of action. These models are based on concentrations and activity levels of various components such as genes, metabolites, and proteins and yields dose-response data by utilizing ordinary differential equations (**Figure 9B**).

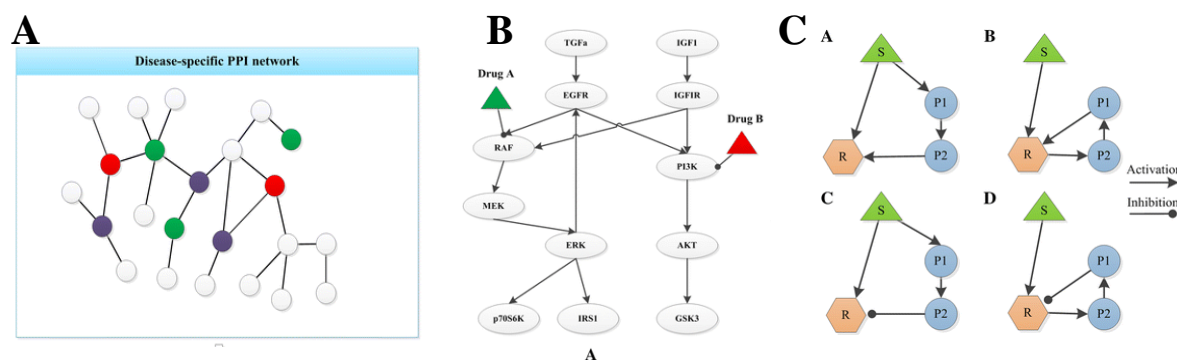


**Figure 9.** Diagrams of (A) PPI network modeling, (B) dynamic pathway modeling, and (C) examples of network motifs that facilitate in determining synergy of drug combinations. Reprinted from [206]. Copyright © 2015, Springer Nature.

PPI and dynamic pathway simulation provide an understanding of which interactions in the pathways can produce a synergism thereby providing the mechanism of action. However, the limitations of these models are that they are either complex or not all encompassing. Instead, network motifs can be used to describe the same number of events in distinct patterns, which can be used to distinguish which characteristic of the pathway produce synergistic activity (**Figure 9C**). Overall, with these models it can still be difficult to predict drug activity in disease-specific pathways as well as overlook drug behavior (absorption and metabolism) and secondary drug activating pathways.

Alternative methods include machine learning based methods [207,208]. Genomics, transcriptomics, and metabolomics have facilitated the development of these drug combination studies

[209,210]. Other consideration for formulating methods are side-effects and addressing those networks in the model. An example of these models is the Petri-net (EPN) model developed by Jin et al. [210]. Overall, there are different approaches that can be taken to understand the interactions and effects of drug combinations. However, due to the complexity of drug interactions and pathways, they can still be challenging to predict. A detailed description of drug combination modeling can be found in [206]. The benefit of this approach is that it provides an understanding of the mechanisms of clinically used therapies as well as predicting synergy of novel combinations [206].

Two examples of network models were developed by Pandey et al. and Jain et al. [211,212] Pandey et al., developed a mathematical model for sequential drug combinations in breast cancer with PI828, an inhibitor of P13K, and cis-platinum nanoparticles. The model explored the interaction of the drugs with three critical proteins: pAkt, XIAP, and caspase-3 and modeled as a feedback reaction loop. The phosphorylation of Akt activates a cascade pathway that activates XIAP which protects the cells from auto-ubiquitination and phosphorylates caspase-9 which is correlated to cell death. Activation of Caspase-3 induces a negative feedback on Akt by inhibiting its activity. The drug activity was modeled based on the assumption that cisplatin nanoparticles increase production of pAkt and caspase-3 and reduce the activity of XIAP and that PI828 inhibits phosphorylation of Akt via inhibition of PI3K. Each of the interactions was modeled by a system of equations to describe production, decay, inhibition, and drug effects of the three proteins. The drug release from the nanoparticles was also accounted for in the model by a biexponential release profile (**Figure 10**) [211]. The model predicted that initial administration of cis-platinum nanoparticles followed by PI828 24 hrs later produced the maximum drug efficacy compared to other sequence schedules (earlier or later than 24 hrs and reverse sequence) and validated with *in vitro* and *in vivo* experiments [211].

Jain et al. examined cancer cells that are resistant to carboplatin and paclitaxel treatment due to Bcl family of proteins and anti-apoptotic protein Bcl-xL. Jain et al. modeled the synergism of

sequential delivery of ABT-737 and carboplatin on ovarian cancer cells. The model suggests that delivering carboplatin followed by ABT-737 produced the highest synergy. It suggests that carboplatin treatment primes cells for ABT-737 by increasing cell dependence on BcL-xL for survival then treating the cells with ABT-737 decreases the activity of BcL-xL below the threshold of cell survival. The model can also be used to determine the minimal dosage necessary for effective treatment [212].

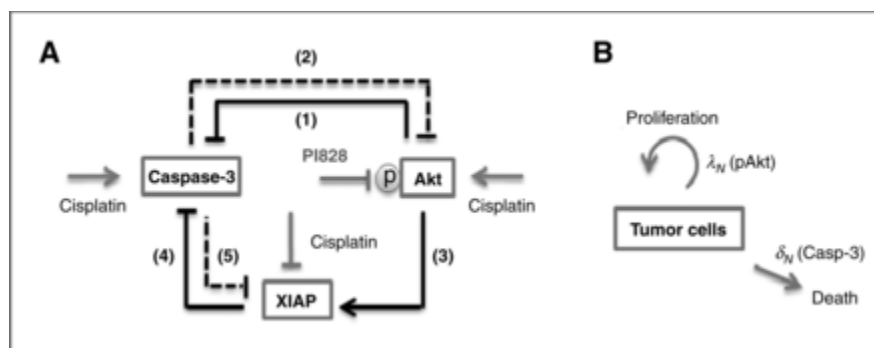


**Figure 10.** Simplified pathway cascade for modeling interaction of cisplatin and PI828. Reprinted (or adapted) from [211], with permission from AACR.

Cancer cells heterogeneity and microenvironments can also have an effect on the drug activity and drug resistance mechanisms [213–215]. Sun et al., developed a stochastic differential equations (SDEs) based model to address cell heterogeneity and adaptability to connect cellular mechanisms of drug resistance to population-level patient survival. This model was used to predict patterns in drug combination synergy. The study found a dose-dependent synergistic effect of co-treating BRAF and PI3K inhibitor compared to BRAF and MEK inhibitors due to different downstream targets of the two inhibitors and the results were confirmed with experimental data [216].

## 1.7. Conclusion

Combination chemotherapy can improve drug efficacy and lower systemic toxicity by targeting multiple pathways to induce cell death, lowering dosages, and overcoming drug resistance mechanisms. Sequential drug delivery has shown to improve the results of drug combinations due to synergistic drug interaction. Overall, drug synergy is highly dependent on cell type due to the

expression levels of key proteins involved either in drug resistance mechanisms or circumventing cell death. Due to the expression of these proteins, selecting appropriate drug combinations that will produce a synergistic or additive effect is an important consideration. Additionally, cells are sensitive to both the ratio of the drugs and to the sequence that they are delivered. This presents an immense challenge of selecting the optimal treatment for ovarian cancer due to the limitless number of combinations.

As a means to narrow in on a course of treatment, modeling the drug interaction with key proteins and gene expression is a vital tool. By first identifying the pathways and proteins involved in inhibiting cell death and promoting proliferation in ovarian cancer cells, models can be applied to determine both the appropriate drug combination as well as sequence of treatment. This can be particularly useful in more complex tumors with various types of cancer cells.

Furthermore, many *in vitro* or *in vivo* sequence schedules that optimize drug synergy are on the order of hours while in the clinic, chemotherapeutic treatment cycles are conducted over the course of a week. This difference in time scales can produce differences in therapeutic outcomes due to a difference in driving mechanisms of synergy. This makes translation of pre-clinical methods to clinical application very difficult due to patient and caregiver compliance. However, nanoparticle drug delivery can alleviate these practical challenges as well as overcome the disadvantages of free drug formulations. Nanoparticles can be designed for controlled and sustained release of drug combinations making them a great vehicle to decrease drug dosage and decrease systemic toxicity but increase bioavailability to improve patient outcomes. Nanoparticle drug delivery can also facilitate drug delivery on the order of hours to the target sight without the need for multiple injections from caregivers. Therefore, nanoparticles provide a natural transition from pre-clinical studies to therapeutic treatment of patients without compromising the drug efficacy of sequential drug delivery. However, delivery of drug combination in nanoparticles is still an emerging area of study and there has been a

limited number of studies investigating sequential drug release from nanoparticles. Therefore, future studies need to examine the synergistic interaction of sequential release from nanoparticles to treat ovarian cancer. These include examining sequential delivery of nanoparticle drug combinations for multiple ovarian cancer cell lines which can be done with multiple single-drug nanoparticles delivered at specific time points, then translating these results to designing controlled drug delivery from a single nanoparticle using approaches such as pH-labile drug release and prodrug formulations. The goal of future studies is designing sequential drug delivery of drug combinations from a single nanoparticle with an optimized sequence schedule.

## 2. Chapter 2: Project Overview

---

### 2.1. Overview

Ovarian cancer is one of the most prevalent forms of cancer in women with over 200,000 new cases each year [1,217–222]. Treating ovarian cancer is inherently challenging due to various genetic mutations, advanced stage diagnosis, and acquired drug resistance mechanisms with continual chemotherapy treatment [1–4,223]. Free drug treatment with chemotherapeutic agents also causes systemic toxicity with low bioavailability and control over drug delivery. Therefore, there is an urgent need to improve chemotherapeutic treatments without the need for formulating new drug agents.

This study focuses on improving drug efficacy of anticancer drugs and overcome challenges in drug resistance, poor drug solubility, and poor bioavailability. Nanoparticle drug delivery will be used to control drug delivery using a pH-labile platform, drug combinations, and a prodrug approach to modulate the drug properties. The advantage of nanoparticle drug delivery is that it can be used to increase drug solubility in the bloodstream as well as control the pharmacokinetics of the drug to minimize side effects and increase activity in target site. Polymer nanoparticles are formulated via Flash NanoPrecipitation which is a rapid and scalable method. Furthermore, by leveraging a pH-labile platform, the drug release can be tuned for sustained release in the bloodstream and rapid drug release upon cellular endocytosis when there is a change in environmental pH [204]. Drug combinations have also been found to improve the cytotoxicity of chemotherapeutic agents with multiple protein targets and pathways to cell death [18,96,224]. Therefore, co-encapsulation of multiple drugs are examined in this



study as a means to increase drug efficacy and synergy. Paclitaxel, a chemotherapeutic agent, and lapatinib, a tyrosine kinase inhibitor, are used as the model system. Lastly, prodrug formulation is investigated as a means to control the relative drug release of the drug combinations for sequential drug delivery to enhance drug efficacy. This approach will improve the understanding of nanoparticle formulation methods that correlate to an increase in drug efficacy, overcome drug resistance, and controlled drug release from nanoparticles.

## 2.2. Significance and Background

Formulating these two anti-cancer drugs, paclitaxel and lapatinib, into a single nanoparticle formulation would address many of the challenges of treating ovarian cancer and provide several advantages over current delivery methods. Furthermore, sequential drug release from pH-labile nanoparticles can significantly improve drug efficacy and overcome multi-drug resistance (MDR). This approach can be applied to treating thousands of patients with ovarian cancer to improve their quality of life.

Tumor sensitivity to chemotherapeutic agents can decrease with continual treatments [225]. Tumor cells can develop resistant mechanisms against chemotherapies via acquired MDR. One of these mechanisms involved overexpression of ATP-binding cassette (ABC) transporters such as ABC subfamily B member 1 (ABCB1) also called P-glycoprotein (P-gp) [226,227]. One of the function of these transporters (e.g. ABCB1) is to remove drugs from tumor cells thereby decreasing the intracellular drug accumulation [226,227]. Without sufficient intracellular accumulation, there is insufficient levels of chemotherapeutic agents for a cytotoxic effect [228]. Furthermore, the ABC transporters are also associated with upregulation of human epidermal growth factor receptors (EGFR). The EGFR proteins are overexpressed resulting in upregulation of several protein kinase signaling pathways such as mitogen-activated protein kinase (MAPK) known to promote tumor

growth, angiogenesis, and metastasis among other effects [226,229,230]. These effects in combination with low anti-cancer drug accumulation in tumor cells due to the ABC transporters make treating patients with MDR extremely difficult.

As a means to overcome MDR in ovarian cancer, current approaches include combination drug therapy [35]. Drug combinations allow for targeting of multiple anticancer pathways, overcome and/or prevent drug resistance mechanisms, increase drug accumulation, lower systemic toxicity, and improve patient outcomes [9,12,57–59]. Furthermore, sequential drug delivery is a developing approach that has been shown to further improve the synergy of drug combinations. Sequential delivery allows for both parallel and interconnected cascade pathways to induce cell death and overcome the multiple drug resistant mechanisms of cancer cells [206].

Research in sequential drug delivery to treat ovarian cancer has been primarily focused on free drug formulations [18,84,88,116,131,133]. However, there are several limitations with free drug delivery. Chemotherapeutic free drug formulations are often hydrophobic and poorly water solubility resulting in poor bioavailability while inducing severe side effect [108,231]. Another challenge with free drugs is sequential delivery has to be done by trained personnel and delivery on the order of hours can be difficult in the clinical setting without drug targeting. Without methods to control drug delivery, increase bioavailability, and reduce toxicity, treating ovarian cancer remains a challenge.

There is a critical need for improving current treatment methods of MDR ovarian cancers. Advances in formulation of combination nanoparticle therapies offer a new paradigm to deliver an effective drug dosage, overcome MDR, control sequential drug delivery, simplify drug regimens to improve patient adherence as well as decrease side effects. Nanoparticle formulations can be designed for passive targeting and controlled drug delivery without use of toxic solvents as well as prevent premature degradation [108,232,233]. Nanoparticle combination therapy has been a growing approach for increasing efficacy of anti-cancer drugs and overcoming effects like MDR. Co-encapsulation of

drug combinations would improve co-localization of the drugs in the tumor tissue and improve spatiotemporal control of drug delivery [108,234–237].

Broadly, this nanoparticle platform can be applied to sequentially delivering other chemotherapeutic agents as well as a broad range of drugs. Encapsulating drug cocktails into pH-labile nanoparticles with controlled sequential release provides cost effective and accelerated improvement in controlled drug delivery and drug efficacy that can be applied to a variety of diseases.

### 2.3. Model Drug Selection

Taxol (paclitaxel) is one of the most widely used chemotherapeutic agents for treating ovarian cancer [103,104]. Paclitaxel binds to the  $\beta$ -subunit of tubulin, which stabilized the tubulin polymers preventing polymerization of microtubules [105–107]. Prolonged stabilization of microtubules prevents mitosis resulting in cell cycle arrests in the G<sub>2</sub>/M phase [107]. Clinically, PTX is used in combination with other drugs to increase the efficacy of treatment by targeting multiple pathways and overcoming drug resistance [115,238,239].

Lapatinib (Tykerb) or lapatinib ditosylate, is a drug that is effective at increasing accumulation of chemotherapeutic agents in MDR cells. Lapatinib is among a family of tyrosine kinase inhibitors which functions by binding to the ATP-binding sites of ABC transporters and inhibiting the transporter's function. Lapatinib thereby increases the intracellular drug accumulation of chemotherapeutics such paclitaxel [226]. Lapatinib has also been found to aid in inhibiting cell growth of MDR cells. It is currently FDA approved for combination therapies in metastatic breast cancer [240–242]. There are several ongoing clinical trials investigating the potential of lapatinib to increase the efficacy of anti-cancer drugs in other advanced solid tumors including ovarian cancer [104,246,247]. Thus lapatinib has the potential to overcome MDR effects in ovarian cancer and increase the efficacy of currently used chemotherapeutic agents (**Figure 11**).

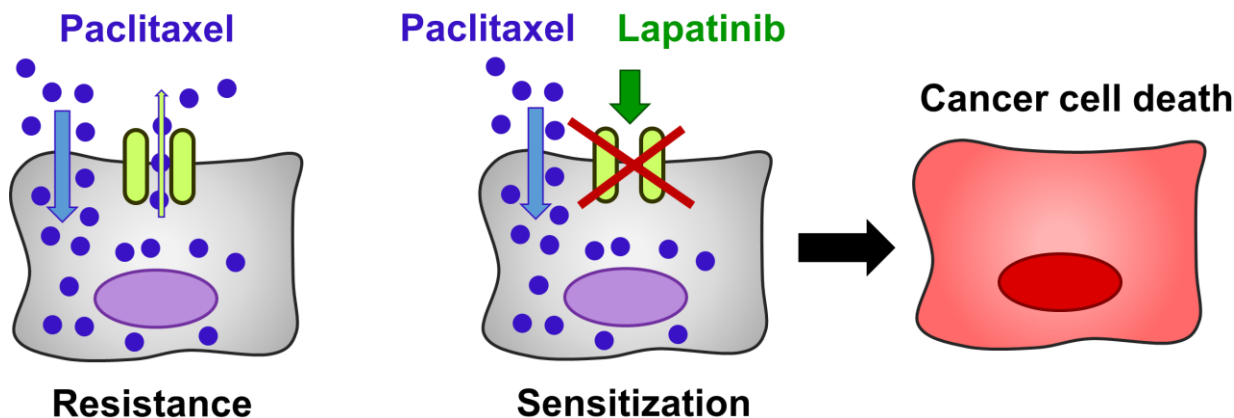


**Figure 11.** ABC transporters are responsible for removing drugs from the cell resulting in drug resistance. Lapatinib inhibits the activity of the transporters which sensitizes the cells and increases intracellular chemotherapeutic accumulation.

There are several obstacles with using paclitaxel and lapatinib in combination therapies. Paclitaxel is a cytotoxic agent that targets microtubules and prevents disassembly resulting in cell death which can be highly toxic for healthy cells [103]. Side effects can include low blood pressure, risk of infection, formation of blood clots, and neurotoxicity [108–110]. Additionally, paclitaxel is formulated with Cremophor EL, polyethoxylated castor oil which can cause severe side effects, including nephrotoxicity and neurotoxicity [108,109]. Both paclitaxel and lapatinib are relatively hydrophobic, poorly water soluble, and have low permeability which limits drug efficacy [248,249]. For treatment with these medications, patients require premedication before injection and complex treatment regimens [250,251]. This can lead to issues with patient compliance. There are ongoing studies on development of new therapeutic agents to overcome MDR and challenges with toxicity [252,253]. Formulating these two anti-cancer drugs into a single nanoparticle formulation would address many of these challenges and provide several advantages over current delivery methods.

Additionally, prior clinical studies have suggested that sequential delivery of paclitaxel and lapatinib improve drug efficacy [240,247]. Sequential delivery of chemotherapeutic agents and

tyrosine kinase inhibitors have been further investigated in free-drug *in vitro* [254–257]. Some of the studies found that delivering the chemotherapeutic drug prior to the tyrosine kinase inhibitors provided a synergistic effect compare the reversed order [254–256]. Another study indicated that treatment with the tyrosine kinase inhibitors prior to the chemotherapeutic drug provided a more effective treatment schedule for MDR cancer cells [257]. While there is still some debate as to which treatment schedule is more effective, these studies do suggest that a sequence-dependent synergistic effect on the cytotoxicity of MDR cancer cells. Incorporating controlled drug release of paclitaxel and lapatinib from nanoparticles can facilitate in further understanding the sequence-dependent drug interaction and improve drug efficacy.

## 2.4. Prior Art

Several nanoparticle formulations encapsulating paclitaxel and lapatinib have been previously considered [108,234–237,258]. Lipopolymer micelles co-encapsulating lapatinib and paclitaxel were found to significantly decrease cell viability of prostate cancer cells *in vitro* and decrease tumor volume *in vivo* relative to drugs delivered individually in nanoparticle form [234]. In another study co-encapsulated lapatinib and paclitaxel in polyelectrolyte nanoparticles with sonication-assisted layer by layer (SLBL) technique produced a paclitaxel core and lapatinib shell. These nanoparticles showed a significant decrease in cell viability compared to nanoparticles containing only paclitaxel [108]. Another study also investigated delivering paclitaxel and lapatinib in a core-shell structure using polymer micelles. Binding lapatinib to PEG resulted in a delayed release of lapatinib relative to paclitaxel. There was an increase in cytotoxicity of approximately 10% when the cells were treated with paclitaxel/lapatinib nanoparticles that release paclitaxel followed by lapatinib compare to paclitaxel nanoparticles [235]. These studies suggest there is a synergistic effect of delivering nanoparticle drug cocktails on chemotherapeutic efficacy for treating drug resistant cancer and provide

the foundation for formulating polymer nanoparticles drug cocktails. However, many of the methods for nanoparticle formation are time-intensive and not scalable. Furthermore, the drug release kinetics is not well understood from polymer nanoparticles as well as the influence of sequential delivery on cell cytotoxicity. Understanding this interaction, it is possible to design a nanoparticle system that maximizes the potency of the drugs.

## 2.5. Flash NanoPrecipitation

Flash NanoPrecipitation is a rapid, scalable process for encapsulating drug combinations. In FNP, PEGylated block copolymers direct self-assembly of kinetically trapped nanoparticles with high drug loading capacities, narrow size distribution, and tunable surface chemistry (**Figure 12**) [259]. By leveraging a pH-labile nanoparticle platform, we can introduce additional control of drug release after a change in pH of localized environment. The pH-labile nanoparticles are formulated by complexing an antioxidant (i.e. tannic acid) with  $\text{Fe}^{3+}$  (aq.) *in situ*. Antioxidant metal complexes are insoluble under basic conditions ( $\text{pH} > 7$ ) and soluble in acidic environments ( $\text{pH} < 5$ ). To achieve pH-labile nanoparticles we will encapsulate antioxidant metal complexes using a block copolymer stabilizer via FNP. The resulting nanoparticles are pH-labile; the nanoparticles are stable under basic conditions ( $\text{pH} > 7$ ) when the complex is insoluble and the nanoparticles disassemble in acidic environments ( $\text{pH} < 2$ ) when the complex is soluble [260].

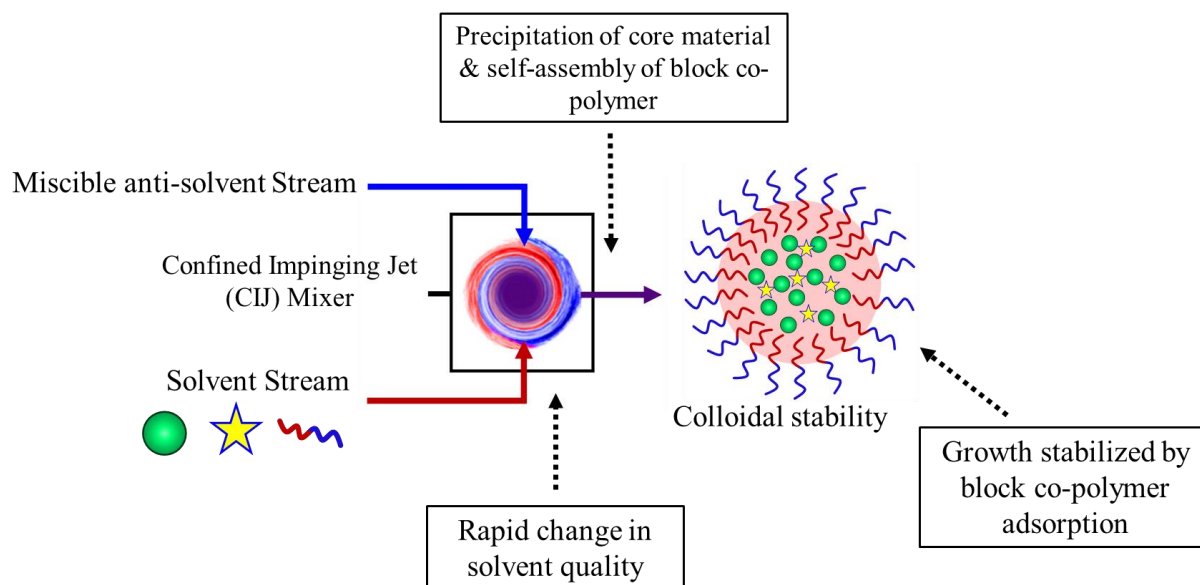


**Figure 12.** Flash NanoPrecipitation (FNP) is a rapid and scalable process with high drug loading. The rapid change in solvent quality during mixing of the solvent stream with the miscible anti-solvent stream in the Confined Impinging Jet (CIJ) Mixer leads to 1) precipitation of core material and 2) self-assembly of block co-polymer. The growth stabilized by block co-polymer adsorption. Nanoparticle size is governed by rate of nucleation and growth relative to self-assembly.

The advantages of pH-labile nanoparticle platform is control over drug release. Ideally, the nanoparticles would minimize the amount of drug released into the bloodstream while delivering the payload to the target sight. A pH-labile nanoparticle will allow for slow, sustained release under pH 7.4 conditions in the bloodstream. With passive targeting using nanoparticles < 200 nm, there is preferential accumulate in the tumor tissue through leaky tumorigenic vasculature [261]. Upon endocytosis by the cancer cells, a change in pH in the lysosome (pH ~4) will induce rapid drug release due to the degradation of the particle core (**Figure 13**).

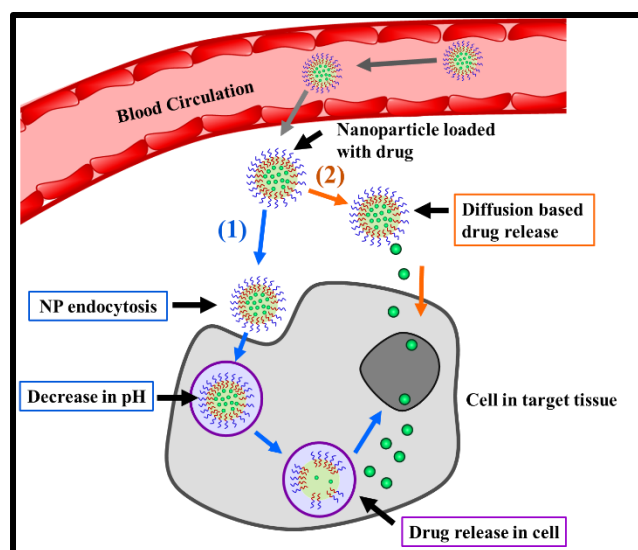


**Figure 13.** Two potential pathways of drug delivery from pH-labile nanoparticles. (1) When the nanoparticles are endocytosed the pH decreases resulting in destabilization and drug release or (2) diffusion-limited drug release from the nanoparticle outside the cell.

## 2.6. Approach

We propose developing a nanoparticle platform for sequential delivery of paclitaxel and lapatinib to decrease drug dosage and improve drug synergy. Our central **hypothesis is that sequential release of paclitaxel and lapatinib from a co-loaded nanoparticle will improve drug potency in terms of cell viability and enhance drug synergy.**

Flash NanoPrecipitation (FNP) is typically performed with highly hydrophobic moieties as indicated by the calculated octanol water partition coefficient,  $\log P > 6$ ; successful nanoparticle self-assembly occurs due to hydrophobic interactions between the precipitating core material and hydrophobic block of the block co-polymer. Previously, FNP has been limited to hydrophobic materials due to instability and particle disassembly with non-hydrophobic materials ( $\log P < 6$ ). In this work, we will develop methods to encapsulate the model drugs which are not highly hydrophobic using Flash NanoPrecipitation. The challenge this work will address is formulating uniform nanoparticles with size control and maintaining strong interaction between the hydrophobic block of the block co-polymer and the particle core. This work will provide the foundation for encapsulation



of a wide variety of drugs into stable polymer nanoparticle without the need for tuning drug hydrophobicity.

Furthermore, to establish sequential release, we have proposed to formulate a hydrophobic paclitaxel-prodrug to control the drug release profile relative to paclitaxel and lapatinib [262]. By tuning the properties of paclitaxel with a prodrug approach, we can control the rate of diffusion from the nanoparticle core. This provides an additional measure of control over the drug release particularly to facilitate sequential delivery of paclitaxel and lapatinib.

## 2.7. Specific Aims

Designing nanoparticles with tunable release kinetics will enable sequential delivery from pH-labile nanoparticles. To accomplish this goal, we will completed three specific aims:

**Aim 1:** Paclitaxel, paclitaxel-prodrug, and lapatinib will be encapsulated in pH-labile nanoparticles. The formulation parameters of weakly hydrophobic drugs ( $\log P < 6$ ) will be determined for formulating monodispersed nanoparticles  $\sim 100$  nm. We will formulated both single-drug loaded nanoparticles as well as co-loaded nanoparticles with paclitaxel/lapatinib or paclitaxel-prodrug/lapatinib (**Figure 14**).

**Aim 2:** The drug release kinetics of paclitaxel, paclitaxel-prodrug, and lapatinib from pH-labile nanoparticles will be determined. The drug release profile will be determined via dialysis under sink-conditions at pH 7.4 and pH 4 as representative biological conditions.

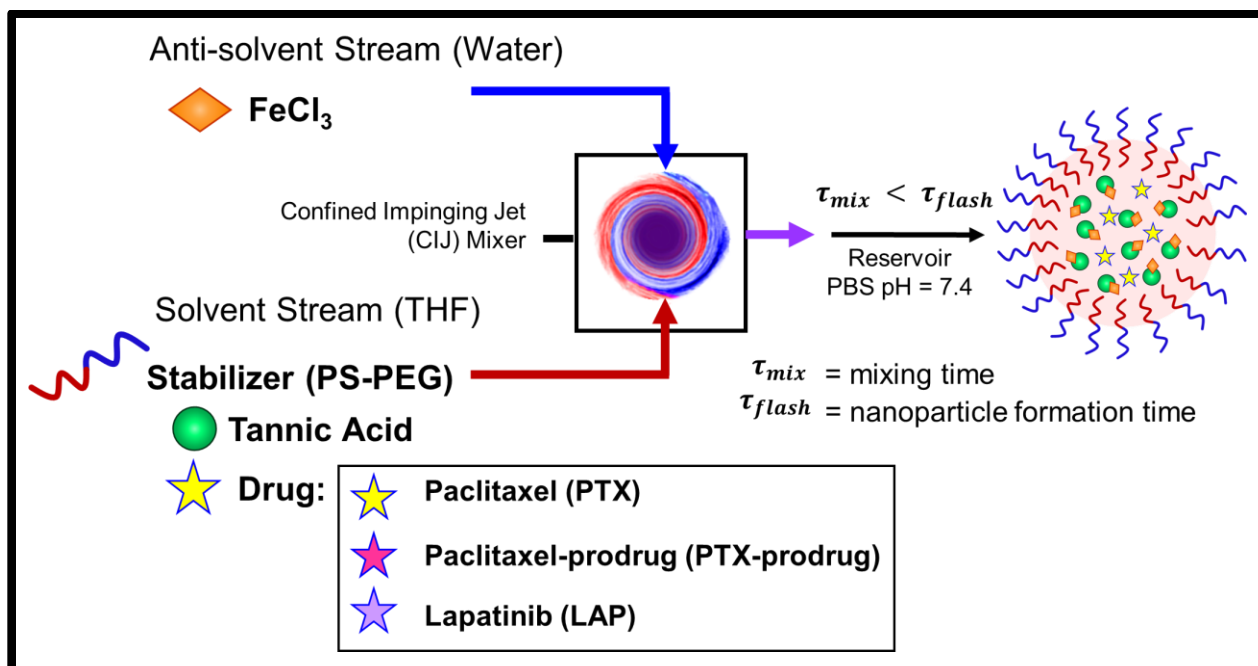


**Figure 14.** Overview of nanoparticle synthesis with Flash NanoPrecipitation to encapsulate paclitaxel and lapatinib with a tannic acid (TA) and iron coordination complex using an amphiphilic block copolymer stabilizer.

**Aim 3:** Finally, we will examine the drug efficacy of the nanoparticles *in vitro* by examining cell viability. Comparisons will be made between the free drug and nanoparticle formulations as well as single-drug and co-loaded nanoparticles and the synergistic drug interaction will be evaluated. Furthermore, sequential delivery of single-drug loaded nanoparticle as well as controlled release from co-loaded nanoparticles will be evaluated. The mechanisms of drug efficacy will also be further assessed by examining the cell cycle distribution following treatment.

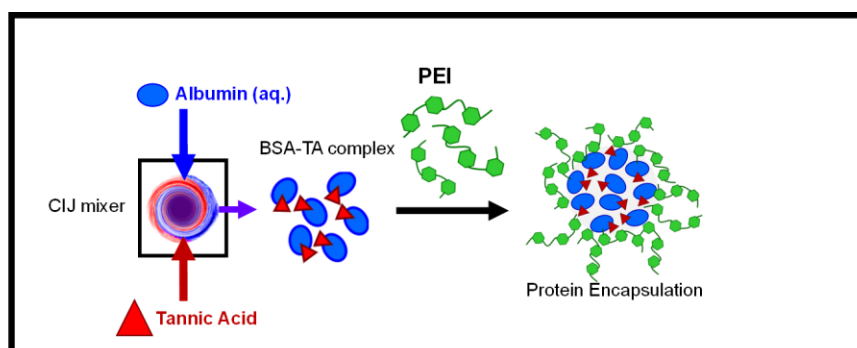
These three aims will enable us to determine whether encapsulating these drugs into nanoparticles can enhance drug efficacy. This research approach will also address if co-loading the drugs into nanoparticles can improve drug synergy. Additionally, whether sequential delivery of paclitaxel and lapatinib from nanoparticles can improve drug efficacy and if the drug release can be controlled by tuning the drug hydrophobicity and environmental pH.

## 2.8. Overview of Dissertation

The main objectives of this study were to developing a method for encapsulating paclitaxel, paclitaxel-prodrug, and lapatinib into nanoparticles and understanding the implications of sequential drug delivery. Then based on these findings a nanoparticle platform for controlled drug release with enhanced drug efficacy was developed. Finally, we addressed clinical limitations of nanoparticles in terms of shelf-stability and reconstitution from dried form (**Figure 15**).

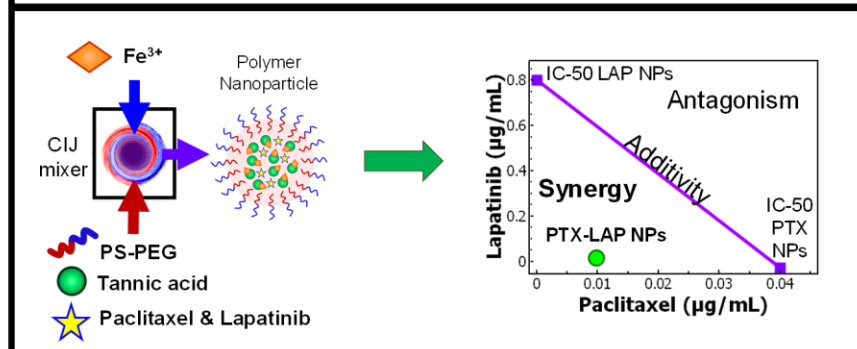
### Chapter 3

Encapsulation of proteins with FNP via electrostatic interaction between the polymer and protein stabilizing the nanoparticles.



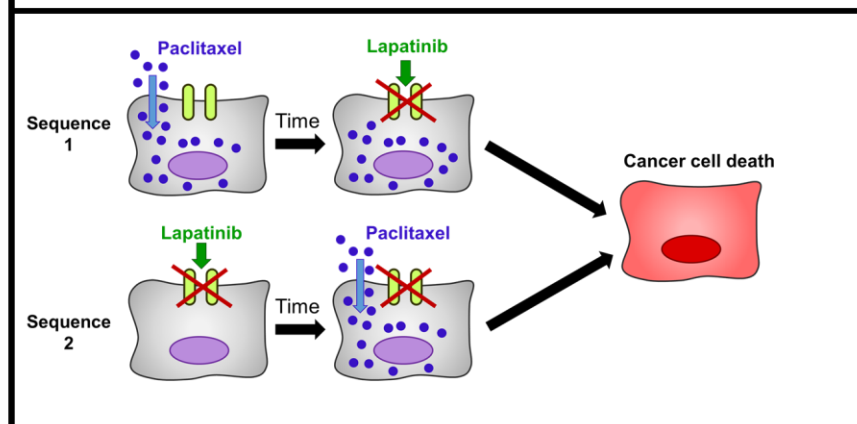
### Chapter 4

Encapsulation of weakly hydrophobic ( $\log P < 6$ ) drug combinations via in situ TA- $\text{Fe}^{3+}$  complexation which produces a synergetic drug interaction *in vitro*.



### Chapter 5

Sequence-dependent cytotoxicity was observed with delivery of paclitaxel and lapatinib encapsulated into nanoparticles.



## Chapter 6

Controlled drug delivery was examined using pH-responsive nanoparticles. The drug efficacy of paclitaxel was enhanced by formulation of a hydrophobic prodrug and encapsulation of the prodrug with lapatinib

## Chapter 7

A rapid, room-temperature nanoparticle drying method was established via electrospinning to facilitate translation of nanoparticle drug products to clinical practice.

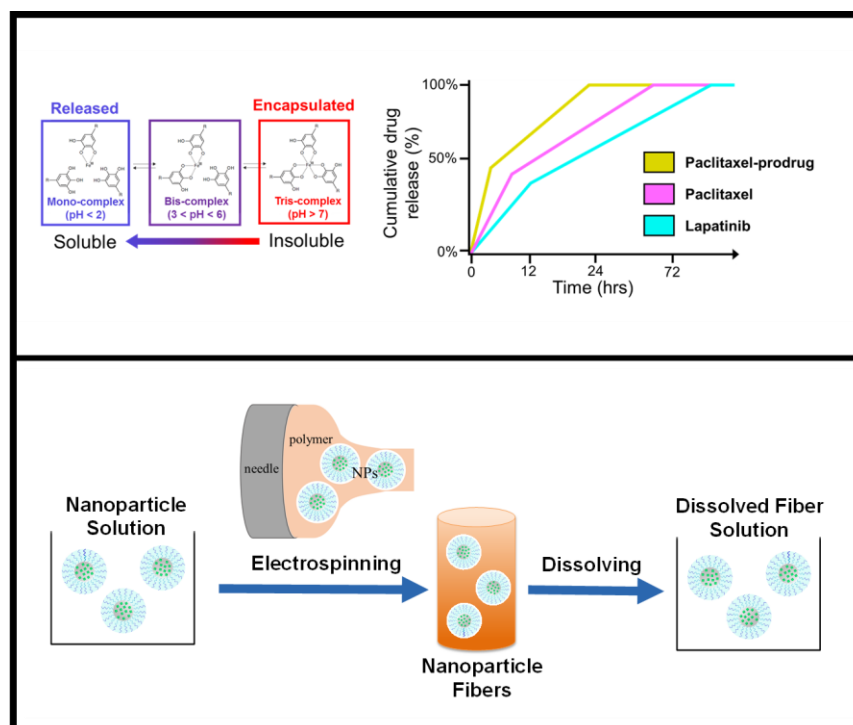


**Figure 15.** Overview of experimental studies covered in this dissertation. In Chapter 3 we discuss encapsulation of protein followed by the nanoparticle formulation process for encapsulating weakly hydrophobic drugs and synergistic activity of co-loaded nanoparticles in Chapter 4. In Chapter 5 we examine sequential drug delivery *in vitro* and in Chapter 6 we investigate formulating nanoparticles for controlled release. Lastly, in Chapter 7 we discuss electrospinning nanoparticles to extend their shelf-life.

First, we investigated an alternative FNP platform for encapsulating non-hydrophobic drugs and macromolecules such as proteins. As FNP has previously been limited to highly hydrophobic materials ( $\log P > 6$ ), it was important to understand the fundamentals for an FNP platform encapsulating non-hydrophobic materials. By encapsulating proteins such as albumin into polymer nanoparticles we can broaden the therapeutic agents that can be co-loaded into polymer nanoparticles such as DNA, RNA, and antibodies. Additionally by conjugating weakly or non-hydrophobic drugs to albumin we can create another vehicle for drug delivery. These findings are discussed in Chapter 3.

Next, another FNP platform was investigated for encapsulating weakly hydrophobic drugs ( $\log P < 6$ ). The formation of tannic acid-iron complexes *in situ* was evaluated as a method for co-encapsulation of weakly hydrophobic drugs (paclitaxel and lapatinib). The parameters for fabricating uniform nanoparticles at  $\sim 100$  nm were investigated to allow for passive targeting. The drug efficacy

was compared between free drug formulations and nanoparticles as well as between co-delivery of two nanoparticles and co-loaded nanoparticles. The synergistic drug interaction and cell cycle were evaluated and these results are presented in Chapter 4.

After determining a platform for encapsulating paclitaxel and lapatinib in polymer nanoparticles, sequential drug delivery was investigated. *In vitro* experiments were conducted and both free drug and nanoparticle formulations were delivered in different sequence schedules. These findings are presented in Chapter 5.

Based on the results from sequential drug delivery, nanoparticles for controlled drug release were investigated. The relative drug release rate of paclitaxel was tuned by formulating a hydrophobic prodrug. The drug release profiles were determined for nanoparticles encapsulating paclitaxel, paclitaxel-prodrug, lapatinib, or combinations of those drugs. Finally the drug efficacy was evaluated for single-drug and co-loaded nanoparticles encapsulating either paclitaxel or paclitaxel-prodrug. The results from these experiments are discussed in Chapter 6.

Lastly, we addressed the limitations of translating nanoparticle technology to clinical practices. Maintaining shelf-stability and nanoparticle integrity during reconstitution is challenging with traditional drying methods. A novel method for rapid, room temperature nanoparticle drying and low-energy reconstitution via electrospinning was presented. The parameters of this technology are discussed in Chapter 7. Finally, the conclusions from the dissertation and final remarks are presented in Chapter 8.

### 3. Chapter 3: Rapid, Single-Step Protein Encapsulation via Flash NanoPrecipitation

---

**Published:** [263] Levit, S.L.; Walker, R.C.; Tang, C. Rapid, Single-Step Protein Encapsulation via Flash NanoPrecipitation. *Polymers* **2019**, 11, 1406.

#### Abstract

Flash NanoPrecipitation (FNP) is a rapid method for encapsulating hydrophobic materials in polymer nanoparticles with high loading capacity. Encapsulating biologics such as proteins remains a challenge due to their low hydrophobicity ( $\log P < 6$ ) and current methods require multiple processing steps. In this work, we report rapid, single-step protein encapsulation via FNP using bovine serum albumin (BSA) as a model protein. Nanoparticle formation involves complexation and precipitation of protein with tannic acid and stabilization with a cationic polyelectrolyte. Nanoparticle self-assembly is driven by hydrogen bonding and electrostatic interactions. Using this approach, high encapsulation efficiency (up to ~80%) of protein can be achieved. The resulting nanoparticles are stable at physiological pH and ionic strengths. Overall, FNP is a rapid, efficient platform for encapsulating proteins for various applications.

#### 3.1. Introduction

Flash NanoPrecipitation (FNP) is a versatile method to incorporate hydrophobic drugs, dyes, or inorganic nanoparticles with hydrophobic coating into polymeric nanoparticles via rapid mixing achieved with confined impinging jets [150]. Typically, nanoparticle self-assembly involves precipitation of the supersaturated hydrophobic material via nucleation, growth and adsorption of a

micellizing amphiphilic block copolymer. The resulting nanoparticles are sterically stabilized with a hydrophobic core – hydrophilic shell structure [150,264]. Due to the rapid precipitation rate and strong hydrophobic interaction with the hydrophobic block of the amphiphilic block co-polymer necessary for stabilization, the use of FNP has generally been limited to encapsulation of hydrophobic materials ( $\log P > 6$ ) [265]. Due to the increasing emphasis on biologically derived therapeutics [266] such as proteins and peptides, encapsulation to prevent rapid clearance from natural mechanisms and enzymatic degradation of the biologic [267,268] via FNP is of considerable interest.

Encapsulation of less hydrophobic materials ( $\log P < 6$ ) [269–272] using FNP has been achieved via *in situ* complexation [269–272]. For example, hydrophobic ion pairs [271] or insoluble coordination complexes can be formed during mixing and stabilized with an amphiphilic block copolymer [272]. To encapsulate peptides, hydrophilic imaging agents, and small proteins (~14 kDa), inverse Flash Nanoprecipitation (iFNP) has recently been reported [273,274]. In iFNP, the biologic and the amphiphilic block copolymer are solubilized in a polar organic solvent (e.g. dimethyl sulfoxide) and rapidly mixed with a miscible nonpolar solvent (e.g. acetone or chloroform) which leads to precipitation of the biologic, adsorption of the hydrophilic block, and stabilization by the hydrophobic block in the nonpolar solvent. These initial particles with a hydrophilic core and hydrophobic coating are then crosslinked for stabilization and dispersed in an appropriate solvent for a second FNP step and encapsulated within a second block copolymer [273,274]. While promising, this approach inherently requires multiple processing steps.

Another approach to encapsulate biologics has been Flash Nanocomplexation in which polyelectrolytes complex with biologics (e.g. negatively charged DNA) to impart stability. For gene delivery, Santos et al. stabilized DNA with linear polyethylenimine (lPEI) (22 kDa) via rapid mixing [275]. This approach of leveraging electrostatic interactions has been successful for strong

polyelectrolytes such as DNA. Use of this approach for encapsulation of diffusely charged, globular proteins has not yet been reported.

Therefore, we investigate a single-step method for encapsulation of proteins via FNP. We use bovine serum albumin (BSA) as the model protein and form an insoluble precipitate *in situ* with tannic acid [276–278]. We study various stabilizers (i.e. amphiphilic block co-polymer and polyelectrolytes). The effects of formulation parameters e.g. stabilizer concentration, molecular weight, pH, and ionic strength on nanoparticle size, zeta potential, stability, protein encapsulation are discussed.

## 3.2. Materials and Methods

### 3.2.1. Materials

ACS grade tannic acid (TA), calcium chloride ( $\text{CaCl}_2$ ), and ACS grade hydrochloric acid (HCl) were purchased from Sigma-Aldrich (St. Louis, MO, USA). The branched polyethylenimine (PEI) at weight averaged molecular weight ( $M_w$ ) of 2,000 g/mol and 10,000 g/mol, were obtained from PolySciences (Warrington, PA, USA), and  $M_w = 750,000$  g/mol 50% (w/v) in  $\text{H}_2\text{O}$  was obtained from Sigma-Aldrich (St. Louis, MO, USA). Bovine serum albumin (BSA), ACS grade acetone, HPLC grade tetrahydrofuran (THF), diethyl ether, ammonium hydroxide ( $\text{NH}_4\text{OH}$ ) (aq. 10% v/v), and ACS certified sodium chloride (NaCl) were obtained from Fisher Scientific (Pittsburg, PA, USA). These reagents were used as received. Phosphate-buffered saline (PBS) was made with 156 mM NaCl, 10mM sodium phosphate dibasic anhydrous ( $\text{Na}_2\text{HPO}_4$ , Fisher Scientific), and 2mM potassium phosphate monobasic ( $\text{KH}_2\text{PO}_4$ , Fisher Scientific). Prior to use, BioRad Protein Assay Dye Reagent (Bradford dye, BioRad, Hercules, CA, USA) was filtered with a  $0.45\mu\text{m}$  PTFE filter (Fisher Scientific) and diluted 4-fold with deionized water. Additionally, polystyrene-b-polyethylene glycol (1600-b-500 g/mol) (PS-b-PEG) obtained from Polymer Source (Product No. P13141-SEO, Montreal, Canada)



was dissolved in THF (500 mg/mL) and precipitated in diethyl ether (1:20 v:v THF:ether). The PS-b-PEG was recovered by centrifuging, decanting, and drying under vacuum at room temperature for two days as previously described [279].

### 3.2.2. *Nanoparticle Preparation*

Flash NanoPrecipitation (FNP) was performed with a hand-operated confined impinging jet (CIJ) mixer similar to previous reports [10]. Using the amphiphilic block co-polymer stabilizer, PS-b-PEG was dissolved with TA (5 mg/mL) in acetone by sonication (~40°C) and rapidly mixed with BSA dispersed in water (9 mg/mL or 20 mg/mL). The block co-polymer to core material (BSA/TA) ratio was 2:1 by mass. The effluent from the CIJ mixer was immediately diluted in deionized water to maintain an acetone:water volume ratio of 1:9. To use PEI as a stabilizer, TA (5 mg/mL) was dissolved in acetone and rapidly mixed with BSA dispersed in water (9 mg/mL); the mixer effluent was immediately diluted into PEI dispersed in water. The amount of PEI was varied relative to the mass of BSA/TA to achieve a final ratio PEI:BSA/TA of 1:1, 2:1, or 3:1 by mass. The volume of aqueous PEI was set to maintain a final acetone/water ratio of 1:9 by volume. To determine the role of TA, FNP was performed without TA using PEI as a stabilizer by rapidly mixing BSA dispersed in water with acetone and immediately diluting with PEI dispersed in water. In some cases, the ionic strength or the pH of the aqueous BSA stream was adjusted with HCl and NH<sub>4</sub>OH to achieve pH values between 2 and 10. In some cases following FNP, dialysis was performed to remove the organic solvent using regenerated cellulose tubing with a molecular weight cutoff of 6-8 kD MWCO (Spectra/Por, Spectrum Laboratories, Houston, TX) against deionized water at a ratio of 1:100. The bath water was replaced four times in a 24-hour period.

### 3.2.3. Nanoparticle Characterization

The size and zeta potential of the resulting nanoparticle dispersions were measured after formulation with a Malvern Zetasizer ZS with a backscatter detection angle of 173° (Malvern Instruments Ltd, Malvern, United Kingdom). The intensity average particle size and distribution are reported using normal resolution mode with an average of 4 measurements. The polydispersity index (PDI) is used as a measure of the breadth of the particle distribution defined from the moments of the cumulant fit of the autocorrelation function calculated by the instrument software as previously described. Nanoparticles with a PDI below 0.300 were considered uniform [10,19].

To assess nanoparticle stability, the pH of the nanoparticle dispersions following FNP was adjusted between pH 2 and 10 with HCl or NH<sub>4</sub>OH. The size and zeta potential were tracked by DLS for up to a week. Additionally, the effect of ionic strength on particle stability by adding NaCl or CaCl<sub>2</sub> (10 to 300 mM) after FNP and the resulting size and zeta potential were tracked for 24 hours.

### 3.2.4. Protein Quantification

The amount of protein encapsulated in the resulting nanoparticles was quantified using a Bradford assay. After FNP, nanoparticles were recovered by centrifugal filtration (Amicon Ultracel 50K, 50,000 NMWL, Merck Millipore Ltd, Burlington, MA). Briefly, filters were centrifuged (5804 R 15 amp version, Eppendorf, Hamburg, Germany) at ~4000 rpm for 30-40 minutes. The recovered nanoparticles were separated from the supernatant. The recovered particles were washed 3 times with acetone (1 mL) to precipitate the BSA and solubilize the other nanoparticle components. The precipitated BSA was recovered from the acetone soluble nanoparticle components by centrifugation (10,000 rpm for 5-10 minutes) and decanting the acetone supernatant. The recovered protein was redispersed in water. A Bradford assay was performed on the sample following the manufacturer's protocol. Briefly, 10 µL of sample and 200 µL of Bradford dye were added to 96-well plate and measured with a microplate reader (VersaMax ELISA microplate reader, Molecular Devices, San Jose,

CA or Cytation 3 multi-mode reader, BioTek, Winooski, VT) at a wavelength of 595 nm. Performing the procedure with a known amount of BSA, we confirmed  $98 \pm 3\%$  protein recovery (**Table 1**).

**Table 1.** BSA recovery in Bradford assay sample preparation

Initial Loading (mg)	Recovered BSA (mg)	Percent Recovered (%)
0.90	$0.88 \pm 0.06$	$98\% \pm 3\%$

### 3.3. Results and Discussion

Tannins such as tannic acid (TA) are known to precipitate proteins. Thus, to encapsulate proteins via Flash NanoPrecipitation (FNP), our approach was to form an insoluble complex with tannins during mixing in the presence of a stabilizer to facilitate nanoparticle self-assembly and impart stability. We use TA and bovine serum albumin (BSA) as a model system. Initially, we examined the precipitation of the BSA-TA complex via FNP. We mixed BSA dispersed in water with TA dissolved in acetone, which immediately formed a cloudy dispersion with a zeta potential of  $-13.1 \pm 0.6$  mV (**Table 2**). Without a stabilizer, the precipitate continued to grow and macroscopic precipitation was observed within 24 hrs. These observations indicate that BSA and TA complex and precipitate sufficiently fast upon mixing for nanoparticle self-assembly with FNP. We varied the ratio of BSA to TA (between 3:7 and 7:3 by mass) and observed the amount of macroscopic precipitate that formed. A mass ratio of 9:5 BSA to TA, produced the greatest amount of macroscopic precipitate (**Figure 16**) and was thus used for subsequent experiments.

**Table 2.** Zeta potential of BSA-TA complex with polymer stabilizers.

Sample	Zeta Potential (mV)
BSA-TA precipitate	$-13.1 \pm 0.6$
BSA-TA with PS-b-PEG	$-18.0 \pm 3.0$
PEI	$+34.3 \pm 4.2$
BSA-TA with PEI	$+18.8 \pm 0.9$

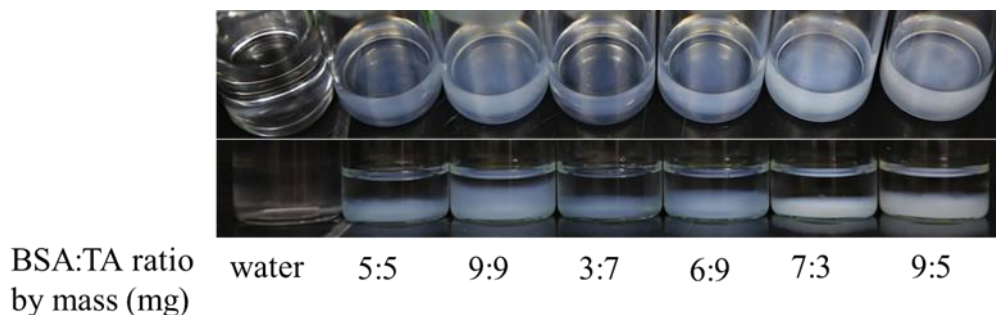


**Figure 16.** Precipitation of BSA and TA - Varying BSA:TA ratio.

Based on these results of rapidly precipitating BSA with TA, we initially formulated nanoparticles using an amphiphilic block co-polymer (PS-*b*-PEG) as a stabilizer. To perform FNP, BSA was dispersed in water and rapidly mixed with TA and PS-*b*-PEG dissolved in acetone. At a BSA to TA mass ratio of 9:5 and a block co-polymer to core mass ratio of 2:1, the nanoparticle dispersion was polydisperse with multiple peaks at ~100 nm, ~20 nm, and ~10 nm (**Figure 17**). The peaks can be attributed to TA/PS-*b*-PEG micelles [10], empty PS-*b*-PEG micelles [281], and soluble BSA [282]. The lack of visible TA/BSA precipitate suggests that TA preferentially interacts with the block copolymer than with BSA during FNP. Further, there is a mismatch in timescales of complexation/precipitation and block copolymer micellization such that the block copolymer rapidly forms micelles and on a longer time scale stabilizes TA [10,22].

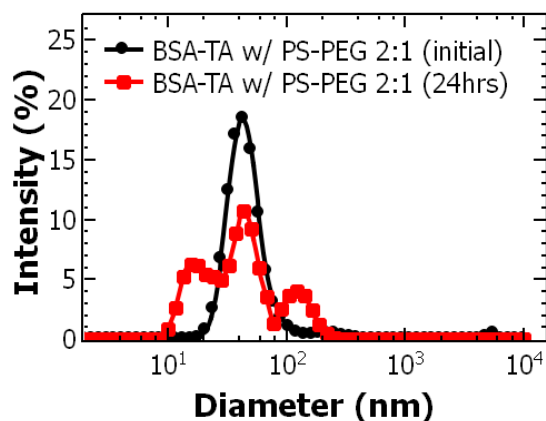


**Figure 17.** Nanoparticles formulated with PS-*b*-PEG (28 mg/mL) and TA (5mg/mL) dissolved in acetone and rapidly mixed with BSA (9mg/mL) dispersed in water via FNP.

To promote BSA/TA interactions, we performed FNP with an excess of protein. When the BSA to TA ratio was increased to 4:1, nanoparticles were initially formed with a size of  $\sim 600$  nm with PDI of  $0.347 \pm 0.045$  similar to BSA-TA without stabilizer (**Figure 18A and Figure 18B**). The measured zeta potential,  $-18.0 \pm 3.0$  mV, is consistent with other PEG based block copolymer stabilized nanoparticles [265,284]. Therefore, it appears that upon mixing, BSA and TA complex and precipitate then the hydrophobic block of the amphiphilic block copolymer stabilizes the precipitate. TA also undergoes intermolecular interactions with the PEG block of the block copolymer via hydrogen bonding forming an insoluble complex that is confined to the nanoparticle core with the TA/BSA precipitate. The hydrophobic block of the block copolymer adsorbs to the precipitating nanoparticle core (hydrophobic PS-block, TA/BSA precipitate, TA:PEG) due to hydrophobic interactions. The PEG that is not complexed with TA microphase separates from the PS-block and orients into the aqueous phase providing steric stabilization. In this case, nanoparticle assembly is driven by a combination of hydrophobic and hydrogen bonding interactions.

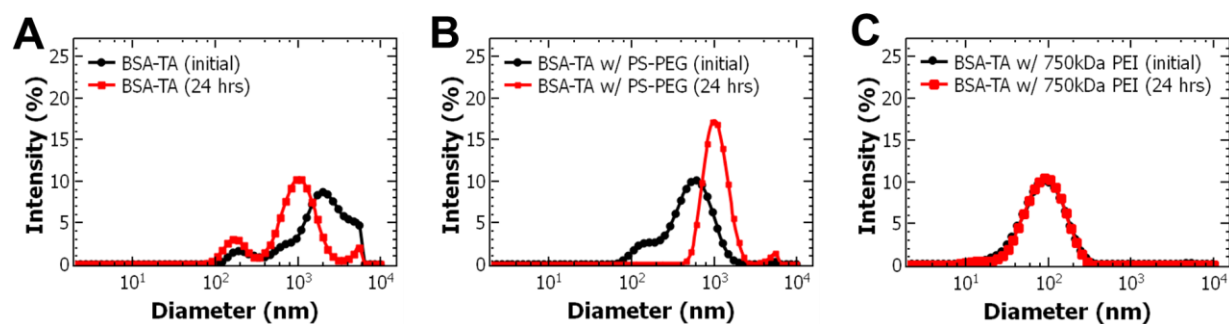


**Figure 18.** Dynamic light scattering (DLS) intensity weighted size distribution results of (A) Bovine serum albumin-tannic acid (BSA-TA) complex without the presence of a stabilizer, (B) BSA-TA complex with an amphiphilic block co-polymer, and (C) the BSA-TA complex stabilized with 750kDa polyethylenimine (PEI), immediately upon mixing and after 24 hrs. The BSA-TA complex stabilized with PEI did not change in size after 24 hrs.

While PS-b-PEG initially facilitated nanoparticle self-assembly, the resulting nanoparticle dispersion, initially transparent, turned cloudy over several hours indicating nanoparticle growth. Over 24 hours, TA and BSA partition out and re-precipitate outside of the nanoparticle core. Similar behavior has been observed with TA [10] and peptides [273] which is attributed to low affinity between the hydrophobic block of PS-b-PEG and the BSA/TA precipitate.

Therefore, we next considered alternative stabilizers. Since we observed the initial BSA/TA complex showed a negative zeta potential of  $-13.1 \pm 0.6$  mV, we considered a cationic polyelectrolyte, polyethylenimine (PEI). To perform FNP, BSA dispersed in water was rapidly mixed with TA dissolved in acetone. The effluent of the mixer was immediately diluted into PEI with a molecular weight of 750,000 g/mol (750kDa PEI) dispersed in water. Introducing PEI stabilizer facilitated nanoparticle self-assembly and conferred nanoparticle stability (**Figure 18c**). The resulting nanoparticles were  $107 \pm 5$  nm with a PDI  $0.285 \pm 0.004$  and a zeta potential of  $+18.8 \pm 0.9$  mV (**Table 3**). No macroscopic precipitate was observed over at least 7 days. The positive zeta potential suggests that PEI was present at the surface of the nanoparticles encapsulating the anionic BSA-TA precipitate providing some degree of steric stabilization as zeta potentials greater than  $+35$  mV are required for entirely electrostatic stabilization [284].

**Table 3.** Effect of polyelectrolyte stabilizer molecular weight on nanoparticle properties and stability.

Sample	Initial			7 days		
	Zeta potential (mV)	Diameter (nm)	PDI	Zeta potential (mV)	Diameter (nm)	PDI
10kDa PEI	$+15.7 \pm 1.0$	$153 \pm 7$	$0.125 \pm 0.022$	$+14.4 \pm 1.9$	$152 \pm 1$	$0.055 \pm 0.013$
750kDa PEI	$+18.5 \pm 1.3$	$107 \pm 5$	$0.285 \pm 0.004$	$+18.5 \pm 1.3$	$94 \pm 3$	$0.259 \pm 0.011$

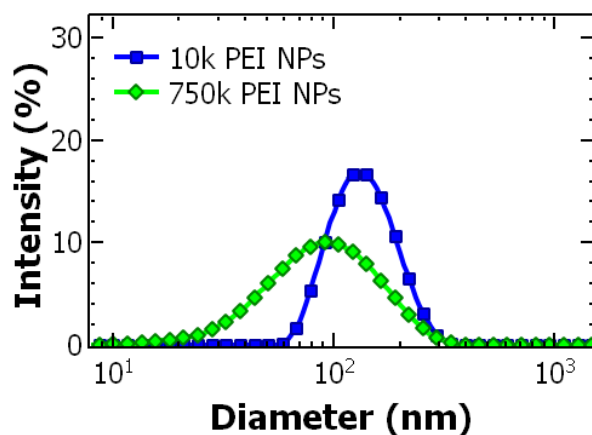


**Figure 19.** Effect of PEI molecular weight on nanoparticle formulation.

Since stabilizer properties can greatly affect resulting nanoparticle properties [265,285–287], we investigated the effect of PEI molecular weight (**Table 4**) on nanoparticle assembly and stability. We used molecular weights of 750kDa, 10kDa, and 2kDa. Interestingly, while 750kDa PEI resulted in  $107 \pm 5$  nm stable nanoparticle, 10kDa PEI formed monodisperse, stable particles with a diameter of  $153 \pm 7$  nm with a PDI of  $0.125 \pm 0.022$  and a zeta potential  $+14.4 \pm 1.9$ mV (**Table 3, Figure 19**). The 2kDa PEI did not facilitate nanoparticle assembly (

**Table 5**) and FNP resulted in macroscopic precipitate. Thus, PEI molecular weights greater than 10kDa were necessary for nanoparticle formation via self-assembly to encapsulate the BSA/TA complex. High molecular weight polyelectrolytes have been reported to strongly absorb onto surfaces which improve the stabilization of dispersions [288,289] such as the BSA/TA precipitate. In contrast, low molecular weight polyelectrolytes have higher intermolecular charge repulsion which limits the electrostatic stabilization of the BSA/TA precipitate [289].

**Table 4.** Size and zeta potential of PEI dispersed in water

Molecular Weight	Diameter (nm)	Zeta Potential (mV)
2kDa PEI	140 ± 99	13.4 ± 2.5
10kDa PEI	5.1 ± 0.7	12.3 ± 3
750kDa PEI	101 ± 7	18 ± 2.9

**Table 5.** Effect of PEI molecular weight on nanoparticle formulation

Molecular Weight	Diameter (nm)	PDI	Zeta Potential (mV)
2kDa PEI	753 ± 230	0.596 ± 0.090	- 4.2 ± 1.1
10kDa PEI	153 ± 7	0.125 ± 0.022	+ 15.7 ± 1.0
750kDa PEI	101 ± 3	0.274 ± 0.007	+ 20.6 ± 1.8

We confirmed the role of electrostatic interactions in nanoparticle assembly and stabilization by examining the effect of pH of the BSA stream on particle formation. First, we confirmed TA precipitates BSA at various pHs; we observed macroscopic precipitation for pHs between 7 and 4.5, and no visible precipitate at pH 2 (**Figure 20**). The maximum amount of visible BSA-TA precipitate was produced at pH ~ 5 which can be attributed to protein aggregation near the isoelectric point of BSA (pI = 4.8) [290] comparable to previous reports [276]. Subsequently, the pH of the BSA stream was adjusted to between 2 and 10 prior to FNP while the PEI reservoir was unbuffered (pH ~ 10) and the nanoparticle size and zeta potential were examined. Varying the pH of the BSA stream did not change the size or zeta potential of the 750kDa PEI NPs (**Table 6**) indicating the measured properties are dictated by the PEI. Interestingly, decreasing the pH to 2 using 10kDa PEI disrupted particle assembly (**Figure 21** and **Table 7**) and instead formation of a visible precipitate was observed. The net charge of BSA is dependent on pH; decreasing pH below the isoelectric point results in protonation of the protein and a net positive charge [276,278]. With a net positive charge, BSA repels the cationic PEI (pKa ~ 10) [288,291] and thus particles do not form. Therefore, particle assembly requires pHs



at or above the isoelectric point of the protein (i.e. pH >5) to ensure electrostatic interaction with the PEI stabilizer.

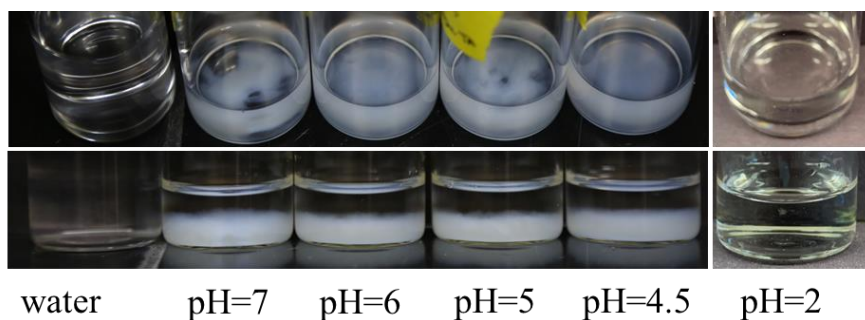


**Figure 20.** Precipitation of BSA and TA at various pH conditions.

**Table 6.** Effect of pH of the BSA stream and PEI reservoir on 750kDa PEI nanoparticles

pH of BSA	pH of PEI	Zeta potential (mV)	Diameter (nm)	PDI
2	10	+ 23.2 ± 1.7	95 ± 8	0.340 ± 0.046
	2	+ 28.7 ± 17.9	115 ± 10	0.324 ± 0.100
5	10	+ 18.9 ± 0.9	105 ± 6	0.289 ± 0.017
	5	+ 38.7 ± 2.0	113 ± 8	0.304 ± 0.096
10	10	+ 24.0 ± 1.8	124 ± 13	0.434 ± 0.085

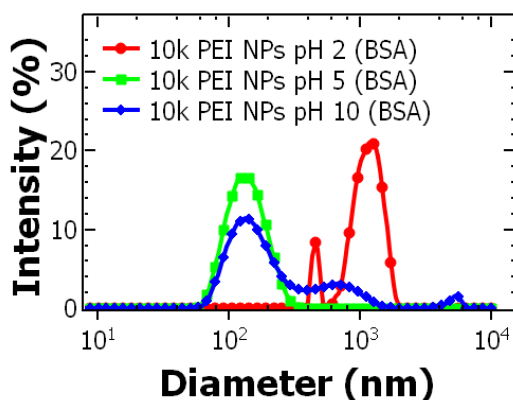


**Figure 21.** DLS of the 10kDa PEI nanoparticles formulated under different pH conditions by varying the pH of the BSA stream.

**Table 7.** Effect of pH of the BSA stream and PEI reservoir on 10kDa PEI nanoparticle formulation

pH of BSA	pH of PEI	Zeta potential (mV)
2	10	+ 23.2 ± 1.7
	2	+ 31.3 ± 3.6
5	10	+ 15.6 ± 0.4
	5	+ 30.2 ± 2.2
10	10	+ 15.7 ± 1.1

Based on these results, we propose that the mechanism of nanoparticle self-assembly differs between the 10kDa and the 750kDa PEI. Interestingly, 750kDa PEI NPs have a size of ~100 nm, similar to the hydrodynamic diameter of 750kDa PEI (**Table 4**). Therefore, the high molecular weight PEI aggregates. These aggregates serve as the nanoparticle template and a sink for absorbing the anionic BSA/TA complex. In contrast, nanoparticles formulated with 10kDa PEI (~150 nm) are much larger than their corresponding polymer in aqueous media (~5 nm). For this stabilizer, BSA/TA complex and precipitate. Particle assembly occurs as cationic 10kDa PEI adsorbs to the anionic BSA/TA precipitate via electrostatic interactions. This mechanism of nanoparticle self-assembly is analogous to previous work with FNP encapsulating coordination complexes or ion pairs formed during mixing [272–274,292,293]. Schematics of the particle self-assembly mechanisms for the 750kDa and 10kDa PEI are shown in **Figure 22**.

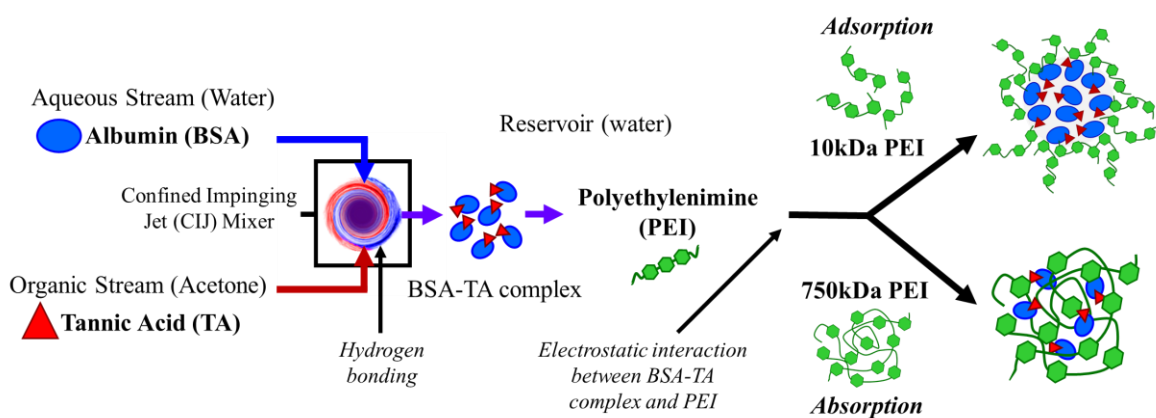


**Figure 22.** Schematic of proposed self-assembly mechanisms using 750kDa and 10kDa polyethylenimine (PEI) via Flash NanoPrecipitation (FNP) with PEI stabilizer. In the confined impinging jet (CIJ) mixer the bovine serum albumin (BSA) and tannic acid (TA) interact via hydrogen bonding to form an insoluble complex. Then the complex is immediately diluted in a reservoir containing PEI. The BSA-TA complex interacts with the PEI via electrostatic interaction. High molecular weight 750kDa PEI aggregates template nanoparticle assembly and absorb the BSA-TA precipitate. In contrast, 10kDa PEI adsorbs on the precipitating BSA-TA complex forming a core-shell structure.

Building on these results, we next sought to understand the effect of formulation parameters on nanoparticle assembly, specifically nanoparticle size. Typically, when nanoparticle assembly occurs due to hydrophobic interactions between the precipitation core material and micellizing block co-polymer, the nanoparticle size can be tuned with the mass ratio of the block co-polymer to the core materials as well as the total solids concentration [294].

The mass ratio of PEI to BSA-TA complex was adjusted from 3:1 to 2:1. However, for the 750kDa PEI, decreasing the relative amount of stabilizer resulted in unstable nanoparticles with visible precipitate forming within 24 hours (**Table 8**). For the 10kDa PEI, stable particles were achieved with lower relative amounts of stabilizer. While the size was not significantly affected, the PDI increased indicating less uniform particles (**Table 9**). Overall, we observe that the range of stabilizer to core ratio that forms stable, uniform nanoparticles is relatively narrow compared to the range used with hydrophobic interactions driving nanoparticle self-assembly. This finding is consistent with particle formation involving *in situ* coordination complexation [10] or cationic polysaccharides [295]. A ratio of 3:1 PEI to BSA-TA complex was used for subsequent experiments.

**Table 8.** Varying ratio of stabilizer to core for 750kDa PEI nanoparticles.

Polymer : Core	Initial		24 hrs	
	Size (nm)	PDI	Size (nm)	PDI
3 : 1	105 ± 2	0.279 ± 0.007	100 ± 3	0.260 ± 0.002
2 : 1	145 ± 39	0.442 ± 0.034	1257 ± 80	0.873 ± 0.109

**Table 9.** Varying total solids concentration and ratio of BSA to TA by mass for nanoparticles made with 10kDa PEI

Polymer : Core	Total solids (mg/mL)	Size (nm)	PDI	Zeta Potential (mV)
3 : 1	5.6	143 ± 8	0.166 ± 0.033	+ 14.8 ± 1.1
3 : 1	11.2	319 ± 185	0.075 ± 0.051	+ 11.8 ± 1.0
2 : 1	4.2	136 ± 42	0.357 ± 0.055	+ 15.0 ± 1.4

To vary particle size, the total solids concentration of the BSA, TA, and PEI in the final dispersion was varied from 5.6 mg/mL to 11.2 mg/mL; the 9:5 ratio of BSA:TA and 3:1 ratio of PEI:BSA/TA were held constant. We note that with the 750kDa PEI stabilizer, the total solids concentration did not affect particle size or stability (**Table 10**). Using 750kDa PEI as a stabilizer, particle assembly was templated by the aggregated polymer [289,291,296]. The results are comparable to previous reports with various PEI systems at constant charge ratios [297,298]. Interestingly, with the 10kDa PEI stabilizer, doubling the total solids concentration resulted in a two-fold increase in particle size from 143 ± 8 nm to 319 ± 185 nm while maintaining a PDI less than 0.300 (**Table 9**). The trend of increasing size with total solids concentration is comparable to previous results with FNP. During FNP, there is a rapid precipitate of the core materials simultaneously with the self-assembly and adsorption of the polymer on the surface of the nanoparticles. The growth of the nanoparticles is arrested by the adsorption of the polymer on the surface of the core, kinetically stabilizing the nanoparticle. By varying the concentration of the polymer relative to the core, the adsorption of the

polymer on the particle surface can be slowed thereby promoting greater core growth producing larger nanoparticles. This result has been attributed to a greater rate of core growth relative to the rate of nucleation which results in larger particle size [150,294]. Overall, these results support the mechanism of particle self-assembly in which TA precipitates the protein and further precipitation is arrested by adsorption of the 10kDa PEI stabilizer.

**Table 10.** Varying Total Solids of 750kDa PEI nanoparticles

Total Solids (mg/mL)	Zeta Potential (mV)	Initial		24 hrs	
		Size (nm)	PDI	Size (nm)	PDI
2.8 mg/mL	+ 23.7 ± 1.8	107 ± 7	0.276 ± 0.005	107 ± 7	0.276 ± 0.005
5.6 mg/mL	+ 19.5 ± 1.2	99 ± 2	0.270 ± 0.009	98 ± 1	0.264 ± 0.006
11.2 mg/mL	+ 18.0 ± 0.4	101 ± 1	0.276 ± 0.009	101 ± 1	0.271 ± 0.005

Salt and pH are expected to greatly affect electrostatic assemblies [299], thus we examine nanoparticle stability as a function of pH and ionic strength. After mixing, the nanoparticle dispersion had a pH of ~10 due to the PEI. As expected, decreasing the pH to 2 caused the nanoparticles with the 10kDa PEI stabilizer to disassemble, as indicated by DLS. The presence of a peak on the order of 10 nm can be attributed to unencapsulated BSA [282] (**Figure 24A**). At acidic conditions, protonation of PEI and BSA leads to a net positive charge on both molecules and charge repulsion, which destabilizes the particles. Similar results were observed after dialysis of the nanoparticles against deionized water (**Figure 23**) due to decrease in pH near the isoelectric point of BSA. Therefore, the pH of the nanoparticle dispersion should be greater than the isoelectric point of the protein to maintain particle stability. Surprisingly, the particles using the 750kDa stabilizer were stable below the isoelectric point of BSA (pH < 4.8) when both the PEI and BSA are expected to carry a net positive charge (**Figure 24B**). The PEI aggregates may provide a localized buffering effect preventing protonation of BSA [291].

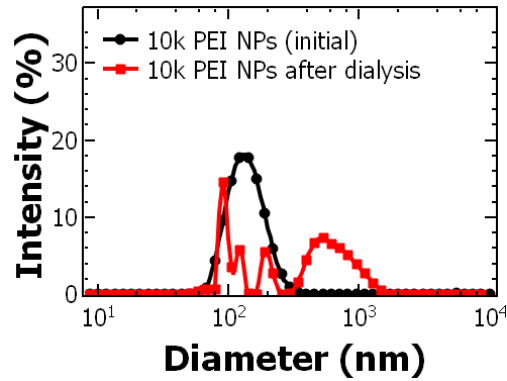


**Figure 23.** DLS of 10kDa PEI nanoparticles after dialysis.

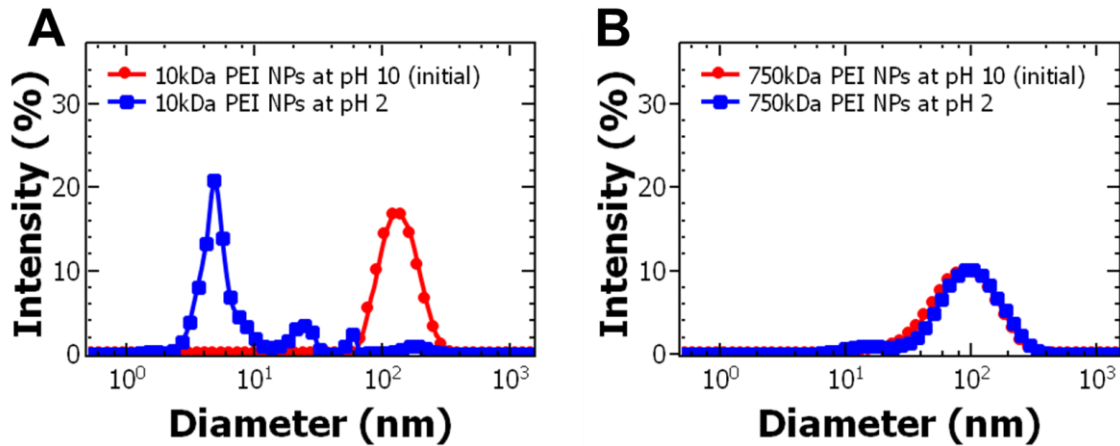


**Figure 24.** Effect of nanoparticle dispersion pH on size for (A) 10kDa polyethylenimine nanoparticles (PEI NPs) and (B) 750kDa PEI NPs. The size of the particles was measured 24 hours after adjusting the pH. The 10kDa PEI NPs destabilized under acidic conditions and released bovine serum albumin (BSA). The 750kDa PEI NPs did not change size at acidic pH.

To further understand particle stability, we investigated the effect of adjusting the ionic strength of the particle dispersion between 0.01 M to 0.3 M with monovalent and divalent salts. With the 750kDa PEI stabilizer, the measured size decreased slightly in the presence of salt at ionic strengths greater than 0.01 M (**Table 11**). The decrease in particle size with ionic strength has been observed previously and was attributed to decreased intra-molecular charge repulsion forces which allow for tighter PEI aggregate formation [291].

**Table 11.** Effect of ionic strength on particle stability of 750kDa PEI nanoparticles

Salt added	Concentration (mM)	Ionic Strength (M)	Diameter (nm)	PDI	Zeta Potential (mV)
Initial 750kDa PEI	0	0	107 ± 5	0.285 ± 0.004	18.5 ± 1.3
NaCl	10	0.01	89 ± 2	0.254 ± 0.007	12.7 ± 0.5
	30	0.03	87 ± 9	0.276 ± 0.039	15.8 ± 1.2
	100	0.1	91 ± 2	0.246 ± 0.004	14.8 ± 3.4
	300	0.3	84 ± 5	0.297 ± 0.032	20.0 ± 4.2
	CaCl <sub>2</sub>	10	0.03	84 ± 5	0.288 ± 0.028
	100	0.3	85 ± 4	0.306 ± 0.024	21.2 ± 4.0

In the presence of NaCl, the size of 10kDa PEI stabilized nanoparticles was not affected at ionic strengths less than 0.03 M and increased two-fold at ionic strength 0.3 M. The presence of salts introduce charge screening and reduce the electrostatic interactions between the 10kDa PEI stabilizer and anionic TA/BSA precipitate leading to the increase in particle size [289,300]. Interestingly, the diameter of the 10kDa PEI stabilized nanoparticles was 290 ± 6 nm in the presence of NaCl, compared to 188 ± 7 nm with CaCl<sub>2</sub> at the same ionic strength (0.3 M) (**Table 12**). The difference in particle size in the presence of Ca<sup>2+</sup> and Na<sup>+</sup> ions at the same ionic strength can be attributed to a 3-fold difference in ion concentration of Na<sup>+</sup> ions compared to Ca<sup>2+</sup> which resulted in greater charge screening and thus larger particle size. Additionally, calcium promotes protein/TA precipitation compared to sodium [278] and specific BSA-calcium interactions promote BSA aggregation compared to sodium [301], which prevents particle swelling.

**Table 12.** Effect of ionic strength on 10kDa PEI nanoparticle properties.

Salt added	Concentration (mM)	Ionic Strength (M)	Diameter (nm)	PDI	Zeta Potential (mV)
Initial 10kDa PEI	0	0	146 ± 2	0.125 ± 0.020	15.7 ± 2.0
NaCl	10	0.01	145 ± 2	0.065 ± 0.019	13.5 ± 2.6
	30	0.03	139 ± 2	0.069 ± 0.007	13.4 ± 2.0
	100	0.1	194 ± 3	0.035 ± 0.023	14.3 ± 0.3
	300	0.3	290 ± 6	0.110 ± 0.024	11.8 ± 1.4
	CaCl <sub>2</sub>	10	0.03	138 ± 6	0.351 ± 0.019
	100	0.3	188 ± 7	0.148 ± 0.022	16.1 ± 0.5

Taken together, these results demonstrate that self-assembled nanoparticles are stable at physiologically relevant ionic strengths (~0.15 M). The particles are pH labile. Specifically, they are stable at basic pH (e.g. 7.4) and disassemble at acidic pH. Such properties may be promising for controlled release application such as intracellular delivery [10,41–43].

Finally, we quantified the amount of BSA in the nanoparticles in terms of encapsulation efficiency and protein loading for both molecular weights of PEI via Bradford assay. To understand the role of TA in nanoparticle assembly, we compared formulations with and without TA. Interestingly, while TA did not affect particle size or zeta potential (**Table 13**), it greatly affected the amount of protein incorporated into the nanoparticles (**Table 14**). For example, using the 750kDa PEI stabilizer, the protein encapsulation increased from 50% with TA to 74% without the presence of TA. This result suggests that the charge density of BSA alone compared to the BSA/TA complex enhances interactions with PEI. Additionally, the absence of TA may increase BSA-PEI interactions. In contrast, with the 10kDa PEI NPs, the protein encapsulation increased from 8% without TA to 79% with TA. This result supports the mechanism of self-assembly in which TA/BSA complex and precipitate and further growth of the precipitate is prevented by adsorption of the 10kDa PEI stabilizer.

**Table 13.** Effect of TA on nanoparticle formulation

PEI MW	Formulated with TA?	Size (nm)	PDI	Zeta Potential (mv)
10kDa	No	141 ± 13	0.196 ± 0.053	+ 16.1 ± 1.4
	Yes	153 ± 7	0.125 ± 0.022	+ 15.7 ± 1.0
750kDa	No	90 ± 11	0.301 ± 0.064	+ 23.5 ± 2.8
	Yes	101 ± 3	0.274 ± 0.007	+ 20.6 ± 1.8



**Table 14.** Effect of tannic acid (TA) on protein encapsulation.

Sample	Condition	Encapsulation Efficiency (EE%)	Drug Loading (DL%)
10kDa PEI NPs	no TA	8% ± 3%	1% ± 0%
	with TA	79% ± 7%	13% ± 1%
750kDa PEI NPs	no TA	74% ± 6%	12% ± 1%
	with TA	50% ± 10%	8% ± 2%

Interestingly, the 10kDa PEI stabilizer resulted in higher protein loading (13% compared to 8%) and encapsulation efficiency (79% compared to 50%) than achieved with the 750kDa PEI stabilizer (**Table 14**). Nanoparticle assembly using the 10kDa PEI that occurs due to adsorption of the stabilizer to the precipitate forms kinetically trapped core-shell structures and enhances protein encapsulation compared to the absorption of the precipitate with the 750kDa PEI aggregates. This improvement in loading is analogous to traditional FNP with hydrophobic small molecules [305]. Interestingly, in the absence of TA, protein encapsulation efficiency in the 750kDa PEI NPs increased from 50% to 74%. This could suggest that proteins can be encapsulated with FNP in the absence of organic solvents and without the need for precipitation limiting protein denaturation and reduction in functionality. Excitingly, the encapsulation efficiency of protein via rapid mixing with 10kDa PEI is greater (~ 80%) than generally reported for encapsulating biologics via nanoprecipitation (7 – 40%) [273,306]. These results suggest that FNP facilitated by TA/BSA complexation and precipitation is a highly efficient, rapid process for encapsulating proteins.

### 3.4. Conclusions

Overall, we have demonstrated a rapid, single-step method using Flash NanoPrecipitation for encapsulating biologics (i.e. proteins) with high encapsulation efficiency (up to ~80%). Nanoparticle formation involves complexation and precipitation with tannic acid and stabilization with a cationic polyelectrolyte. Nanoparticle self-assembly is driven by hydrogen bonding between TA and protein,

then electrostatic interactions between the TA/protein precipitate and polyelectrolyte stabilizer. The resulting particles are stable at physiological ionic strengths and pH labile, i.e. stable above the isoelectric point of the protein and disassemble at pHs below the isoelectric point of the protein, to facilitate potential controlled release applications.

## 4. Chapter 4: Rapid Self-Assembly of Polymer Nanoparticles for Synergistic Codelivery of Paclitaxel and Lapatinib via Flash NanoPrecipitation

---

**Published:** [307] Levit, S.L.; Yang, H.; Tang, C. Rapid Self-Assembly of Polymer Nanoparticles for Synergistic Codelivery of Paclitaxel and Lapatinib via Flash NanoPrecipitation. *Nanomaterials* **2020**, *10*, 561.

### Abstract

Taxol, a formulation of paclitaxel (PTX), is one of the most widely used anticancer drugs, particularly for treating recurring ovarian carcinomas following surgery. Clinically, PTX is used in combination with other drugs such as lapatinib (LAP) to increase treatment efficacy. Delivering drug combinations with nanoparticles has the potential to improve chemotherapy outcomes. In this study, we use Flash NanoPrecipitation, a rapid, scalable process to encapsulate weakly hydrophobic drugs ( $\log P < 6$ ) PTX and LAP into polymer nanoparticles with a coordination complex of tannic acid and iron formed during the mixing process. We determine the formulation parameters required to achieve uniform nanoparticles and evaluate the drug release *in vitro*. The size of the resulting nanoparticles was stable at pH 7.4, facilitating sustained drug release via first-order Fickian diffusion. Encapsulating either PTX or LAP into nanoparticles increases drug potency (as indicated by the decrease in IC-50 concentration); we observe a 1500-fold increase in PTX potency and a 6-fold increase in LAP potency. When PTX and LAP are co-loaded in the same nanoparticle, they have a synergistic effect that is greater than treating with two single-drug loaded nanoparticles as the combination index is 0.23 compared to 0.40, respectively.

## 4.1. Introduction

Ovarian cancer remains one of the most difficult cancers to treat due to late stage diagnosis and its highly malignant nature [102]. Chemotherapies such as Taxol, a formulation of paclitaxel (PTX), remains to be one of the most widely used cancer treatments particularly for recurring ovarian carcinomas following surgery [102–104]. The mechanism of action for PTX is binding to the  $\beta$ -subunit of tubulin at two sites, which stabilized the tubulin polymers preventing cytoskeletal rearrangement for cellular function [105–107]. Stabilizing tubulin results in cell cycle arrests in the G<sub>2</sub>/M phase [107]. However, there are many challenges with the use of Taxol. There are severe systemic side effects associated with PTX treatment such as low blood pressure, risk of infection, formation of blood clots, and neurotoxicity [108–110]. Additionally, PTX is poorly water-soluble and has low permeability which limits drug efficacy due to low drug concentrations reaching the tumor site [248]. Clinically, PTX is used in combination with other drugs to increase the efficacy of treatment by targeting multiple pathways [115,238,239].

Paclitaxel is often used in combination with Lapatinib (Tykerb, LAP), a class of tyrosine kinase inhibitors [111–114]. Several studies observed an increase in drug efficacy in terms of tumor cell death and decrease in tumor volume when PTX and LAP were used in combination [112,308]; in some cases, a synergetic effect was observed [309]. However, combination treatment required premedication before injection, i.e., complex treatment regimens with multiple methods of administration [250,251]. Formulation of drug combinations in nanoparticles could overcome low solubility and permeability of the drugs to deliver an effective drug dosage to the tumor site and simplify drug regimens to improve patient adherence, while decreasing side effects [108,232,233].

Co-encapsulation of PTX and LAP may improve the co-localization of the drugs in the tumor tissue and increase drug efficacy [108,234–237]. For example, PTX and LAP have been co-formulated in a core-shell structure using polymer micelles. Lapatinib was conjugated to a PEGylated block

copolymer and formulated into micelles encapsulating PTX in the core. Interestingly, formulation into the polymer micelles increased the potency of the PTX as indicated by a 2-fold decrease in the half maximal inhibitory concentration (IC-50) concentration in certain types of breast cancer [235]. Although the increase in potency via formulation into nanoparticles is exciting, this approach requires multiple steps and covalent modifications of LAP which results in the formation of a new compound, requiring further testing for FDA approval, a costly and time-consuming process [271].

Nanoparticle formulations co-encapsulating PTX and LAP without chemical modification of LAP has also been considered [108,234–237,258]. Vergara et al. co-encapsulated LAP and PTX in polyelectrolyte nanoparticles by sonication-assisted layer-by-layer (SLBL) technique. To formulate these nanoparticles, PTX-chitosan nanoparticles were first formed, followed by the sequential deposition of alginic acid and chitosan coatings. Lapatinib was co-deposited with chitosan to achieve nanoparticles with a PTX core and LAP shell. The core-shell nanoparticles showed a significant decrease in cell viability *in vitro* compared to PTX loaded nanoparticles and free PTX [108]. While the results are promising, the formulation of the nanoparticles was time intensive as each deposition of each layer required 20-45 minutes.

Co-loading both LAP and PTX in the nanoparticle core has been achieved using lipopolymer [234] or Pluronic F127 polymeric micelles [310]. Formulation using the Pluronic F127 suppressed tumor cell proliferation and decreased IC-50 by 10-fold relative to free drug combination treatment of PTX and LAP [310]. These nanoparticles provide the basis for further improvements of drug combinations; however, the formulation method is challenging to scale up [311]. Furthermore, the drug effect when co-delivering drugs in nanoparticle form in terms of synergy is not well established.

In this study, we extend the use of Flash NanoPrecipitation (FNP) to PTX and LAP by leveraging *in situ* coordination complexation of tannic acid and iron. Flash NanoPrecipitation enables the rapid, scalable formulation of drug combinations [259]. However, this method has generally been

limited to highly hydrophobic materials ( $\log P > 6$ ) [265]. Encapsulating PTX and LAP using FNP is challenging due to their relatively weak hydrophobicity (PTX,  $\log P = 3.2$  and LAP,  $\log P = 5.4$ ). We encapsulate drugs ( $\log P < 6$ ) via *in situ* coordination complex formation of tannic acid-iron (TA-Fe) and stabilization with an amphiphilic block copolymer. Our focus is understanding how incorporating multiple drugs affects nanoparticle self-assembly. Based on our understanding, we establish the formulation parameters to form PTX NPs, LAP NPs and PTX-LAP NPs with comparable size (~100 nm in diameter). We perform initial drug release studies *in vitro*, focusing on the release of PTX. We evaluate the potency of the nanoparticles *in vitro* using an ovarian cancer cell line OVCA-432. The core of our preliminary *in vitro* evaluation is based on IC-50 values; the effect of co-encapsulating the drugs in terms of synergy using the combination index is analyzed.

## 4.2. Materials and Methods

### 4.2.1. Materials

HPLC grade tetrahydrofuran (THF), dimethyl sulfoxide (DMSO), acetonitrile, and Tween 80 were purchased from Fisher Scientific (Pittsburg, PA). ACS grade tannic acid (TA) and ACS grade iron (III) chloride hexahydrate (97%) were purchased from Sigma-Aldrich (St. Louis, MO). Paclitaxel (PTX, >98%) and lapatinib (LAP, >98%) were obtained from Cayman Chemical Company (Ann Arbor, MI); phosphate buffered saline without calcium and magnesium was purchase from Lonza (Basel, Switzerland). Polystyrene-b-polyethylene glycol (1600-b-500 g/mol) (PS-b-PEG) was obtained from Polymer Source (Montreal, Canada) and was purified by dissolving in THF (~40°C) and precipitating into diethyl ether then dried by vacuum for two days as previously described [279].

#### 4.2.2. Cell Culture

Ovarian cancer cell line OVCA-432 was a kind gift from Dr. Xianjun Fang from Virginia Commonwealth University. The OVCA-432 cells were cultured in RPMI-1640 media containing 2 mM L-glutamine (ATCC, Manassas, VA) supplemented with 10% Fortified Bovine Calf Serum (FBS, HyClone Cosmic Calf Serum, Fisher Scientific, Pittsburg, PA), 100 U/mL penicillin and 100 µg/mL streptomycin (Gemini Bio-Products, West Sacramento, CA), and cultured at 37 °C at 5% CO<sub>2</sub>. The cells were passaged once a week.

#### 4.2.3. Nanoparticle Formulation

Flash NanoPrecipitation (FNP) was used to prepare polymer-based nanoparticles encapsulating the anti-cancer drugs with a hand-operated confined impinging jet (CIJ) mixer with dilution as previously described [272,312]. Four nanoparticles were formulated that either encapsulated the TA-Fe complex (TA-Fe NPs), PTX (PTX NPs), LAP (LAP NPs), or both PTX and LAP (PTX-LAP NPs).

To self-assemble the nanoparticles, PS-*b*-PEG, TA (4 mg/mL), and one or more of the drugs (PTX and LAP) were dissolved in a water-miscible organic solvent (e.g. THF or DMSO) by sonicating (~40°C) for 10 minutes to formulate the organic stream. The organic stream was rapidly mixed with the Fe<sup>3+</sup> (aq., 1 mg/mL) at equal volumes, typically 1 mL, in the CIJ mixer. The effluent from the mixer was immediately diluted in 1X PBS at pH 7.4 for a final organic solvent/water ratio of 1:9 by volume. The drug concentration in the organic stream of PTX and LAP was varied from 0.5 mg/ml to 2 mg/mL; the block copolymer concentration was varied relative to the core material. Specifically, the core material was considered the TA and Fe<sup>3+</sup> for the TA-Fe NPs, and for the drug-loaded nanoparticles it was determined as TA and the drugs encapsulated. The ratio of the PS-*b*-PEG to the core material was varied between 1:1 to 2:1 by mass.

Within 24 hrs of formulation, the nanoparticles were filtered to remove the organic solvent, unencapsulated drug(s), and excess TA and  $\text{Fe}^{3+}$  with Amicon Ultra-2 Centrifugal filters (Amicon Ultra centrifuge filter (Ultracel 50K, 50,000 NMWL), Merck Millipore Ltd, Burlington, MA) by centrifuging at 3700 rpm for ~15-30 minutes (5804 R 15 amp version, Eppendorf, Hamburg, Germany). The nanoparticle pellet was resuspended with 1X PBS to a nominal concentration ~25 mg/mL of total solids and stored at ~4 °C. The nanoparticles were used within 5 days of the FNP to ensure there was minimal change in particle size and drug loss.

#### 4.2.4. *Nanoparticle Characterization*

The size, polydispersity (PDI), and zeta potential of the nanoparticles were characterized immediately after FNP and after filtration using dynamic light scattering (Malvern Zetasizer ZS, Malvern Instruments Ltd, Malvern, United Kingdom). The nanoparticle size and PDI were measured by averaging 4 measurements at a scattering angle of 173°. Nanoparticles populations with a PDI of less than 0.400 were considered uniform [313]. The nanoparticle size stability at 4 °C was observed by measuring size and PDI for up to 3 weeks after formulation. The concentration of the nanoparticle dispersion following filtration was determined by thermogravimetric analysis (TGA) (Pyris 1 TGA, Perkin Elmer, Waltham, MA).

Transmission electron microscopy (TEM) samples were prepared by diluting the filtered nanoparticle dispersions with DI water 1:20 by volume ratio and pipetting 5  $\mu\text{L}$  three times onto a TEM grid with Formvar/Carbon support films (200 mesh, Cu, Ted Pella, Inc, Redding, CA) and dried under ambient conditions. Dilution was necessary to prevent aggregation during drying. The samples were imaged with a JEOL JEM-1230 (Peabody, MA) at 120 kV.

To determine the drug content of the nanoparticles, acetonitrile (1.8 mL) was added to nanoparticles (50  $\mu\text{L}$ ) filtered with Amicon filter, as previously described, and the sample was



vortexed so that the nanoparticles would disassemble. The sample was centrifuged at 10,000 rpm for 6 minutes, and then the supernatant was collected for reverse-phase high Performance Liquid Chromatography (RP-HPLC) (1260 HPLC with Quaternary Pump and UV-Vis Diode Array Detector, Agilent, Santa Clara, CA) fitted with a Luna® 5 µm C18 100 Å, LC Column 250 x 4.6 mm (Phenomenex, Torrance, CA). The sample was eluted with degassed acetonitrile and water gradient at a flow rate of 1 mL/min (0-1 minute at 80:20, 1-6 of ramp up to 0:100, 6-8 minutes at 0:100, and ramp down to 80:20 between 8-9 minutes). PTX was measured at a wavelength of 228 nm with a retention time of ~8 minutes and LAP was measured at 332 nm with a retention time of ~9 minutes. The concentration of each drug was determined by comparing the peak areas with the standard calibration curve. Encapsulation efficiency (EE%) and drug loading (DL%) were calculated based on equations 10 and 11, respectively, and the values reported are the average and standard deviation of three trials.

$$\text{encapsulation efficiency (EE\%)} = \frac{\text{Mass of drug encapsulated}}{\text{Initial mass of drug}} \times 100\% \quad (\text{Eq. 10})$$

$$\text{drug loading (DL\%)} = \frac{\text{Mass of drug encapsulated}}{\text{Total nanoparticle mass}} \times 100\% \quad (\text{Eq. 11})$$

#### 4.2.5. Nanoparticle Drug Release In Vitro

To measure the drug release, 500 µL of concentrated nanoparticle dispersion was loaded into 7,000 MWCO dialysis unit (Slide-A-Lyzer® MINI Dialysis Unit, Thermo Scientific, Waltham, MA) and incubated in 0.5% Tween 80 in PBS at pH 7.4 at 37°C, which was replaced every day of the experiment. Samples (32 µL) at 0 h, 3 h, 6 h, 24 h, 48 h, day 4, day 6, and day 10 were taken from the nanoparticle dispersion and the remaining drug concentration was determined by RP-HPLC as previously described. Three replicates of each drug-loaded nanoparticle dispersion were tested.

#### 4.2.6. Cytotoxicity

OVCA-432 cells were seeded at a density of  $15 \times 10^3$  cell/well in a 96-well plate containing 100  $\mu\text{L}$  of complete medium. The cells were incubated at  $37^\circ\text{C}$  in 5%  $\text{CO}_2$  overnight. Then the media was replaced with 100  $\mu\text{L}$  medium containing free-drug or nanoparticles and treated for 48 hrs. Stock solution of free-drug were prepared by dissolving PTX (12 mg/mL) or LAP (5 mg/mL) in DMSO and sonicating for 5 minutes. Then the drugs were diluted with complete media and serial dilutions were performed to achieve concentrations between 200 - 0.0002  $\mu\text{g}/\text{mL}$ . Additional DMSO was added for a final DMSO concentration of 2% v/v. The nanoparticles were concentrated with Amicon filters (50kDa MWCO) as previously described and the nanoparticle pellet was diluted with 1X PBS. The PTX NPs and LAP NPs were individually concentrated to 1000  $\mu\text{g}/\text{mL}$  of drug. The PTX-LAP NPs were concentrated to 500  $\mu\text{g}/\text{mL}$  relative to PTX. The nanoparticle-loaded medium was prepared by diluting the stock nanoparticle dispersion with complete media and performing serial dilutions for final concentrations between 200 - 0.0002  $\mu\text{g}/\text{mL}$ . The cells were also treated with complete media and 2% DMSO media as controls for comparison. There were 6 replicates for each experimental condition. After 48 hrs, the cell viability was measured with WST-1 assay (Sigma-Aldrich, St. Louis, MO) according to manufacturing instructions. Briefly, the drug-loaded medium was removed and 100  $\mu\text{L}$  of RPMI-1640 with Phenol Red (Fisher Scientific, Pittsburg, PA) containing 10% WST-1 solution was added to each well as well as to 6 empty wells. The cells were incubated between 45 - 90 minutes until there was a visible color change to a golden-yellow or the absorbance of control wells reached at least 0.700 measured with a microplate reader (VersaMax ELISA microplate reader, Molecular Devices, San Jose, Ca) at a wavelength of 440 nm with background subtraction of 640 nm. The cell viability was determined by subtracting the background noise (wells containing only 10% WST-1 in media) from the samples and then dividing the sample absorbance by the average absorbance of the

untreated wells. The relative cell viability was expressed as a percentage of the untreated cells with mean  $\pm$  standard deviation of six replicates.

#### 4.2.7. *Cell cycle analysis by flow cytometry*

The cells were seeded at a density of  $20 \times 10^4$  cells/mL in a 35 mm petri dish containing 3 mL of complete media. The cells were incubated at 37°C and 5% CO<sub>2</sub> until 90% confluence and the media was replaced every 2 days. The cells were treated with either free PTX, free LAP, PTX NPs, LAP NPs at the IC-50 concentration or left untreated for 48 hrs at 37 °C. After 48 hrs treatment, the cells were stained with Propidium Iodide (PI Flow Cytometry Kit, Abcam, Cambridge, MA) for flow cytometry according to manufacturing instructions. Briefly, the cells were trypsinized and the aspirated medium and PBS were collected to minimize cell loss. The cells were centrifuged at 700 x g for 5 minutes as necessary. The cells were washed with 1X PBS and fixed with 66 % ethanol by slowly adding ethanol to PBS during vortexing. The cells were stored in ethanol at 4 °C for at least 2 hrs and up to 4 days. The cells were centrifuged and washed with PBS to remove the ethanol. The 1X Propidium Iodide and RNase solution was prepared immediately prior to use by mixing 5% v/v of 20X Propidium Iodide and 0.05% v/v 200X RNase in 1X PBS. Then the cells were resuspended in 200  $\mu$ L/500,000 cells of 1X Propidium Iodide and RNase solution and incubated in the dark at 37 °C for 30 minutes. Prior to flow cytometry, the cell samples were stored on ice and filtered through a cell strainer (Falcon Test Tube with Snap Cap, Fisher Scientific, Pittsburg, PA). Flow cytometry was performed on a BD FACSCanto™ II Analyzer (BD Biosciences, San Diego, CA) and 10,000 cells were analyzed at an excitation of 488 nm and emission of 670 nm. The samples were analyzed in triplicate.

### 4.3. Results and Discussion

#### 4.3.1. Nanoparticle Preparation and Characterization

Flash NanoPrecipitation (FNP) is a well-established polymer-directed self-assembly method for preparing size-tunable nanoparticles encapsulating highly hydrophobic molecules ( $\log P > 6$ ). Since nanoparticle self-assembly involves adsorption of the hydrophobic block of the block copolymer to a precipitating core material, this process has generally been limited to highly hydrophobic materials with  $\log P$  of 6 or greater [259,265]. Since PTX is not sufficiently hydrophobic to form stable particles via FNP directly [314], we explore an alternative approach in which we encapsulate PTX ( $\log P = 3.2$ ) and LAP ( $\log P = 5.4$ ) using a pH-labile, tannic acid-iron (TA-Fe) based nanoparticle platform [272].

To prepare TA-Fe based nanoparticles, FNP was performed by mixing drug(s), TA and PS-b-PEG dissolved in a water-miscible (THF or DMSO) organic solvent with iron (III) chloride dissolved in water in a confined impinging jet mixer. The effluent from the mixer was quenched in a bath of PBS, pH 7.4, conditions under which the TA-Fe coordination complex is expected to be insoluble. Upon rapid mixing, the TA and  $\text{Fe}^{3+}$  form an insoluble coordinate complex which co-precipitates with the drug(s) forming the particle core. Precipitation of the core materials is arrested by adsorption of the hydrophobic block of the block copolymer and the PEGylated end of the block copolymer sterically stabilizes the nanoparticle in dispersion (**Figure 25**). The dispersions appeared red which is consistent with the tris-complex of TA and iron expected at pH 7.4 [294,311]. Nanoparticles encapsulating the TA-Fe complex (TA-Fe NPs) are  $109 \pm 5$  nm (**Figure 26**) with a zeta potential of  $-21.4 \pm 2.1$  mV consistent with other PEGylated nanoparticles [265,284].

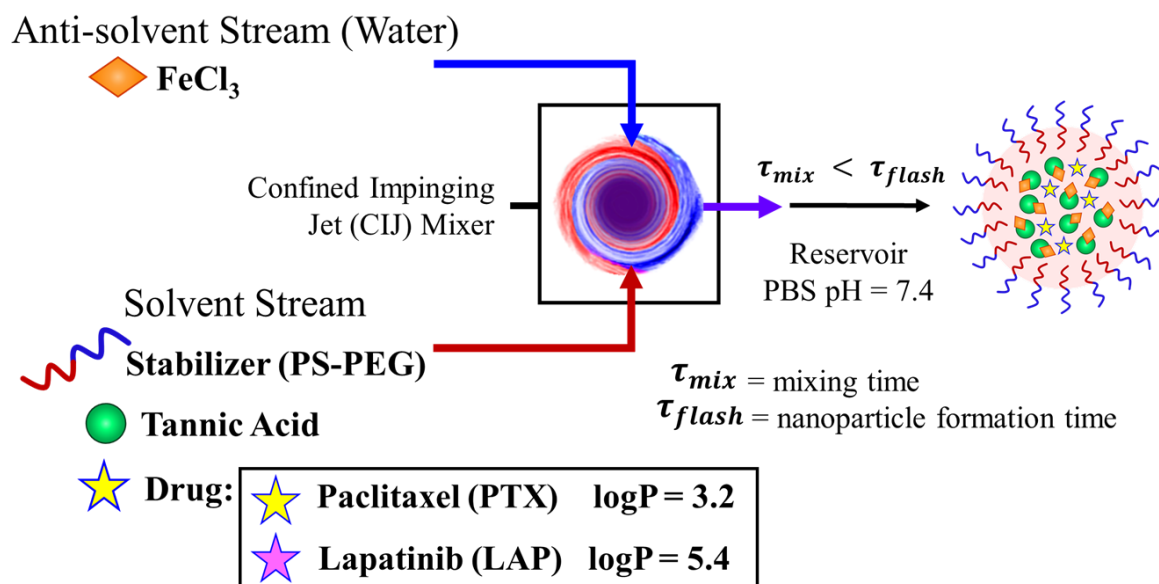


**Figure 25.** Overview of nanoparticle synthesis with Flash NanoPrecipitation to encapsulate paclitaxel and lapatinib with a tannic acid (TA) and iron coordination complex using an amphiphilic block copolymer stabilizer. The organic solvent stream contains the stabilizer, PS-b-PEG, TA, and one or more drugs of interest. The organic stream is rapidly mixed with the aqueous stream containing iron using a CIJ mixer. Upon rapid mixing, the TA and iron form an insoluble complex which facilitates the precipitation and encapsulation of paclitaxel and lapatinib. The resulting nanostructures are kinetically trapped.

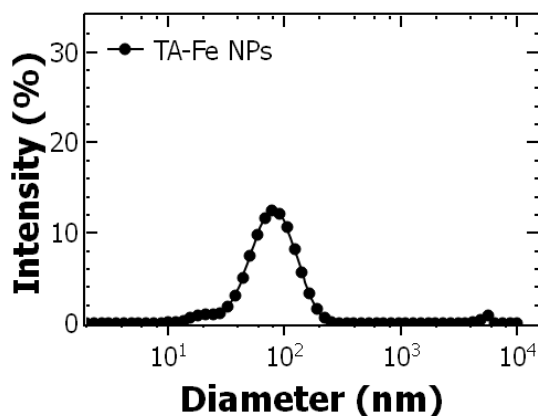


**Figure 26.** Dynamic light scattering of TA-Fe NPs (containing no drugs).

Our initial goal was to achieve uniform PTX-loaded nanoparticles on the order of 100 nm to allow for passive targeting [315]. We examined the effect of organic solvent selection, total solids concentration, ratio of the block copolymer to core materials, and drug concentration on the ability to make uniform particles and resulting nanoparticle size.

Two water-miscible organic solvents were considered, THF and DMSO, as the block copolymer, TA, LAP and PTX were sufficiently soluble for the self-assembly of nanoparticles via FNP. However, when DMSO was used for the organic stream, a visible red-purple precipitate formed immediately upon mixing in the reservoir. With THF, stable PTX-loaded nanoparticle dispersions were achieved with a zeta potential of  $-22.1 \pm 2.1$  mV and no precipitate was observed. These results suggest that co-precipitation of PTX and the TA-Fe complex and the rate of PS-b-PEG self-assembly is more appropriately matched using THF as a solvent than DMSO as a solvent. Thus, THF was used as a solvent in all further experiments.

To further tune the size of the PTX-loaded particles, we examined the effect of other formulation parameters. At a total solids concentration of 18 mg/mL in the streams and above, there are two size populations in the intensity weighted distribution with peak diameter  $\sim 30$  nm and  $\sim 100$  nm. The population with hydrodynamic diameter of  $\sim 30$  nm can be attributed to empty block copolymer micelles [271,280] produced with the PTX-loaded nanoparticles of  $\sim 100$  nm (**Table 15**). The inability to form uniform particles at high concentrations has been previously observed and could be attributed to a limited affinity between stabilizer and TA-Fe precipitate at high iron concentrations [271].

**Table 15.** Summary of paclitaxel nanoparticle formulations.

Total solids (mg/mL)	Ratio of BCP: core	PTX Concentration (mg/mL)	Size 1 (nm)	Size 2 (nm)	PDI
18	2:1	1	$107 \pm 2$	$32 \pm 1$	$0.275 \pm 0.009$
36	2:1	2	$113 \pm 6$	$31 \pm 1$	$0.372 \pm 0.012$
11	1:1	1	$170 \pm 33$	0	$0.142 \pm 0.053$
13.5	1.5:1	1	$128 \pm 7$	0	$0.244 \pm 0.034$
16	2:1	1	$111 \pm 10$	0	$0.255 \pm 0.021$
19	2:1	2	$117 \pm 3$	$20 \pm 1$	$0.268 \pm 0.009$
16	2:1	1	$111 \pm 10$	0	$0.255 \pm 0.021$
14.5	2:1	0.5	$134 \pm 42$	0	$0.232 \pm 0.145$

\* The average  $\pm$  standard deviation of 3 replicates of FNP are reported.

To improve particle uniformity, we next examined the ratio of the block copolymer to core materials (BCP:core with the core defined as concentration of TA and PTX in the formulation) at reduced total solids concentration. Specifically, three BCP:core ratios, i.e., 1:1 1.5:1 and 2:1 were studied with total solids concentration less than 16 mg/mL. All three ratios produced uniform nanoparticles with a PDI < 0.400. At a 1:1 BCP:core ratio, the particles were  $170 \pm 33$  nm. Increasing the amount of block copolymer from a 1:1 to 2:1 BCP:core ratio produced in a 35% decrease in particle size (**Table 15**) and a 2:1 BCP:core ratio uniform PTX-loaded particles with a hydrodynamic diameter of  $117 \pm 3$  nm were achieved. TEM confirmed the nanoparticles were spherical and the size was consistent with DLS (**Figure 27A**). This trend has been attributed to an increase in the rate of self-assembly relative to the rate of core growth, limiting the growth of the core before it is kinetically stabilized. These results are comparable to FNP systems using hydrophobic core materials ( $\log P > 6$ ) in which the particle size can be tuned by varying the ratio of the block copolymer to the core [259,293].

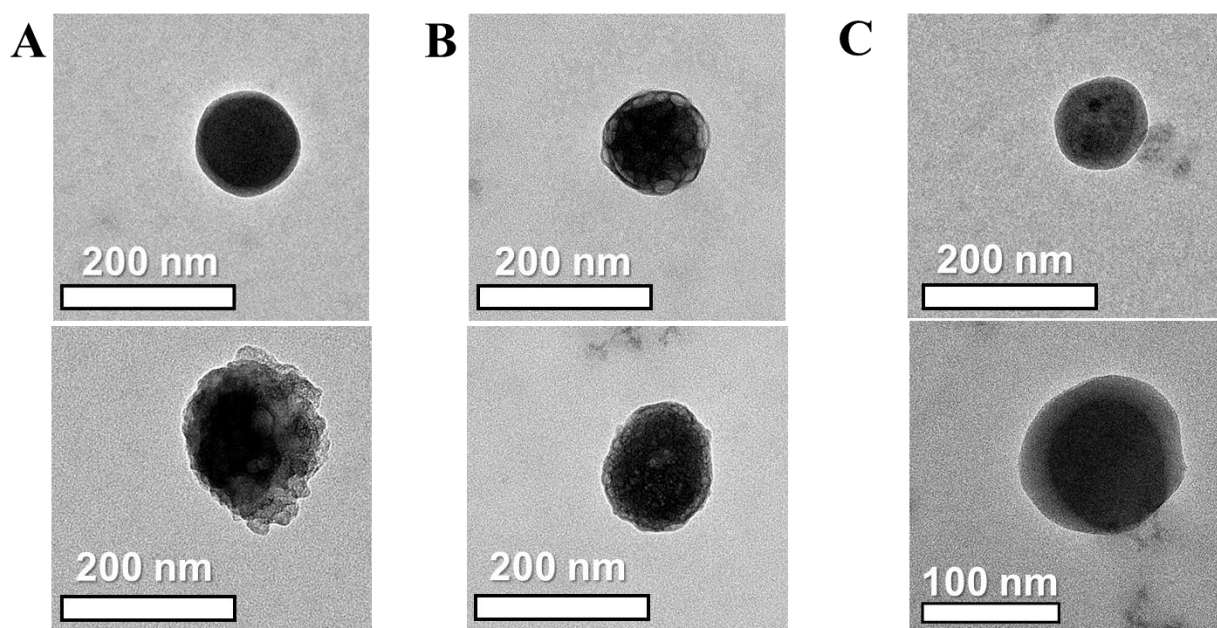


**Figure 27.** TEM images of (A) PTX NPs, (B) LAP NPs, and (C) PTX-LAP NPs.

Thus, we next investigated the effect of PTX concentration to maximize the drug loading in the nanoparticle while maintaining uniform, ~100 nm nanoparticle formulations (**Figure 28**). We varied the PTX concentration from 0.5 to 2 mg/mL in the organic stream. Increasing the PTX concentration to 2 mg/mL resulted in two size populations with peak diameters of ~100 nm and ~20 nm (**Table 15**) possibly due to a mismatch time scales of complexation/precipitation and block copolymer micellization at higher concentrations of drug. The highest concentration that we used that resulted in uniform PTX-loaded particles was 1 mg/mL.

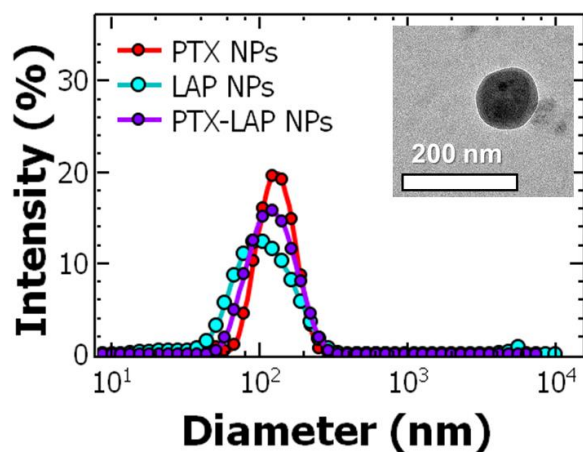


**Figure 28.** Representative dynamic light scattering results of uniform (red) paclitaxel nanoparticle (PTX NPs), (blue) lapatinib nanoparticle (LAP NPs), and (purple) co-loaded paclitaxel-lapatinib nanoparticle (PTX-LAP NPs) samples produced at ~100 nm (each DLS curve is the average of  $n = 4$  measurements). Representative transmission electron microscopy (TEM) image of PTX-LAP NPs (scale bar = 200 nm), as inset.

In parallel with formulating PTX-loaded nanoparticles, we also used FNP to encapsulate LAP within TA-Fe nanoparticles via *in situ* complexation with the aim of achieving uniform LAP nanoparticles ~100 nm in diameter.

Similar to PTX, total solids concentration above 36 mg/mL in the streams resulted in two size populations in the intensity weighted distribution with peak diameter ~30 nm and ~100 nm due to the formation empty block copolymer micelles. Lowering the total solids concentration to 16 mg/mL,



nanoparticle dispersions with uniform size were achieved (**Table 16**). Nanoparticle dispersions with uniform particle size were obtained at BCP to core ratios between 2:1 and 1:1. Interestingly, the size of the LAP-loaded NPs was independent of BCP: core ratio. This result indicates that the concentrations used the rate of LAP/TA-Fe co-precipitation is comparable to the self-assembly of PS-b-PEG micellization.

**Table 16.** Summary of lapatinib nanoparticle formulations.

Total solids (mg/mL)	Ratio of BCP:core	Size 1 (nm)	Size 2 (nm)	PDI
16	2:1	91 ± 10	0	0.214 ± 0.038
36	2:1	106 ± 5	26 ± 4	0.288 ± 0.004
10.5	1:1	134 ± 8	0	0.255 ± 0.012
15.3	2:1	126 ± 7	0	0.380 ± 0.037

\* The average ± standard deviation of 3 replicates of FNP are reported.

Next, we investigated the effect of LAP concentration to maximize the drug loading in the nanoparticle while maintaining uniform size distributions (diameter ~100 nm). At LAP concentrations 2 mg/mL nanoparticle were produced at ~150 nm and ~30 nm (**Figure 29**). These results are comparable to the results observed with PTX. Reducing the drug concentration, uniform, ~100 nm particles were achieved and confirmed with TEM (**Figure 28** and **Figure 27B**). These results suggest co-precipitation of these weakly hydrophobicity drugs ( $\log P < 6$ ) with the TA-Fe core affect timescale of precipitation as well as the affinity of the stabilizer and the core that can result in the formation of empty micelles and need to be considered when formulating these drug-loaded nanoparticles.

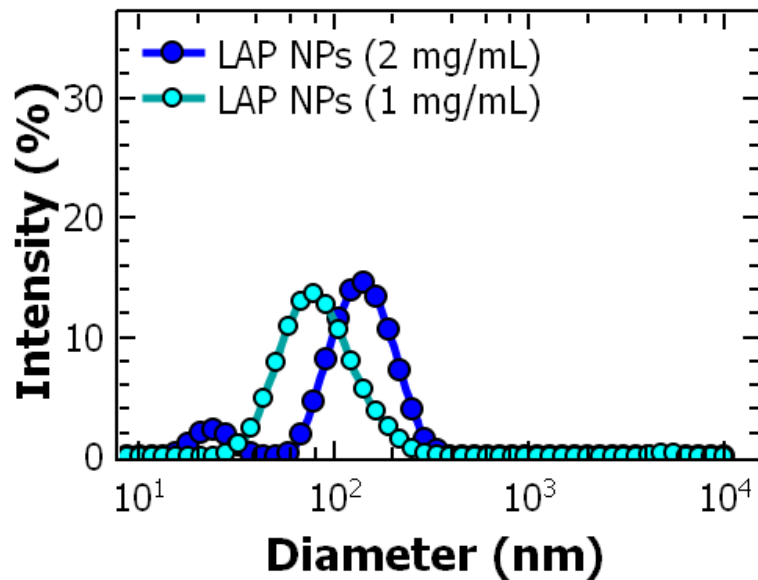


**Figure 29.** Dynamic light scattering of LAP NPs. Nanoparticles were formulated at 1mg/mL and 2mg/mL drug concentration in the organic stream. The LAP NP dispersion produced at 2 mg/mL had multiple size peaks at ~150 nm and ~30 nm, while the LAP NPs produced at 1 mg/mL were uniform at ~100 nm.

Finally, our goal was to produce co-loaded nanoparticles containing both PTX and LAP (PTX-LAP NPs). Based on the findings from formulating PTX NPs and LAP NPs, we first focused on drug concentration using THF as the organic solvent. Using a drug concentration of 1 mg/mL PTX and 1 mg/mL LAP (a total drug concentration of 2 mg/mL), nanoparticles with multiple two size populations (peak diameters of  $119 \pm 28$  nm and  $22 \pm 3$  nm) were observed. When the total drug concentration was decreased to 1 mg/mL (0.5 mg/mL each of PTX and LAP), uniform nanoparticles were produced at  $115 \pm 3$  nm (**Table 17**). These results are comparable with PTX NPs and LAP NPs where a maximum drug concentration of 1 mg/mL could be used in the formation of monodispersed nanoparticles. To maximize the drug loading, a BCP:core ratio of 1:5:1 was used. TEM confirms the particles are spherical and the particle size is consistent with DLS (**Figure 28**). Additionally, the nanoparticle size and polydispersity was unaffected by the filtration process (**Table 18**). Nanoparticle size was stable for up to two weeks after FNP when stored at 4 °C (**Table 19**).

**Table 17.** Effect of varying drug concentration when preparing for formulating PTX-LAP NPs.

Sample	Drug Concentration (mg/mL)		Size 1 (nm)	Size 2 (nm)	PDI
	PTX	LAP			
PTX-LAP NPs	1	1	119 ± 28	22 ± 3	0.330 ± 0.080
	0.5	0.5	115 ± 3	0	0.248 ± 0.007

**Table 18.** Comparing nanoparticles size and polydispersity before and after filtration.

Sample	Unfiltered		Filtered		Change in nanoparticle size (%)
	Size (nm)	PDI	Size (nm)	PDI	
TA-Fe NPs	134 ± 3	0.129 ± 0.012	135 ± 5	0.148 ± 0.022	1%
PTX NPs	170 ± 33	0.142 ± 0.053	164 ± 36	0.175 ± 0.050	-4%
LAP NPs	117 ± 7	0.335 ± 0.025	107 ± 8	0.344 ± 0.041	-9%
PTX-LAP NPs	120 ± 35	0.294 ± 0.085	110 ± 12	0.271 ± 0.068	-8%

**Table 19.** Nanoparticle stability.

Nanoparticles	Initial (T = 0)		T = 2 weeks	
	Size (nm)	PDI	Size (nm)	PDI
TA-Fe NPs	151 ± 5	0.258 ± 0.003	158 ± 2	0.228 ± 0.011
PTX NPs	136 ± 27	0.280 ± 0.059	142 ± 58	0.344 ± 0.225
LAP NPs	117 ± 7	0.247 ± 0.049	132 ± 25	0.332 ± 0.132
PTX-LAP NPs	84 ± 16	0.286 ± 0.026	81 ± 21	0.266 ± 0.058

Following FNP, the drug concentration in the resulting dispersions was determined by HPLC after disassembling the nanoparticles with acetonitrile. From the drug concentration, the encapsulation efficiency and drug loading of PTX and LAP were determined. The encapsulation efficiency of the drug is the amount of drug encapsulated compared to the nominal amount in the formulation. The drug loading of PTX and LAP in the single drug loaded nanoparticles were similar (**Table 20**) and comparable to previous literature using polymer micelles [237,316]. For the single drug loaded nanoparticles, the encapsulation efficiency PTX and the LAP were  $37.6 \pm 14.4\%$  and  $25.0 \pm 1.5\%$ ,

respectively which are comparable to previous reports using polymer micelles [316]. Interestingly, in the co-loaded nanoparticles the encapsulation efficiency of PTX increases from  $37.6 \pm 14.4\%$  to  $67.0 \pm 2.2\%$  while the encapsulation efficiency for LAP in PTX-LAP NPs remained the same as the LAP NPs (**Table 20**). This result could be attributed to a more hydrophobic core environment in the presence of LAP facilitating encapsulation of PTX. Due to the selective increase in encapsulation efficiency of PTX in the presence of LAP, the drug loading of PTX was 2.7-fold higher than the LAP loading ( $2.11 \pm 0.50\%$  compared to  $0.79 \pm 0.49\%$ ) despite using equal amounts of each drug during mixing (0.5 mg/mL of each). Notably, these drug concentrations are comparable to previous studies micelles [237,316].

**Table 20.** Encapsulation Efficiency and Drug Loading of Nanoparticles.

Samples	Encapsulation efficiency (EE%)		Drug loading (DL%)	
	PTX	LAP	PTX	LAP
PTX NPs	$37.6 \pm 14.4$	--	$3.11 \pm 1.88$	--
LAP NPs	--	$25.0 \pm 1.5$	--	$1.82 \pm 0.71$
PTX-LAP NPs	$67.0 \pm 2.2$	$25.9 \pm 3.5$	$2.11 \pm 0.50$	$0.79 \pm 0.40$

\* The average  $\pm$  standard deviation of 3 replicates of FNP are reported.

#### 4.3.2. Drug Release

As a first step to understanding the *in vitro* drug release rates of PTX and LAP from nanoparticles, dialysis was performed with PBS at pH 7.4 with Tween 80 similar to previous studies [317–320]. Examining the PTX-loaded nanoparticles, a burst release was observed within the first 6 hours at which  $\sim 20\%$  of PTX was released. After 6 hours, the burst release was followed by sustained PTX release and the drug release plateaued at  $\sim 40\%$  at day 6 (**Figure 30A**). In comparison,  $\sim 25\%$  of LAP released from LAP-loaded NPs in the first 3 hours ( $\sim 25\%$ ). Following the burst release, the sustained release of LAP release over 6 days was observed with  $\sim 35\%$  total drug release achieved (**Figure 30B**).

PTX release from the co-loaded nanoparticles was comparable to the single drug loaded nanoparticles with burst release in the first 6 hours and cumulative drug release at day 6 of ~40%. We examined the drug release kinetics of PTX from single-drug and co-loaded nanoparticles and fitted it to Korsmeyer-Peppas diffusion model (Eq. 12) [321,322].

$$\frac{M_t}{M_\infty} = at^n \quad (\text{Eq. 12})$$

Where the  $M_t$  is the drug release at time,  $t$ ,  $M_\infty$  is maximum drug release, and  $a$  is the release rate. The diffusion exponent,  $n$ , is determined based on the fit and described the drug release mechanism [321]. The diffusion exponent for PTX released from PTX NPs and from PTX-LAP NPs was 0.34. Since the diffusion exponent was less than 0.45, it indicates first-order Fickian diffusion kinetics [323,324].

Examining LAP release, we observe a slight decrease in cumulative release after 24 hours (**Figure 30B**). The fluctuations for lapatinib release from the nanoparticles are unusual but similar observations have been previously reported in other drug release systems [325,326]. The fluctuations in cumulative release can be potentially attributed to supersaturation of lapatinib in the dialysis media in the first 24 hours due to burst release of the drugs from the nanoparticles. Supersaturation could cause nanoprecipitation of LAP which could result in the apparent drop in cumulative drug accumulation [327]. This phenomena has been observed with other hydrophobic drugs from nanoparticles [325,327].

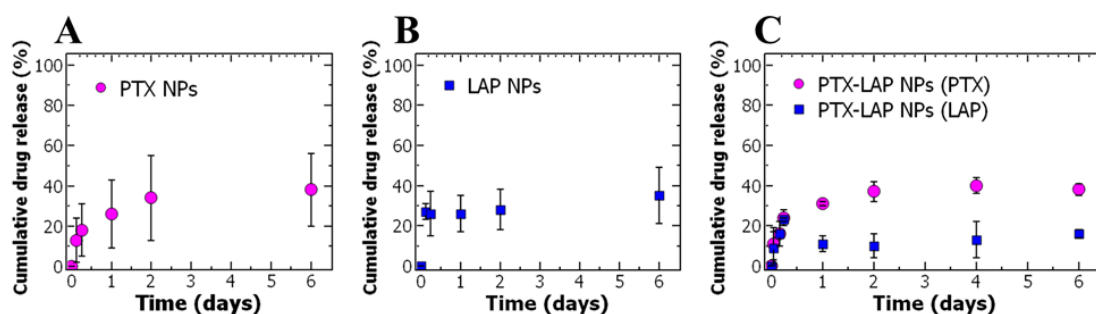


**Figure 30.** The cumulative drug release of paclitaxel (PTX) and lapatinib (LAP) from polymer nanoparticles (NPs) from (A) PTX from PTX NPs, (B) LAP from LAP NPs, and (C) PTX and LAP from co-loaded

nanoparticles. The graph shows the average  $\pm$  standard deviation of 3 replicates of FNP and independent drug release assays.

Investigating release from the PTX-LAP NPs, there is a decrease in cumulative release in LAP between 6 and 24 hours (**Figure 30C**). This result suggests that the release of PTX increases the supersaturation of and nanoprecipitation of LAP. Notably, when comparing LAP release from the co-loaded nanoparticles to the single drug-loaded nanoparticles, burst release occurred over 6 days rather than 3 days and the cumulative LAP release at 6 days was 2-fold lower for co-loaded nanoparticles compared to single-drug nanoparticle (~16% compared to ~35%) (**Figure 30C**). Co-encapsulating PTX and LAP into nanoparticles resulted in a decrease in the cumulative drug release of LAP but the drug release was comparable for PTX to single-drug loaded nanoparticles. The slower burst release of LAP from co-loaded nanoparticles may be attributed to lower drug loading concentrations compared to LAP NPs resulting in a slower dissolution profile, a phenomenon observed with hydrophobic materials [328]. These results are consistent with previous literature indicating LAP has a slower release profile compared to PTX from polymer micelles [309]. Studies to further characterize the drug release, especially LAP, using alternative media (e.g. other surfactants, or biologically relevant media such as full growth medium with serum) will be pursued in future work.

#### 4.3.3. *Assessing Drug Efficacy of Single Drug Nanoparticles*

Finally, the efficacy of the nanoparticle dispersions were assessed *in vitro* with ovarian cancer cells, OVCA-432. Specifically, we used the IC-50 concentration, i.e. the drug concentration that reduces the cell viability by 50%, as a measure of potency. As a control, the cell viability was first examined for cells treated with TA-Fe nanoparticles without drug. When treated with 50  $\mu\text{g/mL}$  based on total solids concentration the cell viability was 95% (**Table 21**). Examining the dose-response, the IC-50 concentration for the TA-Fe nanoparticles was  $\sim 1000 \mu\text{g/mL}$  of total solids concentration. This result

demonstrates that the nanoparticle platform itself has minimal cytotoxic effects consistent with previous reports [271].

**Table 21.** Cell viability of cell treated with Fe-TA NPs.

Total Solids Concentration ( $\mu\text{g/mL}$ )	Cell viability
5000	$7 \pm 1\%$
1000	$38 \pm 3\%$
500	$74 \pm 5\%$
100	$89 \pm 5\%$
50	$95 \pm 4\%$
10	$108 \pm 4\%$
5	$106 \pm 8\%$
1	$101 \pm 6\%$
0.5	$100 \pm 11\%$

Next, we compared the potency of the nanoparticles compared to the free drug at the equivalent free drug concentration. We note at the concentrations of nanoparticles used, the (TA-Fe NPs) alone did not induce cytotoxic effects and the IC-50 was reproducible with OVCA-432 cells. Encapsulating the PTX shifts the dose-response curve to lower concentrations compared to free PTX (**Figure 31**) indicating an increase in potency upon encapsulation. A similar trend was observed for LAP (**Figure 32**). Interestingly, the dose-response curve of PTX NPs and LAP NPs plateaued at ~20% cell viability. At low drug concentrations, the TA in the nanoparticle could counter the effects of the drugs by inducing an antioxidant effect and eliminate free radicals produced with the anticancer drugs [329,330].

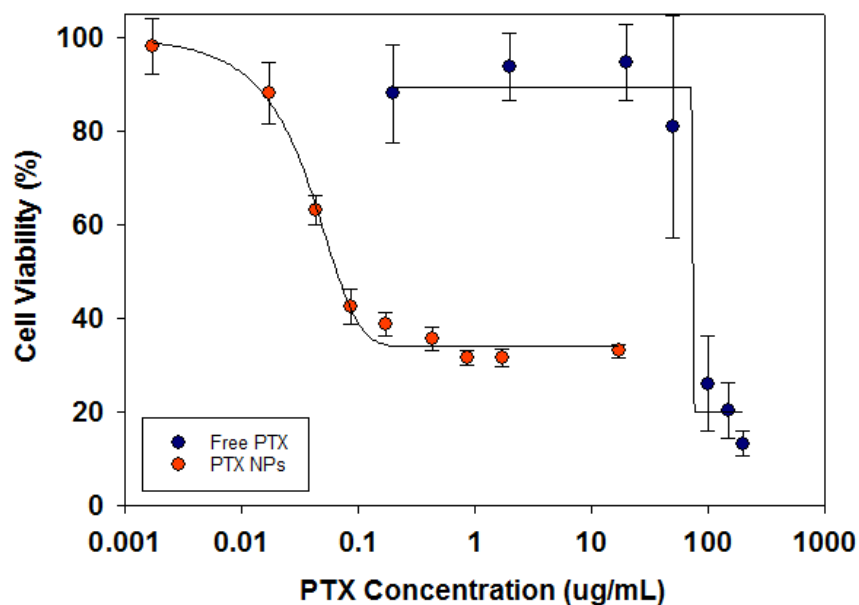


**Figure 31.** Dose response curve for cell treated with free PTX (blue) and PTX NPs (red).

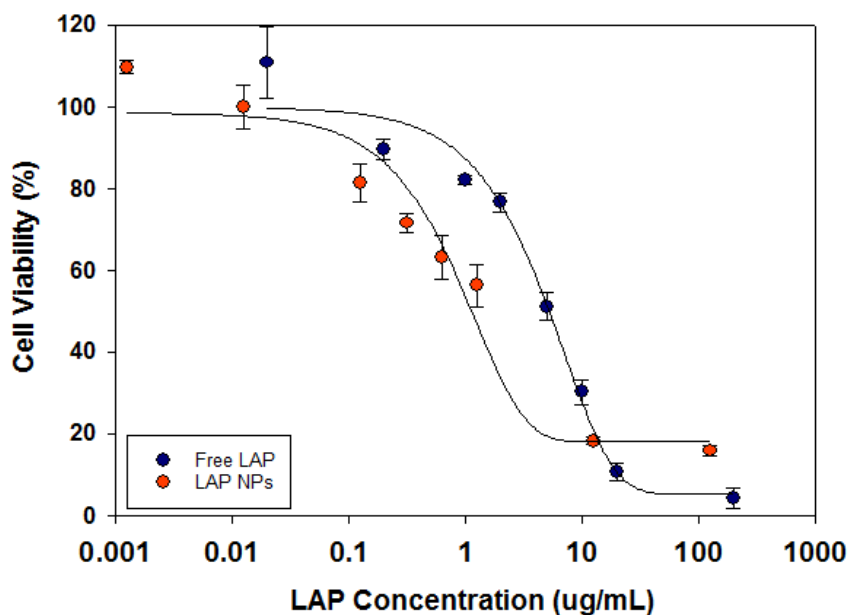


**Figure 32.** Dose response curve for cell treated with free LAP (blue) and LAP NPs (red).

Specifically, the IC-50 concentration decreases from  $70.6 \pm 5.1 \mu\text{g/mL}$  for free PTX to  $0.04 \pm 0.003 \mu\text{g/mL}$  when encapsulated ( $p < 0.05$ ) (**Table 22**). A similar result was observed for LAP; upon encapsulation, there was a nearly 6-fold increase in potency as the IC-50 decreased from  $4.6 \pm 1.3 \mu\text{g/mL}$  for the free drug to  $0.80 \pm 0.26 \mu\text{g/mL}$  when formulated into nanoparticles ( $p < 0.05$ ) (**Table**



22). While decreases in IC-50 concentration compared to the free drug form have been observed in other polymer nanoparticle formulations [234,331,332] and is not fully understood, the 1500-fold increase in PTX potency in this nanoparticle is noteworthy. The significant increase in PTX potency in the TA-Fe could be attributed to several contributing factors including sustained release over the 48 hour treatment period an increased bioavailability due to the nanoparticle formulation [234,333,334].

**Table 22.** IC-50 of paclitaxel, paclitaxel nanoparticles, lapatinib, and lapatinib nanoparticles in OVCA-432 cells

Drug Treatment	IC-50 ( $\mu\text{g/mL}$ )	
	PTX	LAP
Free PTX*	70.6 $\pm$ 5.1	--
Free LAP*	--	4.6 $\pm$ 1.3
PTX NPs	0.040 $\pm$ 0.003	---
LAP NPs	---	0.80 $\pm$ 0.26

\*In 2% DMSO with full growth medium.

\*\*The average  $\pm$  standard deviation (n = 6 treatments) are reported.

#### 4.3.4. Cell Cycle Analysis

To better understand the increase in drug potency upon encapsulation, we examined the effect of treatment on cell cycle using flow cytometry. The difficulty of treating cancer is the rapid proliferation of tumor cells and the propensity for metastasis. It is vital that cancer treatments such as PTX inhibit proliferation. For example, PTX arrests cells in the G<sub>2</sub>/M phase by stabilizing microtubule and preventing their disassembly necessary for cell division [335]. Thus, we examined the effect of the nanoparticles on cell cycle using flow cytometry. Specifically, we compared the cell cycle of cells treated with free PTX and PTX NPs at their respective IC-50 concentrations. The untreated control cells were primarily in the G<sub>0</sub>/G<sub>1</sub> phase with only 9% in the G<sub>2</sub>/M phase. With free PTX, the percentage of cells in the G<sub>0</sub>/G<sub>1</sub> phase drops from 62% to 45% and there is an increase in the number of cells in the G<sub>2</sub>/M phase to 31% (**Figure 33A**). These results indicate that free PTX formulations accumulates

OVCA-432 cells in the G<sub>2</sub>/M phase and likely decrease the cell viability by preventing progression to mitosis [335]. LAP and LAP-NP treated cells remained primarily in the G<sub>0</sub>/G<sub>1</sub> phase (**Figure 33B**) and the proportions for LAP and LAP-NPs were comparable. Thus, free LAP, and LAP NPs seem to stabilize the cells in the G<sub>0</sub>/G<sub>1</sub> phase over the 48 hours treatment with minimal progression to the subG<sub>1</sub> phase as expected since LAP is known to arrest cancer cells in the G<sub>1</sub> phase of the cell cycle [336].

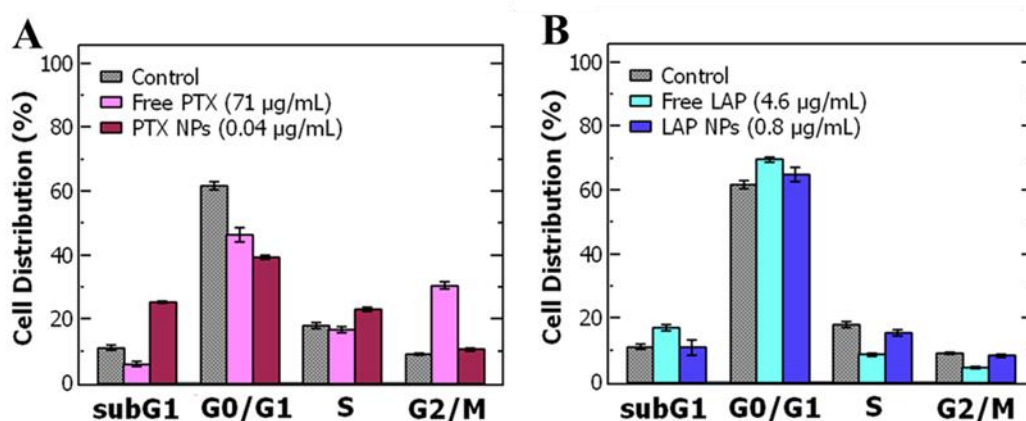


**Figure 33.** Cell cycle analysis of OVCA-432 cells from flow cytometry to compare free drug (in 2% DMSO) and nanoparticle formulations for A) paclitaxel (PTX) and B) lapatinib (LAP). The graph shows the average  $\pm$  standard deviation from 3 replicate wells.

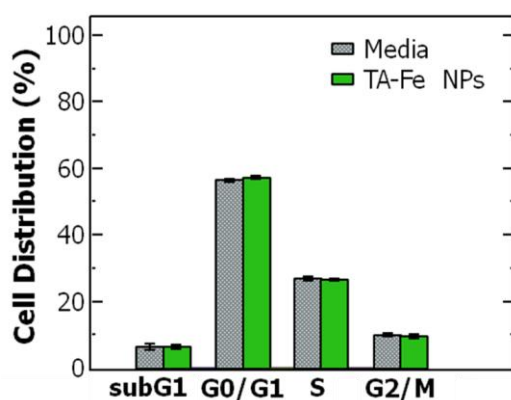


**Figure 34.** Cell cycle distribution of untreated cells and cell treated with TA-Fe NPs.

While the control nanoparticles had no effect on the cell cycle (**Figure 34**), when OVCA-432 cells were treated with PTX NPs the proportion of cells in G<sub>0</sub>/G<sub>1</sub> phase is similar to free PTX treated cells. Notably, treatment with PTX NPs shifted the cells to the subG<sub>1</sub> phase relative to both free PTX and control (**Figure 33A**) and decreased the proportion of cells in the G<sub>2</sub>/M phase from 31% to 11%. Increase proportion in the subG<sub>1</sub> phase could indicate that cells spend a shorter time in the G<sub>2</sub>/M phase with rapid DNA fragmentation [337] or it could be attributed to a short period of G<sub>1</sub> arrest followed by progression to the subG<sub>1</sub> phase during the 48 hour treatment [338]. Importantly, cells in the subG<sub>1</sub> phase undergo DNA damage, which can lead to cell death over time [339]. Overall, these changes in the cell cycle are support our findings that encapsulation increases PTX potency compared to free PTX.

#### 4.3.5. *Drug Combination and Synergy*

Next, we examined the efficacy of the co-loaded formulation. Co-encapsulating encapsulating the PTX with LAP further shifted the dose-response curve to lower concentrations compared to free PTX (**Figure 35**). Co-encapsulating PTX and LAP further increases PTX potency as indicated by the 2-fold-decrease in IC-50.

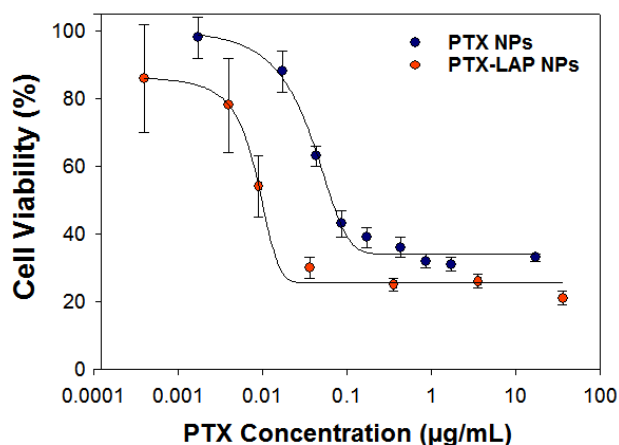


**Figure 35.** The cell viability dose-response curve of OVCA-432 cells when treated with (blue) paclitaxel nanoparticles (PTX NPs) and (red) paclitaxel-lapatinib nanoparticles (PTX-LAP NPs). The PTX-LAP NPs treatment shifts the dose-response curve to lower drug concentrations compared to the PTX NPs treatment. The graph shows the mean  $\pm$  standard deviation from one experiment performed with 6 replicate wells.

Based on the IC-50 of PTX-LAP NPs, we compared the cell viability of OVCA-432 cells treated with a single-drug nanoparticle (0.009  $\mu\text{g/mL}$  PTX or 0.004  $\mu\text{g/mL}$  LAP) to co-loaded PTX-LAP NPs (**Table 23**). The control nanoparticles containing no drug (TA-Fe NPs) at the same total solids concentration ( $\sim 0.5$   $\mu\text{g/mL}$ ) exhibited no cytotoxic effects on the OVCA-432 cells. When the OVCA-432 cells were treated with PTX NPs, there was a slight decrease in the cell viability to  $\sim 80\%$  whereas LAP NPs did not significantly affect cell viability. As expected, the PTX-LAP NPs reduced cell viability to  $\sim 50\%$  which was significantly lower compared to both PTX NPs ( $p = 0.0002$ ) and LAP NPs ( $p = 0.0001$ ) (**Figure 36**). These results indicate that at equivalent drug concentrations, co-loaded PTX-LAP NPs had the greatest potency.

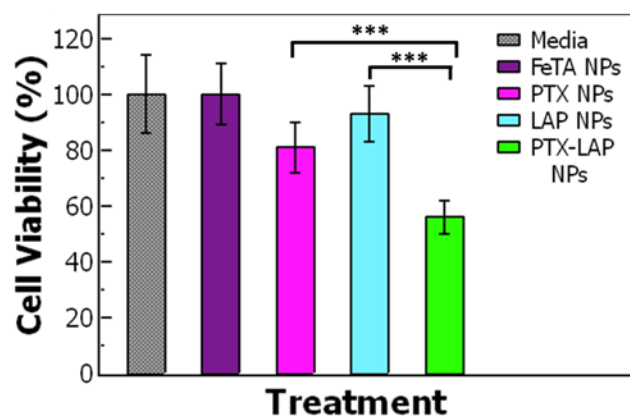


**Figure 36.** Cell viability of OVCA-432 cells after 48-hour treatment with (gray) media, (purple) tannic acid-iron nanoparticles (TA-Fe NPs), (pink) paclitaxel nanoparticles (PTX NPs), (light blue) lapatinib nanoparticles (LAP NPs), (green) paclitaxel-lapatinib nanoparticles (PTX-LAP NPs). The cells were treated with a PTX concentration of 0.009  $\mu\text{g/mL}$  and LAP at 0.004  $\mu\text{g/mL}$  based on IC-50 of the PTX-LAP NPs. The cell viability was significantly lower when the cells were treated with PTX-LAP NPs when compared to PTX NPs ( $p < 0.05$ ) and LAP NPs ( $p < 0.05$ ). The graph shows the mean  $\pm$  standard deviation from one experiment performed with 6 replicate wells.

Building on these results, we compared the combination treatment to the single drug treatment to determine if there was a synergistic effect of co-treating the cells with PTX and LAP. Synergy was examined with the combination index (CI) based on the Chou-Talalay method and when the CI is below 1, the combination treatment is synergistic compared to the sum of the individual drug treatments [340–342]. Free PTX and free LAP can be combined synergistically as indicated by the CI of 0.18. PTX and LAP target different mechanisms of the cell to produce an anticancer effect [8,343]. LAP inhibits the function of ABC transporters, which helps increase the intracellular concentration of PTX thereby increasing drug efficacy [234,344,345]. Similar synergistic effects were seen with chemotherapeutic agents and tyrosine kinase inhibitors [238,239].

Interestingly, the CI of the co-loaded PTX-LAP NPs was 0.23 comparable to the free drug combination and lower than co-delivered nanoparticles, which had a CI of 0.40 (**Table 23**). These results indicate an advantage to co-encapsulation of both drugs within the same particle. The co-loaded nanoparticles could enhance the co-localization of the drugs particularly if the nanoparticles are endocytosed by tumor cells. Overall, we have presented a rapid and scalable approach to

encapsulating chemotherapeutic combinations in a pH-labile nanoparticle platform that enhances the potency treatment ovarian cancer *in vitro*.

**Table 23.** IC-50 and combination index of paclitaxel-lapatinib nanoparticles (PTX-LAP NPs) (co-loaded) compared to simultaneous delivery of paclitaxel nanoparticles (PTX NPs) and lapatinib nanoparticles (LAP NPs) (two single drug-loaded NPs) in OVCA-432 cells.

Drug Treatment	IC-50 ( $\mu\text{g/mL}$ )		Combination Index (CI)
	PTX	LAP	
PTX NPs and LAP NPs	$0.015 \pm 0.003$	$0.007 \pm 0.001$	0.40
PTX-LAP NPs	$0.0090 \pm 0.0009$	$0.0040 \pm 0.0004$	0.23

\* The average  $\pm$  standard deviation from one experiment performed with 6 replicate wells is reported.

#### 4.4. Conclusion

In conclusion, we demonstrated encapsulation of weakly hydrophobic drugs ( $\log P < 6$ ) into polymer nanoparticles in a rapid, scalable FNP process using *in situ* complexation of TA-Fe. The size of the resulting nanoparticles is stable at pH 7.4, facilitating sustained drug release via first-order Fickian diffusion. Importantly, the nanoparticles that encapsulate PTX and LAP are significantly more potent than the free drugs as indicated by the significantly decreased IC-50. Co-encapsulating PTX with LAP further increased potency. Additionally, co-encapsulating PTX and LAP had a synergistic effect comparable to the free drug and greater than co-delivery of the single drug loaded nanoparticles indicating an advantage co-encapsulation of both drugs within the same particle. Building on this promising study, further studies to understand the cytotoxic effects (e.g. apoptosis), nanoparticle uptake and localization within cells, protein adsorption to nanoparticles, as well as evaluation in additional cell lines will be considered in future work. This is an intriguing approach for improving the potency of existing chemotherapeutics.

## 5. Chapter 5: Sequence-Dependent Cytotoxicity of Nanoparticle Delivery of Paclitaxel and Lapatinib in Ovarian Cancer Cells

---

### Abstract

Treating ovarian cancer with acquired drug resistance is challenging with chemotherapeutic agents. Recently approaches of sequentially delivering drug combinations have been found to improve drug efficacy. In this study, we extend this approach to examine the efficacy of sequential drug delivery of two anticancer drugs, paclitaxel and lapatinib, in polymer nanoparticle formulations. Paclitaxel and lapatinib were individually loaded into polymer nanoparticles by Flash NanoPrecipitation via *in situ* tannic acid-iron complexation. *In vitro* experiments were conducted on ovarian cancer cell models (OVCA-432 and OVCAR-3). We examined the cell viability and cell cycle distribution after three sequence schedules; simultaneous delivery, paclitaxel followed by lapatinib, and lapatinib followed by paclitaxel. While the response was cell-dependent, the greatest cytotoxicity was observed when the cells were treated simultaneously with paclitaxel and lapatinib for 48 hours or with paclitaxel for the first 24 hours followed by lapatinib for a second 24 hour period. This reduction in cell viability paralleled the shift observed in the cell cycle distribution to an increase in the G<sub>2</sub>/M and subG<sub>1</sub> phases.

## 5.1. Introduction

Treating ovarian cancer with chemotherapeutic agent (e.g. paclitaxel) remains a challenge due to development of drug resistance mechanisms [7,102]. The drug resistance is also attributed to several factors including drug inactivation, dose intensity, DNA repair, cell death inhibition, and drug efflux [20,21]. Cellular drug resistance mechanism such as increased drug efflux are attributed to an overexpression of ATP-binding cassette (ABC) transporters that have a role in removal of anticancer drugs [344]. ABC transporter inhibitors, e.g. lapatinib (LAP), have been used in combination with chemotherapeutics to reduce drug efflux and increase the efficacy of the chemotherapeutic agent [226,240,246].

Recently, there has been a shift to examining sequential drug delivery of drug combinations for managing recurring ovarian cancers [12,238,346,347]. These studies have found that sequential treatment of two or more drugs can increase anticancer activity through synergistic drug interaction and enable higher drug dosing with tolerable toxicity [12,84,116,117]. Vanhoefer et al. investigated sequential delivery of paclitaxel and cisplatin on ovarian adenocarcinoma cells from patients pretreated with platinum therapies and found that a sequence treatment of paclitaxel 24 hrs prior to cisplatin produced a synergistic effect [84]. When PTX was co-delivered with vorinostat, a histone deacetylase inhibitor, to treat ovarian cancer cells a sequence-dependent synergetic activity was observed *in vitro* and *in vivo*. However the synergetic activity was also cell type dependent attributed to the protein expression of drug targets [116]. Sequential delivery of chemotherapeutic agents and transporter inhibitors similar to lapatinib have also been investigated in free-drug formulations *in vitro* [254–257]. Some of the studies found that delivering the chemotherapeutic drug prior to the inhibitory drug provided a synergistic effect compared to the reversed order [254–256]. Another study indicated that treatment with the inhibitory drug, sorafenib, prior to the chemotherapeutic drug, docetaxel, provided a more effective treatment schedule for drug resistant cancer cells [257]. While there is still



some debate as to which treatment schedule is more effective and if the observed synergy is cell type dependent, these studies do suggest that a sequential drug delivery has the potential to increase treatment efficacy to induce greater cancer cell death.

Overall, these studies suggest that drug delivery sequence schedules can be tailored to increase drug efficacy. The benefit of this approach is targeting multiple interconnecting cascade pathways at specific time points to produce an enhanced anticancer effect [206,341]. Many of the sequential drug delivery studies are limited to free drugs [84,116,254–257]. The limitations of free drug formulations are poorly drug solubility and have low bioavailability while inducing severe systemic toxicity. Additionally, there is poor control over sequential drug delivery with free drug formulations [188,348]. Nanoparticle drug formulations can address these challenges with controlled drug delivery, passive targeting through enhanced permeability and retention (EPR) effect, improve drug solubility and bioavailability, and reduction in systemic toxicity [188,348,349].

Polymer nanoparticles formulations of paclitaxel with other anticancer drugs have been explored for combination treatment of ovarian cancer. These studies found that polymer nanoparticle formulations of drug combinations have been found to enhance synergistic interaction, significantly reduced tumor volume and extended survival time compared to delivery of single-drug nanoparticles in ovarian cancer [154–157]. Nanoparticle combination drug delivery has been extended to explored sequential drug delivery with nanoparticles for other forms of cancer [184–190,194,195]. Two anticancer drugs, doxorubicin and imatinib, were co-loaded into PEGylated nanoparticles for sequential drug delivery (under acidic conditions) and enhanced drug uptake and apoptosis compared to single-drug nanoparticles or co-delivery of free drugs [185]. While this study provides a foundation for pursuing the study of drug combination nanoparticles, there is still limited understanding of which sequence schedule produce optimal drug efficacy. Further studies are needed to explore the effects of sequential drug delivery with polymer nanoparticles on ovarian cancer cells

In this study, we explore sequential drug delivery of paclitaxel and lapatinib on ovarian cancer cell model (OVCA-432 and OVCAR-3). We encapsulate paclitaxel and lapatinib into single-drug nanoparticles via Flash NanoPrecipitation (FNP) [306]. Three different sequence schedules are explored; simultaneous delivery, paclitaxel prior to lapatinib, and lapatinib prior to paclitaxel. Treatment efficacy of nanoparticle formulations were compared to free drug *in vitro* and evaluated using cell viability and cell cycle analysis.

## 5.2. Materials and Methods

### 5.2.1. Materials

HPLC grade tetrahydrofuran (THF), dimethyl sulfoxide (DMSO), and acetonitrile were purchased from Fisher Scientific (Pittsburg, PA). ACS grade tannic acid (TA) and ACS grade iron (III) chloride hexahydrate (97%) were purchased from Sigma-Aldrich (St. Louis, MO). Paclitaxel (PTX, >98%) and lapatinib (LAP, >98%) were obtained from Cayman Chemical Company (Ann Arbor, MI); phosphate buffered saline without calcium and magnesium was purchase from Lonza (Basel, Switzerland). Polystyrene-b-polyethylene glycol (1600-b-500 g/mol) (PS-b-PEG) was obtained from Polymer Source (Montreal, Canada) and was purified by dissolving in THF (~40°C) and precipitating into diethyl ether then dried by vacuum for two days as previously described [278].

### 5.2.2. Cell Culture

Ovarian cancer cell line OVCA-432 was a kind gift from Dr. Xianjun Fang from Virginia Commonwealth University. Ovarian cancer cell line OVCAR-3 was purchased from ATCC (Manassas, VA). The OVCA-432 cells were cultured in RPMI-1640 media containing 2 mM L-glutamine (ATCC, Manassas, VA) supplemented with 10% Fortified Bovine Calf Serum (FBS, HyClone Cosmic Calf Serum, Fisher Scientific, Pittsburg, PA), 100 U/mL penicillin and 100 µg/mL

streptomycin (Gemini Bio-Products, West Sacramento, CA). The OVCAR-3 cells were cultured in RPMI-1640 media supplemented with 20% FBS and 1 mg/mL bovine insulin (Sigma Aldrich, St. Louis, MO). Both cell lines were cultured at 37 °C at 5% CO<sub>2</sub> and passaged once a week.

### 5.2.3. Nanoparticle Formulation

Flash NanoPrecipitation (FNP) was used to prepare polymer-based nanoparticles encapsulating the anti-cancer drugs via tannic acid-iron *in situ* complexation with a hand-operated confined impinging jet (CIJ) mixer, as previously described [271,306]. Briefly, PS-b-PEG (10 mg/mL), TA (4 mg/mL), and either PTX (1 mg/mL) or LAP (1mg/mL) were dissolved in THF by sonicating (~40°C) for 10 minutes to formulate the organic stream. The organic stream was rapidly mixed with the Fe<sup>3+</sup> (aq., 1 mg/mL) at equal volumes (1 mL of each stream) in the CIJ mixer. The effluent from the mixer was immediately diluted in 1X PBS at pH 7.4 for a final organic solvent/water ratio of 1:9 by volume. Nanoparticles encapsulating paclitaxel (PTX NPs) or lapatinib (LAP NPs) were formulated using the described method.

Within 24 hrs of formulation, the nanoparticles were filtered to remove the organic solvent, unencapsulated drug(s), and excess TA and Fe<sup>3+</sup> with Amicon Ultra-2 Centrifugal filters (Amicon Ultra centrifuge filter (Ultracel 50K, 50,000 NMWL), Merck Millipore Ltd, Burlington, Ma) by centrifuging at 3700 rpm for ~15-30 minutes (5804 R 15 amp version, Eppendorf, Hamburg, Germany). The nanoparticle pellet was resuspended with 1X PBS to a nominal concentration ~25 mg/mL of total solids and stored at ~4 °C. The nanoparticles were used within 5 days of the FNP to ensure there was minimal change in particle size and drug loss.

#### 5.2.4. Nanoparticle Characterization

The size and polydispersity (PDI) of the nanoparticles were characterized after FNP using dynamic light scattering (Malvern Zetasizer ZS, Malvern Instruments Ltd, Malvern, United Kingdom). The nanoparticle size and PDI were measured by averaging 4 measurements at a scattering angle of 173°. The average and standard deviation of three replicates of each nanoparticles are reported.

The nanoparticle encapsulation efficiency (EE%) and drug loading (DL%) were determined for the two nanoparticles. The nanoparticles were filtered to remove the organic solvent, unencapsulated drug(s), and excess TA and Fe<sup>3+</sup> with Amicon Ultra-2 Centrifugal filters (Amicon Ultra centrifuge filter (Ultracel 50K, 50,000 NMWL), Merck Millipore Ltd, Burlington, Ma) by centrifuging at 3700 rpm for ~15-30 minutes (5804 R 15 amp version, Eppendorf, Hamburg, Germany) within 24hrs of formulation. The nanoparticle pellet was resuspended with 1X PBS to a nominal concentration ~25 mg/mL of total solids and stored at ~4 °C.

The concentration of the nanoparticle dispersion was determined by thermogravimetric analysis (TGA) (Pyris 1 TGA, Perkin Elmer, Waltham, MA). The nanoparticle dispersion was loaded at 10 uL and the temperature was ramped up from 28°C to 110°C at 10°C/min and held for 30 minutes at 110°C. The final nanoparticle mass was used to determine the nanoparticle drug loading.

To determine the drug content of the nanoparticles, acetonitrile (360 µL) was added to nanoparticles (10 µL) and the sample was vortexed so that the nanoparticles would disassemble. The sample was centrifuged at 10,000 rpm for 7 minutes, and then the supernatant was collected for reverse-phase high Performance Liquid Chromatography (RP-HPLC) (1260 HPLC with Quaternary Pump and UV-Vis Diode Array Detector, Agilent, Santa Clara, CA) fitted with a Luna® 5 µm C18 100 Å, LC Column 250 x 4.6 mm (Phenomenex, Torrance, CA). The sample was eluted with degassed acetonitrile and water gradient at a flow rate of 1 mL/min (0-1 minute at 80:20, 1-6 of ramp up to 0:100, 6-8 minutes at 0:100, and ramp down to 80:20 between 8-9 minutes). PTX was measured

at a wavelength of 228 nm with a retention time of ~8 minutes and LAP was measured at 332 nm with a retention time of ~9 minutes. The concentration of each drug was determined by comparing the peak areas with the standard calibration curve. Encapsulation efficiency (EE%) and drug loading (DL%) were calculated based on equations 10 and 11, respectively, and the values reported are the average and standard deviation of three trials.

$$\text{encapsulation efficiency (EE\%)} = \frac{\text{Mass of drug encapsulated}}{\text{Initial mass of drug}} \times 100\% \quad (\text{Eq. 10})$$

$$\text{drug loading (DL\%)} = \frac{\text{Mass of drug encapsulated}}{\text{Total nanoparticle mass}} \times 100\% \quad (\text{Eq. 11})$$

#### 5.2.5. Determining Half Maximal Inhibitory Concentration

The half maximal inhibitory concentration (IC-50) of free PTX, free LAP, PTX NPs, and LAP NPs for both OVCA-432 cells and OVCAR-3 cells. Cells were seeded at a density of  $15 \times 10^3$  cell/well in a 96-well plate containing 100  $\mu\text{L}$  of complete medium. The cells were incubated at 37 °C in 5%  $\text{CO}_2$  overnight. Then the media was replaced with 100  $\mu\text{L}$  medium containing free-drug or nanoparticles and treated for 48 hrs. Stock solution of free-drug were prepared by dissolving PTX (12 mg/mL) or LAP (5 mg/mL) in DMSO and sonicating for 5 minutes. Then the drugs were diluted with complete media and serial dilutions were performed to achieve concentrations between 200 - 0.0002  $\mu\text{g/mL}$ . Additional DMSO was added for a final DMSO concentration of 2% v/v. The nanoparticles were concentrated with Amicon filters (50kDa MWCO) as previously described and the nanoparticle pellet was diluted with 1X PBS to a concentration of 1000  $\mu\text{g/mL}$  of drug. The nanoparticle-loaded medium was prepared by diluting the stock nanoparticle dispersion with complete medium and performing serial dilutions for final concentrations between 200 - 0.0002  $\mu\text{g/mL}$ . The cells were also treated with complete media and 2% DMSO media as controls for comparison. Cells were treated for 48 hours with 6 replicates of each conditions and the cell viability was measured with a WST-1 assay

(Sigma-Aldrich, St. Louis, MO) according to manufacturing instructions. Briefly, the media was removed and replaced with 10% WST-1 solution. The cells were incubated between 45 - 90 minutes until there was a visible color change to a golden-yellow or the absorbance of control wells reached at least 0.700 measured with a microplate reader (VersaMax ELISA microplate reader, Molecular Devices, San Jose, Ca) at a wavelength of 440 nm with background subtraction of 640 nm. The cell viability was determined by subtracting the background noise (wells containing only 10% WST-1 in media) from the samples and then dividing the sample absorbance by the average absorbance of the untreated wells. The cell viability of cells treated with free drug were normalized with cells treated with 2% DMSO. The relative cell viability was expressed as a percentage of the untreated cells with mean  $\pm$  standard deviation of six replicates.

#### *5.2.6. Cell Viability with Sequential Drug Treatment*

The cell viability was examined for the OVCA-432 and OVCAR-3 cells treated for 24 hrs with either free drugs or nanoparticles. The cells were dosed at half the IC-50 concentrations according to **Table 24** for OVCA-432 cells and **Table 25** for OVCAR-3 cells as indicated under T = 0 treatment. The cell viability was also examined for the OVCA-432 and OVCAR-3 cells following sequential treatment over 48 hours (24 hours with first dose, second 24 hours with second dose). Three different sequences were evaluated: 1) simultaneous treatment of both drugs; 2) treatment with paclitaxel for 24 hours followed by lapatinib for 24 hours; and 3) treatment with lapatinib for 24 hours followed by paclitaxel for 24 hours. Again, the cells were dosed at half the IC-50 concentrations according to **Table 24** for OVCA-432 cells and **Table 25** for OVCAR-3 cells. After total 48 hr treatment period, the cell viability was measured with WST-1 assay, as previously described [306].

**Table 24.** Sequential drug dosing of OVCA-432 cells for evaluating cell viability.

Formulation	Sequence Schedule	Drug Concentration for Treating OVCA-432 cells ( $\mu\text{g/mL}$ )*					
		T = 0 hr		T = 24 hr		Total drug dose	
		Paclitaxel	Lapatinib	Paclitaxel	Lapatinib	Paclitaxel	Lapatinib
Free drug	Simultaneous delivery	17.8	1.2	17.8	1.2	36	2.3
	PTX -> LAP	36	--	--	2.3	36	2.3
	LAP -> PTX	--	2.3	36	--	36	2.3
Nanoparticles	Simultaneous delivery	0.01	0.2	0.01	0.2	0.02	0.4
	PTX NPs -> LAP NPs	0.02	--	--	0.4	0.02	0.4
	LAP NPs -> PTX NPs	--	0.4	0.02	--	0.02	0.4

\*The drug concentrations were selected based on half the IC-50 dose of each drug to allow for a greater range in cell viability results post treatment.

**Table 25.** Sequential drug dosing of OVCAR-3 cells for evaluating cell viability.

Formulation	Sequence Schedule	Drug Concentration for Treating OVCAR-3 cells ( $\mu\text{g/mL}$ )*					
		T = 0 hr		T = 24 hr		Total	
		Paclitaxel	Lapatinib	Paclitaxel	Lapatinib	Paclitaxel	Lapatinib
Free drug	Simultaneous delivery	0.0025	1	0.0025	1	0.005	2.0
	PTX -> LAP	0.005	--	--	2	0.005	2
	LAP -> PTX	--	2	0.005	--	0.005	2
Nanoparticles	Simultaneous delivery	0.0075	7.75	0.0075	7.75	0.015	15.5
	PTX NPs -> LAP NPs	0.015	--	--	15.5	0.015	15.5
	LAP NPs -> PTX NPs	--	15.5	0.015	--	0.015	15.5

\*The drug concentrations were selected based on half the IC-50 dose of each drug to allow for a greater range in cell viability results post treatment.

### 5.2.7. Cell Cycle Analysis by Flow Cytometry

The OVCA-432 and OVCAR-3 cells were seeded at a density of  $20 \times 10^4$  cells/mL in a 35 mm petri dish containing 3 mL of complete media. The cells were incubated at  $37^\circ\text{C}$  and 5%  $\text{CO}_2$  until 90% confluence and the media was replaced every 2 days. The cells were treated with three different sequence schedules using with either free drugs or nanoparticle formulations. Three different sequences were evaluated: 1) simultaneous treatment of both drugs; 2) treatment with paclitaxel for 24 hours followed by lapatinib for 24 hours; and 3) treatment with lapatinib for 24 hours followed by

paclitaxel for 24 hours. The cells were dosed at the IC-50 concentrations for cell cycle analysis according to **Table 26** for OVCA-432 cells and **Table 27** for OVCAR-3 cells.

**Table 26.** Sequential drug dosing of OVCA-432 cells for cell cycle analysis.

Formulation	Sequence Schedule	Drug Concentration for Treating OVCA-432 cells ( $\mu\text{g/mL}$ )*					
		T = 0		T = 24		Total drug dose	
		Paclitaxel	Lapatinib	Paclitaxel	Lapatinib	Paclitaxel	Lapatinib
Free drug	Simultaneous delivery	36	2.3	36	2.3	72	4.6
	PTX -> LAP	72	--	--	4.6	72	4.6
	LAP -> PTX	--	4.6	72	--	72	4.6
Nanoparticles	Simultaneous delivery	0.02	0.4	0.02	0.4	0.04	0.8
	PTX NPs -> LAP NPs	0.04	--	--	0.8	0.04	0.8
	LAP NPs -> PTX NPs	--	0.8	0.04	--	0.04	0.8

\*The drug concentrations were selected based on the IC-50 dose of each drug.

**Table 27.** Sequential drug dosing of OVCAR-3 cells for cell cycle analysis.

Formulation	Sequence Schedule	Drug Concentration for Treating OVCAR-3 cells ( $\mu\text{g/mL}$ )					
		T = 0 hr		T = 24 hr		Total drug dose	
		Paclitaxel	Lapatinib	Paclitaxel	Lapatinib	Paclitaxel	Lapatinib
Free drug	Simultaneous delivery	0.005	2	0.005	2	0.01	4.0
	PTX -> LAP	0.01	--	--	4	0.01	4.0
	LAP -> PTX	--	4	0.01	--	0.01	4.0
Nanoparticles	Simultaneous delivery	0.015	15.5	0.015	15.5	0.03	31.0
	PTX NPs -> LAP NPs	0.03	--	--	31	0.03	31.0
	LAP NPs -> PTX NPs	--	31	0.03	--	0.03	31.0

\*The drug concentrations were selected based on the IC-50 dose of each drug.

The total treatment time was 48 hrs at 37 °C. Then, the cells were stained with Propidium Iodide (PI Flow Cytometry Kit, Abcam, Cambridge, MA) for flow cytometry according to manufacturing instructions. Briefly, the cells were trypsinized and the aspirated medium and PBS were collected to minimize cell loss. The cells were centrifuged at 700 x g for 5 minutes as necessary. The cells were washed with 1X PBS and fixed with 66 % ethanol by slowly adding ethanol to PBS during vortexing. The cells were stored in ethanol at 4 °C for at least 2 hrs and up to 4 days. The cells were



centrifuged and washed with PBS to remove the ethanol. The 1X Propidium Iodide and RNase solution was prepared immediately prior to use by mixing 5% v/v of 20X Propidium Iodide and 0.05% v/v 200X RNase in 1X PBS. Then the cells were resuspended in 200  $\mu$ L/500,000 cells of 1X Propidium Iodide and RNase solution and incubated in the dark at 37°C for 30 minutes. Prior to flow cytometry, the cell samples were stored on ice and filtered through a cell strainer (Falcon Test Tube with Snap Cap, Fisher Scientific, Pittsburg, PA). Flow cytometry was performed on a BD FACSCanto™ II Analyzer (BD Biosciences, San Diego, CA) and 10,000 cells were analyzed at an excitation of 488 nm and emission of 670 nm. The samples were analyzed in triplicate.

## 5.3. Results and Discussion

### 5.3.1. Nanoparticle Formulation

Paclitaxel and lapatinib were encapsulated into single-drug polymer nanoparticles via Flash Nanoprecipitation [306]. Briefly, encapsulation of these weakly hydrophobic drugs ( $\log P < 6$ ) was facilitated via *in situ* tannic acid-iron complexation which forms an insoluble complex under neutral pH conditions [271,306]. To formulate the nanoparticles, an organic stream comprised of the block co-polymer (PS-b-PEG), tannic acid, and one of the drugs was rapidly mixed with  $\text{Fe}^{3+}$  (aq.) in a confined impinging jet (CIJ) mixer. The rapid change in solvent quality forms the tannic acid-iron complex, precipitates the drugs, and self-assembles the block co-polymer. The nanoparticles are kinetically stabilized by the adsorption of the block co-polymer onto the growing core [306].

Polymer nanoparticles were formulated with either paclitaxel (PTX NPs, 1 mg/mL) or lapatinib (LAP NPs 1 mg/mL). The PTX NPs were formulated at  $\sim 130$  nm and the diameter of LAP NPs was  $\sim 120$  nm. Both nanoparticles were monodispersed indicated by a single size peak and a PDI below 0.300 [312] (**Table 28**). These nanoparticles are on the order of 100 nm and allow for passive targeting [349].

**Table 28.** Nanoparticle Characterization.

Nanoparticles	Size (nm)	PDI
PTX NPs	136 ± 27	0.280 ± 0.059
LAP NPs	117 ± 7	0.247 ± 0.049

### 5.3.2. Assessing Potency of Single-Drug Treatment via Cell Viability

Following formulation of the nanoparticles, the drug efficacy of paclitaxel and lapatinib, treated individually were evaluated *in vitro* on two ovarian cancer cells OVCA-432 and OVCAR-3. Cells were treated with the free drug and nanoparticle formulations of paclitaxel and lapatinib. The dose-response was measured with WST-1 assay and the half maximal inhibitory concentration (IC-50) was used as a measure of drug potency.

The free drug treatment with paclitaxel resulted in an IC-50 of  $70.6 \pm 5.1 \mu\text{g/mL}$  for the OVCA-432 cells. The OVCAR-3 cells had a lower IC-50 value of  $0.004 \pm 0.001 \mu\text{g/mL}$  when treated with free paclitaxel. In comparison, treatment with free lapatinib of OVCA-432 and OVCAR-3 cells resulted in equivalent IC-50 concentrations at  $\sim 4 \mu\text{g/mL}$  (**Table 29**). The two ovarian cancer cell lines had significantly different responses to treatment with free paclitaxel on the order of 5-magnitude. These results indicate that the OVCA-432 cells are more resistant to free paclitaxel compared to OVCAR-3 cells and comparable cytotoxicity due to lapatinib. These results are surprising as the OVCA-3 cells are considered resistant [350,351], but the results suggest that the OVCA-432 cell have greater resistance to paclitaxel compared to OVCAR-3 cells. Further investigations are necessary to determine the reason for the differences observed such as examining protein phosphorylation, microtubule polymerization, and P-glycoprotein expression and are outside the scope of this study.

**Table 29.** The IC-50 values for free drug and nanoparticle treated cells.

Drug Treatment	OVCA-432 cell		OVCAR-3 cell	
	IC-50 ( $\mu\text{g/mL}$ )		IC-50 ( $\mu\text{g/mL}$ )	
	PTX	LAP	PTX	LAP
Free PTX	$70.6 \pm 5.1$	--	$0.004 \pm 0.001$	--
Free LAP	--	$4.6 \pm 1.3$	--	$4.1 \pm 0.7$
PTX NPs	$0.040 \pm 0.003$	---	$0.027 \pm 0.005$	---
LAP NPs	---	$0.80 \pm 0.26$	---	$31 \pm 8$

Next, we compared the single-drug treatment potency of nanoparticles to free drug formulations. In OVCA-432 cells, encapsulating PTX in nanoparticles reduced the IC-50 over 1500-fold from  $70.6 \pm 5.1$  to  $0.040 \pm 0.003$   $\mu\text{g/mL}$ . Inversely, the OVCAR-3 cells exhibited an increase in IC-50 when treated with the nanoparticle formulations compared to free drug. The IC-50 increased 7-fold from  $0.004 \pm 0.001$   $\mu\text{g/mL}$  to  $0.027 \pm 0.005$   $\mu\text{g/mL}$  when the OVCAR-3 cells were treated with nanoparticles compared to free PTX (**Table 29**). These results indicate that OVCAR-3 are resistant to nanoparticle formulation of paclitaxel and differ from previous studies that have treated OVCAR-3 cells with paclitaxel loaded polymer nanoparticles [350]. This could possibly be attributed to difference in nanoparticle formulation and drug release, as well as cell-line dependence which has been previously observed but poorly understood [83,88]. Overall, encapsulating paclitaxel into nanoparticles produces similar drug potency between cell lines.

Next, we examined the potency of lapatinib loaded nanoparticles. Encapsulating LAP decreased the IC-50 of OVCA-432 cells from  $4.6 \pm 1.3$   $\mu\text{g/mL}$  with free LAP to  $0.80 \pm 0.26$   $\mu\text{g/mL}$ . When OVCAR-3 cells were treated with LAP NPs, an increase in the IC-50 was observed from  $4.1 \pm 0.7$   $\mu\text{g/mL}$  to  $31 \pm 8$   $\mu\text{g/mL}$ . As with PTX NPs, we observed a resistance in the OVCAR-3 cells to the nanoparticle form of lapatinib. These results are interesting and provide further support that formulation into nanoparticles improves drug potency in the OVCA-432 cell line while decreases drug potency in the OVCAR-3 cell line. The effect may be attributed to aspects of the nanoparticle

formulation such as nanoparticles size (endocytosis mechanisms), surface charge, or additional component (tannic acid-iron complex).

Overall, the OVCA-432 and OVCAR-3 had differing responses to treatment with nanoparticles compared to free drug. The paclitaxel potency was increased by 1500-fold when the OVCA-432 cells were treated with PTX NPs, indicating a significantly improvement in drug potency. However the potency decreased by 7-fold for OVCAR-3 cells when PTX was encapsulated. A similar trend was observed with LAP NPs. The results indicate a 5-fold increase in LAP potency for OVCA-432 cells with the nanoparticle formulation. However the OVCAR-3 cells exhibited a 8-fold decrease in LAP potency when treated with LAP NPs. The results indicate a cell-type dependent potency to nanoparticle formulations which could be attributed to endocytosis mechanism [352] or possibly the presence of tannic acid and iron in the nanoparticle formulation that reduce anticancer effects [353].

### 5.3.3. Comparing Cell Viability after 24 Hour Treatment with Free Drug and Nanoparticles

After we determined the drug potency, we examined the drug cytotoxicity after 24 hour treatment. The cells were treated either simultaneously with paclitaxel and lapatinib or with paclitaxel alone and lapatinib alone. The concentration the OVCA-432 and OVCAR-3 cells are treated with are described in **Table 24** under T = 0 hr. Additionally, the cells were treated with free drug and nanoparticles formulations.

Examining the free drug treatment, the OVCA-432 cells had a significant reduction ( $p < 0.0001$ ) in cell viability to ~17% when treated simultaneously with paclitaxel and lapatinib relative to the control cells. Treatment with free paclitaxel had an even greater reduction in the cell viability of the OVCA-432 cells to ~5% ( $p < 0.001$ ). There was only a slight decrease in cell viability with free lapatinib of ~78%. In comparison, the OVCAR-3 cells exhibited a similar trend with the three treatments. The free lapatinib had no effect on the cell viability of the OVCA-432 cells. The lowest

cell viability of ~75% was attributed to treatment with free paclitaxel (**Figure 37**). Interestingly, these results are opposite to the IC-50 results, as the cell viability of the OVCA-432 cells is lower after 24 hours compared to OVCAR-3 cells.

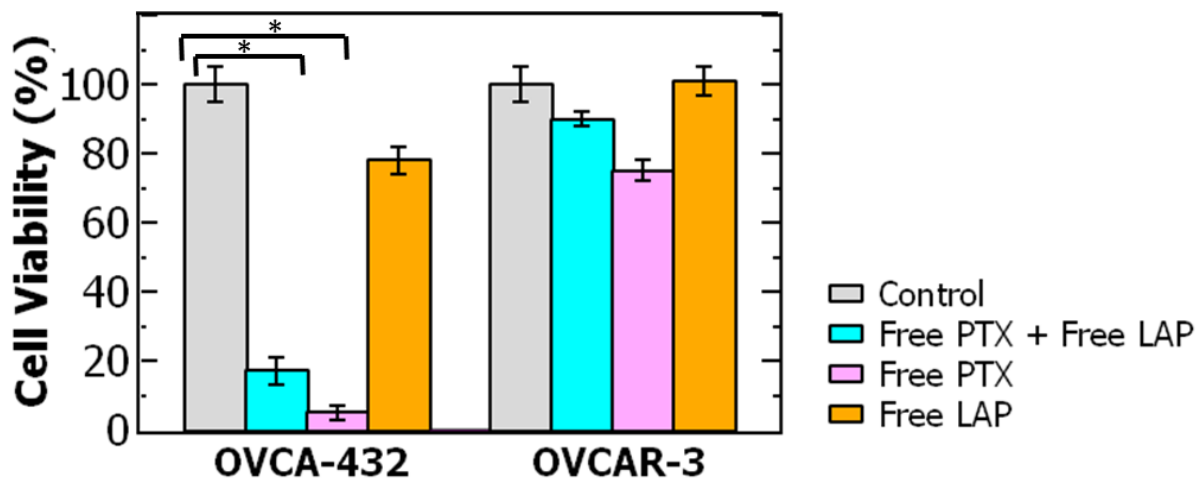


**Figure 37.** The cell viability was examined for OVCA-432 and OVCAR-3 cells following 24 hour treatment with a single free drug dose. Cells were either treated simultaneously with free paclitaxel and free lapatinib (light blue, PTX + LAP), with free paclitaxel alone (pink, Free PTX), with free lapatinib alone (light orange, Free LAP), or untreated (light grey, Control).

The two cell lines were also treated with either with a single nanoparticle or simultaneously with both PTX NPs and LAP NPs. In the case of OVCA-432 cells, there was a slight reduction in cell viability of 76% and 81% when treated simultaneously with two nanoparticles and with LAP NPs individually, respectively. Treatment with PTX NPs significantly reduced the cell viability of the OVCA-432 ( $p < 0.0001$ ) and had the greatest reduction in cell viability relative to the other two nanoparticle treatments. However simultaneous nanoparticle treatment produced the greatest reduction in cell viability of OVCAR-3 cells ( $p < 0.0001$ ) (**Figure 38**).

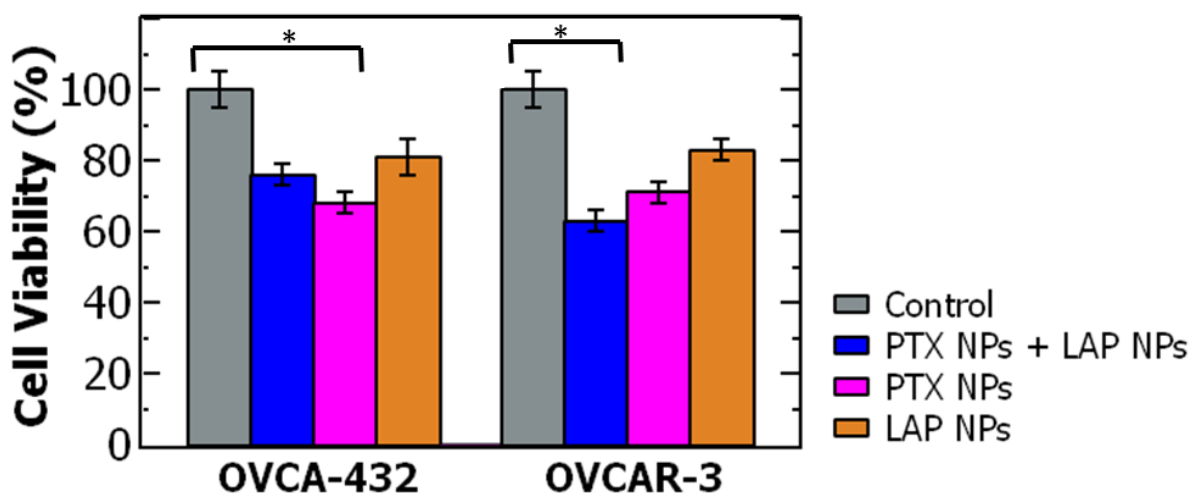


**Figure 38.** The cell viability was examined for OVCA-432 and OVCAR-3 cells following 24 hour treatment with a single nanoparticle drug dose. Cells were either treated simultaneously with PTX NPs and LAP NPs (dark blue, PTX NPs + LAP NPs), with PTX NPs alone (magenta, PTX NPs), with LAP NPs alone (orange, LAP NPs), or untreated (dark grey, Control).

The results from the 24 hour free drug treatment indicate that free paclitaxel had the greatest cytotoxic effects compared to free lapatinib and simultaneous treatment for both cell lines. The trends with the free drug are comparable between the two cell lines, however the OVCAR-3 cells had higher cell viabilities for all three treatments. However the nanoparticle drug efficacy differed between the two cell lines. The lowest cell viability was observed with PTX NPs for the OVCA-432 cells while the simultaneous nanoparticle treated had the greatest drug efficacy for the OVCAR-3 cells. These results indicates that a single 24 hour dose with free drugs produces comparable trends in drug efficacy for ovarian cancer cells such as lower cell viability with simultaneous delivery and paclitaxel relative to lapatinib.

However, with a single 24 hour dose with nanoparticle the drug efficacy is both cell type and treatment dependent. This could be attributed to the activation of signaling cascades and the variabilities of expression of key proteins involved with either tubulin polymerization as well as ABC transporter inhibition in the two cell lines [90,124,354,355]. It is also worth noting, that the OVCA-432 cells exhibit a significant decrease in cell viability after simultaneous and free paclitaxel treatment

compared to OVCAR-3 cells. In comparison, the cell viability following 24 hr treatment with nanoparticle is comparable between the two cell lines. This could be attributed to the slow drug release of paclitaxel and lapatinib from the nanoparticles [306] which facilitates the continuous delivery of a controlled dose. This suggest that nanoparticle drug delivery can produce consistent results between ovarian cancer cell types after a single dose and overcome the mechanisms of drug resistance. Further experiments such as measuring P-glycoprotein activity and nanoparticle endocytosis could facilitate in further understanding this phenomenon.

#### *5.3.4. Comparing Cell Viability Following Sequential Drug Combination Treatment*

Following the 24 hour treatment of the cells, the efficacy of sequential treatment was investigated for the two ovarian cancer cells. The cell viability was examined after treatment with three difference sequence schedules and dosed with the concentrations described in **Table 24** for OVCA-432 cells and **Table 25** for OVCAR-3 cells; 1) simultaneous drug delivery of paclitaxel and lapatinib, 2) paclitaxel followed by lapatinib, and 3) lapatinib followed by paclitaxel. The cells were treated for a total of 48 hours prior to measuring the cell viability.

Sequential treatment with free drugs produced comparable trends between the OVCA-432 and OVCAR-3 cells for the three sequences. Treatment with free paclitaxel followed by lapatinib decreased the cell viability to ~52% for the OVCA-432 cells ( $p < 0.0001$ ) and ~44% for the OVCAR-3 cells ( $p < 0.0001$ ). Simultaneous treatment with paclitaxel and lapatinib produced similar results to paclitaxel first treatment with cell viabilities of 56% and 49%, respectively for OVCA-432 and OVCAR-3 cells (**Figure 39**). The similarities in the trends between OVCA-432 and OVCAR-3 cells suggest that simultaneous delivery or free paclitaxel followed by lapatinib produces the greatest decrease in cell viability.

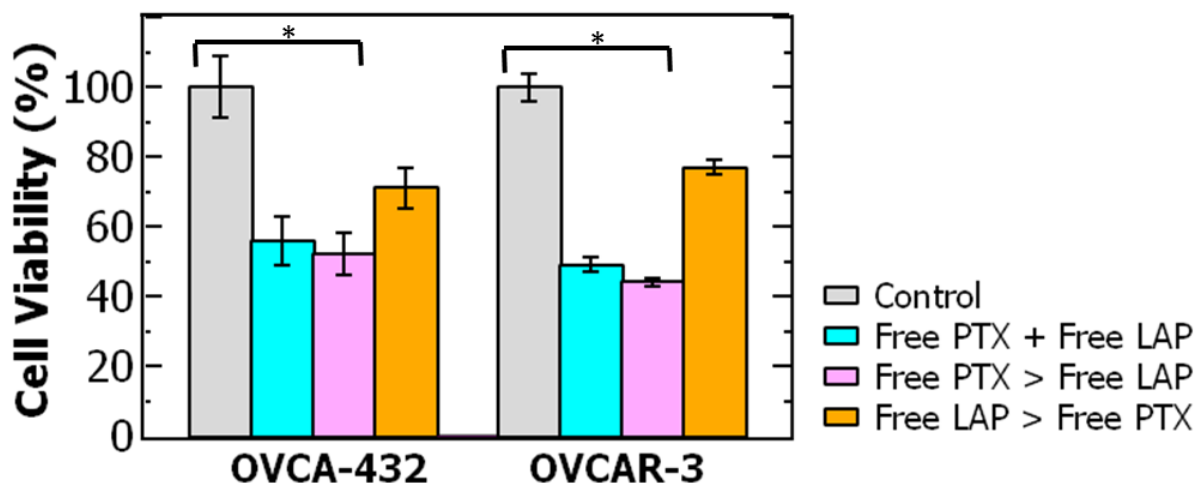


**Figure 39.** The cell viability of OVCA-432 cells and OVCAR-3 cells following 48 hour sequential treatment with free paclitaxel and free lapatinib. The cells were either untreated (light grey, Control), or treated with sequential drug delivery over 48 hours: simultaneous treatment of free paclitaxel and free lapatinib (light blue, Free PTX + Free LAP), (pink) paclitaxel followed by lapatinib (pink, Free PTX > Free LAP), and lapatinib followed by paclitaxel (light orange, Free LAP > Free PTX).

Next, we examined the cell viability of the two cell lines following sequential delivery with nanoparticles. The OVCA-432 cell line exhibited comparable levels of cytotoxicity across the three sequential treatments. In comparison, the three sequence schedule produced widely different results in OVCAR-3 cells. The lowest drug efficacy only resulted in a cell viability of 47% with simultaneous treatment with two nanoparticles, while PTX NPs followed by LAP NPs treated had the greatest drug efficacy resulting in a cell viability of ~3% for OVCAR-3 cells (**Figure 40**).



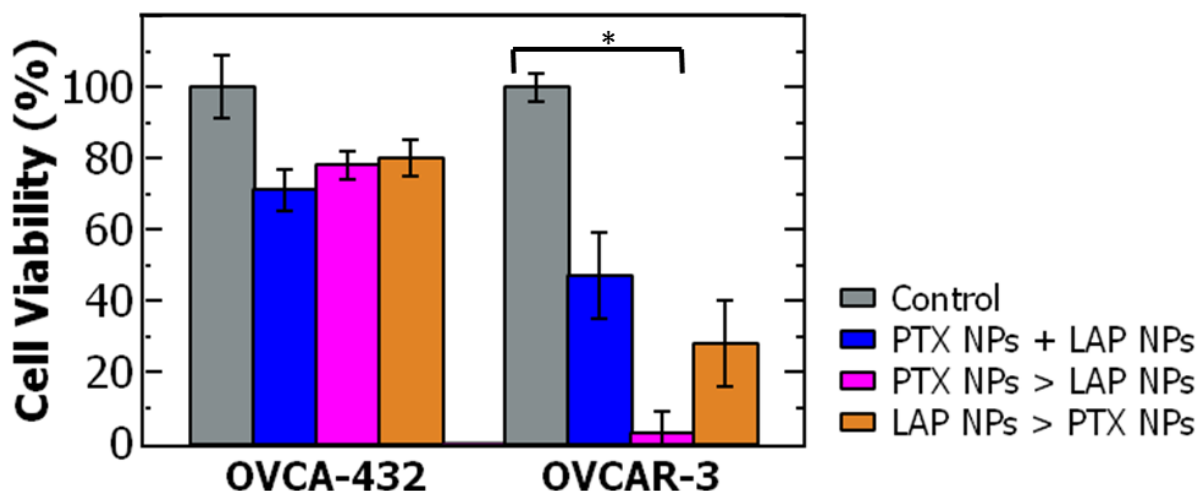


**Figure 40.** The cell viability of OVCA-432 cells and OVCAR-3 cells following 48 hour sequential treatment with PTX NPs and LAP NPs. The cells were either untreated (dark grey, Control), or treated with sequential drug delivery over 48 hours: simultaneous treatment of PTX NPs and LAP NPs (dark blue, PTX NPs + LAP NPs), paclitaxel followed by lapatinib (magenta, PTX NPs > LAP NPs), and lapatinib followed by paclitaxel (orange, LAP NPs > PTX NPs).

Interestingly, the trends observed with sequential treatment with free drug parallel the results from single dose 24 hour treatment. Free paclitaxel produced the greatest cytotoxic effect in both OVCA-432 and OVCAR-3 cells after 24 hours while free lapatinib produced to lowest. These results indicate that the first line of treatment has the greatest impact on the receptibility of the cells to the drugs. This could be attributed to longer incubation time for the drug uptake by the cells in the first 24 hours allowing for regulation of downstream anticancer pathways. The similarity in the trends observed with free drug between the two cell lines is noteworthy. Overall, the results from sequential free drug treatment suggest that either simultaneous delivery of paclitaxel and lapatinib or delivery of paclitaxel followed by lapatinib 24 hrs later produces the greatest cytotoxic effects.

Examining the results from sequential treatment with nanoparticles, there is a wide difference in response between the two cells lines for all three treatment schedules. The OVCAR-3 have substantially lower cell viability for all three treatments compared to OVCA-432 cells. The difference could be attributed to the resistance mechanisms to paclitaxel of OVCA-432 cells observed in the IC-

50 experiments as noted by the higher IC-50 values for paclitaxel which inhibit reduction in cell viability. However, in the case of OVCAR-3 cells, the IC-50 results with nanoparticles showed low potency of both PTX NPs and LAP NPs while delivery of both nanoparticles displayed high potency.

This difference could be attributed to interconnecting signaling cascades activated by the presence of both paclitaxel and lapatinib in OVCAR-3 cells, but perhaps some of the key proteins involved are over- or under-expressed in OVCA-432 cells producing a different outcome over the 48 hour period. Furthermore, the three nanoparticle sequence schedules produce similar cell viabilities over 48hrs in the OVCA-432 cells. These results suggest that the OVCA-432 are not sequence dependent with nanoparticle treatment. Inversely, the OVCAR-3 cells did exhibit sequence dependent cytotoxicity with the greatest cytotoxic effects observed with PTX NPs treatment 24 hours prior to LAP NPs. Cell-dependent cytotoxicity due to sequential and simultaneous drug delivery of paclitaxel and an inhibitor agent were also observed in previous studies [238,256,346,347].

#### *5.3.5. Comparing Cell Cycle Following Sequential Drug Combination Treatment*

The cell cycle was also examined for the OVCA-432 and OVCAR-3 cells following sequential treatment based on drug dosing described in **Table 26** and **Table 27** for each cell line, respectively to understand the interaction of the drugs on the cell activity. Generally, paclitaxel arrests cells in the G<sub>2</sub>/M phase [335], while lapatinib arrests cells in the G<sub>0</sub>/G<sub>1</sub> phase [336]. Thus, the order the order the cells are treated with the drugs could impact the final cell phase. The cell cycle was measured by analyzing the PI absorbance with flow cytometry. The cells were treated with the three sequential schedule previously described at each drug's IC-50 concentration. The cells were treated with both free drug and nanoparticle formulations.

Following treatment with free drugs, the OVCA-432 cells displayed a sequence dependent distribution in the cell cycle. OVCA-432 cells treated simultaneously with paclitaxel and lapatinib had

a decrease in cells compared to the control cells in the  $G_0/G_1$  phase from ~62% to ~20%. There was a large increase in the number of cells in the S and  $G_2/M$  from ~18% to ~29% and ~9% to ~34% when treated simultaneously with paclitaxel and lapatinib. When the OVCA-432 cells were treated with paclitaxel followed by lapatinib, there was also a decrease in cells in the  $G_0/G_1$  phase and an increase in cells in the S phase compared to simultaneous delivery. However, a greater percentage of OVCA-432 cells treated with paclitaxel followed by lapatinib accumulated in the sub $G_1$  phase and decrease in percentage of cells in the  $G_2/M$  compared to the simultaneous treatment. Sequential treatment with free lapatinib followed by paclitaxel resulted in accumulation of the OVCA-432 cells in the  $G_0/G_1$  phase and comparable cell distribution in the other three cell phases to the control cells (**Figure 41**)

Next, we examined the cell cycle distribution of the OVCAR-3 cells after sequential treatment with free drugs. The control cells that were untreated primarily accumulated in the  $G_0/G_1$  phase at ~64%. In comparison, all three sequences accumulated even higher percentage of cells in  $G_0/G_1$  compared to the control. Examining the distribution in the other three phases, all three sequences decreased the percentage of cells in the S and  $G_2/M$ , but saw an increase of cells in the sub $G_1$  phase relative to the control (**Figure 41**). There was no variability in the cell cycle distribution for the three sequential treatments with free drug for OVCAR-3 cells.

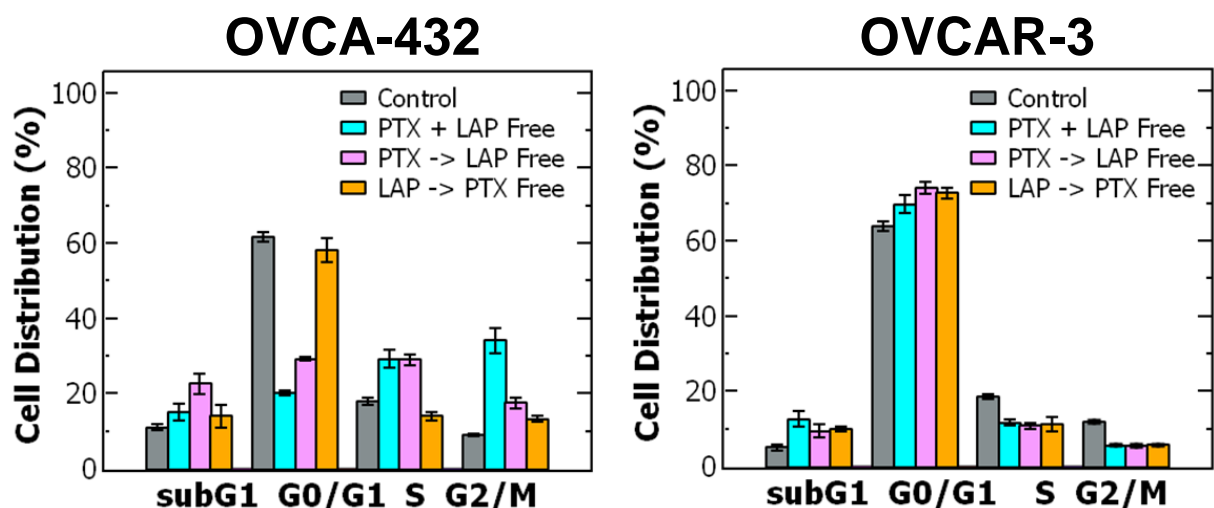


**Figure 41.** The cell cycle distribution for OVCA-432 and OVCAR-3 cells treated with three sequence schedules using free drugs. The cells were either untreated (light grey, Control), simultaneously treated with free paclitaxel and free lapatinib (light blue, PTX + LAP Free), free paclitaxel followed by free lapatinib 24 hrs later (pink, PTX > LAP Free), or free lapatinib followed by free paclitaxel 24 hrs later (light orange, LAP > PTX Free).

The OVCA-432 cells were also treated with nanoparticle formulation delivered in the three sequence schedules. Interestingly, the three nanoparticle sequential treatment produced comparable cell distributions. The notable difference is the cells treated simultaneous with PTX NPs and LAP NPs had decrease in percentage of cells in the G<sub>0</sub>/G<sub>1</sub> and subG<sub>1</sub> phases relative to the control from 62% to 56% and 11% to 4%, respectively. Additionally the simultaneous drug treated cells exhibited a slight increase in the S and G<sub>2</sub>/M phases relative to the control cells (**Figure 42**).

Following sequential treatment with nanoparticles the cell cycle distribution was examined for the OVCAR-3 cells. The untreated cells accumulated in the G<sub>0</sub>/G<sub>1</sub> phase. The distribution is comparable between the simultaneously delivered nanoparticles and PTX NPs followed by LAP NPs. There was a decrease in number of cells in the G<sub>0</sub>/G<sub>1</sub> phase from 64% to 40% and 34%, respectively. The cell distribution primarily accumulated in the subG<sub>1</sub> phases with an increase from the control cell of 5% to 20% and 18%, respectively. Cells treated with LAP NPs followed by PTX NPs exhibited a

smaller decrease in the G<sub>0</sub>/G<sub>1</sub> phase of 52%. Additionally, the cells exhibited only a slight increase in cells in the G<sub>2</sub>/M phases equivalent to the two other sequential treatments (**Figure 42**).

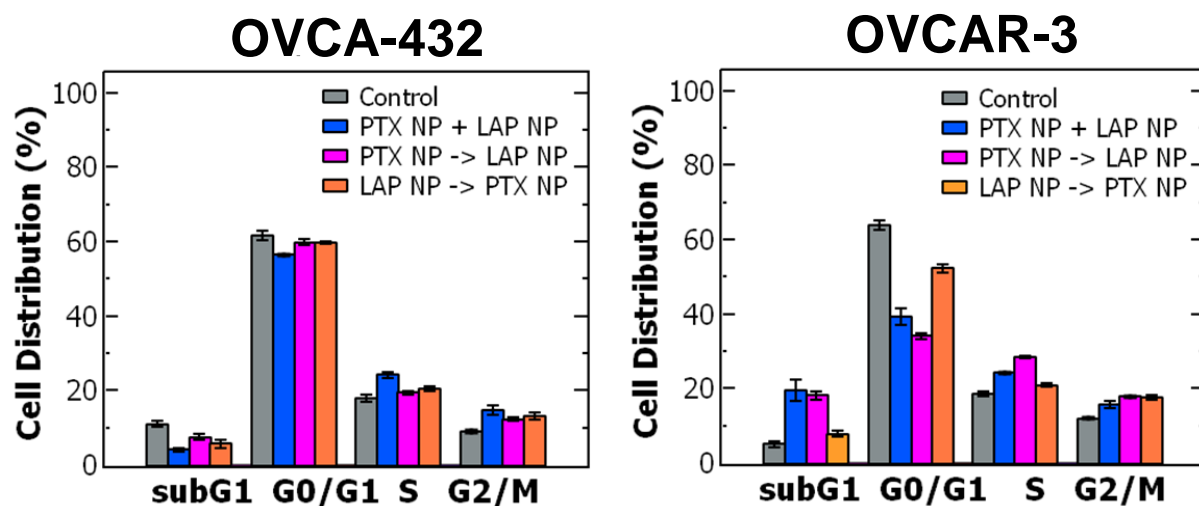


**Figure 42.** The cell cycle distribution for OVCA-432 and OVCAR-3 cells treated with three sequence schedules using nanoparticle formulations. The cells were either untreated (dark grey, Control), simultaneously treated with PTX NPs and LAP NPs (blue, PTX NPs + LAP NPs), PTX NPs followed by LAP NPs 24 hrs later (magenta, PTX NPs > LAP NPs), or LAP NPs followed by PTX NPs 24 hrs later (orange, LAP NPs > PTX NPs).

When we compared the results observed in the cell cycle analysis to the cell viability after sequential treatment. Interestingly, in the case of OVCA-432 cells, when treated with nanoparticles all the sequence schedules reduced the cell viability to ~80%. The similarity in the cell viability results could be attributed to a small shift in the cell cycle distribution of the OVCA-432 cells compared to the control for all three sequences. Therefore, it is not surprising to see that for OVCAR-3 cells when we observed a large reduction in cell viability due to simultaneous nanoparticle treatment as well as PTX NPs followed by LAP NPs we also see a large decrease in cells in the G<sub>0</sub>/G<sub>1</sub> phase and a redistribution to the subG<sub>1</sub> phase. As previously observed, accumulation in the subG<sub>1</sub> phase rather than then G<sub>2</sub>/M phases could indicate cells are spending a shorter period of time in G<sub>2</sub>/M arrest before progressing to subG<sub>1</sub> due to DNA damage leading to cell death [337,339].

Overall examining the results observed from the free drug and nanoparticle sequential treatment, we find that the greatest reduction in cell viability was observed in the cases where there

was either a decrease of cells in the  $G_0/G_1$  phase, increase in  $G_2/M$ , increase in  $subG_1$ , or combination thereof. These results indicate that sequentially delivering paclitaxel and lapatinib has an effect on the cell cycle arrest and the greatest cytotoxicity was observed when there was redistribution to  $G_2/M$  and  $subG_1$  phases. Furthermore, these results suggest that the timing of lapatinib delivery can enhance the effects of paclitaxel to limit proliferation and induce cell death particularly in sequential delivery of paclitaxel followed by lapatinib or simultaneous delivery of both drugs.

#### 5.4. Conclusion

In this study, we have examined *in vitro* sequential delivery of paclitaxel and lapatinib encapsulated into polymer nanoparticles on ovarian cancer cells. We observed a sequence-dependent cytotoxic effect. The greatest reduction in cell viability was observed in the cases with simultaneous delivery of paclitaxel and lapatinib or paclitaxel followed by lapatinib. We observe variability in the cytotoxicity both due to the cell type and the drug formulation (nanoparticle compared to free drug). A parallel was observed between the reduction in cell viability and the cell cycle distribution, with the lowest cell viability observed when there was increase in percentage of cells in the  $G_2/M$  and  $subG_1$  phases indicating an increase in paclitaxel activity. These results are promising for establishing sequential drug delivery with nanoparticles as a method for treating ovarian cancer. Building on this promising study, further studies to examine the gene expression and protein phosphorylation are necessary to understand the effects of sequential drug delivery as well as a broader cell population. Evaluating the rate of drug release from the nanoparticles will be important for designing nanomedicines to achieve sequential delivery paclitaxel and lapatinib from co-loaded nanoparticles for spatiotemporal control of drug release.

## 6. Chapter 6: Controlled Drug Release of a Paclitaxel Prodrug from pH-Labile Nanoparticles to Improve Drug Efficacy

---

### Abstract

The drug efficacy of chemotherapeutic agents such as paclitaxel is limited due to their poor solubility, poor bioavailability, and acquired drug resistance mechanisms in ovarian cancer cells. Prodrug formulations have the potential to enhance the drug efficacy by increasing drug potency. In this study, we examined combining prodrug formulation of paclitaxel with a pH-labile nanoparticle platform to control drug delivery and the effect on drug efficacy. pH-labile nanoparticles were formulated using Flash NanoPrecipitation paired with *in situ* tannic acid-iron complexation. We determined the formulation parameters required to produce monodispersed nanoparticles encapsulating a hydrophobic prodrug of paclitaxel alone and in combination with lapatinib. The nanoparticle drug release profiles were evaluated *in vitro* under pH 7.4 and pH 4 conditions and fit with the Korsmeyer-Peppas model and Hixson-Crowell model, respectively. The drug release at pH 7.4 of paclitaxel-lapatinib nanoparticles is governed by Fickian diffusion, but the release of prodrug-lapatinib nanoparticle is governed by Super Case II transport resulting in sequential drug release. The drug release kinetics at pH 4 are governed by dissolving core due to the solubilization of TA-Fe<sup>3+</sup>. The drug efficacy was evaluated *in vitro* with ovarian cancer cell model (OVCA-432) and we determined that the prodrug formulation of paclitaxel increased drug potency of the nanoparticle formulation by 5-fold. Based on the results of the study, the drug efficacy of paclitaxel could be increased by

formulation of a hydrophobic prodrug, encapsulation into nanoparticles, co-encapsulation with lapatinib, or combination of these approaches.

## 6.1. Introduction

Taxol, a formulation of paclitaxel (PTX), is one of the most widely used anticancer drugs for treating ovarian carcinomas. However, there are challenges associated with Taxol treatment due to its poor solubility, poor bioavailability, and acquired drug resistance mechanisms resulting in low drug efficacy [102–104,248]. There are several approaches to improving drug efficacy of chemotherapeutic agents, such as prodrug formulation, encapsulation into nanoparticles, and co-delivery with other anti-cancer drugs.

Formulation of prodrugs of therapeutic agents is an approach to modulating the properties of the drug molecule such as hydrophobicity, vehicles for targeting, and chemical stability [262,356,357]. By modulating these properties, prodrugs have the potential to overcome challenges of the therapeutic agent. Prodrugs are formulated by conjugating a molecule such as an enzyme or an inactive molecule by linker. Therefore, the properties of the prodrug can be tuned with a combination of the selected molecule and degradation rate of the linker [358]. Previous studies have examined formulation of paclitaxel prodrugs [262,357]. Ansell et al. formulated a series of hydrophobic paclitaxel prodrugs with various lipids conjugated via a nondegradable linker and examined their stability, half-life, and drug efficacy. The study found that while the drug efficacy was decreased *in vitro* when treating breast cancer cells, the half-life was extended compared to paclitaxel [261]. Another study synthesized silicate ester derivatives of paclitaxel with a range of hydrolysis rates and those with relatively fast hydrolysis exhibited comparable cytotoxicity to paclitaxel [357].

Another advantage prodrug formulations is they can facilitate stable encapsulation into polymer nanoparticles [262,357,359]. Nanoparticles drug delivery can be used to control the rate of



drug delivery, control pharmacokinetics, and lower systemic toxicity [188,201,204]. However, it can be challenging to encapsulate therapeutic agents that are not highly hydrophobic into polymer nanoparticles [357,359]. Therefore, combining the benefits of prodrugs approach and nanoparticle drug delivery can be advantageous for treating ovarian cancer. For example, Ansell et al, also examined encapsulation of their prodrugs into polymer nanoparticles by co-encapsulations with a lipid, phosphatidylcholine, via Flash NanoPrecipitation (FNP). This technique facilitated paclitaxel encapsulation and control the drug release by adjusting the length of the alkyl anchor [261]. Other nanoparticle platforms have also been investigated for encapsulating paclitaxel prodrugs [360–363]. Stevens et al. investigated encapsulating a hydrophobic carbonyl cholesterol prodrug of paclitaxel into lipid nanoparticles by co-encapsulation with PEGylated cholesterol. This formulation allowed for high paclitaxel encapsulation efficiencies and improve cytotoxicity *in vitro* and *in vivo* [360].

Encapsulation of hydrophilic paclitaxel prodrugs into nanoparticles has also been investigated such as poly(ethylene glycol)-b-poly(acrylic acid) (PEG-b-PAA) conjugated paclitaxel. The prodrugs were encapsulated into a pH-responsive nanoparticle (i.e. release under acidic conditions) and displayed enhanced drug efficacy *in vitro* [361]. pH-responsive nanoparticle platforms allow for control of drug delivery and can be advantageous in delivery of drug combinations to increase drug efficacy.

Sequential delivery of combination chemotherapeutics has shown improvements in drug efficacy [184,186,190]. By tuning the properties of the paclitaxel with a prodrug approach, we can sequentially deliver it drug combinations to increase cytotoxicity of the treatment. In this study, we will investigate paclitaxel drug efficacy with a hydrophobic prodrug formulated by conjugating  $\alpha$ -tocopherol (vitamin E) using a diglycolic anhydride linker and encapsulation into a pH-responsive nanoparticle platform. The nanoparticles will be formulated with *in situ* complexation with tannic acid-iron complex via Flash NanoPrecipitation, as previously described [271,306]. The nanoparticle

formulation parameters are investigated for encapsulation of the hydrophobic prodrug alone and in combination with lapatinib, an anticancer drug. The drug release kinetics are determined for the nanoparticles under pH 7.4, when the TA-Fe<sup>3+</sup> is insoluble and the nanoparticles are stable and pH 4, when the TA-Fe<sup>3+</sup> is solubilizing and destabilizing the nanoparticles. Lastly, the drug efficacy is compared *in vitro* using ovarian cancer cell model between paclitaxel and its prodrug counterpart in free drug form, encapsulated into nanoparticles alone and in combination with lapatinib.

## 6.2. Materials and Methods

### 6.2.1. Materials

HPLC grade tetrahydrofuran (THF), dimethyl sulfoxide (DMSO), diglycolic anhydride (97%, Alfa Aesar), Diisopropylcarbodiimide (99%, Alfa Aesar), alcohol-free chloroform, acetonitrile, and acetic acid were purchased from Fisher Scientific (Pittsburg, PA). ACS grade tannic acid (TA), ACS grade iron (III) chloride hexahydrate (97%),  $\alpha$ -tocopherol (Vitamin E, >95.5%), and sodium acetate were purchased from Sigma-Aldrich (St. Louis, MO). Paclitaxel (PTX, >98%) and lapatinib (LAP, >98%) were obtained from Cayman Chemical Company (Ann Arbor, MI); phosphate buffered saline without calcium and magnesium was purchase from Lonza (Basel, Switzerland). Pyridine, dichloromethane (DCM), hydrochloric acid (HCl), anhydrous magnesium sulfate, and 4-N,N-dimethylaminopyridine kindly gifted from Dr. Thomas Roper from Virginia Commonwealth University. Polystyrene-b-polyethylene glycol (1600-b-500 g/mol) (PS-b-PEG) was obtained from Polymer Source (Montreal, Canada) and was purified by dissolving in THF (~40°C) and precipitating into diethyl ether then dried by vacuum for two days as previously described [278].

### 6.2.2. Cell Culture

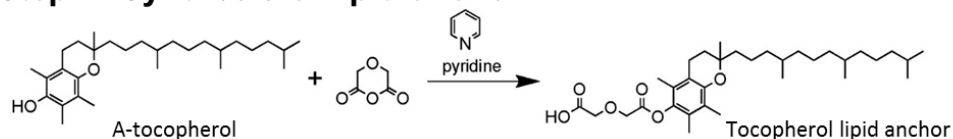
Ovarian cancer cell line OVCA-432 was a kind gift from Dr. Xianjun Fang from Virginia Commonwealth University. The OVCA-432 cells were cultured in RPMI-1640 media containing 2 mM L-glutamine (ATCC, Manassas, VA) supplemented with 10% Fortified Bovine Calf Serum (FBS, HyClone Cosmic Calf Serum, Fisher Scientific, Pittsburg, PA), 100 U/mL penicillin and 100 µg/mL streptomycin (Gemini Bio-Products, West Sacramento, CA). The cells were cultured at 37 °C at 5% CO<sub>2</sub> and passaged once a week.

### 6.2.3. Prodrug Formulation

A hydrophobic paclitaxel-prodrug was formulated via conjugation to  $\alpha$ -tocopherol (vitamin E) lipid anchor which was previously described by Ansell, et al [261]. The paclitaxel-prodrug was formulated by a two-step reaction using a diglycolic anhydride linker. In the first- step of the reaction the lipid anchors were synthesized via an oxidation reaction of tocopherol (1 equiv) and diglycolic anhydride (3 equiv) in pyridine to form a carboxylic acid group on the lipid anchor. The reaction was monitored by TLC. The product from the first reaction was extracted using dichloromethane (DCM) and hydrochloric acid (HCl) and recovered by drying in a rotovap. Then in the second step the lipid anchor was conjugated to paclitaxel via an esterification reaction in which paclitaxel (1 equiv) was reacted with the tocopherol lipid anchor (2 equiv), 4-N,N-dimethylaminopyridine (3 equiv), and diisopropylcarbodiimide (1.3 equiv) in chloroform. This reaction forms a covalent link between the hydroxyl group on the paclitaxel and the carboxylic acid group on the lipid anchor forming an ester (**Figure 43**). The reaction was monitored with TLC until completion. The mixture was then washed with HCl and dried over anhydrous magnesium sulfate. The product was purified with a silica gel column using a hexane/ethyl acetate gradient and the dry formulation was recovered by removal of the solvent with a rotovap. The final product was analyzed with H<sup>1</sup> NMR (**Appendix I, Figure S1**)

and direct-infusion electrospray mass spectrometry (**Appendix I, Figure S2**) performed the Chemical and Proteomic Mass Spectrometry Core Facility at Virginia Commonwealth University. The reaction yield was ~60% and the synthesized paclitaxel-tocopherol prodrug had a molecular weight of 1380 g/mol by mass spectroscopy.

### Step 1: Synthesis of lipid anchor



### Step 2: Synthesis of paclitaxel prodrug

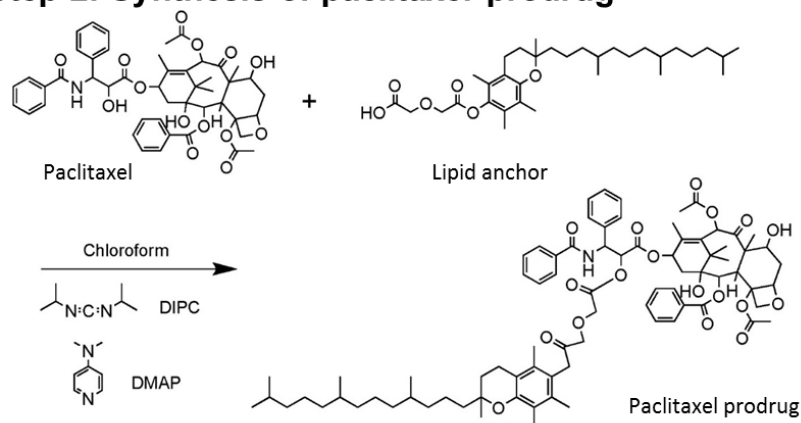


**Figure 43.** Two-step synthesis of the paclitaxel-prodrug with  $\alpha$ -tocopherol as the lipid anchor. In the first step the tocopherol lipid anchor is synthesized and in the second step paclitaxel is conjugated to the lipid anchor to form the prodrug.

#### 6.2.4. Nanoparticle Formulation

Flash NanoPrecipitation (FNP) was used to prepare polymer-based nanoparticles encapsulating the anti-cancer drugs via tannic acid-iron *in situ* complexation with a hand-operated confined impinging jet (CIJ) mixer, as previously described [271,306]. Six nanoparticles were formulated that either encapsulated the TA-Fe complex (TA-Fe NPs), PTX (PTX NPs), LAP (LAP NPs), both PTX and LAP (PTX-LAP NPs), PTX-prodrug (Pro NPs), both PTX-prodrug and LAP (Pro-LAP NPs).

Briefly, PS-b-PEG, TA (4 mg/mL), and one or more drugs were dissolved in THF by sonicating (~40°C) for 10 minutes to formulate the organic stream. The organic stream was rapidly mixed with the Fe<sup>3+</sup> (aq., 1 mg/mL) at equal volumes (1 mL of each stream) in the CIJ mixer. The effluent from the mixer was immediately diluted in 1X PBS at pH 7.4 for a final organic solvent/water ratio of 1:9 by volume. The nanoparticles were formulated based on the concentration and ratios described in **Table 30**.

**Table 30.** Formulation parameters for single-drug and co-loaded nanoparticles with paclitaxel, prodrug, and lapatinib.

Drug	Drug Concentration (mg/mL)	BCP:Core ratio	Total solids Concentration (mg/mL)
PTX	1	2:1	16
LAP	1	2:1	16
PTX-LAP	0.5 / 0.5	1.5:1	13.5
Prodrug	0.5	2:1	14.5
Prodrug-LAP	0.5 / 0.5	1:1	11

Within 24 hrs of formulation, the nanoparticles were filtered to remove the organic solvent, unencapsulated drug(s), and excess TA and Fe<sup>3+</sup> with Amicon Ultra-2 Centrifugal filters (Amicon Ultra centrifuge filter (Ultracel 50K, 50,000 NMWL), Merck Millipore Ltd, Burlington, Ma) by centrifuging at 3700 rpm for ~15-30 minutes (5804 R 15 amp version, Eppendorf, Hamburg, Germany). The nanoparticle pellet was resuspended with 1X PBS to a nominal concentration ~25 mg/mL of total solids and stored at ~4 °C. The nanoparticles were used within 5 days of the FNP to ensure there was minimal change in particle size and drug loss.

#### 6.2.5. Nanoparticle Characterization

The size and polydispersity (PDI) of the nanoparticles were characterized after FNP using dynamic light scattering (Malvern Zetasizer ZS, Malvern Instruments Ltd, Malvern, United Kingdom).

The nanoparticle size and PDI were measured by averaging 4 measurements at a scattering angle of 173°. The average and standard deviation of three replicate FNP samples are reported.

The nanoparticles were analyzed with transmission electron microscopy (TEM). Samples were prepared by diluting the filtered nanoparticle dispersions with DI water 1:20 by volume ratio and pipetting 5  $\mu\text{L}$  three times onto a TEM grid with Formvar/Carbon support films (200 mesh, Cu, Ted Pella, Inc, Redding, CA) and dried under ambient conditions. The samples were imaged with a JEOL JEM-1230 (Peabody, MA) at 120 kV.

The nanoparticle encapsulation efficiency (EE%) and drug loading (DL%) were determined for the size nanoparticles. The nanoparticles were filtered to remove the organic solvent, unencapsulated drug(s), and excess TA and  $\text{Fe}^{3+}$  with Amicon Ultra-2 Centrifugal filters (Ultracel 50K) by centrifuging at 3700 rpm for ~15-30 minutes (5804 R 15 amp version, Eppendorf, Hamburg, Germany) within 24hrs of formulation. The nanoparticle pellet was resuspended with 1X PBS to a nominal concentration ~25 mg/mL of total solids and stored at ~4 °C.

The concentration of the nanoparticle dispersion was determined by thermogravimetric analysis (TGA) (Pyris 1 TGA, Perkin Elmer, Waltham, MA). The nanoparticle dispersion was loaded at 10  $\mu\text{L}$  and the temperature was ramped up from 28°C to 110°C at 10°C/min and held for 30 minutes at 110°C. The final nanoparticle mass was used to determine the nanoparticle drug loading.

To determine the drug content of the nanoparticles, acetonitrile (360  $\mu\text{L}$ ) was added to nanoparticles (10  $\mu\text{L}$ ) and the sample was vortexed so that the nanoparticles would disassemble. The sample was centrifuged at 10,000 rpm for 7 minutes, and then the supernatant was collected for reverse-phase high Performance Liquid Chromatography (RP-HPLC) (1260 HPLC with Quaternary Pump and UV-Vis Diode Array Detector, Agilent, Santa Clara, CA) fitted with a Luna® 5  $\mu\text{m}$  C18 100 Å, LC Column 250 x 4.6 mm (Phenomenex, Torrance, CA).

Chromatography for PTX NPs, LAP NPs, and PTX-LAP NPs samples was eluted with a gradient of degassed water and acetonitrile at a flow rate of 1 mL/min (0-1 minute at 80:20, 1-6 of ramp up to 0:100, 6-8 minutes at 0:100, and ramp down to 80:20 between 8-9 minutes). PTX was measured at a wavelength of 228 nm with a retention time of ~8 minutes and LAP was measured at 332 nm with a retention time of ~9 minutes. The Pro NPs and Pro-LAP NPs samples were eluted with a gradient of degassed 10 mM sodium acetate buffer (pH 5.6) and methanol at a flow rate of 1 mL/min (0-5 minutes at 70:30, 5-16 minutes of ramp up to 0:100, 16-17 minutes of at 0:100, and 17-21 minutes of ramp down to 70:30). PTX-prodrug was measured at a wavelength of 228 nm with a retention time of ~16 minutes and LAP was measured at 332 nm with a retention time of ~9 minutes.

The concentration of each drug was determined by comparing the peak areas with the standard calibration curve. Encapsulation efficiency (EE%) and drug loading (DL%) were calculated based on equations 10 and 11, respectively, and the values reported are the average and standard deviation of three trials.

$$\text{encapsulation efficiency (EE\%)} = \frac{\text{Mass of drug encapsulated}}{\text{Initial mass of drug}} \times 100\% \quad (\text{Eq. 10})$$

$$\text{drug loading (DL\%)} = \frac{\text{Mass of drug encapsulated}}{\text{Total nanoparticle mass}} \times 100\% \quad (\text{Eq. 11})$$

#### 6.2.6. Nanoparticle Drug Release In Vitro

The drug release from the nanoparticles was measured under neutral and acidic conditions. The nanoparticle samples were prepared by concentrating the dispersion to 1000 µg/mL drug concentration for PTX NPs, LAP NPs, and Pro NPs, and 500 µg/mL paclitaxel or prodrug concentration of PTX-LAP NPs and Pro-LAP NPs using Amicon Ultra-2 Centrifugal filters (Ultracel 50K), as previously described. The concentrated nanoparticle dispersion (500 µL) was loaded into 7,000 MWCO dialysis unit (Slide-A-Lyzer® MINI Dialysis Unit, Thermo Scientific, Waltham, MA)

and incubated in dialysis media at 37°C, which was replaced every day of the experiment. Nanoparticles tested under neutral conditions were incubated with PBS at pH 7.4 with 0.5% Tween 80 and the nanoparticle dispersion was sampled (32 µL) at 0 h, 3 h, 6 h, 24 h, 48 h, day 4, day 6, and day 10. Nanoparticles that were tested under acidic conditions were incubated with 50 mM acetate buffer at pH 4 with 0.5% Tween 80. The nanoparticle dispersion under acidic conditions were sampled (32 µL) at 0 h, 10 min, 30 min, 1 h, 2 h, 5 h, 8 h, 24 h, 48 h, day 4, day 6. The drug concentration was determined by RP-HPLC as described for measuring encapsulation efficiency and drug loading. Three replicates of each drug-loaded nanoparticle dispersion were tested.

#### *6.2.7. Determining Half Maximal Inhibitory Concentration*

The half-maximal inhibitor concentration (IC-50) of the free drug and nanoparticle formulation were examined for the OVCA-432 cells to determine drug potency. Cells were seeded at a density of  $15 \times 10^3$  cell/well in a 96-well plate containing 100 µL of complete medium. The cells were incubated at 37 °C in 5% CO<sub>2</sub> overnight. Then the media was replaced with 100 µL medium containing free-drug or nanoparticles and treated for 48 hours. Stock solution of free-drug were prepared by dissolving PTX (12 mg/mL), PTX-prodrug (5 mg/mL), and LAP (5 mg/mL) in DMSO and sonicating for 5 minutes. The nanoparticles were concentrated with Amicon filters (50kDa MWCO) as previously described and the nanoparticle pellet was diluted with 1X PBS to a concentration of 1000 µg/mL of drug. Serial dilutions of the stock free drug and nanoparticle dispersion were prepared with complete medium for a final concentration between 200 - 0.0002 µg/mL and a total volume of 100 µL. Additional DMSO was added to the free drug formulations for a final DMSO concentration of 2% v/v. The cells were also treated with complete media and 2% DMSO media as controls for comparison.

There were 6 replicates for each experimental condition. After 48 hours, the cell viability was measured with WST-1 assay (Sigma-Aldrich, St. Louis, MO) according to manufacturing instructions.



Briefly, the drug-loaded medium was removed and 100  $\mu$ L of RPMI-1640 with Phenol Red (Fisher Scientific, Pittsburg, PA) containing 10% WST-1 solution was added to each well and to 6 additional empty wells. The cells were incubated between 45 - 90 minutes until there was a visible color change to a golden-yellow or the absorbance of control wells reached at least 0.700 measured with a microplate reader (VersaMax ELISA microplate reader, Molecular Devices, San Jose, Ca) at a wavelength of 440 nm with background subtraction of 640 nm. The cell viability was determined by subtracting the background noise (wells containing only 10% WST-1 in media) from the samples and then dividing the sample absorbance by the average absorbance of the untreated wells. The cell viability of cells treated with free drug were normalized with cells treated with 2% DMSO. The relative cell viability was expressed as a percentage of the untreated cells with mean  $\pm$  standard deviation of six replicates.

#### 6.2.8. Cell Cycle Analysis by Flow Cytometry

The OVCA-432 cells were seeded at a density of  $20 \times 10^4$  cells/mL in a 35 mm petri dish containing 3 mL of complete media. The cells were incubated at 37°C and 5% CO<sub>2</sub> until 90% confluence and the media was replaced every 2 days. The cells were treated with either free drug or nanoparticle formulations for 48 hours at the IC-50 of each drug formulation, respectively. Then, the cells were stained with Propidium Iodide (PI Flow Cytometry Kit, Abcam, Cambridge, MA) for flow cytometry according to manufacturing instructions. Briefly, the cells were trypsinized and the aspirated medium and PBS were collected to minimize cell loss. The cells were centrifuged at 700 x g for 5 minutes as necessary. The cells were washed with 1X PBS and fixed with 66 % ethanol by slowly adding ethanol to PBS during vortexing. The cells were stored in ethanol at 4 °C for at least 2 hrs and up to 4 days. The cells were centrifuged and washed with PBS to remove the ethanol. The 1X Propidium Iodide and RNase solution was prepared immediately prior to use by mixing 5% v/v of

20X Propidium Iodide and 0.05% v/v 200X RNase in 1X PBS. Then the cells were resuspended in 200  $\mu$ L/500,000 cells of 1X Propidium Iodide and RNase solution and incubated in the dark at 37 °C for 30 minutes. Prior to flow cytometry, the cell samples were stored on ice and filtered through a cell strainer (Falcon Test Tube with Snap Cap, Fisher Scientific, Pittsburg, PA). Flow cytometry was performed on a BD FACSCanto™ II Analyzer (BD Biosciences, San Diego, CA) and 10,000 cells were analyzed at an excitation of 488 nm and emission of 670 nm. The samples were analyzed in triplicate.

## 6.3. Results and Discussion

### 6.3.1. Formulation of Prodrug Nanoparticles

Polymer nanoparticles were formulated using Flash NanoPrecipitation (FNP), a rapid, scalable process for encapsulating hydrophobic ( $\log P > 6$ ) [259,264] and weakly hydrophobic drugs ( $\log P < 6$ ) [271,306]. Encapsulation of paclitaxel and lapatinib into nanoparticles via FNP via *in situ* coordination complexation of an antioxidant (i.e. tannic acid) with iron was previously described [306]. *In situ* complexation of tannic acid and iron has also been applied to hydrophobic materials [271]; therefore, it was selected to encapsulation the hydrophobic prodrug of paclitaxel ( $\log P = 10.1$ ) alone and in combination with lapatinib. Briefly, nanoparticles were formulated by dissolving the block co-polymer (PS-b-PEG), tannic acid, and one or more drugs in THF to make the organic stream. The organic stream was rapidly mixed with  $\text{Fe}^{3+}$  (aq.) in a confined impinging jet (CIJ) mixer. Upon mixing, an insoluble tannic acid-iron (TA-Fe) complex is formed, precipitation of the drugs, and self-assembly of the PS-b-PEG. The formation of the TA-Fe complex facilitates encapsulation the precipitating drugs and the growth of the nanoparticle core is kinetically stabilized by the adsorption of the block co-polymer onto the surface of the core. This study will focus on parameters of encapsulating hydrophobic drugs and drug combinations.

The goal was to formulate monodispersed nanoparticles <200 nm nanoparticles for passive targeting [314]. We first examined encapsulating the hydrophobic paclitaxel prodrug alone (Pro NPs). Based on previous results, we determined the two parameters that effect nanoparticle size and polydispersity were ratio of the concentration of the drug and the ratio of the block co-polymer to core (BCP: core). Initially, we examined the prodrug concentration relative to the streams and a BCP: core ratio of 2:1 was selected based on previous results for single-drug nanoparticles [306]. At a drug concentration of 1 mg/mL large nanoparticles were produced at  $184 \pm 11$  nm and a secondary particle size of  $26 \pm 2$ . The nanoparticles on the order of  $\sim 30$  nm can be attributed to empty block copolymer micelles [271,280]. When the prodrug concentration was reduced to 0.5 mg/mL the primarily particle size decreased to  $\sim 155$  nm but also contained a secondary micelle peak. By further reducing the drug concentration to 0.25 mg/mL, monodispersed nanoparticle were produced at a size of  $135 \pm 6$  nm and a polydispersity (PDI) of  $0.206 \pm 0.017$  (**Table 31**). However, this resulted in relatively low nominal drug loading. Therefore the BCP: core ratio was examined as a method for increasing the nominal drug loading while maintaining a monodispersed particle distribution.

**Table 31.** Varying the concentration of the PTX-prodrug.

Sample	Ratio	Prodrug Concentration (mg/mL)	Size 1 (nm)	Size 2 (nm)	PDI
Pro NPs	2:1	1	$184 \pm 11$	$26 \pm 2$	$0.373 \pm 0.050$
	2:1	0.5	$156 \pm 18$	$29 \pm 2$	$0.318 \pm 0.021$
	2:1	0.25	$135 \pm 6$	--	$0.206 \pm 0.017$

The maximum drug concentration at a BCP: core ratio of 2:1 was 0.25 mg/mL which is less than the maximum drug concentration previously observed for PTX NPs and LAP NPs (BCP: core = 2:1) of 1 mg/mL [306]. The decrease in maximum drug loading could be attributed to relatively greater affinity of the hydrophobic block of the block co-polymer onto the surface of the growing core of the Pro NPs due to the higher hydrophobicity of the prodrug [261,263].

Varying the ratio of the block co-polymer had an impact on the size and polydispersity of the Pro NPs. A drug concentration of 0.5 mg/mL was used in these experiments in order to increase the nominal drug loading. Decreasing the ratio from 2:1 to 1:1 increased the nanoparticle size from ~155 nm to ~390 nm as well as the PDI to  $0.789 \pm 0.172$ . These nanoparticles were considered polydispersed due to the large PDI. At a ratio of 1.5:1 and a drug concentration of 0.5 mg/mL, monodispersed nanoparticles were produced at  $98 \pm 4$  nm and a PDI of  $0.233 \pm 0.008$  (**Table 32**). TEM analysis confirms the particles are spherical and the particle size is consistent with DLS (**Figure 44**).

From the results we observed that both the BCP: core ratio and the total drug concentration of Pro NPs can be tuned to formulated monodispersed nanoparticles. Interestingly, the intermediate ratio of the BCP: core produced monodispersed nanoparticles on the order of ~100 nm. This could be attributed to an appropriate matching of timescales between nucleation of the core (TA-Fe<sup>3+</sup> complexation and precipitation of the prodrug) and self-assembly of the block co-polymer. By matching the timescales, we minimized the formation of empty micelles and allowed for greater nominal drug loading. This principle has been previously described and studied for other hydrophobic materials encapsulated via FNP [259,265,281,364].

**Table 32.** Varying ratio of the block co-polymer to core ratio.

Sample	BCP: core Ratio	Prodrug Concentration (mg/mL)	Size 1 (nm)	Size 2 (nm)	PDI
Pro NPs	2:1	0.5	$156 \pm 18$	$29 \pm 2$	$0.318 \pm 0.021$
	1.5:1	0.5	$98 \pm 4$	--	$0.233 \pm 0.008$
	1:1	0.5	$389 \pm 138$	$35 \pm 70$	$0.789 \pm 0.172$

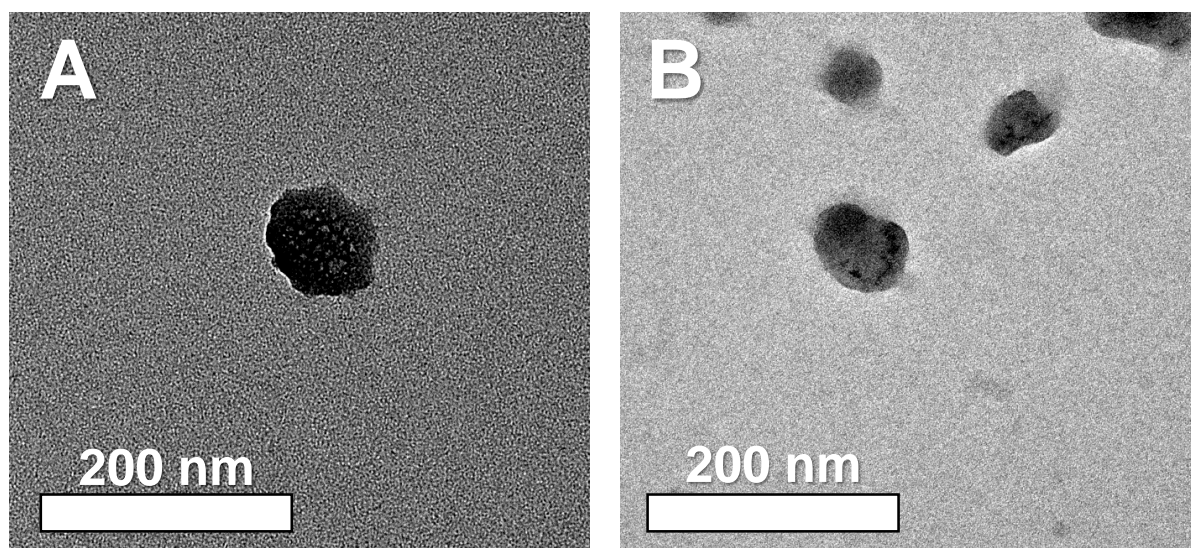


**Figure 44.** Representative transmission electron microscopy (TEM) images of (A) Pro NPs and (B) Pro-LAP NPs taken at 40kX (scale bar = 200 nm).

The parameters for co-encapsulating a hydrophobic drug ( $\log P > 6$ ) with a weakly hydrophobic drug ( $\log P < 6$ ) into monodispersed nanoparticles were also examined. The prodrug was encapsulated with lapatinib to form Pro-LAP NPs. We first examined the ratio of the prodrug to lapatinib. In previous studies, co-loaded nanoparticles of paclitaxel and lapatinib a 1:1 ratio by mass and a total drug concentration of 1 mg/mL produced monodispersed nanoparticles [306]. Therefore, we selected these parameters to determine if they would translate to encapsulating the paclitaxel prodrug and lapatinib. Using equivalent concentrations of prodrug and lapatinib at 0.5 mg/mL of each drug produced polydispersed nanoparticles with two size populations at ~170 nm and ~31 nm (micelles). When the amount of prodrug was decreased to 0.25 mg/mL, there was not a significant impact on the nanoparticle size and polydispersity (**Table 33**).

**Table 33.** Varying the prodrug concentrations of Pro-LAP NPs.

Sample	BCP: Core Ratio	Drug Concentration (mg/mL)		Size 1 (nm)	Size 2 (nm)	PDI
		Prodrug	LAP			
Pro-LAP NPs	2:1	0.5	0.5	169 ± 11	31 ± 3	0.361 ± 0.034
	2:1	0.25	0.5	177 ± 10	36 ± 4	0.271 ± 0.006

Decreasing the prodrug concentration did not facilitate formation of monodispersed nanoparticles or effect the particle size. Therefore, the effect of the BCP: core ratio on nanoparticle formation was investigated. Equivalent drug concentrations of prodrug and lapatinib for a total drug concentration of 1 mg/mL were used to maximize the drug loading to be consistent with the PTX and lapatinib formulation. When the BCP: core ratio was decreased from 2:1 to 1:1 monodispersed nanoparticles were formed. The nanoparticles formulated at a 1:1 BCP: core ratio were  $145 \pm 2$  nm and a PDI of  $0.111 \pm 0.018$  (**Table 34**). These results were confirmed with TEM analysis (**Figure 44**).

These results indicate that decreasing the BCP: core ratio has an impact on the polydispersity of the nanoparticles without impacting the nanoparticle size of drug combination of hydrophobic and weakly hydrophobic drugs. Similar trends were observed with weakly hydrophobic drugs using TA- $\text{Fe}^{3+}$  complexation in which varying the BCP: core ratio had a greater impact on polydispersity rather than size [306] found with system encapsulating only hydrophobic molecules [263,264]. Furthermore, decreasing the BCP: core ratio enabled formation of monodispersed at a total drug concentration of 1 mg/mL which mimic the results previously observed with PTX-LAP NPs [306]. The Pro-LAP NPs required a lower BCP: core ratio of 1:1 rather than 1.5:1 for PTX-LAP NPs, further supports the notion that the hydrophobic block of the BCP has a higher affinity for the prodrug. Also the timescales of self-assembly and precipitation of the core are better matched at a 1:1 BCP: core ratio.

**Table 34.** Varying the BCP: core ratio of Pro-LAP NPs.

Sample	BCP: core Ratio	Drug Concentration (mg/mL)		Size 1 (nm)	Size 2 (nm)	PDI
		Prodrug	LAP			
Pro-LAP NPs	2:1	0.5	0.5	169 ± 11	31 ± 3	0.361 ± 0.034
	1:1	0.5	0.5	145 ± 2	0	0.111 ± 0.018

We determined the parameters necessary for formulating monodispersed nanoparticles < 200 nm with a hydrophobic paclitaxel prodrug as single-drug loaded formulation (Pro NPs) and in combination with a weakly hydrophobic drug (Pro-LAP NPs). The TA-Fe<sup>3+</sup> complexation enabled encapsulation of a hydrophobic drug (logP > 6) as previously described [271]. The polydispersity of the nanoparticle was tunable with both the drug concentration and BCP: core ratio. Furthermore, using the TA-Fe<sup>3+</sup> complexation platform facilitated the co-encapsulation of a hydrophobic (logP > 6) and weakly hydrophobic drug (logP < 6) and monodispersed nanoparticles can be formed by tuning the BCP: core ratio at a total drug concentration of 1 mg/mL, as previously described for combinations of weakly hydrophobic drugs [306].

Next, we formulated TA-Fe NPs, PTX NPs, LAP NPs, and PTX-LAP NPs as previously reported [306]. Nanoparticle encapsulating only the TA-Fe complex were formulated at a BCP: core ratio of 2:1 (core determined as tannic acid and Fe<sup>3+</sup> (aq.)) and a tannic acid to Fe<sup>3+</sup> ratio of 4:1 by mass. Monodispersed single-drug loaded nanoparticles were formulated at a drug concentration of 1 mg/mL and a BCP: core (core determined at tannic acid and paclitaxel or lapatinib) ratio of 2:1. The co-loaded nanoparticles containing paclitaxel and lapatinib were formulated at a 1.5:1 BCP: core ratio (core determined as tannic acid and drugs) and a total drug concentration of 1 mg/mL. A summary of all six nanoparticles used in the subsequent experiments can be found in **Table 35**.

**Table 35.** Size and polydispersity index of nanoparticles.

Nanoparticles	Size (nm)	PDI
TA-Fe NPs	151 ± 5	0.258 ± 0.003
PTX NPs	136 ± 27	0.280 ± 0.059
LAP NPs	117 ± 7	0.247 ± 0.049
PTX-LAP NPs	84 ± 16	0.286 ± 0.026
Pro NPs	91 ± 10	0.280 ± 0.076
Pro-LAP NPs	145 ± 29	0.139 ± 0.026

### 6.3.2. Nanoparticle Encapsulation Efficiency and Drug Loading

Following nanoparticle formulation with FNP, the encapsulation efficiency and drug loading was examined by disassembling the nanoparticles with acetonitrile and measuring the drug concentration and nanoparticle dispersion mass by HPLC and TGA, respectively. The encapsulation efficiency was determined by comparing the drug mass encapsulated to the nominal amount in the formulation using Eq. 10. The encapsulation efficiency was comparable between the single-drug loaded PTX NPs and Pro NPs at ~40%. In comparison, the encapsulation efficiency of prodrug in the co-loaded nanoparticles was 0.5-fold lower compared to paclitaxel. However, the encapsulation efficiency remained ~26% for lapatinib in both co-loaded nanoparticles (**Table 36**).

The drug loading was determined by comparing the encapsulated drug mass to the total mass of the nanoparticle dispersion. Comparing the drug loading of paclitaxel and prodrug in single-drug loaded nanoparticles there was a 2.5-fold greater drug loading of paclitaxel compared to the prodrug. Examining the co-loaded nanoparticles, there is still greater drug loading of paclitaxel compared to prodrug with a 2-fold difference. The drug loading of lapatinib between the two co-loaded nanoparticles is comparable (**Table 36**).



**Table 36.** Summary of the encapsulation efficiency and drug loading.

Samples	Encapsulation efficiency (EE%)		Drug loading (DL%)	
	PTX / Prodrug	LAP	PTX / Prodrug	LAP
PTX NPs	37.6 ± 14.4	--	3.11 ± 1.88	--
LAP NPs	--	25.0 ± 1.5	--	1.82 ± 0.71
PTX-LAP NPs	67.0 ± 2.2	25.9 ± 3.5	2.11 ± 0.50	0.79 ± 0.40
Pro NPs	45.3 ± 1.8	--	1.25 ± 0.22	--
Pro-LAP NPs	37.6 ± 1.7	26.9 ± 10.8	1.01 ± 0.02	0.55 ± 0.15

The encapsulation efficiency and drug loading results suggest that either the properties of the prodrug or the components of the formulation, or combination thereof affect the encapsulation of the prodrug. It is possible that the size and/or high hydrophobicity of the prodrug molecules (1381 g/mol) relative to the other components of the core prevent high concentrations of the prodrug from being encapsulated and resulting in low drug loading. This result suggests that the hydrophobicity of the molecule is an important factor in particle assembly due to greater rate of precipitation and core formation in the case of single-drug loaded nanoparticles. It is worth noting that the encapsulation efficiency and drug loading of lapatinib was not affected by the hydrophobic of the co-loaded molecule. In fact, in the co-loaded nanoparticles there is double the drug loading of paclitaxel and prodrug than lapatinib which suggests a stronger interaction of paclitaxel and its prodrug to the TA-Fe<sup>3+</sup> complex and the hydrophobic block of the block co-polymer compared to lapatinib. This is noteworthy, because in other FNP systems high drug loading is expected of hydrophobic (logP > 6) core materials, however these results suggest that in presences of the TA-Fe<sup>3+</sup>, the interaction with the complex as well as the block co-polymer are the guiding factors for drug encapsulation.

### 6.3.3. Drug Release

The drug release from the nanoparticles was examined under two pH conditions via dialysis.

The presence of the pH-labile TA-Fe<sup>3+</sup> complex in the nanoparticles allows for controlled over drug

release and we expect that when the complex is insoluble under  $\text{pH} > 7$  we expect slow drug release from the nanoparticles and when the  $\text{pH}$  is below 5 the complex becomes soluble we expect rapid drug release. The release was measured under  $\text{pH} 7.4$  to simulate release in the bloodstream and non-acidic tissue as well as  $\text{pH} 4$  to simulate nanoparticles that are endocytosed by the cells into a lysosome or acidic cancerous tissue [365–367]. The nanoparticles were dialyzed against either 1X PBS at  $\text{pH} 7.4$  with 0.5% Tween 80 or 50 mM acetate buffer at  $\text{pH} 4$  with 0.5% Tween 80. The nanoparticles were sampled from the dialysis membranes and measured with HPLC to determine the drug release profile.

The drug release was examined for the single drug nanoparticles; PTX NPs, Pro NPs, and LAP NPs to determine their relative drug release rates. Examining the drug release at  $\text{pH} 7.4$ , the PTX NPs exhibited burst release over the first 6 hours at which ~20% of the paclitaxel was released. Under the same conditions, ~40% of the prodrug was released during 6 hour burst release from the Pro NPs. The LAP NPs exhibited a burst release in the first 3 hours with a cumulative drug release of ~25% (**Figure 45B**). During the sustained drug release period examined for up to 6 days, the release of paclitaxel was slow with a cumulative drug release of ~40%. The maximum drug release of prodrug from single-drug nanoparticles was ~90%. A total drug release of ~35% was achieved with LAP NPs (**Figure 45A**).

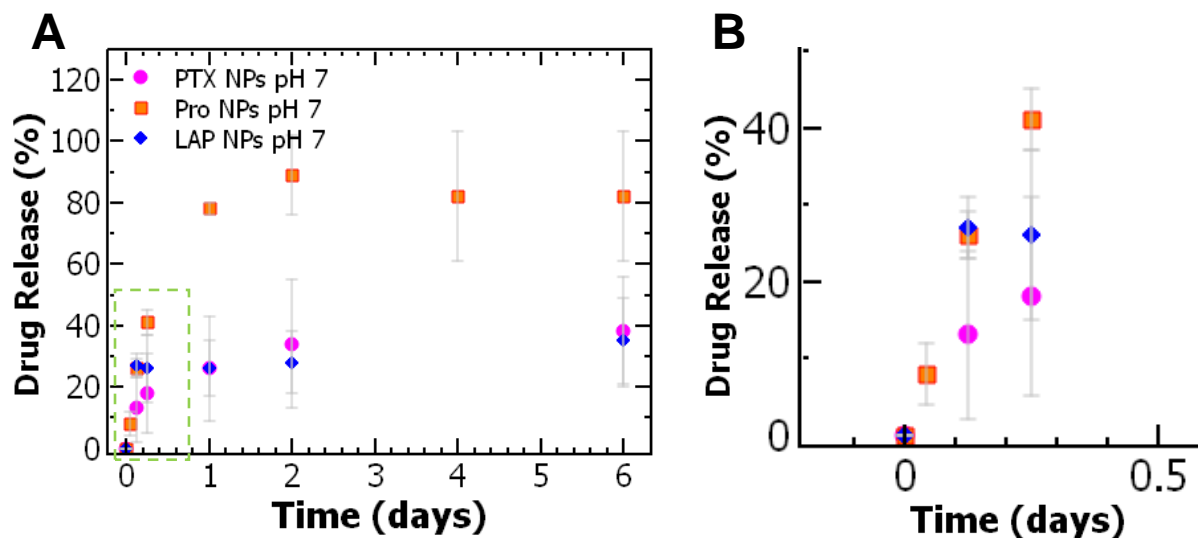


**Figure 45.** (A) The drug release profile of (pink circles) PTX NPs, (orange squares) Pro NPs, (blue rhombus) LAP NPs at pH 7.4 sink conditions. Highlighted in the green square is the (B) close up of the release profile between time 0 to 0.5 days. The average and standard deviation are shown for 3 replicate samples.

The drug release from single-drug loaded nanoparticles was also measured under acidic conditions (pH 4). All three nanoparticles exhibited burst release within the first hour of dialysis. The total paclitaxel released from PTX NPs was ~17%. There was also ~16% of the prodrug released from Pro NPs within the first hour. However, there was twice the amount of lapatinib released compared to paclitaxel or prodrug over the burst release period (**Figure 46B**). The drug release was measured over 6 days during which sustained drug release was exhibited by all three single-drug nanoparticles. The total drug release for the PTX NPs, Pro NPs, and LAP NPs after 6 days was ~26%, ~34%, ~29%, respectively under acidic conditions (**Figure 46A**).

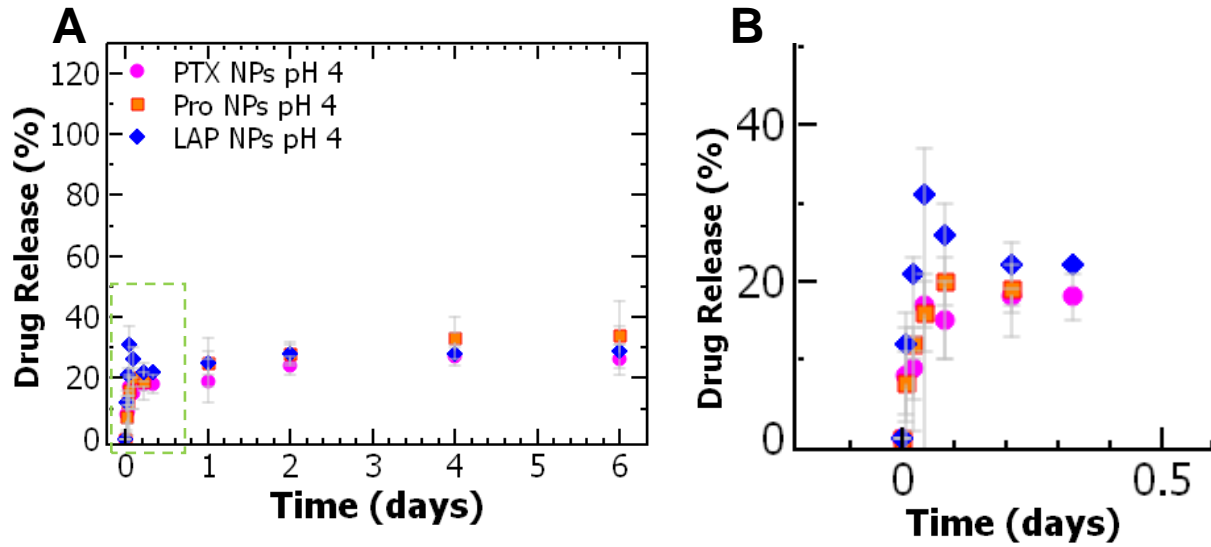


**Figure 46.** (A) The drug release profile of (pink circles) PTX NPs, (orange squares) Pro NPs, (blue rhombus) LAP NPs at pH 4 sink conditions. Highlighted in the green square is the (B) close up of the release profile between time 0 to 0.5 days. The average and standard deviation are shown for 3 replicate samples.

Next, examined the drug release kinetics from the single-drug nanoparticles under pH 7.4 and pH 4 conditions. We fit the data to the Korsmeyer-Peppas diffusion model (Eq. 12):

$$\frac{M_t}{M_\infty} = at^n \quad (\text{Eq. 12})$$

Where the  $M_t$  is the drug release at time,  $t$ ,  $M_\infty$  is maximum drug release, and  $a$  is the release rate. The diffusion exponent,  $n$ , is determined based on the fit and describes the drug release mechanism [321]. The Korsmeyer-Peppas model is used in cases with non-linear regression, as we have in this experiment with an initial burst release followed by a sustained release period and often used to describe diffusion from stable nanoparticles. Based diffusion exponent, the diffusion can be classified (i.g. Fickian diffusion, non-Fickian transport, etc.). To fit the data to the model, we determined the fraction of the cumulative drug released at each time point relative to the maximum drug release at day 6. Then we fit a linear trend to log of the cumulative drug release relative to the log time, excluding

cumulative drug release > 70% and any outliers. From the slope of the line we determined the diffusion exponent,  $n$  [321,322].

The drug release data from pH 7 conditions fit well to the Korsmeyer-Peppas model, with an  $R^2 > 0.7$ . The diffusion exponent for the release of paclitaxel and lapatinib from single-drug nanoparticles is  $< 0.45$  indicating first order Fickian kinetics [323,324] (**Table 37**). Fickian diffusion describe drug release when the rate of diffusion is substantially greater than the polymer chain relaxation of block co-polymer [368]. Under this condition, the release rate of paclitaxel and lapatinib is dependent on drug hydrophobicity and the concentration gradient. Therefore, the initial burst release of paclitaxel and lapatinib can be attributed to the concentration gradient between the nanoparticles and dialysis media. This initial burst release is followed by a faster release rate of paclitaxel compared to lapatinib due to a difference in drug hydrophobicity. The diffusion exponent for the prodrug from Pro NPs was  $> 0.89$  indicating Super Case II transport (**Table 37**). This transport describes a system in which outer layer of the nanoparticles prevents swelling of the nucleus and instead leads to compression of the nucleus and penetration of the solvent which eventually results in disassembly of the nanoparticle [368]. The rate of prodrug release is therefore not dependent on rate of diffusion but instead the compressive stresses on the nanoparticle core leading to rapid drug release. Furthermore, the unexpected rapid release of the prodrug relative to paclitaxel can be attributed to a difference in drug release mechanisms and not on the drug hydrophobicity. The compressive stresses on the nanoparticle core suggest a strong interaction between the hydrophobic block of the block co-polymer and the prodrug and the finding support the previous results observed in the formulation of the Pro NPs.

**Table 37.** Rate constant and R<sup>2</sup> of nanoparticle drug release at pH 7.4 conditions fit to the Korsmeyer-Peppas diffusion model.

Sample	Rate Constant ( <i>a</i> )	Fit (R <sup>2</sup> )
PTX NPs	0.341	0.99
Pro NPs	0.929	0.98
LAP NPs	0.064	0.689
PTX in PTX-LAP NPs	0.339	0.728
LAP in PTX-LAP NPs	0.503	0.994
Pro in Pro-LAP NPs	1.0	1.0
LAP in Pro-LAP NPs	1.0	1.0

When we applied to Korsmeyer-Peppas model to the drug release data under pH 4 conditions, we found that there was very poor fit. Instead, this data was fit to the Hixson-Crowell diffusion model (Eq. 13):

$$\left(1 - \frac{M_t}{M_0}\right)^{1/3} = 1 - K_\beta t \quad (\text{Eq. 13})$$

Where  $M_0$  is the initial amount of drug dose therefore  $M_t/M_0$  is the fraction of total drug released.  $K_\beta$  is the release constant which is dependent upon the change in surface and volume of the nanoparticles. The Hixson-Crowell model describes drug release from a dissolving core or dissolving tablet; [369,370]; therefore, it was an appropriate model to select for this platform as the nanoparticles are pH-labile and we expect a dissolution of our core due to the solubilization of the TA-Fe<sup>3+</sup> complex resulting in a shrinking nanoparticle.

The data was fit to the Hixson-Crowell model by fitting data between T = 0 and 2 hours determined as the period of burst release and the remainder of the data (hour 2 to day 6) during which

sustained release occurred was fit separately. The data was plotted as the cube root of the remaining drug versus time and the slope was determined from the linear fit as the release constant,  $K_{\beta}$ .

With the Hixson-Crowell model, we examining the fit of the experimental data from pH 4 conditions of single-drug loaded nanoparticles. Interestingly, we find during both the burst release and sustained release rate constants for PTX NPs and Pro NPs were equivalent. Interestingly, the cumulative drug release for the prodrug decreases under pH 4 conditions, which can be attributed to a difference in stresses on the nanoparticles with the rate of core dissolution under pH 4 is slower relative to compression of the core under pH 7.4. The burst release constant for LAP NPs was slightly higher compared to PTX NPs and Pro NPs, but the sustained release constant was similar (**Table 38**). Although these three drugs have very different hydrophobicity, the similarity in release rates indicate that the drug release kinetics is not described by diffusion out of the core but by particle deterioration.

**Table 38.** Rate constant and  $R^2$  of nanoparticle drug release at pH 4 conditions fit to the Hixson-Crowell diffusion model.

Sample	Burst Release		Sustained Release	
	Rate Constant ( $K_s$ )	Fit ( $R^2$ )	Rate Constant ( $K_s$ )	Fit ( $R^2$ )
PTX NPs	1.23	0.89	0.0072	0.82
Pro NPs	1.23	0.89	0.012	0.91
LAP NPs	2.56	0.943	0.0051	0.736
PTX-LAP NPs (PTX)	0.61	0.937	0.0073	0.958
Pro-LAP NPs (Pro)	3.07	0.990	0.049	0.732
PTX-LAP NPs (LAP)	0.61	0.937	0.0073	0.958
Pro-LAP NPs (LAP)	1.56	0.702	0.017	0.947

Next, the drug release under pH 7.4 was investigated for the two co-loaded nanoparticles. For the PTX-LAP NPs, burst release was observed within the first 6 hours with equivalent drug release of paclitaxel and lapatinib at ~24%. In comparison, ~31% of the prodrug and ~22% of lapatinib were released during the 6 hour burst release from Pro-LAP NPs (**Figure 47B**). The cumulative drug release following sustained release over 6 days for the PTX-LAP NPs was ~40% of paclitaxel and 16% of lapatinib. There was greater prodrug release from the co-loaded nanoparticles compared to paclitaxel with ~50% release, but approximately the same percentage of lapatinib released as the PTX-LAP NPs (**Figure 47A**).

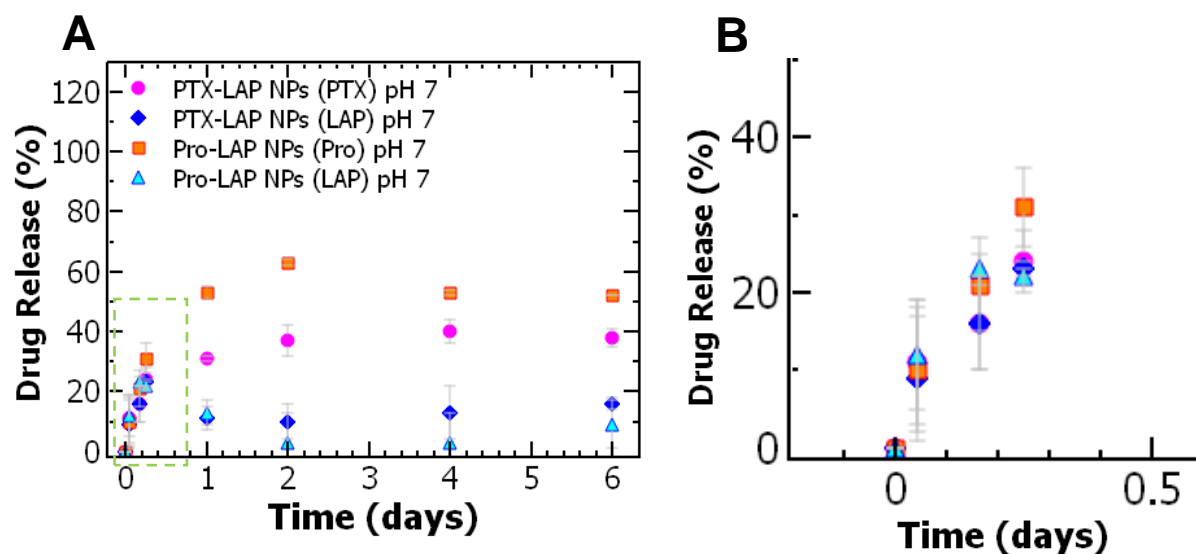


**Figure 47.** (A) The drug release profile of (pink circles) paclitaxel and (blue rhombus) lapatinib from PTX-LAP NPs and (orange squares) prodrug and (light blue triangle) lapatinib from Pro-LAP NPs at pH 7.4 sink conditions. Highlighted in the green square is the (B) close up of the release profile between time 0 to 0.5 days. The average and standard deviation are shown for 3 replicate samples.

The drug release profiles of the co-loaded nanoparticles were also examined under acidic conditions. The burst release for the PTX-LAP NPs was observed within the first 2 hours of dialysis. There was ~16% of the paclitaxel and ~7% of the lapatinib released. In comparison, a burst release was observed over the first hour for the Pro-LAP NPs. Double the prodrug was released relative to



paclitaxel from the co-loaded nanoparticles. Approximately the same percentage of lapatinib was released from PTX-LAP NPs and Pro-LAP NPs during the burst release (**Figure 48B**). Sustained release was observed over 6 days for both co-loaded nanoparticles. The cumulative release of the prodrug was greater at ~52% relative to paclitaxel that only had a cumulative drug release of ~30%. Comparing the cumulative release of lapatinib from the co-loaded nanoparticles we observed that double the lapatinib was released from Pro-LAP NPs compared to the PTX-LAP NPs (**Figure 48A**).

The drug release kinetics for the co-loaded nanoparticles were modeled based on the Korsmeyer-Peppas model for pH 7.4 conditions and the Hixson-Crowell for pH 4 conditions as previously described for single-drug nanoparticles. Examining first the drug release kinetics under pH 7.4 conditions, diffusion exponent for paclitaxel ( $n < 0.45$ ) and lapatinib ( $n \sim 0.5$ ) from co-loaded nanoparticles describes the release kinetics by Fickian diffusion [323,324,368] (**Table 37**). Therefore, the drug release of the PTX-LAP NPs is determined by the drug diffusion from the core based on the drug hydrophobicity and concentration gradient. This driving force explains the greater cumulative drug release over time of paclitaxel due to lower hydrophobicity ( $\log P = 3.2$ ) relative to lapatinib ( $\log P = 5.4$ ) co-loaded nanoparticles. These results suggest sequential drug release of paclitaxel followed by lapatinib. In comparison, the diffusion exponents for prodrug and lapatinib in Pro-LAP NPs are greater than 0.89, similar to Pro NPs, therefore the drug release is described by Super Case II transport [368]. Again, in this case the drug release is dictated by the compression on the nanoparticle likely attributed to the strong hydrophobic interaction between the block co-polymer and the core. However, it is worth noting that the cumulative drug release of the prodrug is greater than lapatinib although the reason for this is not clear.

Next, we examined the rate constant of the co-loaded nanoparticles fit to the Hixson-Crowell model (pH 4). The rate constants for both the burst release and sustained release are comparable between paclitaxel and lapatinib in PTX-LAP NPs. Similarly, the prodrug and lapatinib in Pro-LAP

NPs had similar rate constants (**Table 38**). When we compare paclitaxel to the prodrug released from co-loaded nanoparticles, we observed a substantially higher constant for the prodrug (faster release) relative to paclitaxel. This is noteworthy, since in the single-drug case the two drugs had comparable drug release. While the reason for this is unclear, it could suggest a combination of factors such as both core solubilization, due to the TA-Fe<sup>3+</sup> complex, and compression, due to the block co-polymer and prodrug interaction.

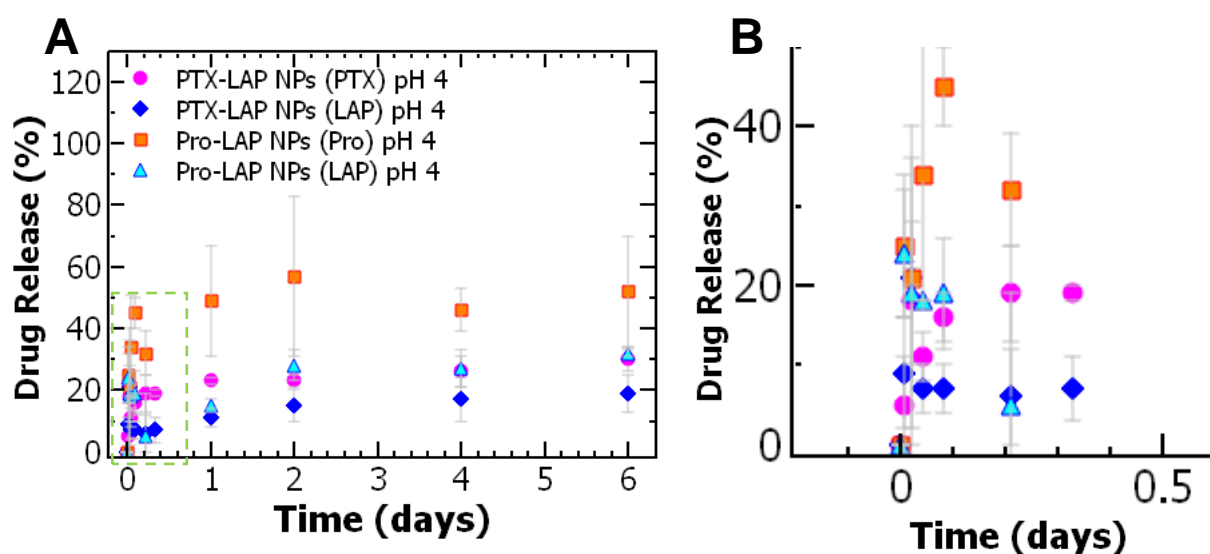


**Figure 48.** (A) The drug release profile of (pink circles) paclitaxel and (blue rhombus) lapatinib from PTX-LAP NPs and (orange squares) prodrug and (light blue triangle) lapatinib from Pro-LAP NPs at pH 4 sink conditions. Highlighted in the green square is the (B) close up of the release profile between time 0 to 0.5 days. The average and standard deviation are shown for 3 replicate samples.

#### 6.3.4. Drug Potency and Evaluating the IC-50

The potency of the nanoparticle dispersion was assessed *in vitro* with ovarian cancer cells, OVCA-432 cells. The cells were treated with free drug or single-drug nanoparticle formulations of paclitaxel, prodrug, and lapatinib. The cell viability was measured with the WST-1 assay from which the half-maximal inhibitory concentration (IC-50) was determined as a measure of potency. We first compared the potency of the free prodrug to free paclitaxel. Treatment with the free prodrug produced

an IC-50 of  $0.010 \pm 0.005$  mM which was over 8-fold lower compared to free paclitaxel (**Table 39**). These results suggest that formulating hydrophobic prodrug of paclitaxel is an approach to increase the potency of paclitaxel to treat ovarian cancer cells.

Free lapatinib had the highest potency with an IC-50 of  $0.008 \pm 0.002$  mM. Next, we compared the potency of the nanoparticle formulations to the free drug. With all three drugs, there was a reduction in IC-50 concentration of the nanoparticles relative to the free drug. The largest increase in potency was observed with paclitaxel from  $\sim 0.083$  mM to  $\sim 47 \times 10^{-6}$  mM followed by the prodrug from  $\sim 0.010$  mM to  $\sim 8.7 \times 10^{-6}$  mM. Formulating lapatinib into nanoparticles decreased the IC-50 to  $\sim 0.0014$  mM (**Table 39**). While decreases in IC-50 concentration compared to the free drug form have been observed in other polymer nanoparticle formulations [234,331,332] and is not fully understood, the 1800-fold increase in paclitaxel potency and 1100-fold increase in prodrug potency in this nanoparticle formulation is noteworthy. The significant increase in paclitaxel and prodrug potency in the TA-Fe could be attributed to several contributing factors including sustained release over the 48 hour treatment period an increased bioavailability due to the nanoparticle formulation [234,333,334].

Additionally, the Pro NPs exhibited greater potency compared to PTX NPs. Specifically, therefore, the Pro NPs were 5-fold more potent compared to the PTX NPs (per mole of PTX). Thus, formulation of the paclitaxel prodrug and encapsulation into nanoparticle is a method to further enhance paclitaxel potency.

Interestingly, these results differ from previous studies investigating the activity of hydrophobic paclitaxel prodrugs [262,356,357]. Ansell et al, observed a 10-fold decrease in potency in ovarian cancer cells (A2780) and a 3-fold decrease in potency in breast tumor cells (MCF-7) when comparing  $\alpha$ -tocopherol conjugated paclitaxel to paclitaxel drugs that were co-encapsulated with phosphatidylcholine (POPC) in polymer nanoparticles via FNP [261]. The difference in the observed results could indicate cell-dependent cytotoxicity due to the gene expression [371,372]. Furthermore,

the difference in nanoparticle formulation methods, co-encapsulation with TA-Fe<sup>3+</sup> versus a hydrophobic polymer, could also play a role in the difference in prodrug potency and could, therefore, be explained by the Hansch-Fujita parabolic relationship between drug hydrophobicity and cell membrane penetration [373].

Examining the drug release profile, the rapid release of the prodrug under pH 7.4 conditions could suggest in greater bioavailability of the prodrug compared to paclitaxel with this nanoparticle platform. Additionally, the diameter of the nanoparticles formulated with TA-Fe<sup>3+</sup> were ~100 nm which are 4-fold larger compared to those formulated by Ansell et al. (~25 nm), which plays a significant role in the mechanisms of endocytosis [374,375]. Additionally the pH-labile platform created with TA-Fe<sup>3+</sup> can also play a role in the drug delivery mechanism *in vitro*. Overall these results suggest that the potency of paclitaxel is cell-type dependent and can be enhanced with a hydrophobic prodrug as well encapsulating in nanoparticles via TA-Fe<sup>3+</sup> complexation.

**Table 39.** The IC-50 of OVCA-432 cells treated with paclitaxel, paclitaxel prodrug, lapatinib in free drug and nanoparticles formulations.

Drug Treatment	IC-50 (µg/mL)		IC-50 (mM)	
	PTX / Prodrug	LAP	PTX/Prodrug	LAP
Free PTX	70.6 ± 5.1	--	0.083 ± 0.006	
Free Prodrug	13.3 ± 6.5	--	0.010 ± 0.005	
Free LAP	--	4.6 ± 1.3	--	0.008 ± 0.002
PTX NPs	0.040 ± 0.003	--	47 x 10 <sup>-6</sup> ± 3.5 x 10 <sup>-6</sup>	--
Pro NPs	0.012 ± 0.027	--	8.7 x 10 <sup>-6</sup> ± 20 x 10 <sup>-6</sup>	--
LAP NPs	---	0.80 ± 0.26	--	0.0014 ± 0.0004

### 6.3.5. Drug Combination and Synergy

Next, we examined the efficacy of the two co-loaded nanoparticle formulations. The benefit of co-loading drug combinations into nanoparticles is spatiotemporal control of drug delivery as well as targeting of multiple anticancer pathways [197,376]. The OVCA-432 cells were treated with co-loaded nanoparticles loaded with either paclitaxel or its prodrug at a range of concentration and the treatment potency was measured with IC-50 concentration. As expected, there was a decrease in the IC-50 concentration for all three drugs in the co-encapsulated nanoparticles compared to the single-drug formulations. Particularly of note, there was a 4-fold decrease for paclitaxel and a 2-fold decrease for prodrug when co-encapsulated with lapatinib compared to single-drug formulations (**Table 39** and **Table 40**). These results suggest that co-delivery of paclitaxel or its prodrug with lapatinib in nanoparticle formulations improved drug efficacy. This could be attributed to targeting multiple anticancer pathways with combined delivery of paclitaxel and lapatinib [111,234,307,309,377]. Additionally, co-localization of the drugs relative to the cells [378,379] as well as controlled release of the two drugs from the pH-labile nanoparticles [201,204] can enhance drug targeting. Interestingly, the IC-50 concentrations was equivalent between PTX-LAP NPs and Pro-LAP NPs for both drugs (**Table 40**). These results indicate that the hydrophobicity of paclitaxel does not impact the efficacy of co-encapsulated nanoparticles. The reason for the similarities between IC-50 of the two co-loaded nanoparticles is unclear. The results do suggest that a method for improving the potency of paclitaxel or its prodrug is co-encapsulation with lapatinib into nanoparticles. Further examination of the cell cycle analysis could provide insight into the efficacy of the drugs on the cell activity.

The synergistic activity was determined with the combination index (CI) for the two co-loaded nanoparticles by Eq. 14:

$$CI = \frac{IC_{50}(A)_{pair}}{IC_{50}(A)} + \frac{IC_{50}(B)_{pair}}{IC_{50}(B)} \quad (\text{Eq. 14})$$

Where the IC-50 concentration for drug A in combination ( $IC_{50(A)}_{pair}$ ) is divided by the IC-50 of drug A alone ( $IC_{50(A)}$ ) and added to that of drug B. A CI less than 1 indicates synergistic drug interaction. We determined that PTX-LAP NPs had a CI of 0.23 and Pro-LAP NPs had a CI of 0.54 indicating drug synergism (**Table 40**). While both nanoparticles are synergistic, the PTX-LAP NPs have a greater synergistic activity compared to co-loaded nanoparticles containing the prodrug. Since the prodrug is more potent than PTX, combining it with LAP has less of an effect which results in the higher CI.

**Table 40.** IC-50 and combination index of co-loaded nanoparticles in OVCA-432 cells.

Drug Treatment	IC-50 ( $\mu\text{g/mL}$ )		IC-50 ( $\times 10^{-6}$ mM)		Combination Index (CI)
	PTX / Prodrug	LAP	PTX/ Prodrug	LAP	
PTX-LAP NPs	$0.0090 \pm 0.0009$	$0.0040 \pm 0.0004$	$1.1 \pm 1.1$	$6.9 \pm 0.69$	0.23
Pro-LAP NPs	$0.0064 \pm 0.0075$	$0.0046 \pm 0.0054$	$4.6 \pm 5.4$	$7.9 \pm 9.3$	0.54

### 6.3.6. Cell Cycle Analysis

To better understand the efficacy of paclitaxel and its hydrophobic prodrug on the ovarian cancer cells, we examined the cell cycle distribution using flow cytometry. Paclitaxel is known to arrest cells in the G<sub>2</sub>/M phase by stabilizing microtubule and preventing their disassembly necessary for cell division [335]. Untreated OVCA-432 cells were primarily distributed in the G<sub>1</sub>/G<sub>0</sub> phase at ~62% and only ~9% of cells were in the G<sub>2</sub>/M phase. Cells were treated with the free drug and nanoparticles at each treatment's IC-50 concentration. We first compared the distribution following treatment with free drugs. Free paclitaxel reduced the percentage of cells in the G<sub>1</sub>/G<sub>0</sub> phase to 46% and stabilized the cells in the G<sub>2</sub>/M phase (~30%). Interestingly, while free prodrug also reduced the percentage of cells in the G<sub>2</sub>/M phase, the cells accumulated in the subG<sub>1</sub> phase (~25%) rather than the G<sub>2</sub>/M phase (~6%) (**Figure 49**). The greater accumulation of cells in the subG<sub>1</sub> phase treated with

the prodrug could indicate that by increasing hydrophobicity of paclitaxel cells spend less time in the G<sub>2</sub>/M phase and transition to the subG<sub>1</sub> phase due to cell damage.

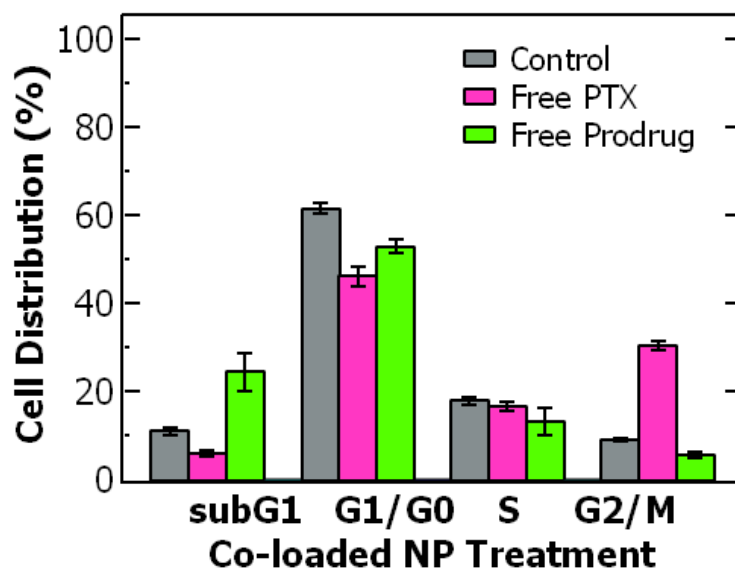


**Figure 49.** Cell cycle analysis of OVCA-432 cells from flow cytometry of (grey) untreated cells, and cells treated with either (pink) free paclitaxel or (green) free prodrug.

Next, we compared the cell cycle distribution when the OVCA-432 cells were treated with single drug nanoparticles containing paclitaxel and prodrug. In this case, the cell distribution was similar between the two nanoparticles with a decrease in the G<sub>1</sub>/G<sub>0</sub> phase to ~40% and an increase in cells in the S and subG<sub>1</sub> phases. There is only a slight increase in cells in the G<sub>2</sub>/M phase for both nanoparticles relative to the control cells. The differences worth noting are that the PTX NPs exhibit a greater percentage of cells in the subG<sub>1</sub> phase of ~25% compared to Pro NPs (~17%) (**Figure 50**). Since the cells were treated at the IC-50 concentrations of both particles and induce similar cell cycle arrest, it suggests that the drugs have a similar effect at these concentrations. As the Pro NPs were treated at a 8-fold lower concentration on a molar basis suggests higher potency of the Pro NPs formulation.

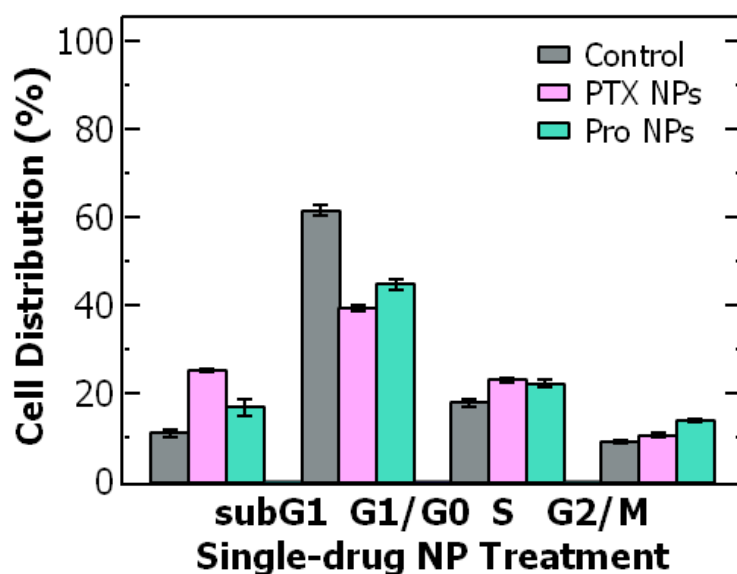


**Figure 50.** Cell cycle analysis of OVCA-432 cells treated with single drug nanoparticles. The cell distribution was compared between (grey) untreated cells, (pink) PTX NPs, and (green) Pro NPs.

Finally, we compared the treatment with the two co-loaded nanoparticles. The PTX-LAP NP treatment did not affect the cell distribution compared to the untreated cells with greatest proportion of cells in  $G_1/G_0$  phase. However, the Pro-LAP NPs reduced the proportion of cells in the  $G_1/G_0$  phase and redistributed the cells among the other three phases. Particularly, there was a large increase in cells in the sub $G_1$  phase from ~11% to ~24% and only a slight increase in the  $G_2/M$  phase from ~9% to ~15% (**Figure 51**). In this case, the cells were treated with similar drug concentrations as the IC-50 concentrations are comparable. Therefore, while they both reduce cell viability by equivalent percentages, there is greater cell cycle arrest observed with Pro-LAP NPs and a more rapid shift to sub $G_1$  phase which could result in greater and more rapid cell death indicating increased potency of co-encapsulation of the prodrug with lapatinib.

Therefore, the difference observed in the cell cycle distribution could be due to a difference in drug release rates. There is a faster rate of prodrug release compared to paclitaxel from co-loaded nanoparticles under both pH 7.4 and pH 4 conditions therefore more prodrug is bioavailable. Furthermore, in previous unpublished data (Chapter 5), when sequential delivery was examined, we



determined the delivery of paclitaxel prior to lapatinib increased drug efficacy. Therefore with Pro-LAP NPs we have an even greater difference in the cumulative drug release of the two drugs suggesting there is enhanced cytotoxic effects observed with cell cycle analysis due to sequential drug delivery.

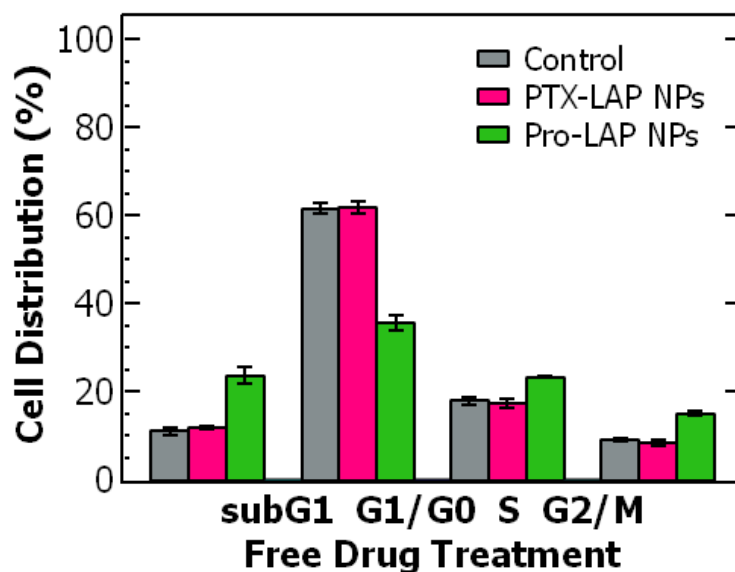


**Figure 51.** Cell cycle analysis of OVCA-432 cells treated with co-loaded nanoparticles. The cell distribution was compared between (grey) untreated cells, (pink) PTX-LAP NPs, and (green) Pro-LAP NPs.

#### 6.4. Conclusion

In this study, we demonstrated the potential of encapsulating a hydrophobic paclitaxel prodrug into pH-labile nanoparticles as a method to enhance drug efficacy and control drug release. Parameters for formulating monodispersed nanoparticles via Flash NanoPrecipitation with a tannic acid-iron complex were determined for encapsulating the hydrophobic drugs ( $\log P > 6$ ) and in combinations with a weakly hydrophobic drug ( $\log P < 6$ ). By examining the drug release profiles, we determined that the prodrug has faster rate of drug release in both pH 7.4 and pH 4 conditions relative to paclitaxel and lapatinib due to a difference in the drug release mechanisms. The drug efficacy of the prodrug was 8-fold higher delivered as a free drug and 5-fold higher in the nanoparticle formulation compared to

equivalent formulations of paclitaxel in ovarian cancer cells. The cytotoxic effects were further enhanced by co-encapsulation with lapatinib, which produces similar levels of potency between paclitaxel and its prodrug counterpart. Overall, these findings provide the foundation for developing co-encapsulated nanoparticles with controlled drug release as well as methods for improving the drug efficacy of paclitaxel.

## 7. Chapter 7: Rapid, Room Temperature Nanoparticle Drying and Low Energy Reconstitution via Electrospinning

---

**Published:** [278] Levit, S.L.; Stwodah, R.M.; Tang, C. Rapid, Room Temperature Nanoparticle Drying and Low-Energy Reconstitution via Electrospinning. *Journal of Pharmaceutical Sciences* **2018**, *107*, 807–813.

### 7.1. Abstract

Nanoparticle formulations offer advantages over free drug; however, stability of the nanoparticle dispersions is a significant obstacle and drying is often required for long-term size stability. The main limitation of current drying methods is particle aggregation upon reconstitution which can be overcome with sonication (impractical in a clinical setting) or large amounts of cryoprotectants (result in hypertonic dispersions). Therefore, new approaches to nanoparticle drying are necessary. We demonstrate conversion of nanoparticle dispersions to a dry, thermostable form via electrospinning. As proof-of-concept, polyethylene glycol stabilized nanoparticles and polyvinyl alcohol were blended and electrospun into ~300 nm fibers. Following electrospinning, nanoparticles were stored for at least seven months and redispersed with low osmolarity to their original size without sonication. The nanoparticle redisperse to their original size when the fiber diameter and nanoparticle diameter are comparable (NP:NF ratio ~ 1). Nanoparticles with liquid cores and larger particles better maintained their size when compared to nanoparticles with solid cores and smaller particles, respectively. Storing the nanoparticles within nanofibers appears to prevent Ostwald ripening improving thermostability. Overall, this novel approach enables rapid, continuous drying of

nanoparticles at room temperature to facilitate long-term nanoparticle storage. Improved nanoparticle drying techniques will enhance clinical translation of nanomedicines.

## 7.2. Introduction

Nanoparticle (NP) drug formulations offer advantages over free-drug formulations such as increased bioavailability and intracellular accumulation with relatively low toxicity [380–382]. However, stability of the NP dispersions is a formidable problem [383]. Often, cold-chain storage is required to prevent Ostwald ripening. The requirement of cold-chain storage is challenging for clinical applications [384]. Often, to achieve stable formulations with long shelf-lives, complete drying of the sample is required [385,386]. However, maintaining NP size during drying remains a significant challenge.

Three techniques commonly used for drying drug-loaded NPs are freeze drying, spray drying, and more recently spray freeze drying [386–392]. Freeze drying is a three-step process in which the water is removed with an initial freezing step followed by sublimation and desorption [393]. Spray drying is a continuous process in which the NP suspension is turned into droplets that are rapidly dried with a hot gas [394–396]. Spray freeze drying is an integration of the two methods, in which the solution is turned into droplets that are immediately frozen followed by sublimation of the remaining liquid [397]. While some particles have had success [396,398], the main limitation of current drying methods is particle aggregation after drying and reconstitution so the nanometer particle size, which is vital for therapeutic efficacy [399,400] cannot be maintained [393,401]. For example, after freeze drying,  $\beta$ -carotene- and paclitaxel-loaded NP made by Flash NanoPrecipitation (FNP) method, redispersions resulted in at least a 2.25-fold increase in particle size even with sonication, a process which is considered impractical in a clinical setting [385,402]. Freeze dried vitamin E (VE) NPs stabilized with polystyrene-*b*-polyethylene glycol (PS-*b*-PEG) that were made via FNP exhibited

a 3-fold increase in size after reconstitution with sonication [385]. Therefore, new approaches to NP drying that maintain NP size after reconstitution are necessary.

Cryoprotectants or excipients, such as glucose, sucrose and trehalose, etc., can prevent aggregation [388,403]. However, significant amounts of protectant/excipient are generally required [388,398,404]. For example, spray freeze drying PCL NPs required concentrations of 70 wt.% mannitol to achieve a final NP size to initial NP size ( $S_f/S_i$ ) ratio of 1.5 [398]. When freeze drying drug-loaded NPs using trehalose as a cryoprotectant, a mass ratio of 5:1 trehalose: NPs was required for redispersion [402]. The large amount of protectant is problematic for parenteral administration because the osmolarity of the protectant results in a hypertonic formulation [385].

We present electrospinning NPs blended with a water soluble polymer as an alternative to freeze drying to rapidly convert NP dispersions to a dry form that can be stored at room temperature. In electrospinning, the polymer blend is extruded at a constant rate and when the force due to an applied electric field overcomes surface tension, a liquid jet forms. As the liquid jet travels to a grounded collector, it is whipped and stretched and the solvent rapidly evaporates creating a solid fiber [405–409]. The fiber is deposited as a random, non-woven material. Electrospinning the blend of NPs and a water soluble polymer, the NPs are encapsulated within the resulting polymer fibers. The nonwoven material can be stored at room temperature and the fibers dissolved in aqueous media to reconstitute the NPs.

Use of polymers as excipients are a promising alternative to saccharides because they can be added at high mass ratios relative to the NPs without creating hypertonic formulations. Polymers, such as polyvinyl alcohol (PVA), used as excipients in traditional drying techniques, spray drying and spray freeze drying [410] have been considered. Approaches using polymers as in techniques such as electrospinning and electroblowing have been employed for preserving amorphous formulations of

small molecules [411]. However, the applicability of such techniques for converting NPs to a dry, stable form have yet to be demonstrated.

In this work, we demonstrate electrospinning as a rapid, room temperature method to convert NP dispersions to a dry, thermostable form that can be redispersed to the original NP size without sonication. We use NP formulations sterically stabilized with polyethylene glycol (PEG) as a model system because PEG coatings increase circulation time and delay clearance by the mononuclear phagocytic system [412–415]. Such particles can be fabricated using FNP, a rapid and scalable method. In FNP, PEGylated block copolymers direct NP self-assembly during rapid mixing of the hydrophobic drug and block copolymer dissolved in an organic stream with a miscible anti-solvent stream. Due to the rapid mixing, the NPs are kinetically trapped with high core loading capacities, narrow size distribution and tunable size [260]. Blends of the PEGylated FNP particles with PVA were electrospun to convert the NPs into a stable, dry form. PVA was selected as a starting point for these experiments because it is often included in freeze dried formulations [393,410]. The NPs were reconstituted to their original size without sonication. The effect of fiber processing on final NP size was explored. Specifically, we examined the effect of NP composition, NP size, and NP to fiber diameter ratio.

### **7.3. Materials and Methods**

#### *7.3.1. Materials*

The NPs were formulated with amphiphilic block co-polymer, polystyrene-b-PEG (1600-b-5000 g/mol) (PS-b-PEG) obtained from Polymer Source (Montreal, Canada). PS-b-PEG was dissolved in THF (~40°C) and precipitated into diethyl ether and dried in vacuum. For the core materials,  $\alpha$ -tocopherol (Vitamin E, VE, Sigma-Aldrich, St. Louis, MO) and polystyrene (PS) with molecular weight (MW) = 800 – 5 000 Da (Polyscience, Inc., Warrington, PA) were used. Tetrahydrofuran

(THF) was used as the solvent (HPLC grade, Fisher Scientific, Pittsburgh, PA). The electrospinning polymer was polyvinyl alcohol (PVA) with MW = 205 000 Da (Mowiol 40-88, Sigma-Aldrich, St. Louis, MO). All other reagents were used as received.

### 7.3.2. Nanoparticle Preparation

NPs were prepared via FNP with a hand-operated confined impinging jet mixer with dilution [260]. In Flash NanoPrecipitation, the hydrophobic core material is initially molecularly dissolved with the amphiphilic block copolymer stabilizer and is rapidly mixed with a miscible, non-solvent for the hydrophobic core. This rapid mixing with the non-solvent decreases the solvent quality for the core material and hydrophobic block of the amphiphilic block copolymer i.e. decreases the solubility of the core material and hydrophobic block of the stabilizer which induces simultaneous precipitation of the core material and micellization of the block copolymer. Adsorption of hydrophobic block on the precipitating core material arrests nanoparticle growth while the hydrophilic block sterically stabilizes the nanoparticle [416]. In a typical experiment, PS-*b*-PEG was dissolved in THF with core material (VE or PS) at a total solids concentration ~30 mg/mL. Typically, 0.5 mL of the organic stream was rapidly mixed with an equal amount of water (miscible non-solvent for the hydrophobic core material) and immediately diluted with 4 mL of water to maintain a THF:water ratio of 1:9 by volume. The ratio of the block copolymer to core material was varied to tune the size of the NPs based on previous studies [260]. Following mixing, the organic solvent was removed by dialysis, using regenerated cellulose tubing with a molecular weight cutoff of 6-8 kDa (Spectra/Por, Spectrum Laboratories, Houston, TX), against a 100-fold volume of water for 24 hours with four changes of the bath. NP size before and after dialysis were measured using Dynamic Light Scattering (DLS).

### 7.3.3. *Initial Nanoparticle Characterization*

The mean particle size and distribution was determined by DLS using a Malvern Zetasizer ZS (Malvern Instruments Ltd, Malvern, UK) with a backscatter detection angle of 173°. Initial particle size distributions are reported using the normal resolution model intensity weighted distribution (average of 4 measurements). For the initial NP size, particle uniformity was defined as size distribution with a single Gaussian peak. The polydispersity index (PDI) is a measure of the breadth of the particle distribution defined from the moments of the cumulant fit of the autocorrelation function calculated by the instrument software as previously described [260].

### 7.3.4. *Electrospinning*

For electrospinning, aqueous solutions of PVA were prepared by dissolving 9.5 wt.% PVA in water. The PVA was stirred at 60°C overnight until the solution was macroscopically homogeneous and then stored at 4°C. The NPs in water (after dialysis) and dissolved PVA were combined in various proportions and stirred for several minutes at room temperature until macroscopically homogenous. The final PVA concentration for electrospinning was 7 wt.% based on previous studies [417]. The NP loading (mass of NPs per mass of PVA) was systematically varied.

The blend of polymer and NPs was electrospun using a conventional set-up [417]. Briefly, polymer-NP blend was pumped (New Era Pump System, Inc., Farmingdale, NY) through a 22-gauge (inner diameter = 0.508 mm) stainless steel needle (Jensen Global, Santa Barbra, CA) at a constant rate while applying a constant voltage (Matsusada High Precision Inc., Shiga, Japan). Typical, process parameters were: tip-to-collector distance of 15 cm, applied voltage of 13-15 kV, flow rate of 0.5 mL/hr. Blends were electrospun for 20 mins so the resulting mat was thick enough to easily remove from the foil. Each solution was electrospun in triplicate and stored at ambient conditions.



### 7.3.5. *Nanofiber Characterization*

The fiber samples were sputter-coated (POLARON E5400 SEM Coating system) with gold (~10 nm) or gold:palladium target 60:40 and analyzed with scanning electron microscopy (SEM) (JEOL LV-5610, JOEL, Peabody, MA) at an accelerating voltage of 20kV. Images were taken at a magnification of 10,000x with a working distance of 10 mm. The average fiber diameter and standard deviation were determined by measuring the diameter of at least 75 fibers from 4-5 fields of view using ImageJ software.

### 7.3.6. *Nanoparticle Reconstitution*

The NPs were reconstituted by dissolving the resulting nanofibers (after being removed from the foil and weighed) in deionized (DI) water. Mass of fibers to volume of DI water ratio was held constant at 0.4 mg fiber per mL of DI water. The redispersions were hand-mixed for ~10 min with brief, intermittent vortexing until there were no visible aggregates. The reconstituted samples were syringe filtered (Whatman 0.45  $\mu\text{m}$  nylon filter) and measured on DLS. The time between reconstitution and syringe filtering was varied and no significant effect of delay time was observed. This fiber to water ratio was selected so that the dissolved polymer and NP sizes could be resolved using DLS to determine the NP size upon reconstitution post-electrospinning. The NP size and PDI were obtained using the Multiple Narrow Modes algorithm based on non-negative least squares fit using Zetasizer software as has been previously reported [418,419]. Since the resolution of DLS is inherently limited to a factor of 3 [420], only samples with a NP intensity peak size (nm)/PVA intensity peak size (nm) > 3 are reported.

## 7.4. Results

### 7.4.1. Proof of Concept

PEG-stabilized NPs loaded with VE or polystyrene homopolymer (PS) were fabricated with FNP. The size of the NPs was tuned by varying the ratio of core material to block copolymer stabilizer in the formulation [260]. The initial VE-loaded NPs were between 95 and 175 nm and PS-loaded NPs were between 110 and 190 nm (**Table 41**).

**Table 41.** Characteristics of NPs electrospun fibers

Core material	Initial NP Diameter (nm)	NP loading (wt.%)	Nanofiber Diameter (nm)
VE	95 ± 4	0.8	365 ± 36
	118 ± 5	0.8	249 ± 32
	129 ± 2	0.8	326 ± 34
	144 ± 9	0.8	322 ± 56
	174 ± 2	0.8	291 ± 37
			1.7
		3.2	292 ± 47
PS	112 ± 5	0.8	354 ± 31
	192 ± 14	0.8	390 ± 37

To demonstrate proof-of-concept of drying NPs via electrospinning, aqueous blends of NPs and a water-soluble polymer, PVA, was used as a model system. PVA was selected because its electrospinning has been well characterized [417,421]. PVA was used at concentration of 7 wt.% because there is sufficient molecular entanglement to facilitate fiber formation [417,421]. At 7 wt.% PVA and NP loading up to 3.2 wt.%, the PVA-NP blend solutions were electrospun to produce continuous, uniform fibers with no evidence of beading (**Figure 52**). Since the fiber diameters were larger than the NPs, the NPs appear encapsulated within smooth PVA fibers. The fiber diameter and

fiber size distribution (relative standard deviation) with and without VE or PS NPs were comparable (**Figure 52**). Therefore, at the NP loadings used, the presence of the NPs did not significantly affect the PVA entanglement required for fiber formation. This result is comparable to other PVA-blend systems [421]. Thus, these results demonstrate that NPs can be converted into a dry form, i.e. encapsulated within polymer fibers, by electrospinning a blend with a spinnable polymer.

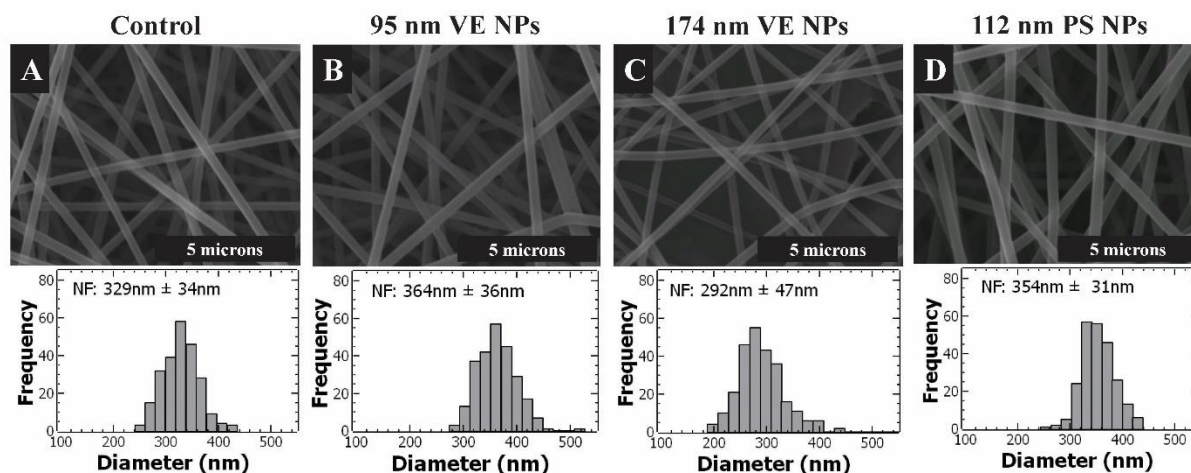


**Figure 52.** SEM images of electrospun PVA fibers loaded with NPs. A) PVA only fibers with an average nanofiber (NF) diameter of  $329 \text{ nm} \pm 34 \text{ nm}$ , B) PVA fibers with 95 nm VE NPs at 0.8 wt.% with an average NF diameter of  $364 \text{ nm} \pm 36 \text{ nm}$ , C) PVA NF with 3.2 wt.% loading of 174 nm VE NPs with an average diameter of  $292 \text{ nm} \pm 47 \text{ nm}$ , and D) PVA fiber with 0.8 wt.% loading of 112 nm PS NPs and NF diameter of  $354 \text{ nm} \pm 31 \text{ nm}$ . All samples electrospun to form continuous, uniform fibers.

#### 7.4.1.1. Nanoparticle Reconstitution

For nanoparticle reconstitution, water was added to the PVA fibers followed by hand-mixing. The polymer fibers start to dissolve immediately after the addition of water and appear completely dissolved after 5 minutes of hand-mixing (**Figure 53**). These results show that the NPs can be rapidly reconstituted using hand-mixing (low-energy mixing). Nanoparticles reconstituted with hand-mixing retain their initial size ( $S_f/S_i = 1.0 - 1.2$ ) (**Table 42**). Notably, previous results freeze drying (without excipient) similar particles stabilized by PS-b-PEG did not retain their size as well. Sonication was required to obtain a  $S_f/S_i$  of 2.9 [385]. Using PS-b-PEG-stabilized nanoparticles as a model system

suggests that drying NPs via electrospinning with PVA is a promising approach for converting nanoparticles to a dry form while maintaining particle size.

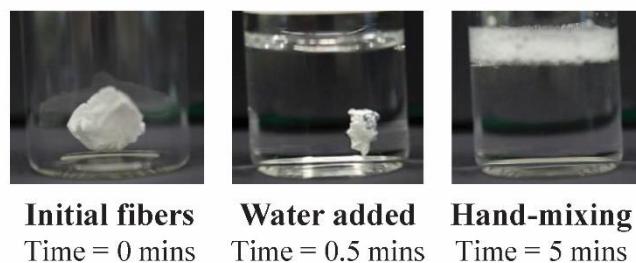


**Figure 53.** Rapid NP reconstitution using low-energy mixing. A) Initial NP-loaded fibers B) Immediate dissolution of PVA fibers upon addition of DI water, and C) Visible confirmation of NP reconstitution after 5 mins of hand-mixing.

**Table 42.** Comparing reconstitution techniques

VE NPs	Initial NPs Diameter (nm)	Reconstituted NPs Diameter (nm)	Change in Size (%)	$S_f/S_i$
20 min hand-mix & vortex	$174 \pm 2$	$174 \pm 20$	0%	1.0
5 min hand-mix		$174 \pm 17$	0%	1.0

The reconstitution of the NPs was examined by dissolving the fibers in phosphate buffer solution (PBS) and compared with water. All samples have 15-16% change in size and a  $S_f/S_i$  of 1.1-1.2 (**Table 43**). Thus, the buffer does not appear to alter the reconstitution of the NPs compared to dissolution in water. NPs can be reconstituted in PBS or water for potential clinical applications. Since the results were comparable when reconstituting in water or buffer, water was used in further experiments.

**Table 43.** Dissolving fibers in PBS

VE NPs in PVA	Change in Size (%)	$S_f / S_i$
dissolved in DI	16%	1.2
dissolved in PBS w/ KCl	15%	1.1
dissolved in PBS w/out KCl	16%	1.2

The osmolarity of the dispersion upon reconstitution is an important consideration in intravenous formulations. The PVA in the reconstituted solution of NPs has an approximate osmolarity of 0.002 mOsM. For comparison, the osmolarity of saline solution and PBS are 300 mOsM and 150 mOsM, respectively. Therefore, the polymer has a negligible contribution to the osmolarity of the final formulation when reconstituting in saline or buffer.

#### 7.4.1.2. Nanoparticle Storage

The shelf-life of the dry NPs in nanofibers at ambient temperature was examined using 120 nm VE NPs at a loading of 0.8 wt.%. The fiber sample was stored for 7 months at ambient conditions and then reconstituted. The NPs reconstituted from fibers after 1 day and after 7 months were comparable (**Figure 54**). Notably, for the original NP dispersion stored at 4°C for 7 months, there was a 54% increase in diameter likely due to Ostwald ripening [399] (**Table 44**). These results suggest that converting the NP dispersion to a dry form, i.e. encapsulated within the polymer fibers, prevents Ostwald ripening. Therefore, NP storage in nanofibers improves the size stability of NPs enabling storage of the NP formulations at room temperature and avoids the need for cold chain storage.

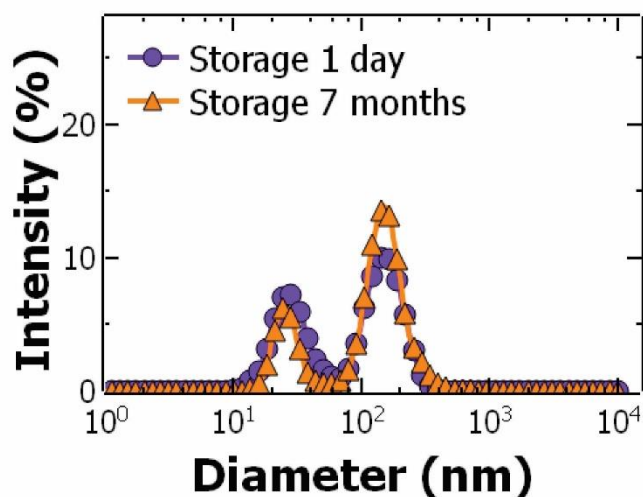


**Figure 54.** Particle size distribution measured by dynamic light scattering of 118 nm VE NPs reconstituted within 1 day of drying and after 7 months of storage at ambient conditions. The peak at ~30 nm is attributed to the dissolved polymer in the solution and the solution and the peak at ~160 nm is attributed to the reconstituted NPs. The NP size is comparable upon reconstitution after 1 day and 7 months of storage at ambient conditions.

**Table 44.** Comparing size stability of NPs after storage for 7 months

Sample	Storage temperature	Change in size (%)
NPs in solution	4°C	54%
Dried NPs	~23°C	4%

#### 7.4.2. *Effect of Particle Properties*

##### 7.4.2.1. *Nanoparticle Composition*

Building on the results demonstrating proof-of-concept, we further probed the effect of fiber processing and particle properties on redispersed NP size. First, we investigated the effect of the composition of the NP core by comparing VE- and PS-loaded NPs. The melting point of VE is 3°C which is below the working temperature of the NP processing; therefore, VE core is expected to be in liquid phase. PS has a glass transition temperature of 100°C [422], which is above the working temperature; therefore, the PS core is expected to behave as a solid. NPs of similar size were compared:

the VE NPs has an initial diameter of  $118 \text{ nm} \pm 5 \text{ nm}$  and the PS NPs has an initial diameter of  $112 \text{ nm} \pm 5 \text{ nm}$  (**Table 41**). The fiber diameter was  $\sim 300 \text{ nm}$  so the initial NP to nanofiber diameter ratio (NP:NF) was 0.47 for both samples.

Using the Multiple Narrow Modes algorithm, the DLS results of the reconstituted NPs showed a bimodal distribution (**Figure 55**). We attribute the peak at  $\sim 30 \text{ nm}$  to the dissolved PVA and the second peak to the reconstituted NPs. The reconstituted NP size was taken as the NP peak intensity. For both VE and PS NPs, there was an increase in NP diameter upon reconstitution in water. When compared to the initial NP size, the final size to initial size ( $S_f/S_i$ ) was 1.3 for the liquid core NPs and 1.7 for the solid core NPs (**Table 45**).

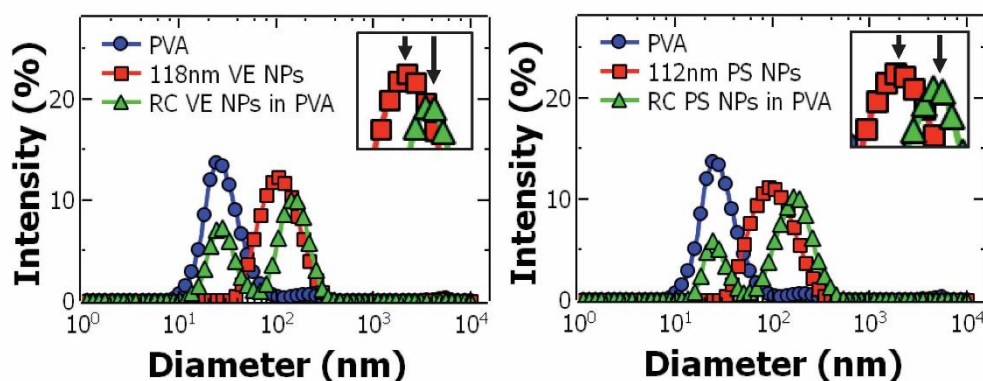


**Figure 55.** Particle size distribution measured by dynamic light scattering of the initial NPs, PVA control, and reconstituted (RC) NPs for A) VE NP and B) PS NPs. The second peak for RC NPs shifts to the right indicative of an increase in particle size relative to initial NPs.

**Table 45.** NP core composition and size influences NP size stability after reconstitution

NP Core	Initial NPs Diameter (nm)	Nanofiber Diameter (nm)	NP:NF Ratio	Reconstituted NPs Diameter (nm)	Change in Size (%)	$S_f/S_i$
VE	118 ± 5	249 ± 32	0.47	159 ± 18	35%	1.3
	144 ± 9	322 ± 56	0.45	169 ± 10	17%	1.2
PS	112 ± 5	240 ± 32	0.47	189 ± 43	69%	1.7
	192 ± 14	390 ± 37	0.49	223 ± 24	16%	1.2

Interestingly, the increase in PS NPs was almost 2-fold greater than the VE NPs (i.e. 77 nm for PS NPs compared to 41 nm for VE NPs) (Table 45). This result suggests that NPs with a liquid core are more resistant to changes in size during fiber processing. Similar results have been observed with lyophilization [402] and was attributed to ability of a NP with a liquid core to deform much more than a NP with a solid core. Since the liquid-core particles deform, the forces experienced during drying are distributed over a larger area. In contrast, solid-core particles that do not deform experience higher stresses (same force over a smaller area) which may cause aggregation [402]. In this method of drying, fiber formation involves uniaxial elongation of a viscous liquid jet [423], as the solvent evaporates there is a transition from a liquid jet to a solid fiber, followed by stretching and thinning of the solid fiber. Since the diameter of the liquid jet is typically on the order of millimeters and much larger than the NP, we posit the shear forces have minimal influence on the NP deformation. As the jet is elongated and the solvent evaporates, it transitions from a liquid jet to a solid fiber (micron to nanometer diameter) resulting in high elongational stresses [424]. The elongational force as the fiber thins can cause the NPs to rotate and deform along the axis of shear stresses [425,426]. The liquid core particles are expected to deform during fiber formation and redisperse into spheres close to the original



size upon reconstitution. In contrast, the solid-core particles may undergo some degree of aggregation during fiber formation and subsequent redispersion.

#### 7.4.2.2. *Effect of Nanoparticle Size*

Next, we varied the initial size of the NPs at comparable NP:NF ratios. For VE NPs, the size of the NPs varied from 118 nm to 144 nm and the NP:NF ratio was  $\sim 0.5$ , i.e. the NP diameter was approximately half of the final nanofiber diameter. For PS NPs, the NP size varied from 112 nm to 192 nm and the NP:NF ratio was  $\sim 0.5$ . In both cases, the larger NPs better maintained their size upon electrospinning and redispersion compared to the smaller particles. For PS NPs, when the NP size increased from 112 to 192 nm, the change in NP size after reconstitution decreased from 69% to 16% resulting in a decrease in  $S_f/S_i$  from 1.7 to 1.2 (**Table 45**). A similar trend was observed with VE NPs. The change in VE NP size after reconstitution decreased from 35% to 17% resulting in a  $S_f/S_i$  from 1.3 to 1.2. This result may be because larger particles have larger surface area to distribute the force the NPs are subjected to during fiber formation which reduced potential aggregation.

#### 7.4.2.3. *Effect of nanoparticle size relative to nanofiber size*

Based on these results, we investigated the effect of fiber size relative to the particle using VE NPs. The size of the VE NPs was varied between 95 nm and 175 nm (**Table 41**). When electrospun, the resulting fibers diameter was comparable and we examined the ratio of the NP diameter to nanofiber diameter (NP:NF diameter). For NPs  $\sim 95$  nm and fiber diameter  $\sim 300$  nm (NP:NF ratio 0.26), the change in size upon electrospinning and redispersion was 39%, i.e. a  $S_f/S_i$  ratio of 1.4. As the NP size increased relative to the nanofiber size (increasing NP:NF ratio), there was a decrease in the  $S_f/S_i$  ratio. Specifically, for the large NPs (NP:NF ratio 0.60), there was no significant change in NP size and a  $S_f/S_i$  ratio of 1.0 (**Table 46**).

**Table 46.** NP:NF ratio influences NP size stability after reconstitution

Initial NPs Diameter (nm)	Nanofiber Diameter (nm)	NP: NF Ratio	Reconstituted NPs Diameter (nm)	Change in Size (%)	$S_f/S_i$
95 ± 4	365 ± 36	0.26	133 ± 36	39%	1.4
129 ± 2	326 ± 34	0.40	150 ± 18	16%	1.2
174 ± 2	291 ± 37	0.60	174 ± 20	0%	1.0

These results indicate that matching the NP size to the NF size, i.e. NP:NF ratio ~1, better maintain NP size upon redispersion compared to when the NP diameter is much smaller (less than half) than the nanofiber diameter. When the NPs are small relative to the fiber diameter, multiple small particles in close proximity could aggregate as the liquid jet elongates and transitions to a solid fiber. In contrast, when the NP is similar in size to the resulting nanofiber, the number of particles in the liquid jet as it transitions to a solid fiber is geometrically constrained to one particle. This geometric constraint may prevent NP-NP interactions that can lead to aggregation. Notably, given the appropriate NP size relative to NF diameter ratio, drying NPs by blending and electrospinning with a water soluble polymer is a promising approach that enables drying and redispersion with no significant change in NP size.

This observation related to NP:NF ratio is important for extending this approach to additional nanoparticle systems in future studies. Since NPs are often designed to be a certain size, varying nanofiber size will be an important consideration. Fiber diameter of electrospun nanofibers is a complex function of electrospinning polymer properties, solvent, and process parameters [427,428].

#### 7.4.2.4. *Practical Considerations*

Building on these results, the NP loading in the polymer fibers was also examined. The loading of VE NPs (174 nm) was varied from 0.8 to 3.2 wt.% (mass of NP/mass of polymer). NP loading of 0.8 wt.% was the minimum NP concentration required to resolve the NP and PVA peaks using DLS.

The final size was not significantly affected by the 4-fold increase in NP loading; the  $S_f/S_i$  ratios were 1.0 for the range of loadings examined (**Table 47**). These loadings are comparable to drying FNP nanoparticles via freeze drying [429] and spray freeze drying [430].

**Table 47.** NP loading concentration

NPs loading	<u>Initial NPs Diameter (nm)</u>	<u>Nanofiber Diameter (nm)</u>	NP:NF Ratio	<u>Reconstituted NPs Diameter (nm)</u>	Change in Size (%)	$S_f/S_i$
0.8%	174 ± 2	291 ± 37	0.60	174 ± 20	0%	1.0
1.7%	174 ± 2	303 ± 34	0.57	171 ± 11	-2%	1.0
3.2%	174 ± 2	292 ± 47	0.60	173 ± 10	-2%	1.0

Our focus has been demonstrating electrospinning is a viable approach to converting nanoparticles to a dry form and that the nanoparticles can be reconstituted to their original size. These preliminary results indicate the reconstituted particle size is not significantly affected by the nanoparticle loading for the nanoparticle loadings examined. Further increasing the nanoparticle loading is of practical interest. Promising results maintaining nanoparticle size at high nanoparticles using PVA excipients in spray freeze drying have been reported [410] thus higher loadings may be possible and will be addressed in future studies. Extension to electrospinnable polymers and biocompatible nanoparticle formulations that are FDA approved for parenteral formulations will also be considered [431–433].

Finally, preliminary experiments electrospinning nanoparticles (VE core, PS-b-PEG stabilizer) with and without dialysis indicate that the presence of the organic solvent does not significantly affect fiber formation or nanoparticle reconstitution. In contrast, freeze drying (without excipient) after dialysis resulted in smaller redispersed particles when compared to non-dialyzed samples [402].

Therefore, it may be possible to directly electrospin after FNP and avoid the purification step to remove the organic solvent. The presence of the organic solvent considering solvents other than tetrahydrofuran, e.g. DMSO, during electrospinning will be further explored in future studies.

**Table 48.** Comparing drying and reconstitution of dialyzed particles to non-dialyzed particles

VE NPs	<u>Initial NPs</u> Diameter (nm)	<u>Nanofiber</u> Diameter (nm)	NP:NF Ratio	<u>Reconstituted NPs</u> Diameter (nm)	Change in Size (%)	$S_f/S_i$
Dialyzed	174 ± 2	291 ± 37	0.60	174 ± 20	0%	1.0
Non-Dialyzed	157 ± 6	223 ± 28	0.70	164 ± 21	4%	1.0

## 7.5. Conclusion

We demonstrate electrospinning as a new method to convert NP dispersions to a dry, stable form for long-term storage at room temperature. Using PEGylated NPs and PVA fibers as a model system, we show NPs can be stored at room temperature for at least seven months and redispersed to their original size without sonication. Thus, encapsulating NPs in polymer fibers prevents changes in size due to Ostwald ripening. The dissolved polymer following electrospinning contributes negligibly to the osmolarity of the final NP dispersion.

The final NP size is affected by polymer fiber formation and NP properties. NP composition, NP size, and nanofiber diameter relative to NP diameter are important considerations. Sizes of the NPs upon redispersion are maintained when the fiber diameter and NP diameter are comparable (NP:NF ratio ~ 1). NPs with liquid cores and larger particles better maintained their size when compared to NPs with solid cores and smaller particles, respectively. We attribute the observed differences to deformation during liquid jet-to-solid fiber transition during electrospinning.

Overall, electrospinning blends of NP dispersions and water-soluble, spinnable polymer is a novel approach for rapid, continuous drying of NPs at room temperature and redispersion to their original size at low osmolarity without sonication. This method overcomes the long standing challenge of particle aggregation that occurs with traditional drying methods (freeze drying and spray drying). Converting NP dispersions to dry, thermostable formulations will avoid the need for cold chain storage and enhance translation of nanomedicines to clinical practice.

## 8. Chapter 8: Conclusion

---

### 8.1. Overview of Project Goals

The goal of this study was to co-encapsulate paclitaxel and lapatinib in pH-labile PEGylated nanoparticles to reduce drug dosages and increase drug efficacy. We formulated a controlled release platform by tuning the hydrophobicity of the drugs and pH-labile nanoparticle core. This enabled sequential delivery of drug combinations to further improve drug efficacy through synergistic interactions [261]. There were three aims set out to achieve these goals and they were presented in this research study. First, we developed formulation parameters for encapsulation of weakly hydrophobic drugs alone and in combination via *in situ* tannic-acid iron complexation using Flash NanoPrecipitation (FNP). Next, the drug release profile was measured under pH 7.4 and pH 4 sink conditions and then the kinetics were determined using two drug release models. Finally, the drug efficacy of the nanoparticles were examining *in vitro* with an ovarian cancer cell model and the synergistic drug interaction was evaluated.

### 8.2. Conclusions from Study

The main objective of this study was to determine if co-encapsulation of paclitaxel and lapatinib into nanoparticles would enhance drug efficacy and if sequentially delivering these drugs would further improve synergy as a means to improve current chemotherapeutic treatments and translation to clinical practice. Ovarian cancer cells with multi-drug resistance (MDR) can be difficult

to treat due to an increase in the efflux of chemotherapeutic agents and low drug bioavailability; therefore, nanoparticle drug delivery of paclitaxel, a chemotherapeutic agent, with lapatinib, a tyrosine kinase inhibitor, is an advantageous approach for increasing drug bioavailability and lowering drug dosage and overcoming MDR.

Two nanoparticle platforms were developed in this study to encapsulate hydrophilic macromolecules and weakly hydrophobic drugs via Flash NanoPrecipitation (FNP). To encapsulate biologics like albumin, we developed a rapid, single-step method by leveraging tannic acid-protein complexation *in situ* during FNP. The complexes were electrostatically stabilized with a cationic polyelectrolyte. This formulation allows for high protein encapsulation efficiency (~80%) as well as pH-labile controlled release. These experiments provided the foundation to extend FNP to encapsulation of weakly hydrophobic drugs ( $\log P < 6$ ). Again, *in situ* complexation of an antioxidant complex was critical for encapsulation of the target drugs. Paclitaxel and lapatinib were encapsulated into polymer nanoparticles via *in situ* complexation of tannic acid and iron. The tannic acid-iron complex also provided advantages of a pH-labile drug release. In this study we develop the principles for formulating monodispersed nanoparticles at ~100 nm encapsulating both single drug and drug combinations. These experiments provide the foundation for controlled delivery of multiple drugs.

Following formulation of the nanoparticles, the drug release kinetics was characterized *in vitro*. The drug release profile was determined for paclitaxel, paclitaxel-prodrug, and lapatinib in both pH 7.4 and pH 4 sink conditions. We identified that the paclitaxel-prodrug was released as a faster rate relative to both paclitaxel and lapatinib as the drug transport of the prodrug was guided by different mechanisms than for paclitaxel and lapatinib. The drug release under pH 4 conditions was guided by core dissolution due to the solubilization of the TA-Fe<sup>3+</sup> complex. These results provide the foundation for understanding methods for controlling drug release from tannic acid-iron nanoparticle platform by tuning drug hydrophobicity. The efficacy of the nanoparticles was determined *in vitro* with an ovarian

cancer cell model. Firstly, we determined the encapsulation of the drugs into nanoparticles improved the drug efficacy by over 1500-fold for paclitaxel and its prodrug and by 5-fold for lapatinib when formulated with the TA-Fe<sup>3+</sup> complex. The potency of paclitaxel was also improved by the conjugation to a hydrophobic lipid (vitamin E) in both free drug and nanoparticle formulations. Furthermore, co-encapsulation had a synergistic effect relative to single-drug nanoparticles for both paclitaxel-lapatinib and prodrug-lapatinib combinations due to spatiotemporal control.

Translating nanoparticle drug delivery research into clinical practice is a challenge due to poor shelf-stability and reconstitution of nanoparticles with traditional methods (e.g. freeze drying). To address these limitations, we developed a novel method for drying nanoparticles via electrospinning. We demonstrate electrospinning as a new method for converting nanoparticle dispersions into dry, stable form for long-term storage at room temperature by electrospinning the nanoparticles with a water-soluble polymer as well as rapid redispersion to original nanoparticle size at low osmolality. This technology provides the platform for translating controlled release nanoparticles into clinical practice.

### **8.3. Future Work and Potential Impact**

Sequential delivery of paclitaxel and lapatinib was investigated in this study. We observed cell-dependent synergy due to sequential drug delivery, which was confirmed with cell cycle analysis. These experiments provided direction for further improvement in cytotoxicity of the anticancer drugs through controlled release. We investigated the effects of tuning paclitaxel hydrophobicity by formulating a hydrophobic prodrug. We determined that nanoparticles loaded with the prodrug were more cytotoxic compared to nanoparticles loaded with paclitaxel. Additionally, co-encapsulating paclitaxel or the prodrug with lapatinib enhanced the drug efficacy through synergistic drug interaction. Overall, the results from these experiments have shown that we can control the drug



release from nanoparticles by leveraging the pH-labile nature of the tannic acid-iron nanoparticle platform and tune of the drug release profiles by modulating drug hydrophobicity. More importantly, this controlled delivery platform sequentially delivers drug combinations on the order of hours which enhances drug cytotoxicity and reduces dosages improving chemotherapeutic treatment.

The results from this study display great promise for sequential drug delivery of chemotherapeutic agents from nanoparticles for treating ovarian cancer. This area of research opens up many avenues for further investigation in future studies. This includes studies on the synergistic effects of sequential drug delivery on a wide range of ovarian cancer cells with different levels of expression of key proteins and receptors. Furthermore, creating a correlation between sequential delivery results observed with free drugs and nanoparticles will be of significant importance in a larger population of cells. This will provide the foundation for translating previous studies with free drugs to nanoparticle research. Other markers of cell death and cytotoxicity can also be explored such as live/dead stains, apoptosis assays to determine mechanism of cell death (necrosis vs apoptosis) such as analysis of subG<sub>1</sub> peaks and TUNEL assay, and microtubule polymerization. Additional examination of nanoparticles could also facilitate translation to clinical practices such as replacing the polymer used in FNP with an FDA approved biodegradable polymer such as poly(lactic-co-glycolic acid)-b-poly(ethylene glycol) (PLGA-b-PEG). Exploring this line of research will facilitate future nanomedicine design of sequential treatments and optimize chemotherapeutic treatment with paclitaxel.

Another important future step is examining sequentially release from nanoparticles *in vivo* to better understand the drug efficacy for progressing the research to clinical studies. These experiments will be done with a xenograft model using human ovarian cancer cells. The tumor cells will be subcutaneously implanted in immunocompromised mice and the nanoparticle treatment will be administered intravenously to parallel typical administration of paclitaxel in clinical settings as well

as the intended administration of the nanoparticle treatment. This method of administration will provide evidence of selective nanoparticle accumulation in the tumor tissue compared to free drug formulations. This will be examined by conjugating a fluorescent marker on paclitaxel and lapatinib. From the *in vivo* experiments will evaluate drug biodistribution in key tissues (i.g. tumor, liver, kidney, heart, etc.), systemic toxicity, tumor volume and weight over time, the pharmacokinetics, drug clearance, and survival time. Furthermore, we will compare the nanoparticle drug formulations to pharmaceutical grade Taxol (paclitaxel) and Tykerb (lapatinib). As a method to further improve selective accumulation of the nanoparticles in the tumor tissue and minimize side effects, targeting moieties on the nanoparticles will also be explored *in vivo*. Selection of an appropriate target will be an important consideration. For example, CD44 is a good choice because it is a membrane receptor that is overexpressed on ovarian cancer cells and can be targeted with an antibody conjugated to the PEGylated amphiphilic polymer. Exploring this line of research will facilitate future nanomedicine design of sequential treatments and optimize chemotherapeutic treatment with paclitaxel. Additionally, this future work can provide a better understanding of methods to overcome drug resistance in ovarian cancer as well facilitate in translation to phase I clinical trials. The culmination of the research covered in this dissertation as well as the proposed studies for future work will facilitate in translation of this platform into a clinical study and eventually clinical practice for treating ovarian cancer.

Translating sequential drug release from nanoparticles to clinical practice is the first step for improving clinical practices in the areas of ovarian cancer. The research in this dissertation present two platform for encapsulation and controlled delivery of hydrophobic, weakly hydrophobic, hydrophilic small molecules, and hydrophilic macromolecules. These nanoparticle platforms could be extended to encapsulate a wide variety of drug combinations not only to treat ovarian cancer but other forms of cancer. Other small molecule chemotherapeutic agents can be encapsulated such as

carboplatin as well as macromolecules such as DNA or RNA for gene therapy through controlled release from polymer nanoparticles. While this opens up the possibility for limitless combinations of therapeutic agents there is still a need to understand the effects of sequential delivery of these combination on different cancer cells. Therefore, there needs to be a greater focus on developing an index for key pro-survival pathways for a wide range of cancer cells types. Based on this information, we can use network modeling to facilitate predicting the combinations and sequences which will improve drug efficacy and patient outcomes. Finally, these results can be applied to animal models and clinical trials using nanoparticle drug delivery to improve patient's lives.

## 9. Vita

### Shani Levit

601 West Main St., Richmond VA. 23284 | levitsl@vcu.edu | LinkedIn/shani-levit

#### EDUCATION

---

<b>Virginia Commonwealth University, School of Engineering</b>	Fall 2015 – Spring 2020
Ph.D. Candidate in Chemical and Life Sciences Engineering	
<u>Dissertation</u> : Sequential Delivery of Nanoparticle Drug-Cocktails for Chemotherapy	
<b>University of Virginia, School of Engineering and Applied Science</b>	2011 – 2015
B.S. in Biomedical Engineering	
<u>Technical Thesis</u> : Optimizing Cell Compatibility on Electrospun Poly-L-lactic Acid Scaffolds	

#### AWARDS

---

<b>College of Engineering Dissertation Assistantship Award</b> (Awarded \$19,500)	Fall 2019 – Spring 2020
<b>Second Place at College of Engineering Three-Minute-Thesis (3MT) Competition</b> (Awarded \$300)	2019
<b>Outstanding Graduate Service Award</b> (Awarded \$300)	2019
<b>Second Place at the Graduate Student Symposium</b> (Awarded \$200)	2017

#### WORK EXPERINCES

---

<b>Sequential Delivery of Nanoparticle Drug-Cocktails for Chemotherapy</b>	Fall 2015 – Spring 2020
<ul style="list-style-type: none"><li>Formulated combination drug product with polymer nanoparticles via Flash NanoPrecipitation.</li><li>Optimized nanoparticle fabrication and characterization for uniformity and size control of nanoparticles.</li><li>Established a standard operating procedure (SOP) for measuring multiple-component drug release with liquid chromatography (HPLC).</li><li>Executed strategies for ensured quality control of nanoparticle formulations.</li><li>Examined the effects of controlled drug release from nanoparticles <u>in vitro</u> and enhanced bioavailability of API.</li></ul>	
<b>Rapid, Single-Step Protein Encapsulation via Flash NanoPrecipitation</b>	2016 – 2019
<ul style="list-style-type: none"><li>Designed a rapid, single-step method for encapsulating biologics into polymer nanoparticles.</li><li>Achieved stable nanoparticles with protein encapsulation efficiency of ~80%.</li><li>Initiated collaboration with a pulse-electric field laboratory to develop a cross-functional team to investigate the effect of protein nanoparticles on enhancing irreversible electroporation for improving cancer treatment.</li><li>Contributed to team effort to execute project targets and acted as liaison between team members, collaborators, and principal investigator.</li></ul>	
<b>Thermochromic Polymer-Liquid Crystal Fibers</b>	2017 – 2019
<ul style="list-style-type: none"><li>Characterized cholesterol liquid crystal blends with techniques such as polarized light microscopy (PLM) and differential scanning calorimetry (DSC).</li><li>Developed electrospinning process for formulating liquid crystal-polymer blends to create temperature-responsive fibers for applications in color-changing medical scaffold design.</li><li>Lead a team of 7 students as part of Dean's Research Initiative program and was responsible for provided mentorship on day-to-day operations such as early phase procedure development to reviewing technical reports.</li></ul>	

## Rapid Nanoparticle Drying and Low Energy Reconstitution via Electrospinning Fall 2015 – 2017

- Developed a novel nanoparticle drying technique via electrospinning to increase nanoparticle shelf-life.
- Preserved nanoparticles with 0% change in size after 7 months of storage with simple, rapid reconstitution as a low-energy alternative to freeze drying and spray drying as well as formulation of dry powders inhalers.
- Submitted a provisional patent and authored published based on this work.

## LABORATORY QUALIFICATIONS

---

Flash NanoPrecipitation (FNP)	Scanning Electron Microscopy (SEM)	Electrospinning
Mammalian Cell Culture	Differential Scanning Calorimetry (DSC)	WST-1 Assay
Liquid Chromatography (HPLC)	Dynamic Light Scattering (DLS)	MATLAB
Flow Cytometry	UV-vis Spectroscopy	Bradford Assay
Polarized Light Microscopy (PLM)	Rheology	

## PUBLICATIONS

---

**Levit, S.L.**; Yang, H.; Tang, C. (2020). Rapid Self-Assembly of Polymer Nanoparticles for Synergistic Codelivery of Paclitaxel and Lapatinib via Flash NanoPrecipitation. *Nanomaterials*. 10, 561.

**Levit, S.L.**; Nguyen, J.; Hattrup, N.P.; Rabatin, B.E.; Stwodah, R.; Vasey, C.L.; Zeevi, M.P.; Gillard, M.; D'Angelo, P.A.; Swana, K.W.; et al. (2020). Color Space Transformation-Based Algorithm for Evaluation of Thermochromic Behavior of Cholesteric Liquid Crystals Using Polarized Light Microscopy. *ACS Omega*. 5, 7149–7157.

**Levit, S. L.** Walker, R., Tang, C., (2019). Rapid, Single-Step Protein Encapsulation via Flash NanoPrecipitation. In *Polymers*. 11 (9), 1406.

Smith, R. A., Walker, R. C., **Levit, S. L.**, Tang, C. (2019). Single Step Self-Assembly and Crosslinking of Chitosan-based Nanoparticles. In *Polymers*. 11 (5), 749.

**Levit, S. L.**, Walker, R., Pham, A. L., Tang, C., (2019). Polymer-Free Electrospinning. Green Electrospinning, De Gruyter, Ed. Hozrum, N., Demir, M.M., Crespy, D., Muñoz-Espí, R. ISBN: 978-3-11-058139-3.

**Levit, S. L.**, Stwodah, R. M., Tang, C. (2018). Rapid, Room Temperature Nanoparticle Drying and Low-Energy Reconstitution via Electrospinning. In *Journal of Pharmaceutical Sciences*, 107(3), 807-813.

Tang, C., **Levit, S. L.**, Zeevi, M., Vasey, C., Fromen, C. (2019). Polymer Colloids Enable Medical Applications. In *Polymer Colloids*, Royal Society of Chemistry. 358-398.

Tang C., **Levit, S. L.**, Wang, K. F., Edwards, B. T., Corson, J. L., Dotivala, A. C. (2017) Electrospinning Process and Nanofiber Characteristics, *Polymer Nanofibers: Science, Technology and Applications*. (Submitted).

## PATENTS

---

U. S. Provisional Patent No. 62/853,429: “Rapid, one-step process for encapsulating biologics”. Filed May 28 2019.

U. S. Provisional Patent No. 62/434,614: “Converting nanoparticle dispersions to dry fibers for long-term storage and compatibility”. Filed June 8 2017.

Invention Disclosure: “Nanoparticle-based Chronotherapies”. Filed Nov 10, 2016

## PRESENTATIONS

---

**Levit, S. L.**, and Tang, C., “Formulation of Small and Large Molecules using Flash NanoPrecipitation via in situ Complexation”, Accepted to Preclinical Form and Formulation for Drug Discovery, Gordon Research Conference, Poster Presentation, Waterville Valley, NH, June 9 – 14, 2019.

**Levit, S. L.**, and Tang, C., “Nanoparticle Drug Cocktails for Improving Chemotherapy of Multi-drug Resistant Cancers”, Accepted to 2018 AIChE Annual Meeting, Oral Presentation, Pittsburg, PA, October 28 – November 2, 2018.

**Levit, S. L.**, Nguyen, J., Stwodah R., Gillar, M., Swana, K., Tang C., “Characterization of Thermo-Responsive Polymer-Liquid Crystal Nonwovens”, Accepted to 92<sup>nd</sup> ACS Colloid & Surface Science Symposium, Poster Presentation, State College, PA, June 10-13, 2018.

**Levit, S. L.**, Stwodah R., Tang C., “Rapid Nanoparticle Drying and Low Energy Reconstitution via Electrospinning”, Accepted to 2<sup>nd</sup> Bioengineering & Translational Medicine Conference, Oral Presentation, Minneapolis, MN, October 28- 28, 2017.

**Levit, S. L.**, Stwodah R., Tang C., “Electrospinning Polymer Nanomedicines Extends Shelf-Life and Size Stability”, Accepted to 2017 AIChE Annual Meeting, Oral Presentation, Minneapolis, MN, October 29 – November 3, 2017.

**Levit, S. L.**, Smith, R., Tang C., “Formulation of pH-responsive Nanoparticles for Controlled Release”, Accepted to 91<sup>nd</sup> ACS Colloid & Surface Science Symposium, Oral Presentation, New York, NY, July 9 – 12, 2017.

**Levit, S. L.**, Tang C., “Nanofibers as a Dry Form of Drug-Loaded Nanoparticles for Long-Term Storage”, Accepted to Nanofiber, Applications and Related Technologies (NART) Conference, Oral Presentation, Raleigh, NC, September 13 – 15, 2016.

## MENTORSHIP & TEACHING EXPERINCES

---

**Teaching Assistant, Chemical and Life Sciences Courses, VCU** Fall 2015 – Spring 2017

- Facilitated teaching 4 courses of 30-50 students and assessed student work in a timely manner.
- Communicated with instructors to assesses and improve students’ understanding of the course material.

**Undergraduate Teaching Assistant for Biomedical Engineering Lab Course, UVA**

May 2014 – June 2015

- Prepared materials for experiments such as methods for determining gene expression (RT-PCR).
- Guided students in statistical analysis of laboratory results and support in writing technical reports.

## PROFESSSIONAL ORGANIZATIONS & SERVICE

---

**Engineering Graduate Student Association (EGSA) at VCU** Senior Board Member

2016 – Present

- Lead in coordinating 2-3 events per month to encourage student collaboration and a positive work environment.
- Dedicated to providing colleagues professional development opportunities through workshops and career panels.

## 10. References

1. Reid, B.M.; Permut, J.B.; Sellers, T.A. Epidemiology of ovarian cancer: a review. *Cancer Biol Med* **2017**, *14*, 9–32, doi:10.20892/j.issn.2095-3941.2016.0084.
2. Gadducci, A.; Cosio, S. Surveillance of patients after initial treatment of ovarian cancer. *Crit. Rev. Oncol. Hematol.* **2009**, *71*, 43–52, doi:10.1016/j.critrevonc.2008.12.008.
3. Marcus, C.S.; Maxwell, G.L.; Darcy, K.M.; Hamilton, C.A.; McGuire, W.P. Current Approaches and Challenges in Managing and Monitoring Treatment Response in Ovarian Cancer. *J Cancer* **2014**, *5*, 25–30, doi:10.7150/jca.7810.
4. Jayson, G.C.; Kohn, E.C.; Kitchener, H.C.; Ledermann, J.A. Ovarian cancer. *The Lancet* **2014**, *384*, 1376–1388, doi:10.1016/S0140-6736(13)62146-7.
5. Shih, I.-M.; Kurman, R.J. Ovarian tumorigenesis: a proposed model based on morphological and molecular genetic analysis. *Am. J. Pathol.* **2004**, *164*, 1511–1518, doi:10.1016/s0002-9440(10)63708-x.
6. King, M.-C.; Marks, J.H.; Mandell, J.B.; New York Breast Cancer Study Group. Breast and ovarian cancer risks due to inherited mutations in BRCA1 and BRCA2. *Science* **2003**, *302*, 643–646, doi:10.1126/science.1088759.
7. Ozols, R.F. Challenges for chemotherapy in ovarian cancer. *Ann Oncol* **2006**, *17*, v181–v187, doi:10.1093/annonc/mdj978.
8. Rowinsky, E.K.; Donehower, R.C. Paclitaxel (Taxol). *New England Journal of Medicine* **1995**, *332*, 1004–1014, doi:10.1056/NEJM199504133321507.
9. Armstrong, D.K. Relapsed Ovarian Cancer: Challenges and Management Strategies for a Chronic Disease. *The Oncologist* **2002**, *7*, 20–28, doi:10.1634/theoncologist.7-suppl\_5-20.
10. Rubin, S.C.; Hoskins, W.J.; Hakes, T.B.; Markman, M.; Cain, J.M.; Lewis, J.L. Recurrence after negative second-look laparotomy for ovarian cancer: analysis of risk factors. *Am. J. Obstet. Gynecol.* **1988**, *159*, 1094–1098, doi:10.1016/0002-9378(88)90420-6.
11. Parhi, P.; Mohanty, C.; Sahoo, S.K. Nanotechnology-based combinational drug delivery: an emerging approach for cancer therapy. *Drug Discovery Today* **2012**, *17*, 1044–1052, doi:10.1016/j.drudis.2012.05.010.
12. Poole, C.J.; Perren, T.; Gawande, S.; Ridderheim, M.; Cook, J.; Jenkins, A.; Roychowdhury, D. Optimized sequence of drug administration and schedule leads to improved dose delivery for gemcitabine and paclitaxel in combination: a phase I trial in patients with recurrent ovarian cancer. *International Journal of Gynecologic Cancer* **2006**, *16*, 507–514, doi:10.1136/ijgc-00009577-200603000-00008.
13. Rowinsky, E.K.; Citardi, M.J.; Noe, D.A.; Donehower, R.C. Sequence-dependent cytotoxic effects due to combinations of cisplatin and the antimicrotubule agents taxol and vincristine. *J Cancer Res Clin Oncol* **1993**, *119*, 727–733, doi:10.1007/BF01195344.
14. Waltmire, C.N.; Alberts, D.S.; Dorr, R.T. Sequence-dependent cytotoxicity of combination chemotherapy using paclitaxel, carboplatin and bleomycin in human lung and ovarian cancer. *Anti-Cancer Drugs* **2001**, *12*, 595.
15. Carducci, M.A.; Gilbert, J.; Bowling, M.K.; Noe, D.; Eisenberger, M.A.; Sinibaldi, V.; Zabelina, Y.; Chen, T.; Grochow, L.B.; Donehower, R.C. A Phase I Clinical and Pharmacological Evaluation of Sodium Phenylbutyrate on an 120-h Infusion Schedule. *Clin Cancer Res* **2001**, *7*, 3047–3055.
16. Ghielmini, M.; Schmitz, S.-F.H.; Cogliatti, S.; Bertoni, F.; Waltzer, U.; Fey, M.F.; Betticher, D.C.; Schefer, H.; Pichert, G.; Stahel, R.; et al. Effect of Single-Agent Rituximab Given at the Standard Schedule or As Prolonged Treatment in Patients With Mantle Cell Lymphoma: A Study of the Swiss Group for Clinical Cancer Research (SAKK). *JCO* **2005**, *23*, 705–711, doi:10.1200/JCO.2005.04.164.
17. Gerrits, C.J.H.; Schellens, J.H.M.; Burris, H.; Eckardt, J.R.; Planting, A.S.T.; Burg, M.E.L. van der; Rodriguez, G.I.; Loos, W.J.; Beurden, V. van; Hudson, I.; et al. A Comparison of Clinical Pharmacodynamics of Different Administration Schedules of Oral Topotecan (Hycamtin). *Clin Cancer Res* **1999**, *5*, 69–75.

18. Yunos, N.M.; Beale, P.; Yu, J.Q.; Huq, F. Synergism from Sequenced Combinations of Curcumin and Epigallocatechin-3-gallate with Cisplatin in the Killing of Human Ovarian Cancer Cells. *Anticancer Res* **2011**, *31*, 1131–1140.
19. Morelli, M.P.; Cascone, T.; Troiani, T.; De Vita, F.; Orditura, M.; Laus, G.; Eckhardt, S.G.; Pepe, S.; Tortora, G.; Ciardiello, F. Sequence-dependent antiproliferative effects of cytotoxic drugs and epidermal growth factor receptor inhibitors. *Ann. Oncol.* **2005**, *16 Suppl 4*, iv61-68, doi:10.1093/annonc/mdi910.
20. Johnson, S.W.; Ozols, R.F.; Hamilton, T.C. Mechanisms of drug resistance in ovarian cancer. *Cancer* **1993**, *71*, 644–649, doi:10.1002/cncr.2820710224.
21. Housman, G.; Byler, S.; Heerboth, S.; Lapinska, K.; Longacre, M.; Snyder, N.; Sarkar, S. Drug Resistance in Cancer: An Overview. *Cancers* **2014**, *6*, 1769–1792, doi:10.3390/cancers6031769.
22. Eastman, A. Cross-linking of glutathione to DNA by cancer chemotherapeutic platinum coordination complexes. *Chem. Biol. Interact.* **1987**, *61*, 241–248, doi:10.1016/0009-2797(87)90004-4.
23. Mistry, P.; Kelland, L.R.; Abel, G.; Sidhar, S.; Harrap, K.R. The relationships between glutathione, glutathione-S-transferase and cytotoxicity of platinum drugs and melphalan in eight human ovarian carcinoma cell lines. *Br. J. Cancer* **1991**, *64*, 215–220, doi:10.1038/bjc.1991.279.
24. Michael, M.; Doherty, M. m. Tumoral Drug Metabolism: Overview and Its Implications for Cancer Therapy. *JCO* **2005**, *23*, 205–229, doi:10.1200/JCO.2005.02.120.
25. Sampath, D.; Cortes, J.; Estrov, Z.; Du, M.; Shi, Z.; Andreeff, M.; Gandhi, V.; Plunkett, W. Pharmacodynamics of cytarabine alone and in combination with 7-hydroxystaurosporine (UCN-01) in AML blasts in vitro and during a clinical trial. *Blood* **2006**, *107*, 2517–2524, doi:10.1182/blood-2005-08-3351.
26. Gottesman, M.M.; Fojo, T.; Bates, S.E. Multidrug resistance in cancer: role of ATP-dependent transporters. *Nature Reviews Cancer* **2002**, *2*, 48–58, doi:10.1038/nrc706.
27. Szakács, G.; Annereau, J.-P.; Lababidi, S.; Shankavaram, U.; Arciello, A.; Bussey, K.J.; Reinhold, W.; Guo, Y.; Kruh, G.D.; Reimers, M.; et al. Predicting drug sensitivity and resistance: Profiling ABC transporter genes in cancer cells. *Cancer Cell* **2004**, *6*, 129–137, doi:10.1016/j.ccr.2004.06.026.
28. Perera, D.; Poulos, R.C.; Shah, A.; Beck, D.; Pimanda, J.E.; Wong, J.W.H. Differential DNA repair underlies mutation hotspots at active promoters in cancer genomes. *Nature* **2016**, *532*, 259–263, doi:10.1038/nature17437.
29. Hanawalt, P.C. Heterogeneity of DNA repair at the gene level. *Mutat. Res.* **1991**, *247*, 203–211, doi:10.1016/0027-5107(91)90016-h.
30. Bonanno, L.; Favaretto, A.; Rosell, R. Platinum drugs and DNA repair mechanisms in lung cancer. *Anticancer Res.* **2014**, *34*, 493–501.
31. Selvakumaran, M.; Pisarcik, D.A.; Bao, R.; Yeung, A.T.; Hamilton, T.C. Enhanced cisplatin cytotoxicity by disturbing the nucleotide excision repair pathway in ovarian cancer cell lines. *Cancer Res.* **2003**, *63*, 1311–1316.
32. Agarwal, R.; Kaye, S.B. Ovarian cancer: strategies for overcoming resistance to chemotherapy. *Nature Reviews Cancer* **2003**, *3*, 502–516, doi:10.1038/nrc1123.
33. Sui, X.; Chen, R.; Wang, Z.; Huang, Z.; Kong, N.; Zhang, M.; Han, W.; Lou, F.; Yang, J.; Zhang, Q.; et al. Autophagy and chemotherapy resistance: a promising therapeutic target for cancer treatment. *Cell Death & Disease* **2013**, *4*, e838–e838, doi:10.1038/cddis.2013.350.
34. Kapse-Mistry, S.; Govender, T.; Srivastava, R.; Yergeri, M. Nanodrug delivery in reversing multidrug resistance in cancer cells. *Front Pharmacol* **2014**, *5*, doi:10.3389/fphar.2014.00159.
35. Vasey, P.A. Resistance to chemotherapy in advanced ovarian cancer: mechanisms and current strategies. *Br J Cancer* **2003**, *89*, S23–S28, doi:10.1038/sj.bjc.6601497.
36. Markman, M.; Rothman, R.; Hakes, T.; Reichman, B.; Hoskins, W.; Rubin, S.; Jones, W.; Almadrones, L.; Lewis, J.L. Second-line platinum therapy in patients with ovarian cancer previously treated with cisplatin. *J. Clin. Oncol.* **1991**, *9*, 389–393, doi:10.1200/JCO.1991.9.3.389.
37. Pfisterer, J.; Plante, M.; Vergote, I.; Du Bois, A.; Wagner, U.; Hirte, H.; Lacave, A.J.; Stähle, A.; Kimmig, R.; Eisenhauer, E. Gemcitabine/carboplatin (GC) vs. carboplatin (C) in platinum sensitive recurrent ovarian cancer (OVCA). Results of a Gynecologic Cancer Intergroup randomized phase III



- trial of the AGO OVAR, the NCIC CTG and the EORTC GCG. *JCO* **2004**, *22*, 5005–5005, doi:10.1200/jco.2004.22.90140.5005.
38. D'Agostino, G.; Ferrandina, G.; Ludovisi, M.; Testa, A.; Lorusso, D.; Gbaguidi, N.; Breda, E.; Mancuso, S.; Scambia, G. Phase II study of liposomal doxorubicin and gemcitabine in the salvage treatment of ovarian cancer. *Br J Cancer* **2003**, *89*, 1180–1184, doi:10.1038/sj.bjc.6601284.
  39. Bookman, M.A.; Malmström, H.; Bolis, G.; Gordon, A.; Lissoni, A.; Krebs, J.B.; Fields, S.Z. Topotecan for the treatment of advanced epithelial ovarian cancer: an open-label phase II study in patients treated after prior chemotherapy that contained cisplatin or carboplatin and paclitaxel. *J. Clin. Oncol.* **1998**, *16*, 3345–3352, doi:10.1200/JCO.1998.16.10.3345.
  40. McGuire, W.P.; Blessing, J.A.; Bookman, M.A.; Lentz, S.S.; Dunton, C.J. Topotecan has substantial antitumor activity as first-line salvage therapy in platinum-sensitive epithelial ovarian carcinoma: A Gynecologic Oncology Group Study. *J. Clin. Oncol.* **2000**, *18*, 1062–1067, doi:10.1200/JCO.2000.18.5.1062.
  41. Ozols, R.F. Maintenance therapy in advanced ovarian cancer: progression-free survival and clinical benefit. *J. Clin. Oncol.* **2003**, *21*, 2451–2453, doi:10.1200/JCO.2003.03.039.
  42. Pfisterer, J.; Weber, B.; Du Bois, A.; Lortholary, A.; Schade-Brittinger, C.; Wagner, U.; Bourgeois, H.; Jackisch, C.; Moebus, V.; Mayer, F. Paclitaxel/carboplatin (TC) vs. paclitaxel/carboplatin followed by topotecan (TOP) in first-line treatment of advanced ovarian cancer. Mature results of a Gynecologic Cancer Intergroup phase III trial of the AGO OVAR and GINECO. *JCO* **2005**, *23*, LBA5007–LBA5007, doi:10.1200/jco.2005.23.16\_suppl.lba5007.
  43. De Placido, S.; Scambia, G.; Di Vagno, G.; Naglieri, E.; Lombardi, A.V.; Biamonte, R.; Marinaccio, M.; Carteni, G.; Manzione, L.; Febbraro, A.; et al. Topotecan compared with no therapy after response to surgery and carboplatin/paclitaxel in patients with ovarian cancer: Multicenter Italian Trials in Ovarian Cancer (MITO-1) randomized study. *J. Clin. Oncol.* **2004**, *22*, 2635–2642, doi:10.1200/JCO.2004.09.088.
  44. Markman, M.; Bundy, B.N.; Alberts, D.S.; Fowler, J.M.; Clark-Pearson, D.L.; Carson, L.F.; Wadler, S.; Sickel, J. Phase III trial of standard-dose intravenous cisplatin plus paclitaxel versus moderately high-dose carboplatin followed by intravenous paclitaxel and intraperitoneal cisplatin in small-volume stage III ovarian carcinoma: an intergroup study of the Gynecologic Oncology Group, Southwestern Oncology Group, and Eastern Cooperative Oncology Group. *J. Clin. Oncol.* **2001**, *19*, 1001–1007, doi:10.1200/JCO.2001.19.4.1001.
  45. Markman, M. Point: Intraperitoneal chemotherapy in the management of ovarian cancer. *J Natl Compr Canc Netw* **2004**, *2*, 549–554, doi:10.6004/jnccn.2004.0045.
  46. McGuire, W.P.; Hoskins, W.J.; Brady, M.F.; Kucera, P.R.; Partridge, E.E.; Look, K.Y.; Clarke-Pearson, D.L.; Davidson, M. Cyclophosphamide and Cisplatin Compared with Paclitaxel and Cisplatin in Patients with Stage III and Stage IV Ovarian Cancer. *New England Journal of Medicine* **1996**, *334*, 1–6, doi:10.1056/NEJM199601043340101.
  47. Armstrong, D.K.; Bundy, B.; Wenzel, L.; Huang, H.Q.; Baergen, R.; Lele, S.; Copeland, L.J.; Walker, J.L.; Burger, R.A.; Gynecologic Oncology Group Intraperitoneal cisplatin and paclitaxel in ovarian cancer. *N. Engl. J. Med.* **2006**, *354*, 34–43, doi:10.1056/NEJMoa052985.
  48. Piccart, M.J.; Bertelsen, K.; James, K.; Cassidy, J.; Mangioni, C.; Simonsen, E.; Stuart, G.; Kaye, S.; Vergote, I.; Blom, R.; et al. Randomized Intergroup Trial of Cisplatin–Paclitaxel Versus Cisplatin–Cyclophosphamide in Women With Advanced Epithelial Ovarian Cancer: Three-Year Results. *J Natl Cancer Inst* **2000**, *92*, 699–708, doi:10.1093/jnci/92.9.699.
  49. Katsumata, N.; Yasuda, M.; Takahashi, F.; Isonishi, S.; Jobo, T.; Aoki, D.; Tsuda, H.; Sugiyama, T.; Kodama, S.; Kimura, E.; et al. Dose-dense paclitaxel once a week in combination with carboplatin every 3 weeks for advanced ovarian cancer: a phase 3, open-label, randomised controlled trial. *The Lancet* **2009**, *374*, 1331–1338, doi:10.1016/S0140-6736(09)61157-0.
  50. Katsumata, N.; Yasuda, M.; Isonishi, S.; Takahashi, F.; Michimae, H.; Kimura, E.; Aoki, D.; Jobo, T.; Kodama, S.; Terauchi, F.; et al. Long-term results of dose-dense paclitaxel and carboplatin versus conventional paclitaxel and carboplatin for treatment of advanced epithelial ovarian, fallopian tube, or

- primary peritoneal cancer (JGOG 3016): a randomised, controlled, open-label trial. *The Lancet Oncology* **2013**, *14*, 1020–1026, doi:10.1016/S1470-2045(13)70363-2.
51. Dunton, C.J. Management of treatment-related toxicity in advanced ovarian cancer. *Oncologist* **2002**, *7* Suppl 5, 11–19, doi:10.1634/theoncologist.7-suppl\_5-11.
  52. Kane, R.; Harvey, H.; Andrews, T.; Bernath, A.; Curry, S.; Dixon, R.; Gottlieb, R.; Kukrika, M.; Lipton, A.; Mortel, R.; et al. Phase II trial of cyclophosphamide, hexamethylmelamine, adriamycin, and cis-dichlorodiammineplatinum(II) combination chemotherapy in advanced ovarian carcinoma. *Cancer Treat Rep* **1979**, *63*, 307–309.
  53. Schütz, C.A.; Juillerat-Jeanneret, L.; Mueller, H.; Lynch, I.; Riediker, M. Therapeutic nanoparticles in clinics and under clinical evaluation. *Nanomedicine* **2013**, *8*, 449–467, doi:10.2217/nnm.13.8.
  54. Gordon, A.N.; Granai, C.O.; Rose, P.G.; Hainsworth, J.; Lopez, A.; Weissman, C.; Rosales, R.; Sharpington, T. Phase II study of liposomal doxorubicin in platinum- and paclitaxel-refractory epithelial ovarian cancer. *J. Clin. Oncol.* **2000**, *18*, 3093–3100, doi:10.1200/JCO.2000.18.17.3093.
  55. Muggia, F.M.; Hainsworth, J.D.; Jeffers, S.; Miller, P.; Groshen, S.; Tan, M.; Roman, L.; Uziely, B.; Muderspach, L.; Garcia, A.; et al. Phase II study of liposomal doxorubicin in refractory ovarian cancer: antitumor activity and toxicity modification by liposomal encapsulation. *J. Clin. Oncol.* **1997**, *15*, 987–993, doi:10.1200/JCO.1997.15.3.987.
  56. Rose, P.G.; Maxson, J.H.; Fusco, N.; Mossbrugger, K.; Rodriguez, M. Liposomal doxorubicin in ovarian, peritoneal, and tubal carcinoma: a retrospective comparative study of single-agent dosages. *Gynecol. Oncol.* **2001**, *82*, 323–328, doi:10.1006/gyno.2001.6272.
  57. Rose, P.G. Pegylated Liposomal Doxorubicin: Optimizing the Dosing Schedule in Ovarian Cancer. *The Oncologist* **2005**, *10*, 205–214, doi:10.1634/theoncologist.10-3-205.
  58. D'Agostino, G.; Ferrandina, G.; Garganese, G.; Salerno, M.G.; Lorusso, D.; Farnetano, M.G.; Mancuso, S.; Scambia, G. Phase I study of gemcitabine and liposomal doxorubicin in relapsed ovarian cancer. *Oncology* **2002**, *62*, 110–114, doi:10.1159/000048255.
  59. Holloway, R.W.; Finkler, N.J.; Nye, L.P.; Bigsby, G.E.; Ortiz, B.H. Doxil and gemcitabine combination therapy for recurrent ovarian cancer: Results of a phase II trial. *JCO* **2004**, *22*, 5090–5090, doi:10.1200/jco.2004.22.90140.5090.
  60. Breiting, H.-G. Drug Synergy – Mechanisms and Methods of Analysis. *Toxicity and Drug Testing* **2012**, doi:10.5772/30922.
  61. Elion, G.B.; Singer, S.; Hitchings, G.H. Antagonists of nucleic acid derivatives. VIII. Synergism in combinations of biochemically related antimetabolites. *J. Biol. Chem.* **1954**, *208*, 477–488.
  62. Hall, M.J.; Middleton, R.F.; Westmacott, D. The fractional inhibitory concentration (FIC) index as a measure of synergy. *J Antimicrob Chemother* **1983**, *11*, 427–433, doi:10.1093/jac/11.5.427.
  63. Botelho, M.G. Fractional inhibitory concentration index of combinations of antibacterial agents against cariogenic organisms. *Journal of Dentistry* **2000**, *28*, 565–570, doi:10.1016/S0300-5712(00)00039-7.
  64. Konaté, K.; Mavoungou, J.F.; Lepengué, A.N.; Aworet-Samseny, R.R.; Hilou, A.; Souza, A.; Dicko, M.H.; M'Batchi, B. Antibacterial activity against  $\beta$ -lactamase producing Methicillin and Ampicillin-resistant Staphylococcus aureus: fractional Inhibitory Concentration Index (FICI) determination. *Ann Clin Microbiol Antimicrob* **2012**, *11*, 18, doi:10.1186/1476-0711-11-18.
  65. Berenbaum, M.C. Synergy, additivism and antagonism in immunosuppression. A critical review. *Clin Exp Immunol* **1977**, *28*, 1–18.
  66. Fraser, T.R. Lecture on the Antagonism between the Actions of Active Substances. *Br Med J* **1872**, *2*, 485–487.
  67. Chou, T.C.; Talalay, P. Generalized equations for the analysis of inhibitions of Michaelis-Menten and higher-order kinetic systems with two or more mutually exclusive and nonexclusive inhibitors. *Eur. J. Biochem.* **1981**, *115*, 207–216, doi:10.1111/j.1432-1033.1981.tb06218.x.
  68. Chou, T.C.; Talalay, P. A simple generalized equation for the analysis of multiple inhibitions of Michaelis-Menten kinetic systems. *J. Biol. Chem.* **1977**, *252*, 6438–6442.
  69. Chou, T.-C.; Talalay, P. Analysis of combined drug effects: a new look at a very old problem. *Trends in Pharmacological Sciences* **1983**, *4*, 450–454, doi:10.1016/0165-6147(83)90490-X.
  70. Berenbaum, M.C. What is synergy? *Pharmacol. Rev.* **1989**, *41*, 93–141.

71. Chou, T.-C. Theoretical basis, experimental design, and computerized simulation of synergism and antagonism in drug combination studies. *Pharmacol. Rev.* **2006**, *58*, 621–681, doi:10.1124/pr.58.3.10.
72. Greco, W.R.; Bravo, G.; Parsons, J.C. The search for synergy: a critical review from a response surface perspective. *Pharmacol. Rev.* **1995**, *47*, 331–385.
73. Zhao, W.; Sachsenmeier, K.; Zhang, L.; Sult, E.; Hollingsworth, R.E.; Yang, H. A New Bliss Independence Model to Analyze Drug Combination Data. *J Biomol Screen* **2014**, *19*, 817–821, doi:10.1177/1087057114521867.
74. Goldoni, M.; Johansson, C. A mathematical approach to study combined effects of toxicants in vitro: Evaluation of the Bliss independence criterion and the Loewe additivity model. *Toxicology in Vitro* **2007**, *21*, 759–769, doi:10.1016/j.tiv.2007.03.003.
75. Lederer, S.; Dijkstra, T.M.H.; Heskens, T. Additive Dose Response Models: Explicit Formulation and the Loewe Additivity Consistency Condition. *Front Pharmacol* **2018**, *9*, doi:10.3389/fphar.2018.00031.
76. Smith, J.A.; Ngo, H.; Martin, M.C.; Wolf, J.K. An evaluation of cytotoxicity of the taxane and platinum agents combination treatment in a panel of human ovarian carcinoma cell lines. *Gynecologic Oncology* **2005**, *98*, 141–145, doi:10.1016/j.ygyno.2005.02.006.
77. Bissery, M.-C.; Nohynek, G.; Sanderink, G.-J.; Lavelie, F. Docetaxel (Taxotere®) a review of preclinical and clinical experience. Part I: preclinical experience. *Anti-cancer Drugs* **1995**, *6*, 339–355.
78. Kornblith, P.; Wells, A.; Gabrin, M.J.; Piwowar, J.; Chattopadhyay, A.; George, L.D.; Ochs, R.L.; Burholt, D. In vitro responses of ovarian cancers to platinum and taxanes. *Anticancer Res.* **2003**, *23*, 543–548.
79. Ozols, R.F. Systemic Therapy for Ovarian Cancer: Current Status and New Treatments. *Seminars in Oncology* **2006**, *33*, 3–11, doi:10.1053/j.seminoncol.2006.03.011.
80. du Bois, A. Treatment of advanced ovarian cancer. *European Journal of Cancer* **2001**, *37*, 1–7, doi:10.1016/S0959-8049(01)00328-8.
81. Jekunen, A.P.; Christen, R.D.; Shalinsky, D.R.; Howell, S.B. Synergistic interaction between cisplatin and taxol in human ovarian carcinoma cells in vitro. *Br J Cancer* **1994**, *69*, 299–306, doi:10.1038/bjc.1994.55.
82. Kano, Y.; Akutsu, M.; Tsunoda, S.; Suzuki, K.; Yazawa, Y. In vitro schedule-dependent interaction between paclitaxel and cisplatin in human carcinoma cell lines. *Cancer Chemother Pharmacol* **1996**, *37*, 525–530, doi:10.1007/s002800050424.
83. Judson, P.L.; Watson, J.M.; Gehrig, P.A.; Fowler, W.C.; Haskill, J.S. Cisplatin Inhibits Paclitaxel-induced Apoptosis in Cisplatin-resistant Ovarian Cancer Cell Lines: Possible Explanation for Failure of Combination Therapy. *Cancer Res* **1999**, *59*, 2425–2432.
84. Vanhoefer, U.; Harstrick, A.; Wilke, H.; Schleucher, N.; Walles, H.; Schröder, J.; Seeber, S. Schedule-dependent antagonism of paclitaxel and cisplatin in human gastric and ovarian carcinoma cell Lines in vitro. *European Journal of Cancer* **1995**, *31*, 92–97, doi:10.1016/0959-8049(94)00440-G.
85. Muggia, F.M. Relevance of chemotherapy dose and schedule to outcomes in ovarian cancer. *Seminars in Oncology* **2004**, *31*, 19–24, doi:10.1053/j.seminoncol.2004.11.024.
86. Tan, D.S.P.; Ang, J.E.; Kaye, S.B. Ovarian Cancer: Can We Reverse Drug Resistance? In Proceedings of the Ovarian Cancer; Coukos, G., Berchuck, A., Ozols, R., Eds.; Springer: New York, NY, 2008; pp. 153–167.
87. Bookman, M.A.; Brady, M.F.; McGuire, W.P.; Harper, P.G.; Alberts, D.S.; Friedlander, M.; Colombo, N.; Fowler, J.M.; Argenta, P.A.; De Geest, K.; et al. Evaluation of New Platinum-Based Treatment Regimens in Advanced-Stage Ovarian Cancer: A Phase III Trial of the Gynecologic Cancer InterGroup. *J Clin Oncol* **2009**, *27*, 1419–1425, doi:10.1200/JCO.2008.19.1684.
88. Rogers, P.; Boxall, F.E.; Allott, C.P.; Stephens, T.C.; Kelland, L.R. Sequence-dependent synergism between the new generation platinum agent ZD0473 and paclitaxel in cisplatin-sensitive and -resistant human ovarian carcinoma cell lines. *European Journal of Cancer* **2002**, *38*, 1653–1660, doi:10.1016/S0959-8049(02)00107-7.

89. Konecny, G.E.; Glas, R.; Dering, J.; Manivong, K.; Qi, J.; Finn, R.S.; Yang, G.R.; Hong, K.-L.; Ginther, C.; Winterhoff, B.; et al. Activity of the multikinase inhibitor dasatinib against ovarian cancer cells. *British Journal of Cancer* **2009**, *101*, 1699–1708, doi:10.1038/sj.bjc.6605381.
90. Cheaib, B.; Auguste, A.; Leary, A. The PI3K/Akt/mTOR pathway in ovarian cancer: therapeutic opportunities and challenges. *Chin J Cancer* **2015**, *34*, 4–16, doi:10.5732/cjc.014.10289.
91. Qian, X.; LaRochelle, W.J.; Ara, G.; Wu, F.; Petersen, K.D.; Thougard, A.; Sehested, M.; Lichenstein, H.S.; Jeffers, M. Activity of PXD101, a histone deacetylase inhibitor, in preclinical ovarian cancer studies. *Mol Cancer Ther* **2006**, *5*, 2086–2095, doi:10.1158/1535-7163.MCT-06-0111.
92. Banerjee, S.; Kaye, S.B.; Ashworth, A. Making the best of PARP inhibitors in ovarian cancer. *Nature Reviews Clinical Oncology* **2010**, *7*, 508–519, doi:10.1038/nrclinonc.2010.116.
93. Luo, H.; Jiang, B.-H.; King, S.M.; Chen, Y.C. Inhibition of Cell Growth and VEGF Expression in Ovarian Cancer Cells by Flavonoids. *Nutrition and Cancer* **2008**, *60*, 800–809, doi:10.1080/01635580802100851.
94. Coley, H.M.; Shotton, C.F.; Ajose-Adeogun, A.; Modjtahedi, H.; Thomas, H. Receptor tyrosine kinase (RTK) inhibition is effective in chemosensitising EGFR-expressing drug resistant human ovarian cancer cell lines when used in combination with cytotoxic agents. *Biochemical Pharmacology* **2006**, *72*, 941–948, doi:10.1016/j.bcp.2006.07.022.
95. Arend, R.C.; Londoño-Joshi, A.I.; Samant, R.S.; Li, Y.; Conner, M.; Hidalgo, B.; Alvarez, R.D.; Landen, C.N.; Straughn, J.M.; Buchsbaum, D.J. Inhibition of Wnt/ $\beta$ -catenin pathway by niclosamide: A therapeutic target for ovarian cancer. *Gynecologic Oncology* **2014**, *134*, 112–120, doi:10.1016/j.ygyno.2014.04.005.
96. Al-Eisawi, Z.; Beale, P.; Chan, C.; Yu, J.Q.; Huq, F. Carboplatin and oxaliplatin in sequenced combination with bortezomib in ovarian tumour models. *Journal of Ovarian Research* **2013**, *6*, 78, doi:10.1186/1757-2215-6-78.
97. Qian, W.; Wang, J.; Roginskaya, V.; McDermott, L.A.; Edwards, R.P.; Stolz, D.B.; Llambi, F.; Green, D.R.; Houten, B.V. Novel combination of mitochondrial division inhibitor 1 (mdivi-1) and platinum agents produces synergistic pro-apoptotic effect in drug resistant tumor cells. *Oncotarget* **2014**, *5*, 4180–4194.
98. Hoskins, P.; Vergote, I.; Cervantes, A.; Tu, D.; Stuart, G.; Zola, P.; Poveda, A.; Provencher, D.; Katsaros, D.; Ojeda, B.; et al. Advanced Ovarian Cancer: Phase III Randomized Study of Sequential Cisplatin–Topotecan and Carboplatin–Paclitaxel vs Carboplatin–Paclitaxel. *J Natl Cancer Inst* **2010**, *102*, 1547–1556, doi:10.1093/jnci/djq362.
99. Bolis, G.; Scarfone, G.; Sciatta, C.; Polverino, G.P.; Rosa, C.; Guarnerio, P.; Parazzini, F. A Phase I/II Study of Topotecan in Combination with Carboplatin in Recurrent Epithelial Ovarian Cancer. *Gynecologic Oncology* **2001**, *83*, 477–480, doi:10.1006/gyno.2001.6399.
100. Pfisterer, J.; Vergote, I.; Bois, A.D.; Eisenhauer, E. Combination therapy with gemcitabine and carboplatin in recurrent ovarian cancer. *International Journal of Gynecologic Cancer* **2005**, *15*, doi:10.1136/ijgc-00009577-200505001-00007.
101. Zhang, N.; Wu, Z.-M.; McGowan, E.; Shi, J.; Hong, Z.-B.; Ding, C.-W.; Xia, P.; Di, W. Arsenic trioxide and cisplatin synergism increase cytotoxicity in human ovarian cancer cells: Therapeutic potential for ovarian cancer. *Cancer Science* **2009**, *100*, 2459–2464, doi:10.1111/j.1349-7006.2009.01340.x.
102. Torre, L.A.; Trabert, B.; DeSantis, C.E.; Miller, K.D.; Samimi, G.; Runowicz, C.D.; Gaudet, M.M.; Jemal, A.; Siegel, R.L. Ovarian cancer statistics, 2018. *CA: A Cancer Journal for Clinicians* **2018**, *68*, 284–296, doi:10.3322/caac.21456.
103. Ueno, N.T.; Mamounas, E.P. Neoadjuvant nab-paclitaxel in the treatment of breast cancer. *Breast Cancer Res. Treat.* **2016**, *156*, 427–440, doi:10.1007/s10549-016-3778-z.
104. Sridhar, S.S.; Hotte, S.J.; Chin, J.L.; Hudes, G.R.; Gregg, R.; Trachtenberg, J.; Wang, L.; Tran-Thanh, D.; Pham, N.-A.; Tsao, M.-S.; et al. A multicenter phase II clinical trial of lapatinib (GW572016) in hormonally untreated advanced prostate cancer. *Am. J. Clin. Oncol.* **2010**, *33*, 609–613, doi:10.1097/COC.0b013e3181beac33.

105. Rao, S.; Krauss, N.E.; Heerding, J.M.; Swindell, C.S.; Ringel, I.; Orr, G.A.; Horwitz, S.B. 3'-(p-azidobenzamido)taxol photolabels the N-terminal 31 amino acids of beta-tubulin. *J. Biol. Chem.* **1994**, *269*, 3132–3134.
106. Rao, S.; He, L.; Chakravarty, S.; Ojima, I.; Orr, G.A.; Horwitz, S.B. Characterization of the Taxol binding site on the microtubule. Identification of Arg(282) in beta-tubulin as the site of photoincorporation of a 7-benzophenone analogue of Taxol. *J. Biol. Chem.* **1999**, *274*, 37990–37994, doi:10.1074/jbc.274.53.37990.
107. Schiff, P.B.; Horwitz, S.B. Taxol stabilizes microtubules in mouse fibroblast cells. *Proc. Natl. Acad. Sci. U.S.A.* **1980**, *77*, 1561–1565, doi:10.1073/pnas.77.3.1561.
108. Vergara, D.; Bellomo, C.; Zhang, X.; Vergaro, V.; Tinelli, A.; Lorusso, V.; Rinaldi, R.; Lvov, Y.M.; Leporatti, S.; Maffia, M. Lapatinib/Paclitaxel polyelectrolyte nanocapsules for overcoming multidrug resistance in ovarian cancer. *Nanomedicine* **2012**, *8*, 891–899, doi:10.1016/j.nano.2011.10.014.
109. van Zuylen, L.; Verweij, J.; Sparreboom, A. Role of formulation vehicles in taxane pharmacology. *Invest New Drugs* **2001**, *19*, 125–141.
110. Markman, M.; Kennedy, A.; Webster, K.; Kulp, B.; Peterson, G.; Belinson, J. Phase I Trial of Paclitaxel Plus Megestrol Acetate in Patients with Paclitaxel-refractory Ovarian Cancer. *Clin Cancer Res* **2000**, *6*, 4201–4204.
111. Di Leo, A.; Gomez, H.L.; Aziz, Z.; Zvirbule, Z.; Bines, J.; Arbushites, M.C.; Guerrero, S.F.; Koehler, M.; Oliva, C.; Stein, S.H.; et al. Phase III, Double-Blind, Randomized Study Comparing Lapatinib Plus Paclitaxel With Placebo Plus Paclitaxel As First-Line Treatment for Metastatic Breast Cancer. *J Clin Oncol* **2008**, *26*, 5544–5552, doi:10.1200/JCO.2008.16.2578.
112. Satoh, T.; Xu, R.-H.; Chung, H.C.; Sun, G.-P.; Doi, T.; Xu, J.-M.; Tsuchi, A.; Omuro, Y.; Li, J.; Wang, J.-W.; et al. Lapatinib plus paclitaxel versus paclitaxel alone in the second-line treatment of HER2-amplified advanced gastric cancer in Asian populations: TyTAN--a randomized, phase III study. *J. Clin. Oncol.* **2014**, *32*, 2039–2049, doi:10.1200/JCO.2013.53.6136.
113. Martin, L.; Schilder, R. Novel Approaches in Advancing the Treatment of Epithelial Ovarian Cancer: The Role of Angiogenesis Inhibition. *JCO* **2007**, *25*, 2894–2901, doi:10.1200/JCO.2007.11.1088.
114. Teplinsky, E.; Muggia, F. Targeting HER2 in ovarian and uterine cancers: Challenges and future directions. *Gynecologic Oncology* **2014**, *135*, 364–370, doi:10.1016/j.ygyno.2014.09.003.
115. Yagi, H.; Yotsumoto, F.; Sonoda, K.; Kuroki, M.; Mekada, E.; Miyamoto, S. Synergistic anti-tumor effect of paclitaxel with CRM197, an inhibitor of HB-EGF, in ovarian cancer. *International Journal of Cancer* **2009**, *124*, 1429–1439, doi:10.1002/ijc.24031.
116. Modesitt, S.C.; Parsons, S.J. In vitro and in vivo histone deacetylase inhibitor therapy with vorinostat and paclitaxel in ovarian cancer models: Does timing matter? *Gynecologic Oncology* **2010**, *119*, 351–357, doi:10.1016/j.ygyno.2010.06.030.
117. Hirai, H.; Sootome, H.; Nakatsuru, Y.; Miyama, K.; Taguchi, S.; Tsuchioka, K.; Ueno, Y.; Hatch, H.; Majumder, P.K.; Pan, B.-S.; et al. MK-2206, an allosteric Akt inhibitor, enhances antitumor efficacy by standard chemotherapeutic agents or molecular targeted drugs in vitro and in vivo. *Mol. Cancer Ther.* **2010**, *9*, 1956–1967, doi:10.1158/1535-7163.MCT-09-1012.
118. Lassus, H.; Sihto, H.; Leminen, A.; Joensuu, H.; Isola, J.; Nupponen, N.N.; Butzow, R. Gene amplification, mutation, and protein expression of EGFR and mutations of ERBB2 in serous ovarian carcinoma. *J Mol Med* **2006**, *84*, 671–681, doi:10.1007/s00109-006-0054-4.
119. Palayekar, M.J.; Herzog, T.J. The emerging role of epidermal growth factor receptor inhibitors in ovarian cancer. *International Journal of Gynecologic Cancer* **2008**, *18*, doi:10.1111/j.1525-1438.2007.01144.x.
120. Glaysher, S.; Bolton, L.M.; Johnson, P.; Atkey, N.; Dyson, M.; Torrance, C.; Cree, I.A. Targeting EGFR and PI3K pathways in ovarian cancer. *British Journal of Cancer* **2013**, *109*, 1786–1794, doi:10.1038/bjc.2013.529.
121. Cao, C.; Lu, S.; Sowa, A.; Kivlin, R.; Amaral, A.; Chu, W.; Yang, H.; Di, W.; Wan, Y. Priming with EGFR tyrosine kinase inhibitor and EGF sensitizes ovarian cancer cells to respond to chemotherapeutic drugs. *Cancer Letters* **2008**, *266*, 249–262, doi:10.1016/j.canlet.2008.02.062.

122. Schwartz, P.A.; Kuzmic, P.; Solowiej, J.; Bergqvist, S.; Bolanos, B.; Almaden, C.; Nagata, A.; Ryan, K.; Feng, J.; Dalvie, D.; et al. Covalent EGFR inhibitor analysis reveals importance of reversible interactions to potency and mechanisms of drug resistance. *PNAS* **2014**, *111*, 173–178, doi:10.1073/pnas.1313733111.
123. Vara, J.Á.F.; Casado, E.; de Castro, J.; Cejas, P.; Belda-Iniesta, C.; González-Barón, M. PI3K/Akt signalling pathway and cancer. *Cancer Treatment Reviews* **2004**, *30*, 193–204, doi:10.1016/j.ctrv.2003.07.007.
124. Osaki, M.; Oshimura, M.; Ito, H. PI3K-Akt pathway: Its functions and alterations in human cancer. *Apoptosis* **2004**, *9*, 667–676, doi:10.1023/B:APPT.0000045801.15585.dd.
125. Butler, L.M.; Zhou, X.; Xu, W.-S.; Scher, H.I.; Rifkind, R.A.; Marks, P.A.; Richon, V.M. The histone deacetylase inhibitor SAHA arrests cancer cell growth, up-regulates thioredoxin-binding protein-2, and down-regulates thioredoxin. *PNAS* **2002**, *99*, 11700–11705, doi:10.1073/pnas.182372299.
126. Kelly, W.K.; O'Connor, O.A.; Lee Krug, M.; Chiao, J.H.; Heaney, M.; Curley, T.; MacGregore-Cortelli, B.; Tong, W.; Secrist, J.P.; Schwartz, L.; et al. Phase I Study of an Oral Histone Deacetylase Inhibitor, Suberoylanilide Hydroxamic Acid, in Patients With Advanced Cancer. *J Clin Oncol* **2005**, *23*, 3923–3931, doi:10.1200/JCO.2005.14.167.
127. Vigushin, D.M.; Ali, S.; Pace, P.E.; Mirsaidi, N.; Ito, K.; Adcock, I.; Coombes, R.C. Trichostatin A Is a Histone Deacetylase Inhibitor with Potent Antitumor Activity against Breast Cancer in Vivo. *Clin Cancer Res* **2001**, *7*, 971–976.
128. Subbaramaiah, K.; Zakim, D.; Weksler, B.B.; Dannenberg, A.J. Inhibition of Cyclooxygenase: A Novel Approach to Cancer Prevention. *Proceedings of the Society for Experimental Biology and Medicine* **1997**, *216*, 201–210, doi:10.3181/00379727-216-44170.
129. Williams, C.S.; Mann, M.; DuBois, R.N. The role of cyclooxygenases in inflammation, cancer, and development. *Oncogene* **1999**, *18*, 7908–7916, doi:10.1038/sj.onc.1203286.
130. Tsujii, M.; Kawano, S.; Tsuji, S.; Sawaoka, H.; Hori, M.; DuBois, R.N. Cyclooxygenase Regulates Angiogenesis Induced by Colon Cancer Cells. *Cell* **1998**, *93*, 705–716, doi:10.1016/S0092-8674(00)81433-6.
131. Li, W.; Cai, J.-H.; Zhang, J.; Tang, Y.-X.; Wan, L. Effects of Cyclooxygenase Inhibitors in Combination with Taxol on Expression of Cyclin D1 and Ki-67 in a Xenograft Model of Ovarian Carcinoma. *International Journal of Molecular Sciences* **2012**, *13*, 9741–9753, doi:10.3390/ijms13089741.
132. Rosanò, L.; Cianfrocca, R.; Spinella, F.; Di Castro, V.; Natali, P.G.; Bagnato, A. Combination therapy of zibotentan with cisplatin and paclitaxel is an effective regimen for epithelial ovarian cancer. This article is one of a selection of papers published in the two-part special issue entitled 20 Years of Endothelin Research. *Can. J. Physiol. Pharmacol.* **2010**, *88*, 676–681, doi:10.1139/Y10-053.
133. Song, Y.; Xin, X.; Zhai, X.; Xia, Z.; Shen, K. Sequential combination of flavopiridol with Taxol synergistically suppresses human ovarian carcinoma growth. *Arch Gynecol Obstet* **2015**, *291*, 143–150, doi:10.1007/s00404-014-3408-0.
134. Ayyagari, V.N.; Diaz-Sylvester, P.L.; Hsieh, T.J.; Brard, L. Evaluation of the cytotoxicity of the Bithionol-paclitaxel combination in a panel of human ovarian cancer cell lines. *PLoS One* **2017**, *12*, doi:10.1371/journal.pone.0185111.
135. McDaid, H.M.; Johnston, P.G. Synergistic Interaction between Paclitaxel and 8-Chloro-adenosine 3',5'-Monophosphate in Human Ovarian Carcinoma Cell Lines. *Clin Cancer Res* **1999**, *5*, 215–220.
136. Orlandi, L.; Zaffaroni, N.; Bearzatto, A.; Villa, R.; Marco, C.D.; Silvestrini, R. Lonidamine as a modulator of taxol activity in human ovarian cancer cells: effects on cell cycle and induction of apoptosis. *International Journal of Cancer* **1998**, *78*, 377–384, doi:10.1002/(SICI)1097-0215(19981029)78:3<377::AID-IJC20>3.0.CO;2-2.
137. Mudshinge, S.R.; Deore, A.B.; Patil, S.; Bhalgat, C.M. Nanoparticles: Emerging carriers for drug delivery. *Saudi Pharmaceutical Journal* **2011**, *19*, 129–141, doi:10.1016/j.jsps.2011.04.001.
138. Rahman, M.; Ahmad, M.Z.; Kazmi, I.; Akhter, S.; Afzal, M.; Gupta, G.; Ahmed, F.J.; Anwar, F. Advancement in multifunctional nanoparticles for the effective treatment of cancer. *Expert Opinion on Drug Delivery* **2012**, *9*, 367–381, doi:10.1517/17425247.2012.668522.

139. Kharkwal, H.; Janaswamy, S. *Natural Polymers for Drug Delivery*; CABI, 2016; ISBN 978-1-78064-447-9.
140. Suk, J.S.; Xu, Q.; Kim, N.; Hanes, J.; Ensign, L.M. PEGylation as a strategy for improving nanoparticle-based drug and gene delivery. *Adv Drug Deliv Rev* **2016**, *99*, 28–51, doi:10.1016/j.addr.2015.09.012.
141. Gregoriadis, G.; Swain, C.P.; Wills, E.J.; Tavill, A.S. DRUG-CARRIER POTENTIAL OF LIPOSOMES IN CANCER CHEMOTHERAPY. *The Lancet* **1974**, *303*, 1313–1316, doi:10.1016/S0140-6736(74)90682-5.
142. Zununi Vahed, S.; Salehi, R.; Davaran, S.; Sharifi, S. Liposome-based drug co-delivery systems in cancer cells. *Materials Science and Engineering: C* **2017**, *71*, 1327–1341, doi:10.1016/j.msec.2016.11.073.
143. Shen, H.; Zhang, L.; Eisenberg, A. Multiple pH-Induced Morphological Changes in Aggregates of Polystyrene-block-poly(4-vinylpyridine) in DMF/H<sub>2</sub>O Mixtures. *J. Am. Chem. Soc.* **1999**, *121*, 2728–2740, doi:10.1021/ja983712m.
144. Yu, Y.; Zhang, L.; Eisenberg, A. Morphogenic Effect of Solvent on Crew-Cut Aggregates of Amphiphilic Diblock Copolymers. *Macromolecules* **1998**, *31*, 1144–1154, doi:10.1021/ma971254g.
145. Choucair, A.; Eisenberg, A. Control of amphiphilic block copolymer morphologies using solution conditions. *Eur. Phys. J. E* **2003**, *10*, 37–44, doi:10.1140/epje/e2003-00002-5.
146. Choucair, A.; Eisenberg, A. Interfacial Solubilization of Model Amphiphilic Molecules in Block Copolymer Micelles. *J. Am. Chem. Soc.* **2003**, *125*, 11993–12000, doi:10.1021/ja036667d.
147. Sutton, D.; Nasongkla, N.; Blanco, E.; Gao, J. Functionalized Micellar Systems for Cancer Targeted Drug Delivery. *Pharm Res* **2007**, *24*, 1029–1046, doi:10.1007/s11095-006-9223-y.
148. Devulapally, R.; Paulmurugan, R. Polymer nanoparticles for drug and small silencing RNA delivery to treat cancers of different phenotypes. *WIREs Nanomedicine and Nanobiotechnology* **2014**, *6*, 40–60, doi:10.1002/wnan.1242.
149. Yallapu, M.M.; Jaggi, M.; Chauhan, S.C. Scope of nanotechnology in ovarian cancer therapeutics. *J Ovarian Res* **2010**, *3*, 19, doi:10.1186/1757-2215-3-19.
150. Tang, C.; Prud'homme, R.K. Targeted Theragnostic Nanoparticles Via Flash Nanoprecipitation: Principles of Material Selection. In *Polymer Nanoparticles for Nanomedicines: A Guide for their Design, Preparation and Development*; Vauthier, C., Ponchel, G., Eds.; Springer International Publishing: Cham, 2016; pp. 55–85 ISBN 978-3-319-41421-8.
151. Poon, C.; Duan, X.; Chan, C.; Han, W.; Lin, W. Nanoscale Coordination Polymers Codeliver Carboplatin and Gemcitabine for Highly Effective Treatment of Platinum-Resistant Ovarian Cancer. *Mol. Pharmaceutics* **2016**, *13*, 3665–3675, doi:10.1021/acs.molpharmaceut.6b00466.
152. Scarano, W.; Souza, P. de; H. Stenzel, M. Dual-drug delivery of curcumin and platinum drugs in polymeric micelles enhances the synergistic effects: a double act for the treatment of multidrug-resistant cancer. *Biomaterials Science* **2015**, *3*, 163–174, doi:10.1039/C4BM00272E.
153. Liu, D.; Chen, Y.; Feng, X.; Deng, M.; Xie, G.; Wang, J.; Zhang, L.; Liu, Q.; Yuan, P. Micellar nanoparticles loaded with gemcitabine and doxorubicin showed synergistic effect. *Colloids and Surfaces B: Biointerfaces* **2014**, *113*, 158–168, doi:10.1016/j.colsurfb.2013.08.010.
154. Devalapally, H.; Duan, Z.; Seiden, M.V.; Amiji, M.M. Modulation of Drug Resistance in Ovarian Adenocarcinoma by Enhancing Intracellular Ceramide Using Tamoxifen-Loaded Biodegradable Polymeric Nanoparticles. *Clin Cancer Res* **2008**, *14*, 3193–3203, doi:10.1158/1078-0432.CCR-07-4973.
155. Cho, H.; Lai, T.C.; Kwon, G.S. Poly(ethylene glycol)-block-poly( $\epsilon$ -caprolactone) micelles for combination drug delivery: Evaluation of paclitaxel, cyclophosphamide and gossypol in intraperitoneal xenograft models of ovarian cancer. *Journal of Controlled Release* **2013**, *166*, 1–9, doi:10.1016/j.jconrel.2012.12.005.
156. Katragadda, U.; Fan, W.; Wang, Y.; Teng, Q.; Tan, C. Combined Delivery of Paclitaxel and Tanespimycin via Micellar Nanocarriers: Pharmacokinetics, Efficacy and Metabolomic Analysis. *PLoS One* **2013**, *8*, doi:10.1371/journal.pone.0058619.

157. Milane, L.; Duan, Z.; Amiji, M. Development of EGFR-Targeted Polymer Blend Nanocarriers for Combination Paclitaxel/Lonidamine Delivery To Treat Multi-Drug Resistance in Human Breast and Ovarian Tumor Cells. *Mol. Pharmaceutics* **2011**, *8*, 185–203, doi:10.1021/mp1002653.
158. Boztas, A.O.; Karakuzu, O.; Galante, G.; Ugur, Z.; Kocabas, F.; Altuntas, C.Z.; Yazaydin, A.O. Synergistic Interaction of Paclitaxel and Curcumin with Cyclodextrin Polymer Complexation in Human Cancer Cells. *Mol. Pharmaceutics* **2013**, *10*, 2676–2683, doi:10.1021/mp400101k.
159. Abouzeid, A.H.; Patel, N.R.; Torchilin, V.P. Polyethylene glycol-phosphatidylethanolamine (PEG-PE)/vitamin E micelles for co-delivery of paclitaxel and curcumin to overcome multi-drug resistance in ovarian cancer. *International Journal of Pharmaceutics* **2014**, *464*, 178–184, doi:10.1016/j.ijpharm.2014.01.009.
160. Gawde, K.A.; Sau, S.; Tatiparti, K.; Kashaw, S.K.; Mehrmohammadi, M.; Azmi, A.S.; Iyer, A.K. Paclitaxel and di-fluorinated curcumin loaded in albumin nanoparticles for targeted synergistic combination therapy of ovarian and cervical cancers. *Colloids and Surfaces B: Biointerfaces* **2018**, *167*, 8–19, doi:10.1016/j.colsurfb.2018.03.046.
161. Liu, Z.; Zhu, Y.-Y.; Li, Z.-Y.; Ning, S.-Q. Evaluation of the efficacy of paclitaxel with curcumin combination in ovarian cancer cells. *Oncology Letters* **2016**, *12*, 3944–3948, doi:10.3892/ol.2016.5192.
162. Ganta, S.; Devalapally, H.; Amiji, M. Curcumin Enhances Oral Bioavailability and Anti-Tumor Therapeutic Efficacy of Paclitaxel upon Administration in Nanoemulsion Formulation. *Journal of Pharmaceutical Sciences* **2010**, *99*, 4630–4641, doi:10.1002/jps.22157.
163. Wang, N.; He, T.; Shen, Y.; Song, L.; Li, L.; Yang, X.; Li, X.; Pang, M.; Su, W.; Liu, X.; et al. Paclitaxel and Tacrolimus Coencapsulated Polymeric Micelles That Enhance the Therapeutic Effect of Drug-Resistant Ovarian Cancer. *ACS Appl. Mater. Interfaces* **2016**, *8*, 4368–4377, doi:10.1021/acsami.5b09340.
164. Yang, H. Targeted nanosystems: Advances in targeted dendrimers for cancer therapy. *Nanomedicine: Nanotechnology, Biology and Medicine* **2016**, *12*, 309–316, doi:10.1016/j.nano.2015.11.012.
165. Gillies, E.R.; Fréchet, J.M.J. Dendrimers and dendritic polymers in drug delivery. *Drug Discovery Today* **2005**, *10*, 35–43, doi:10.1016/S1359-6446(04)03276-3.
166. Boas, U.; H. Heegaard, P.M. Dendrimers in drug research. *Chemical Society Reviews* **2004**, *33*, 43–63, doi:10.1039/B309043B.
167. Cai, L.; Xu, G.; Shi, C.; Guo, D.; Wang, X.; Luo, J. Telodendrimer nanocarrier for co-delivery of paclitaxel and cisplatin: A synergistic combination nanotherapy for ovarian cancer treatment. *Biomaterials* **2015**, *37*, 456–468, doi:10.1016/j.biomaterials.2014.10.044.
168. Guo, X.-L.; Kang, X.-X.; Wang, Y.-Q.; Zhang, X.-J.; Li, C.-J.; Liu, Y.; Du, L.-B. Co-delivery of cisplatin and doxorubicin by covalently conjugating with polyamidoamine dendrimer for enhanced synergistic cancer therapy. *Acta Biomaterialia* **2019**, *84*, 367–377, doi:10.1016/j.actbio.2018.12.007.
169. Zou, L.; Wang, D.; Hu, Y.; Fu, C.; Li, W.; Dai, L.; Yang, L.; Zhang, J. Drug resistance reversal in ovarian cancer cells of paclitaxel and borneol combination therapy mediated by PEG-PAMAM nanoparticles. *Oncotarget* **2017**, *8*, 60453–60468, doi:10.18632/oncotarget.19728.
170. Wang, L.; Shi, C.; Wright, F.A.; Guo, D.; Wang, X.; Wang, D.; Wojcikiewicz, R.J.H.; Luo, J. Multifunctional Telodendrimer Nanocarriers Restore Synergy of Bortezomib and Doxorubicin in Ovarian Cancer Treatment. *Cancer Res* **2017**, *77*, 3293–3305, doi:10.1158/0008-5472.CAN-16-3119.
171. Zhang, C.; Pan, D.; Luo, K.; Li, N.; Guo, C.; Zheng, X.; Gu, Z. Dendrimer–doxorubicin conjugate as enzyme-sensitive and polymeric nanoscale drug delivery vehicle for ovarian cancer therapy. *Polymer Chemistry* **2014**, *5*, 5227–5235, doi:10.1039/C4PY00601A.
172. Tekade, R.K.; Dutta, T.; Tyagi, A.; Bharti, A.C.; Das, B.C.; Jain, N.K. Surface-engineered dendrimers for dual drug delivery: A receptor up-regulation and enhanced cancer targeting strategy. *Journal of Drug Targeting* **2008**, *16*, 758–772, doi:10.1080/10611860802473154.
173. Tekade, R.K.; Dutta, T.; Gajbhiye, V.; Jain, N.K. Exploring dendrimer towards dual drug delivery: pH responsive simultaneous drug-release kinetics. *Journal of Microencapsulation* **2009**, *26*, 287–296, doi:10.1080/02652040802312572.



174. Zhao, Z.; Lou, S.; Hu, Y.; Zhu, J.; Zhang, C. A Nano-in-Nano Polymer–Dendrimer Nanoparticle-Based Nanosystem for Controlled Multidrug Delivery. *Mol. Pharmaceutics* **2017**, *14*, 2697–2710, doi:10.1021/acs.molpharmaceut.7b00219.
175. He, H.; Li, Y.; Jia, X.-R.; Du, J.; Ying, X.; Lu, W.-L.; Lou, J.-N.; Wei, Y. PEGylated Poly(amidoamine) dendrimer-based dual-targeting carrier for treating brain tumors. *Biomaterials* **2011**, *32*, 478–487, doi:10.1016/j.biomaterials.2010.09.002.
176. Mehnert, W.; Mäder, K. Solid lipid nanoparticles: Production, characterization and applications. *Advanced Drug Delivery Reviews* **2012**, *64*, 83–101, doi:10.1016/j.addr.2012.09.021.
177. Wissing, S.A.; Kayser, O.; Müller, R.H. Solid lipid nanoparticles for parenteral drug delivery. *Advanced Drug Delivery Reviews* **2004**, *56*, 1257–1272, doi:10.1016/j.addr.2003.12.002.
178. Ganta, S.; Amiji, M. Coadministration of Paclitaxel and Curcumin in Nanoemulsion Formulations To Overcome Multidrug Resistance in Tumor Cells. *Mol. Pharmaceutics* **2009**, *6*, 928–939, doi:10.1021/mp800240j.
179. Zhang, J.; Wang, L.; Fai Chan, H.; Xie, W.; Chen, S.; He, C.; Wang, Y.; Chen, M. Co-delivery of paclitaxel and tetrandrine via iRGD peptide conjugated lipid-polymer hybrid nanoparticles overcome multidrug resistance in cancer cells. *Scientific Reports* **2017**, *7*, 1–14, doi:10.1038/srep46057.
180. Wu, B.; Lu, S.-T.; Zhang, L.-J.; Zhuo, R.-X.; Xu, H.-B.; Huang, S.-W. Codelivery of doxorubicin and triptolide with reduction-sensitive lipid–polymer hybrid nanoparticles for in vitro and in vivo synergistic cancer treatment. *Int J Nanomedicine* **2017**, *12*, 1853–1862, doi:10.2147/IJN.S131235.
181. Lee, S.-M.; O’Halloran, T.V.; Nguyen, S.T. Polymer-Caged Nanobins for Synergistic Cisplatin–Doxorubicin Combination Chemotherapy. *J. Am. Chem. Soc.* **2010**, *132*, 17130–17138, doi:10.1021/ja107333g.
182. Rui, M.; Xin, Y.; Li, R.; Ge, Y.; Feng, C.; Xu, X. Targeted Biomimetic Nanoparticles for Synergistic Combination Chemotherapy of Paclitaxel and Doxorubicin. *Mol. Pharmaceutics* **2017**, *14*, 107–123, doi:10.1021/acs.molpharmaceut.6b00732.
183. Zheng, M.; Yue, C.; Ma, Y.; Gong, P.; Zhao, P.; Zheng, C.; Sheng, Z.; Zhang, P.; Wang, Z.; Cai, L. Single-Step Assembly of DOX/ICG Loaded Lipid–Polymer Nanoparticles for Highly Effective Chemo-photothermal Combination Therapy. *ACS Nano* **2013**, *7*, 2056–2067, doi:10.1021/nn400334y.
184. Fan, L.; Zhang, Y.; Wang, F.; Yang, Q.; Tan, J.; Grifantini, R.; Wu, H.; Song, C.; Jin, B. Multifunctional all-in-one drug delivery systems for tumor targeting and sequential release of three different anti-tumor drugs. *Biomaterials* **2016**, *76*, 399–407, doi:10.1016/j.biomaterials.2015.10.069.
185. Gupta, B.; Ramasamy, T.; Poudel, B.K.; Pathak, S.; Regmi, S.; Choi, J.Y.; Son, Y.; Thapa, R.K.; Jeong, J.-H.; Kim, J.R.; et al. Development of Bioactive PEGylated Nanostructured Platforms for Sequential Delivery of Doxorubicin and Imatinib to Overcome Drug Resistance in Metastatic Tumors. *ACS Appl. Mater. Interfaces* **2017**, *9*, 9280–9290, doi:10.1021/acsami.6b09163.
186. B. Pacardo, D.; S. Ligler, F.; Gu, Z. Programmable nanomedicine: synergistic and sequential drug delivery systems. *Nanoscale* **2015**, *7*, 3381–3391, doi:10.1039/C4NR07677J.
187. Blanco, E.; Shen, H.; Ferrari, M. Principles of nanoparticle design for overcoming biological barriers to drug delivery. *Nature Biotechnology* **2015**, *33*, 941–951, doi:10.1038/nbt.3330.
188. Shapira, A.; Livney, Y.D.; Broxterman, H.J.; Assaraf, Y.G. Nanomedicine for targeted cancer therapy: Towards the overcoming of drug resistance. *Drug Resistance Updates* **2011**, *14*, 150–163, doi:10.1016/j.drug.2011.01.003.
189. Jabr-Milane, L.S.; van Vlerken, L.E.; Yadav, S.; Amiji, M.M. Multi-functional nanocarriers to overcome tumor drug resistance. *Cancer Treatment Reviews* **2008**, *34*, 592–602, doi:10.1016/j.ctrv.2008.04.003.
190. Hariri, G.; Edwards, A.D.; Merrill, T.B.; Greenbaum, J.M.; van der Ende, A.E.; Harth, E. Sequential Targeted Delivery of Paclitaxel and Camptothecin Using a Cross-Linked “Nanosponge” Network for Lung Cancer Chemotherapy. *Mol. Pharmaceutics* **2014**, *11*, 265–275, doi:10.1021/mp400432b.
191. Ansell, S.M.; Johnstone, S.A.; Tardi, P.G.; Lo, L.; Xie, S.; Shu, Y.; Harasym, T.O.; Harasym, N.L.; Williams, L.; Bermudes, D.; et al. Modulating the Therapeutic Activity of Nanoparticle Delivered Paclitaxel by Manipulating the Hydrophobicity of Prodrug Conjugates. *J. Med. Chem.* **2008**, *51*, 3288–3296, doi:10.1021/jm800002y.

192. Kamaly, N.; Yameen, B.; Wu, J.; Farokhzad, O.C. Degradable Controlled-Release Polymers and Polymeric Nanoparticles: Mechanisms of Controlling Drug Release. *Chem. Rev.* **2016**, *116*, 2602–2663, doi:10.1021/acs.chemrev.5b00346.
193. Zhang, R.X.; Wong, H.L.; Xue, H.Y.; Eoh, J.Y.; Wu, X.Y. Nanomedicine of synergistic drug combinations for cancer therapy – Strategies and perspectives. *Journal of Controlled Release* **2016**, *240*, 489–503, doi:10.1016/j.jconrel.2016.06.012.
194. Shin, H.-C.; Alani, A.W.G.; Cho, H.; Bae, Y.; Kolesar, J.M.; Kwon, G.S. A 3-in-1 Polymeric Micelle Nanocontainer for Poorly Water-Soluble Drugs. *Mol. Pharmaceutics* **2011**, *8*, 1257–1265, doi:10.1021/mp2000549.
195. Hasenstein, J.R.; Shin, H.-C.; Kasmerchak, K.; Buehler, D.; Kwon, G.S.; Kozak, K.R. Antitumor activity of Triolimus: a novel multidrug-loaded micelle containing Paclitaxel, Rapamycin, and 17-AAG. *Mol. Cancer Ther.* **2012**, *11*, 2233–2242, doi:10.1158/1535-7163.MCT-11-0987.
196. Morton, S.W.; Lee, M.J.; Deng, Z.J.; Dreaden, E.C.; Siouve, E.; Shopsowitz, K.E.; Shah, N.J.; Yaffe, M.B.; Hammond, P.T. A Nanoparticle-Based Combination Chemotherapy Delivery System for Enhanced Tumor Killing by Dynamic Rewiring of Signaling Pathways. *Sci Signal* **2014**, *7*, ra44, doi:10.1126/scisignal.2005261.
197. Choi, J.Y.; Thapa, R.K.; Yong, C.S.; Kim, J.O. Nanoparticle-based combination drug delivery systems for synergistic cancer treatment. *Journal of Pharmaceutical Investigation* **2016**, *46*, 325–339, doi:10.1007/s40005-016-0252-1.
198. Ma, L.; Kohli, M.; Smith, A. Nanoparticles for Combination Drug Therapy. *ACS Nano* **2013**, *7*, 9518–9525, doi:10.1021/nn405674m.
199. Gao, W.; Chan, J.M.; Farokhzad, O.C. pH-Responsive Nanoparticles for Drug Delivery. *Mol. Pharmaceutics* **2010**, *7*, 1913–1920, doi:10.1021/mp100253e.
200. de la Rica, R.; Aili, D.; Stevens, M.M. Enzyme-responsive nanoparticles for drug release and diagnostics. *Advanced Drug Delivery Reviews* **2012**, *64*, 967–978, doi:10.1016/j.addr.2012.01.002.
201. Motornov, M.; Roiter, Y.; Tokarev, I.; Minko, S. Stimuli-responsive nanoparticles, nanogels and capsules for integrated multifunctional intelligent systems. *Progress in Polymer Science* **2010**, *35*, 174–211, doi:10.1016/j.progpolymsci.2009.10.004.
202. Zhang, L.; Guo, R.; Yang, M.; Jiang, X.; Liu, B. Thermo and pH Dual-Responsive Nanoparticles for Anti-Cancer Drug Delivery. *Advanced Materials* **2007**, *19*, 2988–2992, doi:10.1002/adma.200601817.
203. Zhou, K.; Wang, Y.; Huang, X.; Luby-Phelps, K.; Sumer, B.D.; Gao, J. Tunable, Ultrasensitive pH-Responsive Nanoparticles Targeting Specific Endocytic Organelles in Living Cells. *Angewandte Chemie International Edition* **2011**, *50*, 6109–6114, doi:10.1002/anie.201100884.
204. Du, J.; Lane, L.A.; Nie, S. Stimuli-responsive nanoparticles for targeting the tumor microenvironment. *Journal of Controlled Release* **2015**, *219*, 205–214, doi:10.1016/j.jconrel.2015.08.050.
205. Shen, Y.T.; Evans, J.C.; Zafarana, G.; Allen, C.; Piquette-Miller, M. BRCA Status Does Not Predict Synergism of a Carboplatin and Olaparib Combination in High-Grade Serous Ovarian Cancer Cell Lines. *Mol. Pharmaceutics* **2018**, *15*, 2742–2753, doi:10.1021/acs.molpharmaceut.8b00246.
206. Chen, D.; Liu, X.; Yang, Y.; Yang, H.; Lu, P. Systematic synergy modeling: understanding drug synergy from a systems biology perspective. *BMC Systems Biology* **2015**, *9*, 56, doi:10.1186/s12918-015-0202-y.
207. Chen, L.; Li, B.-Q.; Zheng, M.-Y.; Zhang, J.; Feng, K.-Y.; Cai, Y.-D. Prediction of Effective Drug Combinations by Chemical Interaction, Protein Interaction and Target Enrichment of KEGG Pathways. *Biomed Res Int* **2013**, *2013*, doi:10.1155/2013/723780.
208. Zhao, X.-M.; Iskar, M.; Zeller, G.; Kuhn, M.; van Noort, V.; Bork, P. Prediction of Drug Combinations by Integrating Molecular and Pharmacological Data. *PLoS Comput Biol* **2011**, *7*, doi:10.1371/journal.pcbi.1002323.
209. Wu, Z.; Zhao, X.-M.; Chen, L. A systems biology approach to identify effective cocktail drugs. *BMC Syst Biol* **2010**, *4*, S7, doi:10.1186/1752-0509-4-S2-S7.
210. Jin, G.; Zhao, H.; Zhou, X.; Wong, S.T.C. An enhanced Petri-net model to predict synergistic effects of pairwise drug combinations from gene microarray data. *Bioinformatics* **2011**, *27*, i310–i316, doi:10.1093/bioinformatics/btr202.

211. Pandey, A.; Kulkarni, A.; Roy, B.; Goldman, A.; Sarangi, S.; Sengupta, P.; Phipps, C.; Koppam, J.; Oh, M.; Basu, S.; et al. Sequential Application of a Cytotoxic Nanoparticle and a PI3K Inhibitor Enhances Antitumor Efficacy. *Cancer Res* **2014**, *74*, 675–685, doi:10.1158/0008-5472.CAN-12-3783.
212. Jain, H.V.; Meyer-Hermann, M. The Molecular Basis of Synergism between Carboplatin and ABT-737 Therapy Targeting Ovarian Carcinomas. *Cancer Res* **2011**, *71*, 705–715, doi:10.1158/0008-5472.CAN-10-3174.
213. Turner, N.C.; Reis-Filho, J.S. Genetic heterogeneity and cancer drug resistance. *Lancet Oncol.* **2012**, *13*, e178-185, doi:10.1016/S1470-2045(11)70335-7.
214. Wilting, R.H.; Dannenberg, J.-H. Epigenetic mechanisms in tumorigenesis, tumor cell heterogeneity and drug resistance. *Drug Resistance Updates* **2012**, *15*, 21–38, doi:10.1016/j.drug.2012.01.008.
215. Taniguchi, K.; Okami, J.; Kodama, K.; Higashiyama, M.; Kato, K. Intratumor heterogeneity of epidermal growth factor receptor mutations in lung cancer and its correlation to the response to gefitinib. *Cancer Sci.* **2008**, *99*, 929–935, doi:10.1111/j.1349-7006.2008.00782.x.
216. Sun, X.; Bao, J.; Shao, Y. Mathematical Modeling of Therapy-induced Cancer Drug Resistance: Connecting Cancer Mechanisms to Population Survival Rates. *Scientific Reports* **2016**, *6*, 22498, doi:10.1038/srep22498.
217. De Marzo, A.M.; DeWeese, T.L.; Platz, E.A.; Meeker, A.K.; Nakayama, M.; Epstein, J.I.; Isaacs, W.B.; Nelson, W.G. Pathological and molecular mechanisms of prostate carcinogenesis: implications for diagnosis, detection, prevention, and treatment. *J. Cell. Biochem.* **2004**, *91*, 459–477, doi:10.1002/jcb.10747.
218. Landis, S.H.; Murray, T.; Bolden, S.; Wingo, P.A. Cancer statistics, 1999. *CA Cancer J Clin* **1999**, *49*, 8–31, 1.
219. Grönberg, H. Prostate cancer epidemiology. *Lancet* **2003**, *361*, 859–864, doi:10.1016/S0140-6736(03)12713-4.
220. What are the key statistics about prostate cancer? Available online: <http://www.cancer.org/cancer/prostatecancer/detailedguide/prostate-cancer-key-statistics> (accessed on Nov 9, 2016).
221. Ovarian Cancer | Who is at Risk? | Symptoms & Treatment Available online: <https://www.plannedparenthood.org/learn/womens-health/ovarian-cancer> (accessed on Nov 9, 2016).
222. U.S. Breast Cancer Statistics Available online: [http://www.breastcancer.org/symptoms/understand\\_bc/statistics](http://www.breastcancer.org/symptoms/understand_bc/statistics) (accessed on Nov 9, 2016).
223. Ramaswamy, S.; Ross, K.N.; Lander, E.S.; Golub, T.R. A molecular signature of metastasis in primary solid tumors. *Nat Genet* **2003**, *33*, 49–54, doi:10.1038/ng1060.
224. Chi, K.N.; Higano, C.S.; Blumenstein, B.A.; Reeves, J.A.; Feyereabend, S.; Gravis, G.; Ferrero, J.-M.; Jacobs, C.; De Bono, J.S. Phase III SYNERGY trial: Docetaxel +/- custirsen and overall survival in patients (pts) with metastatic castration-resistant prostate cancer (mCRPC) and poor prognosis. *JCO* **2015**, *33*, 5009–5009, doi:10.1200/jco.2015.33.15\_suppl.5009.
225. Ryan, C.J.; Small, E.J. Advances in prostate cancer. *Curr Opin Oncol* **2004**, *16*, 242–246.
226. Dai, C.; Tiwari, A.K.; Wu, C.-P.; Su, X.-D.; Wang, S.-R.; Liu, D.; Ashby, C.R.; Huang, Y.; Robey, R.W.; Liang, Y.; et al. Lapatinib (Tykerb, GW572016) reverses multidrug resistance in cancer cells by inhibiting the activity of ATP-binding cassette subfamily B member 1 and G member 2. *Cancer Res.* **2008**, *68*, 7905–7914, doi:10.1158/0008-5472.CAN-08-0499.
227. Sánchez, C.; Mendoza, P.; Contreras, H.R.; Vergara, J.; McCubrey, J.A.; Huidobro, C.; Castellón, E.A. Expression of multidrug resistance proteins in prostate cancer is related with cell sensitivity to chemotherapeutic drugs. *Prostate* **2009**, *69*, 1448–1459, doi:10.1002/pros.20991.
228. Li, F.; Danquah, M.; Singh, S.; Wu, H.; Mahato, R.I. Paclitaxel- and lapatinib-loaded lipopolymer micelles overcome multidrug resistance in prostate cancer. *Drug Deliv Transl Res* **2011**, *1*, 420–428, doi:10.1007/s13346-011-0042-2.
229. Grant, S.; Qiao, L.; Dent, P. Roles of ERBB family receptor tyrosine kinases, and downstream signaling pathways, in the control of cell growth and survival. *Front. Biosci.* **2002**, *7*, d376-389.

230. Normanno, N.; De Luca, A.; Bianco, C.; Strizzi, L.; Mancino, M.; Maiello, M.R.; Carotenuto, A.; De Feo, G.; Caponigro, F.; Salomon, D.S. Epidermal growth factor receptor (EGFR) signaling in cancer. *Gene* **2006**, *366*, 2–16, doi:10.1016/j.gene.2005.10.018.
231. Gao, H.; Cao, S.; Chen, C.; Cao, S.; Yang, Z.; Pang, Z.; Xi, Z.; Pan, S.; Zhang, Q.; Jiang, X. Incorporation of lapatinib into lipoprotein-like nanoparticles with enhanced water solubility and anti-tumor effect in breast cancer. *Nanomedicine (Lond)* **2013**, *8*, 1429–1442, doi:10.2217/nnm.12.180.
232. Peer, D.; Karp, J.M.; Hong, S.; Farokhzad, O.C.; Margalit, R.; Langer, R. Nanocarriers as an emerging platform for cancer therapy. *Nat Nano* **2007**, *2*, 751–760, doi:10.1038/nano.2007.387.
233. Yeh, T.K.; Lu, Z.; Wientjes, M.G.; Au, J.L.-S. Formulating Paclitaxel in Nanoparticles Alters Its Disposition. *Pharm Res* **2005**, *22*, 867–874, doi:10.1007/s11095-005-4581-4.
234. Li, F.; Danquah, M.; Singh, S.; Wu, H.; Mahato, R.I. Paclitaxel- and lapatinib-loaded lipopolymer micelles overcome multidrug resistance in prostate cancer. *Drug Deliv Transl Res* **2011**, *1*, 420–428, doi:10.1007/s13346-011-0042-2.
235. Wei, Y.; Xu, S.; Wang, F.; Zou, A.; Zhang, S.; Xiong, Y.; Cao, S.; Zhang, Q.; Wang, Y.; Jiang, X. A Novel Combined Micellar System of Lapatinib and Paclitaxel with Enhanced Antineoplastic Effect Against Human Epidermal Growth Factor Receptor-2 Positive Breast Tumor In Vitro. *JPharmSci* **2015**, *104*, 165–177, doi:10.1002/jps.24234.
236. Ravar, F.; Saadat, E.; Kelishadi, P.D.; Dorkoosh, F.A. Liposomal formulation for co-delivery of paclitaxel and lapatinib, preparation, characterization and optimization. *Journal of Liposome Research* **2016**, *26*, 175–187, doi:10.3109/08982104.2015.1070174.
237. Dehghankelishadi, P.; Saadat, E.; Ravar, F.; Safavi, M.; Pordeli, M.; Gholami, M.; Dorkoosh, F.A. In vitro and in vivo evaluation of paclitaxel–lapatinib-loaded F127 pluronic micelles. *Drug Development and Industrial Pharmacy* **2017**, *43*, 390–398, doi:10.1080/03639045.2016.1254238.
238. Cheng, H.; An, S.-J.; Zhang, X.-C.; Dong, S.; Zhang, Y.-F.; Chen, Z.-H.; Chen, H.-J.; Guo, A.-L.; Lin, Q.-X.; Wu, Y.-L. In vitro sequence-dependent synergism between paclitaxel and gefitinib in human lung cancer cell lines. *Cancer Chemother. Pharmacol.* **2011**, *67*, 637–646, doi:10.1007/s00280-010-1347-4.
239. He, X.; Zhang, T. Alteration in the Balance of Prosurvival and Proapoptotic Signalling Pathways Leads to Sequence-Dependent Synergism Between Docetaxel and Sorafenib in Human Non-small Cell Lung Cancer Cell Lines. *Cell Biochem Biophys* **2014**, *68*, 411–418, doi:10.1007/s12013-013-9722-5.
240. Di Leo, A.; Gomez, H.L.; Aziz, Z.; Zvirbule, Z.; Bines, J.; Arbushites, M.C.; Guerrero, S.F.; Koehler, M.; Oliva, C.; Stein, S.H.; et al. Phase III, double-blind, randomized study comparing lapatinib plus paclitaxel with placebo plus paclitaxel as first-line treatment for metastatic breast cancer. *J. Clin. Oncol.* **2008**, *26*, 5544–5552, doi:10.1200/JCO.2008.16.2578.
241. Li, X.; Lewis, M.T.; Huang, J.; Gutierrez, C.; Osborne, C.K.; Wu, M.-F.; Hilsenbeck, S.G.; Pavlick, A.; Zhang, X.; Chamness, G.C.; et al. Intrinsic resistance of tumorigenic breast cancer cells to chemotherapy. *J. Natl. Cancer Inst.* **2008**, *100*, 672–679, doi:10.1093/jnci/djn123.
242. Medina, P.J.; Goodin, S. Lapatinib: a dual inhibitor of human epidermal growth factor receptor tyrosine kinases. *Clin Ther* **2008**, *30*, 1426–1447, doi:10.1016/j.clinthera.2008.08.008.
243. Johnston, S.R.D. Clinical trials of intracellular signal transductions inhibitors for breast cancer--a strategy to overcome endocrine resistance. *Endocr. Relat. Cancer* **2005**, *12 Suppl 1*, S145-157, doi:10.1677/erc.1.00992.
244. Chu, I.; Blackwell, K.; Chen, S.; Slingerland, J. The dual ErbB1/ErbB2 inhibitor, lapatinib (GW572016), cooperates with tamoxifen to inhibit both cell proliferation- and estrogen-dependent gene expression in antiestrogen-resistant breast cancer. *Cancer Res.* **2005**, *65*, 18–25.
245. Geyer, C.E.; Forster, J.; Lindquist, D.; Chan, S.; Romieu, C.G.; Pienkowski, T.; Jagiello-Gruszfeld, A.; Crown, J.; Chan, A.; Kaufman, B.; et al. Lapatinib plus capecitabine for HER2-positive advanced breast cancer. *N. Engl. J. Med.* **2006**, *355*, 2733–2743, doi:10.1056/NEJMoa064320.
246. Chien, A.J.; Illi, J.A.; Ko, A.H.; Korn, W.M.; Fong, L.; Chen, L.; Kashani-Sabet, M.; Ryan, C.J.; Rosenberg, J.E.; Dubey, S.; et al. A phase I study of a 2-day lapatinib chemosensitization pulse preceding nanoparticle albumin-bound Paclitaxel for advanced solid malignancies. *Clin. Cancer Res.* **2009**, *15*, 5569–5575, doi:10.1158/1078-0432.CCR-09-0522.

247. Satoh, T.; Xu, R.-H.; Chung, H.C.; Sun, G.-P.; Doi, T.; Xu, J.-M.; Tsuji, A.; Omuro, Y.; Li, J.; Wang, J.-W.; et al. Lapatinib plus paclitaxel versus paclitaxel alone in the second-line treatment of HER2-amplified advanced gastric cancer in Asian populations: TyTAN--a randomized, phase III study. *J. Clin. Oncol.* **2014**, *32*, 2039–2049, doi:10.1200/JCO.2013.53.6136.
248. Varma, M.V.S.; Panchagnula, R. Enhanced oral paclitaxel absorption with vitamin E-TPGS: Effect on solubility and permeability in vitro, in situ and in vivo. *European Journal of Pharmaceutical Sciences* **2005**, *25*, 445–453, doi:10.1016/j.ejps.2005.04.003.
249. Frankel, C.; Palmieri, F.M. Lapatinib Side-Effect Management. *Clinical Journal of Oncology Nursing* **2010**, *14*, 223–233, doi:10.1188/10.CJON.223-233.
250. Weiss, R.B.; Donehower, R.C.; Wiernik, P.H.; Ohnuma, T.; Gralla, R.J.; Trump, D.L.; Baker, J.R.; Van Echo, D.A.; Von Hoff, D.D.; Leyland-Jones, B. Hypersensitivity reactions from taxol. *J. Clin. Oncol.* **1990**, *8*, 1263–1268.
251. Schiller, J.H.; Harrington, D.; Belani, C.P.; Langer, C.; Sandler, A.; Krook, J.; Zhu, J.; Johnson, D.H. Comparison of Four Chemotherapy Regimens for Advanced Non-Small-Cell Lung Cancer. *New England Journal of Medicine* **2002**, *346*, 92–98, doi:10.1056/NEJMoa011954.
252. Szakács, G.; Paterson, J.K.; Ludwig, J.A.; Booth-Genthe, C.; Gottesman, M.M. Targeting multidrug resistance in cancer. *Nature Reviews Drug Discovery* **2006**, *5*, 219–234, doi:10.1038/nrd1984.
253. Thomas, H.; Coley, H.M. Overcoming Multidrug Resistance in Cancer: An Update on the Clinical Strategy of Inhibiting P-Glycoprotein  
Overcoming Multidrug Resistance in Cancer: An Update on the Clinical Strategy of Inhibiting P-Glycoprotein. *Cancer Control* **2003**, *10*, 159–165, doi:10.1177/107327480301000207.
254. Cheng, H.; An, S.-J.; Zhang, X.-C.; Dong, S.; Zhang, Y.-F.; Chen, Z.-H.; Chen, H.-J.; Guo, A.-L.; Lin, Q.; Wu, Y.-L. In vitro sequence-dependent synergism between paclitaxel and gefitinib in human lung cancer cell lines. *Cancer Chemother Pharmacol* **2011**, *67*, 637–646, doi:10.1007/s00280-010-1347-4.
255. Morelli, M.P.; Cascone, T.; Troiani, T.; De Vita, F.; Orditura, M.; Laus, G.; Eckhardt, S.G.; Pepe, S.; Tortora, G.; Ciardiello, F. Sequence-dependent antiproliferative effects of cytotoxic drugs and epidermal growth factor receptor inhibitors. *Ann Oncol* **2005**, *16*, iv61–iv68, doi:10.1093/annonc/mdi910.
256. Hirai, H.; Sootome, H.; Nakatsuru, Y.; Miyama, K.; Taguchi, S.; Tsujioka, K.; Ueno, Y.; Hatch, H.; Majumder, P.K.; Pan, B.-S.; et al. MK-2206, an Allosteric Akt Inhibitor, Enhances Antitumor Efficacy by Standard Chemotherapeutic Agents or Molecular Targeted Drugs In vitro and In vivo. *Mol Cancer Ther* **2010**, 1535-7163.MCT-09–1012, doi:10.1158/1535-7163.MCT-09-1012.
257. He, X.; Zhang, T. Alteration in the Balance of Prosurvival and Proapoptotic Signalling Pathways Leads to Sequence-Dependent Synergism Between Docetaxel and Sorafenib in Human Non-small Cell Lung Cancer Cell Lines. *Cell Biochem Biophys* **2014**, *68*, 411–418, doi:10.1007/s12013-013-9722-5.
258. Ganta, S.; Amiji, M. Coadministration of Paclitaxel and curcumin in nanoemulsion formulations to overcome multidrug resistance in tumor cells. *Mol. Pharm.* **2009**, *6*, 928–939, doi:10.1021/mp800240j.
259. Tang, C.; Prud'homme, R.K. Targeted Theragnostic Nanoparticles Via Flash Nanoprecipitation: Principles of Material Selection. In *Polymer Nanoparticles for Nanomedicines*; Springer, Cham, 2016; pp. 55–85 ISBN 978-3-319-41419-5.
260. Tang, C.; Amin, D.; Messersmith, P.B.; Anthony, J.E.; Prud'homme, R.K. Polymer Directed Self-Assembly of pH-Responsive Antioxidant Nanoparticles. *Langmuir* **2015**, *31*, 3612–3620, doi:10.1021/acs.langmuir.5b00213.
261. Bazak, R.; Hourri, M.; El Achy, S.; Hussein, W.; Refaat, T. Passive targeting of nanoparticles to cancer: A comprehensive review of the literature. *Molecular and Clinical Oncology* **2014**, *2*, 904–908, doi:10.3892/mco.2014.356.
262. Ansell, S.M.; Johnstone, S.A.; Tardi, P.G.; Lo, L.; Xie, S.; Shu, Y.; Harasym, T.O.; Harasym, N.L.; Williams, L.; Bermudes, D.; et al. Modulating the Therapeutic Activity of Nanoparticle Delivered Paclitaxel by Manipulating the Hydrophobicity of Prodrug Conjugates. *J. Med. Chem.* **2008**, *51*, 3288–3296, doi:10.1021/jm800002y.
263. Levit, S.L.; Walker, R.C.; Tang, C. Rapid, Single-Step Protein Encapsulation via Flash NanoPrecipitation. *Polymers* **2019**, *11*, 1406, doi:10.3390/polym11091406.

264. Zhang, C.; J. Pansare, V.; K. Prud'homme, R.; D. Priestley, R. Flash nanoprecipitation of polystyrene nanoparticles. *Soft Matter* **2012**, *8*, 86–93, doi:10.1039/C1SM06182H.
265. Pustulka, K.M.; Wohl, A.R.; Lee, H.S.; Michel, A.R.; Han, J.; Hoyer, T.R.; McCormick, A.V.; Panyam, J.; Macosko, C.W. Flash nanoprecipitation: particle structure and stability. *Mol. Pharm.* **2013**, *10*, 4367–4377, doi:10.1021/mp400337f.
266. Calo-Fernández, B.; Martínez-Hurtado, J.L. Biosimilars: Company Strategies to Capture Value from the Biologics Market. *Pharmaceuticals* **2012**, *5*, 1393–1408, doi:10.3390/ph5121393.
267. Sato, A.K.; Viswanathan, M.; Kent, R.B.; Wood, C.R. Therapeutic peptides: technological advances driving peptides into development. *Current Opinion in Biotechnology* **2006**, *17*, 638–642, doi:10.1016/j.copbio.2006.10.002.
268. Desai, N. Challenges in Development of Nanoparticle-Based Therapeutics. *AAPS J* **2012**, *14*, 282–295, doi:10.1208/s12248-012-9339-4.
269. M. Pinkerton, N.; Behar, L.; Hadri, K.; Amouroux, B.; Mingotaud, C.; R. Talham, D.; Chassaing, S.; Marty, J.-D. Ionic Flash NanoPrecipitation (iFNP) for the facile, one-step synthesis of inorganic–organic hybrid nanoparticles in water. *Nanoscale* **2017**, *9*, 1403–1408, doi:10.1039/C6NR09364G.
270. M. Pinkerton, N.; Hadri, K.; Amouroux, B.; Behar, L.; Mingotaud, C.; Destarac, M.; Kulai, I.; Mazières, S.; Chassaing, S.; Marty, J.-D. Quench ionic flash nano precipitation as a simple and tunable approach to decouple growth and functionalization for the one-step synthesis of functional LnPO 4 -based nanoparticles in water. *Chemical Communications* **2018**, *54*, 9438–9441, doi:10.1039/C8CC04163F.
271. Pinkerton, N.M.; Grandeur, A.; Fisch, A.; Brozio, J.; Riebesehl, B.U.; Prud'homme, R.K. Formation of Stable Nanocarriers by in Situ Ion Pairing during Block-Copolymer-Directed Rapid Precipitation. *Mol. Pharmaceutics* **2013**, *10*, 319–328, doi:10.1021/mp300452g.
272. Tang, C.; Amin, D.; Messersmith, P.B.; Anthony, J.E.; Prud'homme, R.K. Polymer Directed Self-Assembly of pH-Responsive Antioxidant Nanoparticles. *Langmuir* **2015**, *31*, 3612–3620, doi:10.1021/acs.langmuir.5b00213.
273. Pagels, R.F.; Prud'homme, R.K. Polymeric nanoparticles and microparticles for the delivery of peptides, biologics, and soluble therapeutics. *Journal of Controlled Release* **2015**, *219*, 519–535, doi:10.1016/j.jconrel.2015.09.001.
274. Markwalter, C.E.; Prud'homme, R.K. Design of a Small-Scale Multi-Inlet Vortex Mixer for Scalable Nanoparticle Production and Application to the Encapsulation of Biologics by Inverse Flash NanoPrecipitation. *JPharmSci* **2018**, *107*, 2465–2471, doi:10.1016/j.xphs.2018.05.003.
275. Santos, J.L.; Ren, Y.; Vandermark, J.; Archang, M.M.; Williford, J.-M.; Liu, H.-W.; Lee, J.; Wang, T.-H.; Mao, H.-Q. Continuous Production of Discrete Plasmid DNA-Polycation Nanoparticles Using Flash Nanocomplexation. *Small* **2016**, *12*, 6214–6222, doi:10.1002/smll.201601425.
276. Van Buren, J.P.; Robinson, W.B. Formation of Complexes between Protein and Tannic Acid. *J. Agric. Food Chem* **1969**, *17*, 772–777.
277. Hagerman, A.E.; Butler, L.G. Determination of Protein in Tannin-Protein Precipitates. *J. Agric. Food Chem* **1980**, *28*, 944–947.
278. Martin, M.M.; Rockholm, D.C.; Martin, J.S. Effects of surfactants, pH, and certain cations on precipitation of proteins by tannins. *J Chem Ecol* **1985**, *11*, 485–494, doi:10.1007/BF00989559.
279. Levit, S.L.; Stwodah, R.M.; Tang, C. Rapid, Room Temperature Nanoparticle Drying and Low-Energy Reconstitution via Electrospinning. *Journal of Pharmaceutical Sciences* **2018**, *107*, 807–813, doi:10.1016/j.xphs.2017.10.026.
280. Nanocomposix's Guide to Dynamic Light Scattering Measurement and Analysis 2015.
281. Johnson, B.K.; Prud homme, R.K. Flash NanoPrecipitation of Organic Actives and Block Copolymers using a Confined Impinging Jets Mixer. *AUSTRALIAN JOURNAL OF CHEMISTRY* **2003**, *56*, 1021–1024.
282. Meechai, N.; Jamieson, A.M.; Blackwell, J. Translational Diffusion Coefficients of Bovine Serum Albumin in Aqueous Solution at High Ionic Strength. *Journal of Colloid and Interface Science* **1999**, *218*, 167–175, doi:10.1006/jcis.1999.6401.

283. Johnson, B.K.; Prud'homme, R.K. Mechanism for Rapid Self-Assembly of Block Copolymer Nanoparticles. *Phys. Rev. Lett.* **2003**, *91*, 118302, doi:10.1103/PhysRevLett.91.118302.
284. Tang, C.; L. Sosa, C.; F. Pagels, R.; D. Priestley, R.; K. Prud'homme, R. Efficient preparation of size tunable PEGylated gold nanoparticles. *Journal of Materials Chemistry B* **2016**, *4*, 4813–4817, doi:10.1039/C6TB00886K.
285. Saad, W.S.; Prud'homme, R.K. Principles of nanoparticle formation by flash nanoprecipitation. *Nano Today* **2016**, *11*, 212–227, doi:10.1016/j.nantod.2016.04.006.
286. Zhu, Z. Effects of amphiphilic diblock copolymer on drug nanoparticle formation and stability. *Biomaterials* **2013**, *34*, 10238–10248, doi:10.1016/j.biomaterials.2013.09.015.
287. Kumar, V.; Wang, L.; Riebe, M.; Tung, H.-H.; Prud'homme, R.K. Formulation and stability of itraconazole and odanacatib nanoparticles: governing physical parameters. *Mol. Pharm.* **2009**, *6*, 1118–1124, doi:10.1021/mp900002t.
288. Dietrich, A.; Neubrand, A. Effects of Particle Size and Molecular Weight of Polyethylenimine on Properties of Nanoparticulate Silicon Dispersions. *Journal of the American Ceramic Society* **2001**, *84*, 806–812, doi:10.1111/j.1151-2916.2001.tb00745.x.
289. Lindquist, G.M.; Stratton, R.A. The role of polyelectrolyte charge density and molecular weight on the adsorption and flocculation of colloidal silica with polyethylenimine. *Journal of Colloid and Interface Science* **1976**, *55*, 45–59, doi:10.1016/0021-9797(76)90007-2.
290. Shi, Q.; Zhou, Y.; Sun, Y. Influence of pH and ionic strength on the steric mass-action model parameters around the isoelectric point of protein. *Biotechnol. Prog.* **2005**, *21*, 516–523, doi:10.1021/bp049735o.
291. Curtis, K.A.; Miller, D.; Millard, P.; Basu, S.; Horkay, F.; Chandran, P.L. Unusual Salt and pH Induced Changes in Polyethylenimine Solutions. *PLoS One* **2016**, *11*, doi:10.1371/journal.pone.0158147.
292. M. Pinkerton, N.; Behar, L.; Hadri, K.; Amouroux, B.; Mingotaud, C.; R. Talham, D.; Chassaing, S.; Marty, J.-D. Ionic Flash NanoPrecipitation (iFNP) for the facile, one-step synthesis of inorganic–organic hybrid nanoparticles in water. *Nanoscale* **2017**, *9*, 1403–1408, doi:10.1039/C6NR09364G.
293. Jo, A.; Zhang, R.; Allen, I.C.; Riffle, J.S.; Davis, R.M. Design and Fabrication of Streptavidin-Functionalized, Fluorescently Labeled Polymeric Nanocarriers. *Langmuir* **2018**, *34*, 15783–15794, doi:10.1021/acs.langmuir.8b02423.
294. Pagels, R.F.; Edelstein, J.; Tang, C.; Prud'homme, R.K. Controlling and Predicting Nanoparticle Formation by Block Copolymer Directed Rapid Precipitations. *Nano Lett.* **2018**, *18*, 1139–1144, doi:10.1021/acs.nanolett.7b04674.
295. Zhu, Z. It; Margulis-Goshen, K.; Magdassi, S.; Talmon, Y.; Macosko, C.W. Polyelectrolyte stabilized drug nanoparticles via flash nanoprecipitation: a model study with beta-carotene. *Journal of pharmaceutical sciences* **2010**, *99*, 4295–4306, doi:10.1002/jps.22090.
296. Kosacheva, E.M.; Kudryavtsev, D.B.; Bakeeva, R.F.; Kuklin, A.I.; Islamov, A.K.; Kudryavtseva, L.A.; Sopin, V.F.; Konovalov, A.I. The aggregation of branched polyethylenimine and cationic surfactants in aqueous systems. *Colloid J* **2006**, *68*, 713–720, doi:10.1134/S1061933X0606007X.
297. Zhang, M.; Xue, Y.-N.; Liu, M.; Zhuo, R.-X.; Huang, S.-W. Biocleavable Polycationic Micelles as Highly Efficient Gene Delivery Vectors. *Nanoscale Res Lett* **2010**, *5*, 1804, doi:10.1007/s11671-010-9716-9.
298. Dai, Z.; Wu, C. How Does DNA Complex with Polyethylenimine with Different Chain Lengths and Topologies in Their Aqueous Solution Mixtures? *Macromolecules* **2012**, *45*, 4346–4353, doi:10.1021/ma2027963.
299. Blocher, W.C.; Perry, S.L. Complex coacervate-based materials for biomedicine. *Wiley Interdiscip Rev Nanomed Nanobiotechnol* **2017**, *9*, doi:10.1002/wnan.1442.
300. Salt-Induced Charge Screening and Significant Conductivity Enhancement of Conducting Poly(3,4-ethylenedioxythiophene):Poly(styrenesulfonate) - *Macromolecules* (ACS Publications) Available online: <https://pubs.acs.org/doi/10.1021/ma900327d> (accessed on Feb 14, 2019).

301. Donato, L.; Garnier, C.; Doublier, J.-L.; Nicolai, T. Influence of the NaCl or CaCl<sub>2</sub> Concentration on the Structure of Heat-Set Bovine Serum Albumin Gels at pH 7. *Biomacromolecules* **2005**, *6*, 2157–2163, doi:10.1021/bm050132q.
302. Meng, F.; Zhong, Y.; Cheng, R.; Deng, C.; Zhong, Z. pH-sensitive polymeric nanoparticles for tumor-targeting doxorubicin delivery: concept and recent advances. *Nanomedicine* **2014**, *9*, 487–499, doi:10.2217/nmm.13.212.
303. Lynn, D.M.; Amiji, M.M.; Langer, R. pH-Responsive Polymer Microspheres: Rapid Release of Encapsulated Material within the Range of Intracellular pH. *Angewandte Chemie International Edition* **2001**, *40*, 1707–1710, doi:10.1002/1521-3773(20010504)40:9<1707::AID-ANIE17070>3.0.CO;2-F.
304. Du, J.-Z.; Du, X.-J.; Mao, C.-Q.; Wang, J. Tailor-Made Dual pH-Sensitive Polymer–Doxorubicin Nanoparticles for Efficient Anticancer Drug Delivery. *J. Am. Chem. Soc.* **2011**, *133*, 17560–17563, doi:10.1021/ja207150n.
305. Kumar, V.; Prud'homme, R.K. Thermodynamic limits on drug loading in nanoparticle cores. *Journal of Pharmaceutical Sciences* **2008**, *97*, 4904–4914, doi:10.1002/jps.21342.
306. Barichello, J.M.; Morishita, M.; Takayama, K.; Nagai, T. Encapsulation of Hydrophilic and Lipophilic Drugs in PLGA Nanoparticles by the Nanoprecipitation Method. *Drug Development and Industrial Pharmacy* **1999**, *25*, 471–476, doi:10.1081/DDC-100102197.
307. Levit, S.L.; Yang, H.; Tang, C. Rapid Self-Assembly of Polymer Nanoparticles for Synergistic Codelivery of Paclitaxel and Lapatinib via Flash NanoPrecipitation. *Nanomaterials* **2020**, *10*, 561, doi:10.3390/nano10030561.
308. Kondo, N.; Tsukuda, M.; Ishiguro, Y.; Kimura, M.; Fujita, K.; Sakakibara, A.; Takahashi, H.; Toth, G.; Matsuda, H. Antitumor effects of lapatinib (GW572016), a dual inhibitor of EGFR and HER-2, in combination with cisplatin or paclitaxel on head and neck squamous cell carcinoma. *Oncology Reports* **2010**, *23*, 957–963, doi:10.3892/or\_00000720.
309. Guo, X.; Li, S.; Zhu, X.; Dou, Q.; Liu, D. Lapatinib in combination with paclitaxel plays synergistic antitumor effects on esophageal squamous cancer. *Cancer Chemother Pharmacol* **2018**, *82*, 383–394, doi:10.1007/s00280-018-3627-3.
310. Kelishady, P.D.; Saadat, E.; Ravar, F.; Akbari, H.; Dorkoosh, F. Pluronic F127 polymeric micelles for co-delivery of paclitaxel and lapatinib against metastatic breast cancer: preparation, optimization and in vitro evaluation. *Pharmaceutical Development and Technology* **2015**, *20*, 1009–1017, doi:10.3109/10837450.2014.965323.
311. Duong, A.D.; Ruan, G.; Mahajan, K.; Winter, J.O.; Wyslouzil, B.E. Scalable, semicontinuous production of micelles encapsulating nanoparticles via electrospray. *Langmuir : the ACS journal of surfaces and colloids* **2014**, *30*, 3939–3948, doi:10.1021/la404679r.
312. Han, J.; Zhu, Z.; Qian, H.; Wohl, A.R.; Beaman, C.J.; Hoyer, T.R.; Macosko, C.W. A simple confined impingement jets mixer for flash nanoprecipitation. *Journal of Pharmaceutical Sciences* **2012**, *101*, 4018–4023, doi:10.1002/jps.23259.
313. Understanding the colloidal stability of protein therapeutics using dynamic light scattering.
314. Han, J.; Michel, A.R.; Lee, H.; Kalscheuer, S.; Wohl, A.; Hoyer, T.R.; McCormick, A.V.; Panyam, J.; Macosko, C. Nanoparticles Containing High Loads of Paclitaxel-Silicate Prodrugs: Formulation, Drug Release, and Anticancer Efficacy. *Current heart failure reports* **2015**, *12*, 4329–4335, doi:10.1021/acs.molpharmaceut.5b00530.
315. Tang, C.; Levit, S.; Zeevi, M.; Vasey, C.; Fromen, C. Chapter 12: Polymer Colloids Enable Medical Applications. In *Polymer Colloids*; 2019; pp. 358–398.
316. Zajdel, A.; Wilczok, A.; Jelonek, K.; Musiał-Kulik, M.; Forys, A.; Li, S.; Kasperczyk, J. Cytotoxic Effect of Paclitaxel and Lapatinib Co-Delivered in Poly(lactide-co-Poly(ethylene glycol) Micelles on HER-2-Negative Breast Cancer Cells. *Pharmaceutics* **2019**, *11*, doi:10.3390/pharmaceutics11040169.
317. Jia, L.; Shen, J.; Li, Z.; Zhang, D.; Zhang, Q.; Liu, G.; Zheng, D.; Tian, X. In vitro and in vivo evaluation of paclitaxel-loaded mesoporous silica nanoparticles with three pore sizes. *International Journal of Pharmaceutics* **2013**, *445*, 12–19, doi:10.1016/j.ijpharm.2013.01.058.



318. Chavanpatil, M.D.; Patil, Y.; Panyam, J. Susceptibility of nanoparticle-encapsulated paclitaxel to P-glycoprotein-mediated drug efflux. *International Journal of Pharmaceutics* **2006**, *320*, 150–156, doi:10.1016/j.ijpharm.2006.03.045.
319. Modi, S.; Anderson, B.D. Determination of Drug Release Kinetics from Nanoparticles: Overcoming Pitfalls of the Dynamic Dialysis Method. *Mol. Pharmaceutics* **2013**, *10*, 3076–3089, doi:10.1021/mp400154a.
320. D'Souza, S.S.; DeLuca, P.P. Methods to Assess in Vitro Drug Release from Injectable Polymeric Particulate Systems. *Pharm Res* **2006**, *23*, 460–474, doi:10.1007/s11095-005-9397-8.
321. Dash, S.; Murthy, P.N.; Nath, L.; Chowdhury, P. Kinetic modeling on drug release from controlled drug delivery systems. *Acta Pol Pharm* **2010**, *67*, 217–223.
322. Korsmeyer, R.W.; Gurny, R.; Doelker, E.; Buri, P.; Peppas, N.A. Mechanisms of solute release from porous hydrophilic polymers. *International Journal of Pharmaceutics* **1983**, *15*, 25–35, doi:10.1016/0378-5173(83)90064-9.
323. *Simple Brownian Diffusion: An Introduction to the Standard Theoretical Models*; Oxford University Press: Oxford, New York, 2012; ISBN 978-0-19-966450-4.
324. Wu, I.Y.; Bala, S.; Škalko-Basnet, N.; di Cagno, M.P. Interpreting non-linear drug diffusion data: Utilizing Korsmeyer-Peppas model to study drug release from liposomes. *European Journal of Pharmaceutical Sciences* **2019**, *138*, 105026, doi:10.1016/j.ejps.2019.105026.
325. Liu, P.; De Wulf, O.; Laru, J.; Heikkilä, T.; van Veen, B.; Kiesvaara, J.; Hirvonen, J.; Peltonen, L.; Laaksonen, T. Dissolution Studies of Poorly Soluble Drug Nanosuspensions in Non-sink Conditions. *AAPS PharmSciTech* **2013**, *14*, 748–756, doi:10.1208/s12249-013-9960-2.
326. Mobasserri, R.; Karimi, M.; Tian, L.; Naderi-Manesh, H.; Ramakrishna, S. Hydrophobic lapatinib encapsulated dextran-chitosan nanoparticles using a toxic solvent free method: fabrication, release property & in vitro anti-cancer activity. *Materials Science and Engineering: C* **2017**, *74*, 413–421, doi:10.1016/j.msec.2016.12.027.
327. Bullock, J. Dissolution of Nanoparticle Drug Formulations Available online: <https://www.taylorfrancis.com/> (accessed on Mar 5, 2020).
328. D'Addio, S.M.; Bukari, A.A.; Dawoud, M.; Bunjes, H.; Rinaldi, C.; Prud'homme, R.K. Determining drug release rates of hydrophobic compounds from nanocarriers. *Philos Trans A Math Phys Eng Sci* **2016**, *374*, doi:10.1098/rsta.2015.0128.
329. Gülçin, İ.; Huyut, Z.; Elmastaş, M.; Aboul-Enein, H.Y. Radical scavenging and antioxidant activity of tannic acid. *Arabian Journal of Chemistry* **2010**, *3*, 43–53, doi:10.1016/j.arabjc.2009.12.008.
330. Varbiro, G.; Veres, B.; Gallyas, F.; Sumegi, B. Direct effect of Taxol on free radical formation and mitochondrial permeability transition. *Free Radical Biology and Medicine* **2001**, *31*, 548–558, doi:10.1016/S0891-5849(01)00616-5.
331. Fonseca, C.; Simões, S.; Gaspar, R. Paclitaxel-loaded PLGA nanoparticles: preparation, physicochemical characterization and in vitro anti-tumoral activity. *Journal of Controlled Release* **2002**, *83*, 273–286, doi:10.1016/S0168-3659(02)00212-2.
332. Lee, Y.; Graeser, R.; Kratz, F.; Geckeler, K.E. Paclitaxel-Loaded Polymer Nanoparticles for the Reversal of Multidrug Resistance in Breast Cancer Cells. *Advanced Functional Materials* **2011**, *21*, 4211–4218, doi:10.1002/adfm.201100853.
333. Hirota, K.; Ter, H. Endocytosis of Particle Formulations by Macrophages and Its Application to Clinical Treatment. In *Molecular Regulation of Endocytosis*; Ceresa, B., Ed.; InTech, 2012 ISBN 978-953-51-0662-3.
334. Swanson, J.A.; Watts, C. Macropinocytosis. *Trends in Cell Biology* **1995**, *5*, 424–428, doi:10.1016/S0962-8924(00)89101-1.
335. Shu, C.-H.; Yang, W.K.; Shih, Y.-L.; Kuo, M.-L.; Huang, T.-S. Cell cycle G2/M arrest and activation of cyclin-dependent kinases associated with low-dose paclitaxel-induced sub-G1 apoptosis. *Apoptosis* **1997**, *2*, 463–470, doi:10.1023/A:1026422111457.
336. Tang, L.; Wang, Y.; Strom, A.; Gustafsson, J.-Å.; Guan, X. Lapatinib induces p27Kip1-dependent G<sub>1</sub> arrest through both transcriptional and post-translational mechanisms. *Cell Cycle* **2013**, *12*, 2665–2674, doi:10.4161/cc.25728.

337. Wang, T.-H.; Wang, H.-S.; Soong, Y.-K. Paclitaxel-induced cell death. *Cancer* **2000**, *88*, 2619–2628, doi:10.1002/1097-0142(20000601)88:11<2619::AID-CNCR26>3.0.CO;2-J.
338. Demidenko, Z.N.; Kalurupalle, S.; Hanko, C.; Lim, C.-.; Broude, E.; Blagosklonny, M.V. Mechanism of G1-like arrest by low concentrations of paclitaxel: next cell cycle p53-dependent arrest with sub G1 DNA content mediated by prolonged mitosis. *Oncogene* **2008**, *27*, 4402–4410, doi:10.1038/onc.2008.82.
339. Hsiao, J.-R.; Leu, S.-F.; Huang, B.-M. Apoptotic mechanism of paclitaxel-induced cell death in human head and neck tumor cell lines. *Journal of Oral Pathology & Medicine* **2009**, *38*, 188–197, doi:10.1111/j.1600-0714.2008.00732.x.
340. Chou, T.-C. Drug combination studies and their synergy quantification using the Chou-Talalay method. *Cancer Res.* **2010**, *70*, 440–446, doi:10.1158/0008-5472.CAN-09-1947.
341. Azmi, A.S.; Banerjee, S.; Ali, S.; Wang, Z.; Bao, B.; Beck, F.W.J.; Maitah, M.; Choi, M.; Shields, T.F.; Philip, P.A.; et al. Network Modeling of MDM2 Inhibitor-Oxaliplatin Combination Reveals Biological Synergy in wt-p53 solid tumors. *Oncotarget* **2011**, *2*, 378–392.
342. Ashton, J.C. Drug Combination Studies and Their Synergy Quantification Using the Chou–Talalay Method—Letter. *Cancer Res* **2015**, *75*, 2400–2400, doi:10.1158/0008-5472.CAN-14-3763.
343. Moy, B.; Kirkpatrick, P.; Kar, S.; Goss, P. Lapatinib Available online: <https://www.nature.com/articles/nrd2332> (accessed on Jan 27, 2020).
344. Dai, C.; Tiwari, A.K.; Wu, C.-P.; Su, X.; Wang, S.-R.; Liu, D.; Ashby, C.R.; Huang, Y.; Robey, R.W.; Liang, Y.; et al. Lapatinib (Tykerb, GW572016) Reverses Multidrug Resistance in Cancer Cells by Inhibiting the Activity of ATP-Binding Cassette Subfamily B Member 1 and G Member 2. *Cancer Res* **2008**, *68*, 7905–7914, doi:10.1158/0008-5472.CAN-08-0499.
345. Dai, C.; Ma, S.; Wang, F.; Zhao, H.; Wu, X.; Huang, Z.; Chen, Z.; To, K.; Fu, L. Lapatinib promotes the incidence of hepatotoxicity by increasing chemotherapeutic agent accumulation in hepatocytes. *Oncotarget* **2015**, *6*, 17738–17752.
346. Tanaka, R.; Takii, Y.; Shibata, Y.; Ariyama, H.; Qin, B.; Baba, E.; Kusaba, H.; Mitsugi, K.; Harada, M.; Nakano, S. In vitro sequence-dependent interaction between nedaplatin and paclitaxel in human cancer cell lines. *Cancer Chemother Pharmacol* **2005**, *56*, 279–285, doi:10.1007/s00280-004-0991-y.
347. Waltmire, C.N.; Alberts, D.S.; Dorr, R.T. Sequence-dependent cytotoxicity of combination chemotherapy using paclitaxel, carboplatin and bleomycin in human lung and ovarian cancer. *Anti-Cancer Drugs* **2001**, *12*, 595.
348. B. Pacardo, D.; S. Ligler, F.; Gu, Z. Programmable nanomedicine: synergistic and sequential drug delivery systems. *Nanoscale* **2015**, *7*, 3381–3391, doi:10.1039/C4NR07677J.
349. Desai, P.P.; Date, A.A.; Patravale, V.B. Overcoming poor oral bioavailability using nanoparticle formulations – opportunities and limitations. *Drug Discovery Today: Technologies* **2012**, *9*, e87–e95, doi:10.1016/j.ddtec.2011.12.001.
350. Vergara, D.; Bellomo, C.; Zhang, X.; Vergaro, V.; Tinelli, A.; Lorusso, V.; Rinaldi, R.; Lvov, Y.M.; Leporatti, S.; Maffia, M. Lapatinib/Paclitaxel polyelectrolyte nanocapsules for overcoming multidrug resistance in ovarian cancer. *Nanomedicine: Nanotechnology, Biology and Medicine* **2012**, *8*, 891–899, doi:10.1016/j.nano.2011.10.014.
351. Yan, B.-.; Ma, J.-.; Zhang, J.; Guo, Y.; Mueller, M.D.; Remick, S.C.; Yu, J.J. Prostatin may contribute to chemoresistance, repress cancer cells in ovarian cancer, and is involved in the signaling pathways of CASP/PAK2-p34/actin. *Cell Death & Disease* **2014**, *5*, e995–e995, doi:10.1038/cddis.2013.523.
352. Ekkapongpisit, M.; Giovia, A.; Follo, C.; Caputo, G.; Isidoro, C. Biocompatibility, endocytosis, and intracellular trafficking of mesoporous silica and polystyrene nanoparticles in ovarian cancer cells: effects of size and surface charge groups. *Int J Nanomedicine* **2012**, *7*, 4147–4158, doi:10.2147/IJN.S33803.
353. Devine, P.J.; Perreault, S.D.; Luderer, U. Roles of Reactive Oxygen Species and Antioxidants in Ovarian Toxicity. *Biol Reprod* **2012**, *86*, doi:10.1095/biolreprod.111.095224.

354. Wang, L.; Zhang, Q.; Zhang, J.; Sun, S.; Guo, H.; Jia, Z.; Wang, B.; Shao, Z.; Wang, Z.; Hu, X. PI3K pathway activation results in low efficacy of both trastuzumab and lapatinib. *BMC Cancer* **2011**, *11*, 248, doi:10.1186/1471-2407-11-248.
355. Nicolini, G.; Rigolio, R.; Scuteri, A.; Miloso, M.; Saccomanno, D.; Cavaletti, G.; Tredici, G. Effect of trans-resveratrol on signal transduction pathways involved in paclitaxel-induced apoptosis in human neuroblastoma SH-SY5Y cells. *Neurochemistry International* **2003**, *42*, 419–429, doi:10.1016/S0197-0186(02)00132-8.
356. Luo, C.; Sun, J.; Sun, B.; He, Z. Prodrug-based nanoparticulate drug delivery strategies for cancer therapy. *Trends in Pharmacological Sciences* **2014**, *35*, 556–566, doi:10.1016/j.tips.2014.09.008.
357. Wohl, A.R.; Michel, A.R.; Kalscheuer, S.; Macosko, C.W.; Panyam, J.; Hoye, T.R. Silicate Esters of Paclitaxel and Docetaxel: Synthesis, Hydrophobicity, Hydrolytic Stability, Cytotoxicity, and Prodrug Potential. *J. Med. Chem.* **2014**, *57*, 2368–2379, doi:10.1021/jm401708f.
358. Han, H.-K.; Amidon, G.L. Targeted prodrug design to optimize drug delivery. *AAPS PharmSci* **2000**, *2*, 48–58, doi:10.1208/ps020106.
359. Delplace, V.; Couvreur, P.; Nicolas, J. Recent trends in the design of anticancer polymer prodrug nanocarriers. *Polym. Chem.* **2014**, *5*, 1529–1544, doi:10.1039/C3PY01384G.
360. Stevens, P.J.; Sekido, M.; Lee, R.J. A Folate Receptor–Targeted Lipid Nanoparticle Formulation for a Lipophilic Paclitaxel Prodrug. *Pharm Res* **2004**, *21*, 2153–2157, doi:10.1007/s11095-004-7667-5.
361. Gu, Y.; Zhong, Y.; Meng, F.; Cheng, R.; Deng, C.; Zhong, Z. Acetal-Linked Paclitaxel Prodrug Micellar Nanoparticles as a Versatile and Potent Platform for Cancer Therapy. *Biomacromolecules* **2013**, *14*, 2772–2780, doi:10.1021/bm400615n.
362. Li, N.; Cai, H.; Jiang, L.; Hu, J.; Bains, A.; Hu, J.; Gong, Q.; Luo, K.; Gu, Z. Enzyme-Sensitive and Amphiphilic PEGylated Dendrimer-Paclitaxel Prodrug-Based Nanoparticles for Enhanced Stability and Anticancer Efficacy. *ACS Appl. Mater. Interfaces* **2017**, *9*, 6865–6877, doi:10.1021/acsami.6b15505.
363. Hu, X.; Li, J.; Lin, W.; Huang, Y.; Jing, X.; Xie, Z. Paclitaxel prodrug nanoparticles combining chemical conjugation and physical entrapment for enhanced antitumor efficacy. *RSC Adv.* **2014**, *4*, 38405–38411, doi:10.1039/C4RA06270A.
364. Zhu, Z. Flash Nanoprecipitation: Prediction and Enhancement of Particle Stability via Drug Structure. *Mol. Pharmaceutics* **2014**, *11*, 776–786, doi:10.1021/mp500025e.
365. Davoust, J.; Gruenberg, J.; Howell, K.E. Two threshold values of low pH block endocytosis at different stages. *The EMBO Journal* **1987**, *6*, 3601–3609, doi:10.1002/j.1460-2075.1987.tb02691.x.
366. Fu, Y.; Zhang, J.; Wang, H.; Chen, J.-L.; Zhao, P.; Chen, G.-R.; He, X.-P. Intracellular pH sensing and targeted imaging of lysosome by a galactosyl naphthalimide-piperazine probe. *Dyes and Pigments* **2016**, *133*, 372–379, doi:10.1016/j.dyepig.2016.06.022.
367. Swietach, P.; Vaughan-Jones, R.D.; Harris, A.L.; Hulikova, A. The chemistry, physiology and pathology of pH in cancer. *Philosophical Transactions of the Royal Society B: Biological Sciences* **2014**, *369*, 20130099, doi:10.1098/rstb.2013.0099.
368. 5 - Mathematical models of drug release. In *Strategies to Modify the Drug Release from Pharmaceutical Systems*; Bruschi, M.L., Ed.; Woodhead Publishing, 2015; pp. 63–86 ISBN 978-0-08-100092-2.
369. Dash, S.; Murthy, P.N.; Nath, L.; Chowdhury, P. Kinetic modeling on drug release from controlled drug delivery systems. *Acta Pol Pharm* **2010**, *67*, 217–223.
370. Costa, P.; Sousa Lobo, J.M. Modeling and comparison of dissolution profiles. *European Journal of Pharmaceutical Sciences* **2001**, *13*, 123–133, doi:10.1016/S0928-0987(01)00095-1.
371. Nagaraja, G.M.; Othman, M.; Fox, B.P.; Alsaber, R.; Pellegrino, C.M.; Zeng, Y.; Khanna, R.; Tamburini, P.; Swaroop, A.; Kandpal, R.P. Gene expression signatures and biomarkers of noninvasive and invasive breast cancer cells: comprehensive profiles by representational difference analysis, microarrays and proteomics. *Oncogene* **2006**, *25*, 2328–2338, doi:10.1038/sj.onc.1209265.
372. Liang, P.; Pardee, A.B. Analysing differential gene expression in cancer. *Nature Reviews Cancer* **2003**, *3*, 869–876, doi:10.1038/nrc1214.

373. McFarland, J.W. On the parabolic relationship between drug potency and hydrophobicity. *J. Med. Chem.* **1970**, *13*, 1192–1196, doi:10.1021/jm00300a040.
374. Zhang, S.; Li, J.; Lykotrafitis, G.; Bao, G.; Suresh, S. Size-Dependent Endocytosis of Nanoparticles. *Advanced Materials* **2009**, *21*, 419–424, doi:10.1002/adma.200801393.
375. Sahay, G.; Alakhova, D.Y.; Kabanov, A.V. Endocytosis of nanomedicines. *Journal of Controlled Release* **2010**, *145*, 182–195, doi:10.1016/j.jconrel.2010.01.036.
376. El-Far, S.W.; Helmy, M.W.; Khattab, S.N.; Bekhit, A.A.; Hussein, A.A.; Elzoghby, A.O. Folate conjugated vs PEGylated phytosomal casein nanocarriers for codelivery of fungal- and herbal-derived anticancer drugs. *Nanomedicine* **2018**, *13*, 1463–1480, doi:10.2217/nmm-2018-0006.
377. Ravar, F.; Saadat, E.; Kelishadi, P.D.; Dorkoosh, F.A. Liposomal formulation for co-delivery of paclitaxel and lapatinib, preparation, characterization and optimization. *Journal of Liposome Research* **2016**, *26*, 175–187, doi:10.3109/08982104.2015.1070174.
378. Nam, J.; La, W.-G.; Hwang, S.; Ha, Y.S.; Park, N.; Won, N.; Jung, S.; Bhang, S.H.; Ma, Y.-J.; Cho, Y.-M.; et al. pH-Responsive Assembly of Gold Nanoparticles and “Spatiotemporally Concerted” Drug Release for Synergistic Cancer Therapy. *ACS Nano* **2013**, *7*, 3388–3402, doi:10.1021/nn400223a.
379. Kong, M.; Zuo, Y.; Wang, M.; Bai, X.; Feng, C.; Chen, X. Simply constructed chitosan nanocarriers with precise spatiotemporal control for efficient intracellular drug delivery. *Carbohydrate Polymers* **2017**, *169*, 341–350, doi:10.1016/j.carbpol.2017.03.090.
380. Gindy, M.E.; Prud’homme, R.K. Multifunctional nanoparticles for imaging, delivery and targeting in cancer therapy. *Expert Opinion on Drug Delivery* **2009**, *6*, 865–878, doi:10.1517/17425240902932908.
381. Desai, M.P.; Labhassetwar, V.; Walter, E.; Levy, R.J.; Amidon, G.L. The mechanism of uptake of biodegradable microparticles in Caco-2 cells is size dependent. *Pharm. Res.* **1997**, *14*, 1568–1573.
382. Peer, D.; Karp, J.M.; Hong, S.; Farokhzad, O.C.; Margalit, R.; Langer, R. Nanocarriers as an emerging platform for cancer therapy. *Nat Nano* **2007**, *2*, 751–760, doi:10.1038/nnano.2007.387.
383. Liu, Y.; Kathan, K.; Saad, W.; Prud’homme, R.K. Ostwald ripening of beta-carotene nanoparticles. *Phys. Rev. Lett.* **2007**, *98*, 036102, doi:10.1103/PhysRevLett.98.036102.
384. Yusuf, H.; Nugraheni, R.; Mulyadi, N.A.; Setyawan, D.; Rosita, N. Phase Behavior of Dried–DDA Liposomal Formulation Dispersed in HPMC Matrix in the presence of Saccharides. *International Journal of PharmTech Research* **2017**, *10*, 50–56, doi:2455 - 9563.
385. Figueroa, C.E.; Adamson, D.H.; Prud’homme, R.K. Effervescent redispersion of lyophilized polymeric nanoparticles. *Ther Deliv* **2013**, *4*, 177–190, doi:10.4155/tde.12.138.
386. D’Addio, S.M.; Kafka, C.; Akbulut, M.; Beattie, P.; Saad, W.; Herrera, M.; Kennedy, M.T.; Prud’homme, R.K. Novel Method for Concentrating and Drying Polymeric Nanoparticles: Hydrogen Bonding Coacervate Precipitation. *Mol. Pharmaceutics* **2010**, *7*, 557–564, doi:10.1021/mp900260q.
387. Franks, F. Freeze-drying of bioproducts: putting principles into practice. *European Journal of Pharmaceutics and Biopharmaceutics* **1998**, *45*, 221–229, doi:10.1016/S0939-6411(98)00004-6.
388. Freitas, C.; Müllerä, R.H. Spray-drying of solid lipid nanoparticles (SLN TM). *Eur J Pharm Biopharm* **1998**, *46*, 145–151.
389. Iskandar, F.; Gradon, L.; Okuyama, K. Control of the morphology of nanostructured particles prepared by the spray drying of a nanoparticle sol. *Journal of Colloid and Interface Science* **2003**, *265*, 296–303, doi:10.1016/S0021-9797(03)00519-8.
390. Anhorn, M.G.; Mahler, H.-C.; Langer, K. Freeze drying of human serum albumin (HSA) nanoparticles with different excipients. *International Journal of Pharmaceutics* **2008**, *363*, 162–169, doi:10.1016/j.ijpharm.2008.07.004.
391. Cavalli, R.; Caputo, O.; Carlotti, M.E.; Trotta, M.; Scarnecchia, C.; Gasco, M.R. Sterilization and freeze-drying of drug-free and drug-loaded solid lipid nanoparticles. *International Journal of Pharmaceutics* **1997**, *148*, 47–54, doi:10.1016/S0378-5173(96)04822-3.
392. Schwarz, null; Mehnert, null Freeze-drying of drug-free and drug-loaded solid lipid nanoparticles (SLN). *Int J Pharm* **1997**, *157*, 171–179.

393. Abdelwahed, W.; Degobert, G.; Stainmesse, S.; Fessi, H. Freeze-drying of nanoparticles: Formulation, process and storage considerations. *Advanced Drug Delivery Reviews* **2006**, *58*, 1688–1713, doi:10.1016/j.addr.2006.09.017.
394. Vehring, R. Pharmaceutical Particle Engineering via Spray Drying. *Pharm Res* **2008**, *25*, 999–1022, doi:10.1007/s11095-007-9475-1.
395. Suzuki, H.; Hamao, S.; Seto, Y.; Sato, H.; Wong, J.; Prud'homme, R.K.; Chan, H.-K.; Onoue, S. New nano-matrix oral formulation of nanoprecipitated cyclosporine A prepared with multi-inlet vortex mixer. *International Journal of Pharmaceutics* **2017**, *516*, 116–119, doi:10.1016/j.ijpharm.2016.11.031.
396. Jab&#x142; czy&#x144; Ska, K.; Janczewska, M.; Kulikowska, A.; Sosnowski, T.R. Preparation and Characterization of Biocompatible Polymer Particles as Potential Nanocarriers for Inhalation Therapy Available online: <https://www.hindawi.com/journals/ijps/2015/763020/abs/> (accessed on Sep 26, 2017).
397. Wanning, S.; Süverkrüp, R.; Lamprecht, A. Pharmaceutical spray freeze drying. *International Journal of Pharmaceutics* **2015**, *488*, 136–153, doi:10.1016/j.ijpharm.2015.04.053.
398. Cheow, W.S.; Ng, M.L.L.; Kho, K.; Hadinoto, K. Spray-freeze-drying production of thermally sensitive polymeric nanoparticle aggregates for inhaled drug delivery: effect of freeze-drying adjuvants. *Int J Pharm* **2011**, *404*, 289–300, doi:10.1016/j.ijpharm.2010.11.021.
399. Tang, C.; Prud'homme, R.K. Targeted Theragnostic Nanoparticles Via Flash Nanoprecipitation: Principles of Material Selection. In *Polymer Nanoparticles for Nanomedicines*; Vauthier, C., Ponchel, G., Eds.; Springer International Publishing, 2016; pp. 55–85 ISBN 978-3-319-41419-5.
400. Chacón, M.; Molpeceres, J.; Berges, L.; Guzmán, M.; Aberturas, M.R. Stability and freeze-drying of cyclosporine loaded poly(D,L lactide–glycolide) carriers. *European Journal of Pharmaceutical Sciences* **1999**, *8*, 99–107, doi:10.1016/S0928-0987(98)00066-9.
401. Hinrichs, W.L.J.; Manceñido, F.A.; Sanders, N.N.; Braeckmans, K.; De Smedt, S.C.; Demeester, J.; Frijlink, H.W. The choice of a suitable oligosaccharide to prevent aggregation of PEGylated nanoparticles during freeze thawing and freeze drying. *International Journal of Pharmaceutics* **2006**, *311*, 237–244, doi:10.1016/j.ijpharm.2005.12.032.
402. Figueroa, C.E. Engineering Nanoparticles for Pharmaceutical Applications: Formulation and Freeze-Drying Techniques. **2014**.
403. Abdelwahed, W.; Degobert, G.; Fessi, H. A pilot study of freeze drying of poly(epsilon-caprolactone) nanocapsules stabilized by poly(vinyl alcohol): Formulation and process optimization. *International Journal of Pharmaceutics* **2006**, *309*, 178–188, doi:10.1016/j.ijpharm.2005.10.003.
404. Saez, A.; Guzmán, M.; Molpeceres, J.; Aberturas, M.R. Freeze-drying of polycaprolactone and poly(D,L-lactic-glycolic) nanoparticles induce minor particle size changes affecting the oral pharmacokinetics of loaded drugs. *European Journal of Pharmaceutics and Biopharmaceutics* **2000**, *50*, 379–387, doi:10.1016/S0939-6411(00)00125-9.
405. Burger, C.; Hsiao, B.S.; Chu, B. Nanofibrous Materials and Their Applications. *Annual Review of Materials Research* **2006**, *36*, 333–368, doi:10.1146/annurev.matsci.36.011205.123537.
406. Reneker, D.H.; Chun, I. Nanometre diameter fibres of polymer, produced by electrospinning. *Nanotechnology* **1996**, *7*, 216, doi:10.1088/0957-4484/7/3/009.
407. Li, D.; Xia, Y. Electrospinning of Nanofibers: Reinventing the Wheel? *Adv. Mater.* **2004**, *16*, 1151–1170, doi:10.1002/adma.200400719.
408. Huang, Z.-M.; Zhang, Y.-Z.; Kotaki, M.; Ramakrishna, S. A review on polymer nanofibers by electrospinning and their applications in nanocomposites. *Composites Science and Technology* **2003**, *63*, 2223–2253, doi:10.1016/S0266-3538(03)00178-7.
409. Fridrikh, S.V.; Yu, J.H.; Brenner, M.P.; Rutledge, G.C. Controlling the Fiber Diameter during Electrospinning. *Phys. Rev. Lett.* **2003**, *90*, 144502, doi:10.1103/PhysRevLett.90.144502.
410. Wang, Y.; Kho, K.; Cheow, W.S.; Hadinoto, K. A comparison between spray drying and spray freeze drying for dry powder inhaler formulation of drug-loaded lipid–polymer hybrid nanoparticles. *International Journal of Pharmaceutics* **2012**, *424*, 98–106, doi:10.1016/j.ijpharm.2011.12.045.

411. Sóti, P.L.; Bocz, K.; Pataki, H.; Eke, Z.; Farkas, A.; Verreck, G.; Kiss, É.; Fekete, P.; Vigh, T.; Wagner, I.; et al. Comparison of spray drying, electroblowing and electrospinning for preparation of Eudragit E and itraconazole solid dispersions. *International Journal of Pharmaceutics* **2015**, *494*, 23–30, doi:10.1016/j.ijpharm.2015.07.076.
412. Torchilin, V.P. Multifunctional nanocarriers. *Advanced Drug Delivery Reviews* **2012**, *64*, 302–315, doi:10.1016/j.addr.2012.09.031.
413. Bao, G.; Mitragotri, S.; Tong, S. Multifunctional Nanoparticles for Drug Delivery and Molecular Imaging. *Annual Review of Biomedical Engineering* **2013**, *15*, 253–282, doi:10.1146/annurev-bioeng-071812-152409.
414. Levine, D.H.; Ghoroghchian, P.P.; Freudenberg, J.; Zhang, G.; Therien, M.J.; Greene, M.I.; Hammer, D.A.; Murali, R. Polymersomes: A new multi-functional tool for cancer diagnosis and therapy. *Methods* **2008**, *46*, 25–32, doi:10.1016/j.ymeth.2008.05.006.
415. Tyrrell, Z.L.; Shen, Y.; Radosz, M. Fabrication of micellar nanoparticles for drug delivery through the self-assembly of block copolymers. *Progress in Polymer Science* **2010**, *35*, 1128–1143, doi:10.1016/j.progpolymsci.2010.06.003.
416. Johnson, B.K.; Prud'homme, R.K. Flash NanoPrecipitation of Organic Actives and Block Copolymers using a Confined Impinging Jets Mixer. *Aust. J. Chem.* **2003**, *56*, 1021–1024, doi:10.1071/ch03115.
417. Tang, C.; Saquing, C.D.; Harding, J.R.; Khan, S.A. In Situ Cross-Linking of Electrospun Poly(vinyl alcohol) Nanofibers. *Macromolecules* **2010**, *43*, 630–637, doi:10.1021/ma902269p.
418. Dumas, C.; Meledandri, C.J. Insights into the Partitioning Behavior of Secondary Surfactants in a Microemulsion-Based Synthesis of Metal Nanoparticles: A DLS and 2D NMR Spectroscopic Investigation. *Langmuir* **2015**, *31*, 7193–7203, doi:10.1021/acs.langmuir.5b00417.
419. Mishael, Y.G.; Dubin, P.L. Toluene Solubilization Induces Different Modes of Mixed Micelle Growth. *Langmuir* **2005**, *21*, 9803–9808, doi:10.1021/la050513p.
420. Understanding the colloidal stability of protein therapeutics using dynamic light scattering Available online: <https://www.malvern.com/en/support/resource-center/Whitepapers/WP140422ColloidalStabilityProteinTheraDLS.html> (accessed on Sep 29, 2017).
421. Tang, C.; Ozcam, A.E.; Stout, B.; Khan, S.A. Effect of pH on Protein Distribution in Electrospun PVA/BSA Composite Nanofibers. *Biomacromolecules* **2012**, *13*, 1269–1278, doi:10.1021/bm2017146.
422. Rieger, J. The glass transition temperature of polystyrene. *Journal of Thermal Analysis* **1996**, *46*, 965–972, doi:10.1007/BF01983614.
423. Yarin, A.L.; Koombhongse, S.; Reneker, D.H. Bending instability in electrospinning of nanofibers. *Journal of Applied Physics* **2001**, *89*, 3018–3026, doi:10.1063/1.1333035.
424. Naraghi, M.; Arshad, S.N.; Chasiotis, I. Molecular orientation and mechanical property size effects in electrospun polyacrylonitrile nanofibers. *Polymer* **2011**, *52*, 1612–1618, doi:10.1016/j.polymer.2011.02.013.
425. Komrakova, A.E.; Shardt, O.; Eskin, D.; Derksen, J.J. Lattice Boltzmann simulations of drop deformation and breakup in shear flow. *International Journal of Multiphase Flow* **2014**, *59*, 24–43, doi:10.1016/j.ijmultiphaseflow.2013.10.009.
426. Ramanujan, S.; Pozrikidis, C. Deformation of liquid capsules enclosed by elastic membranes in simple shear flow: large deformations and the effect of fluid viscosities. *Journal of Fluid Mechanics* **1998**, *361*, 117–143, doi:10.1017/S0022112098008714.
427. Tan, S.-H.; Inai, R.; Kotaki, M.; Ramakrishna, S. Systematic parameter study for ultra-fine fiber fabrication via electrospinning process. *Polymer* **2005**, *46*, 6128–6134, doi:10.1016/j.polymer.2005.05.068.
428. Ding, B.; Kim, H.-Y.; Lee, S.-C.; Shao, C.-L.; Lee, D.-R.; Park, S.-J.; Kwag, G.-B.; Choi, K.-J. Preparation and characterization of a nanoscale poly(vinyl alcohol) fiber aggregate produced by an electrospinning method. *J. Polym. Sci. B Polym. Phys.* **2002**, *40*, 1261–1268, doi:10.1002/polb.10191.
429. Chow, S.F.; Wan, K.Y.; Cheng, K.K.; Wong, K.W.; Sun, C.C.; Baum, L.; Chow, A.H.L. Development of highly stabilized curcumin nanoparticles by flash nanoprecipitation and lyophilization. *Eur J Pharm Biopharm* **2015**, *94*, 436–449, doi:10.1016/j.ejpb.2015.06.022.

430. D'Addio, S.M.; Chan, J.G.Y.; Kwok, P.C.L.; Benson, B.R.; Prud'homme, R.K.; Chan, H.-K. Aerosol delivery of nanoparticles in uniform mannitol carriers formulated by ultrasonic spray freeze drying. *Pharm. Res.* **2013**, *30*, 2891–2901, doi:10.1007/s11095-013-1120-6.
431. Yu, D.-G.; Shen, X.-X.; Branford-White, C.; White, K.; Zhu, L.-M.; Bligh, S.W.A. Oral fast-dissolving drug delivery membranes prepared from electrospun polyvinylpyrrolidone ultrafine fibers. *Nanotechnology* **2009**, *20*, 055104, doi:10.1088/0957-4484/20/5/055104.
432. Mansour, H.M.; Sohn, M.; Al-Ghananeem, A.; DeLuca, P.P. Materials for Pharmaceutical Dosage Forms: Molecular Pharmaceutics and Controlled Release Drug Delivery Aspects. *International Journal of Molecular Sciences* **2010**, *11*, 3298–3322, doi:10.3390/ijms11093298.
433. Wendorf, J.; Singh, M.; Chesko, J.; Kazzaz, J.; Soewanan, E.; Ugozzoli, M.; O'Hagan, D. A practical approach to the use of nanoparticles for vaccine delivery. *J Pharm Sci* **2006**, *95*, 2738–2750, doi:10.1002/jps.20728.







r180521r01 #1-50 RT: 0.00-0.40 AV: 50 NL: 3.86E6  
T: FTMS + p NSI Full ms [150.00-2000.00]

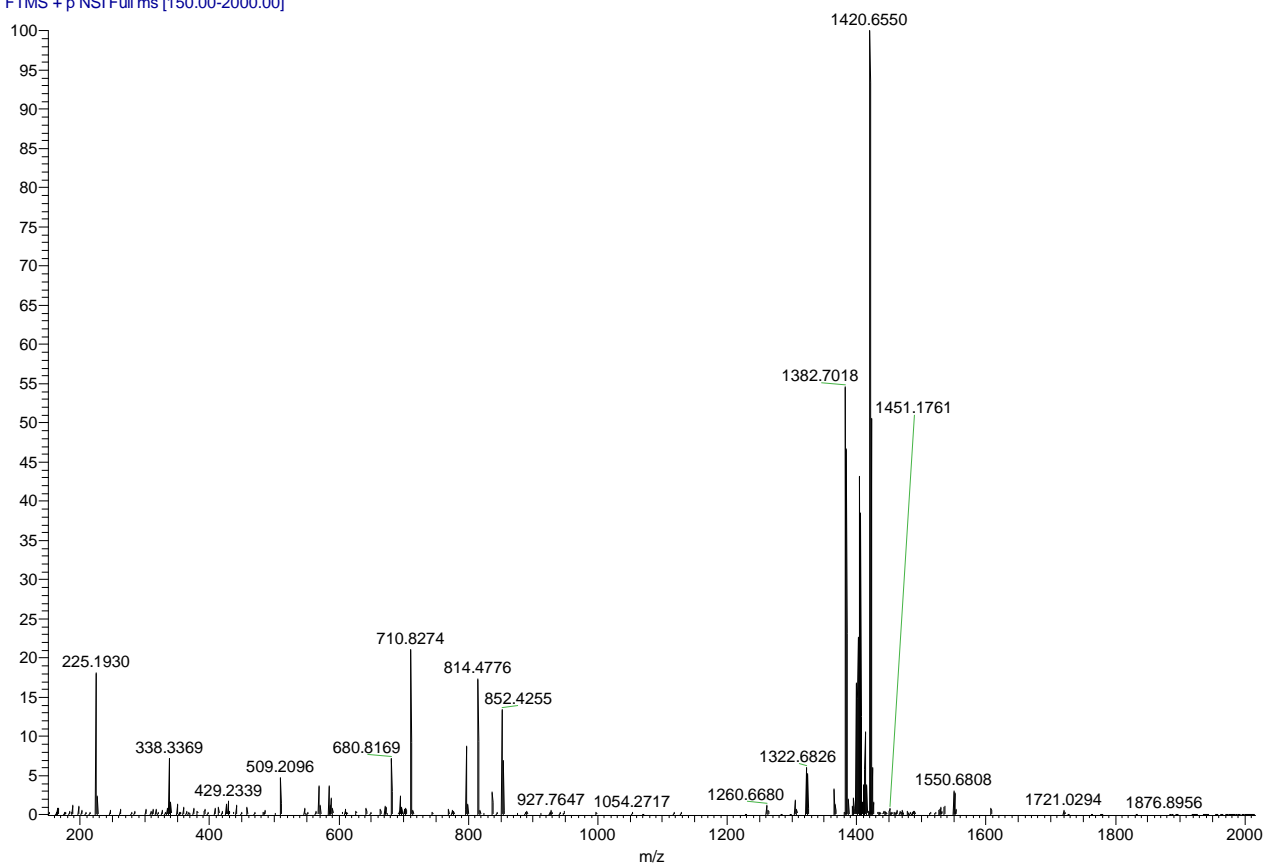


Figure S2: Direct Infusion Mass-Spectroscopy of the prodrug.